Montana Bureau of Mines and Geology

PROCEEDINGS

Original artwork by Bulbul Majumder, MBMG.

Montana Mining and Mineral Symposium 2021
September 9–September 11, 2021
Montana Bureau of Mines and Geology
Special Publication 123

UUNO SAHINEN MEDALLION AWARD

The Montana Bureau of Mines and Geology at Montana Tech has named John F. Childs the recipient of the 2021 Uuno Sahinen Silver Medallion. The award is named after the late Uuno Sahinen, the MBMG's first director, widely recognized for the MBMG's growth. The Uuno Sahinen Award acknowledges "outstanding contributions in understanding and development of energy, mineral, or groundwater resources in Montana" and is awarded each year.

Childs earned a BSc degree in geology from Syracuse University in 1966. He completed his education with an MSc from the University of British Columbia in 1969 and a Ph.D. from the University of California at Santa Cruz in 1982.

He is a member of the Society for Mining, Metallurgy, and Exploration; the Society of Economic Geologists; the Association of Applied Geochemists; the Geological Society of America; and the Geological Association of Canada. Childs has published on a wide variety of topics including structural geology, talc, gold, porphyry deposits, palladium-platinum, gemstones, Arizona geology, various field trip guides, and working relationships with small miners in Brazil.

Childs has worked for several companies including Cyprus Mines Corporation, Pegasus Gold, and Sibanye-Stillwater. However, most of his career has been spent as an independent consultant through Childs Geoscience Inc. and its predecessor companies.

John Childs examining an outcrop in the Elkhorn Ghost Town, Elkhorn, MT. Photo by Chris Gammons.

TABLE OF CONTENTS

Green sphalerite with coarse, white, dolomitic marble from the Elkhorn (Holter) mine. Photo by Chris Gammons.

PROCEEDINGS,
MONTANA MINING AND MINERAL SYMPOSIUM 2022
TECHNICAL PAPERS

Special Publication 123

Edited by Kaleb C. Scarberry,[1] Christopher H. Gammons,[2] and Susan Barth[1]

[1]*Montana Bureau of Mines and Geology, Butte, Montana*

[2]*Montana Technological University, Butte, Montana*

Sulfide-rich sample with Mn-rich calcite, from display case at Montana Tunnels Mine. Photo by Chris Gammons.

An Update on Hard Rock Mining in Montana

Garrett Smith

Montana Department of Environmental Quality, Helena, Montana

Background and Duties

The Hard Rock Mining Section (HRMS) is the program within the Montana Department of Environmental Quality (DEQ) that regulates the mechanized exploration and development of all ore, rock, or mineral substances from hard rock sources. Although that definition encompasses a wide range of operations, the resources that are excluded from the HRMS's permitting authority include bentonite, clay, coal, natural gas, oil, peat, sand and alluvial gravel, scoria, soil materials, and uranium. The HRMS oversees the mining operations conducted under small miner exclusion statements (SMES, ≤5 acres), exploration licenses, and mine operating permits.

The administrative duties and the permitting procedures that apply to the HRMS originate primarily from the Metal Mine Reclamation Act (MMRA) and Montana Environmental Policy Act (MEPA; see § 82-4-301 et seq., Montana Code Annotated (MCA) and 75-1-101 et seq., MCA). These duties include issuing timely and complete decisions for permit applications and modifications, and ensuring permitted mineral development occurs with adequate protection of other resources. The development of environmental assessments (EA) or environmental impact statements (EIS) is coordinated with other permits obtained through State or Federal agencies. HRMS reviews the annual reports or renewal statements submitted by active operations, while also conducting annual inspections to review the mining and reclamation status at each site and to offer compliance assistance. Performance bonds (i.e., financial assurances) are held for operating permits, exploration projects, and some SMES sites, in order to perform any potential reclamation work that is not completed by the operator. The bonds are reviewed on an annual basis and they are recalculated at a minimum of every 5 years or following significant permit modifications.

Recent Legislative Updates

During the 2021 Montana State Legislative Session, amendments were made to the MMRA to account for the different environmental conditions that may exist between hard rock operating permits that produce metalliferous ores, industrial minerals, and rock products. The newly adopted MMRA language specifically addresses the permitting of rock product operations, as summarized below:

82-4-301, MCA (Legislative Intent and Findings)

> (4) The legislature finds that the mining of rock products from or just below the ground surface not containing sulfides is subject to fewer permitting requirements than other minerals because:
>
> (a) the mining of nonsulfide rock products from or just below the ground surface creates fewer and more limited environmental concerns than the mining of other minerals;
>
> (b) nonsulfide rock products are typically used in their natural state and not subject to chemical processing; and
>
> (c) water quality and quantity are not significantly affected by mining of nonsulfide rock products from or just below the ground surface.

82-4-303, MCA (Definitions)

> (29) (a) "Rock products" means decorative rock, building stone, riprap, mineral aggregates, and other minerals produced by typical quarrying activities or collected from or just below the ground surface that do not contain sulfides with the potential to produce acid, toxic, or otherwise pollutive solutions.
>
> (b) The term does not include talc, gypsum, limestone, metalliferous ores, gemstones, or materials extracted by underground mining.

82-4-337, MCA (Inspection, issuance of operating permit, modification, amendment, or revision)

(1) (a) The department shall review all applications for operating permits for completeness and compliance with the requirements of this part and rules adopted pursuant to this part within:

(i) for rock products, 60 days of receipt of the initial application and within 20 days of receipt of responses to notices of deficiencies. If an applicant for a rock products operating permit responds to a notice of deficiency more than 1 year after its receipt, the department has 60 days to review the response to the notice of deficiency.

(ii) for all other applications not covered under subsection (1)(a)(i), 90 days of receipt of the initial application and within 30 days of receipt of responses to notices of deficiencies.

Other details regarding the eligibility requirements for a rock product permit and the procedural elements for permit application and fee are provided in 82-4-343, MCA (Operating permits, rock products, fees). This section is not reproduced in its entirety here, but a few important components include:

82-4-343, MCA (Operating permit, rock products, fees)—Abridged

(2) (a) A person mining rock products or a landowner allowing another person to mine rock products from the landowner's land may obtain an operating permit for a single site or multiple sites if the operation or operations cumulatively disturb no more than 100 acres of the earth's surface and the single site or each of the multiple sites do not:

(i) operate within 100 feet of surface water or in ground water or impact any wetland, surface water, or ground water;

(ii) have any water impounding structures other than for storm water control;

(iii) adversely impact a member of or the critical habitat of a member of a wildlife species that is listed as threatened or endangered under the Endangered Species Act of 1973; or

(iv) impact significant historic or archaeological features.

(b) A landowner who is a permittee and allows another person to mine on the landowner's land is responsible for compliance with this part, the rules adopted pursuant to this part, and the permit for mining activities conducted on sites permitted pursuant to this subsection (2) with the landowner's permission. The performance bond required under this part is and must be conditioned upon compliance with this part, the rules adopted pursuant to this part, and the permit of the landowner and any person who mines with the landowner's consent.

(7) The department's action on an application submitted under this section does not require an environmental review under Title 75, chapter 1, for the following:

(a) an application for a new permit resulting in less than 15 acres of total disturbance;

(b) an application to amend a permit resulting in less than 15 acres of total disturbance; and

(c) an application to amend a permit that has been analyzed under Title 75, chapter 1, that results in less than 25 acres of new disturbance.

Operating Permit Updates

The following discussion provides updates about hard rock operating permits and proposed projects that are currently under development and/or environmental review. It does not summarize the many SMES sites (>400) and exploration license projects (>150) that occur across the state (fig. 1). As of September 2021, there are 71 individual operating permits administered by HRMS, with a total of 255 project sites associated with the permits (figs. 1, 2). These additional project sites may include product load-out facilities, processing sites, and/or disposal facilities that are not adjacent to the mine area. The project sites also reflect the number of multiple-site permits, which allow for more than one mining location under a single operation and reclamation plan. These are more common with rock product quarries and surficial rock picking operations, which typically acquire specific types of rock from relatively small disturbance areas spread over a large region.

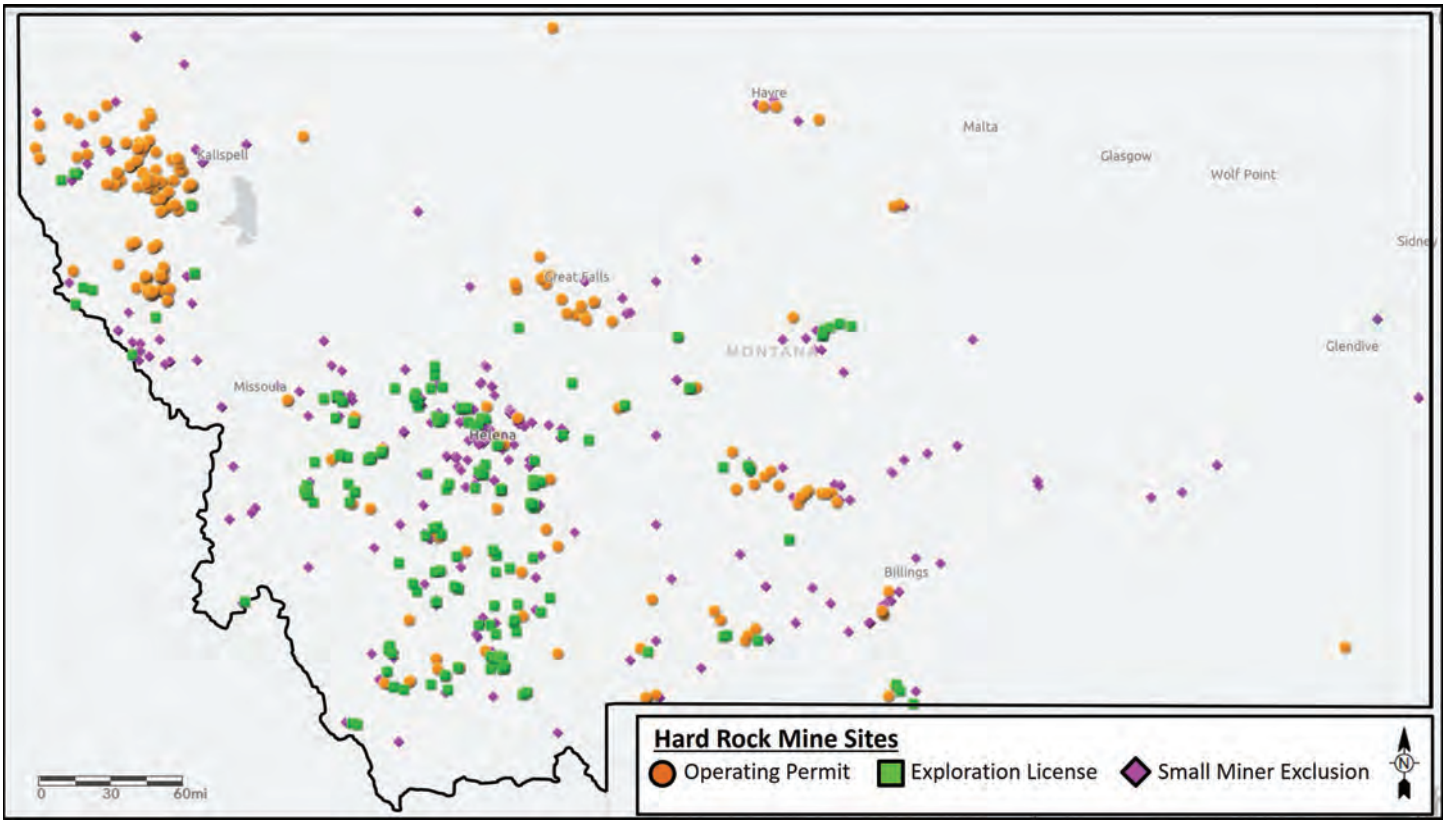

Figure 1. Locations of Hard Rock Mine Sites across Montana. The symbols represent project sites and indicate the permitting category (Operating Permit, Exploration License, or Small Miner Exclusion), but not the commodity or activity status of each site.

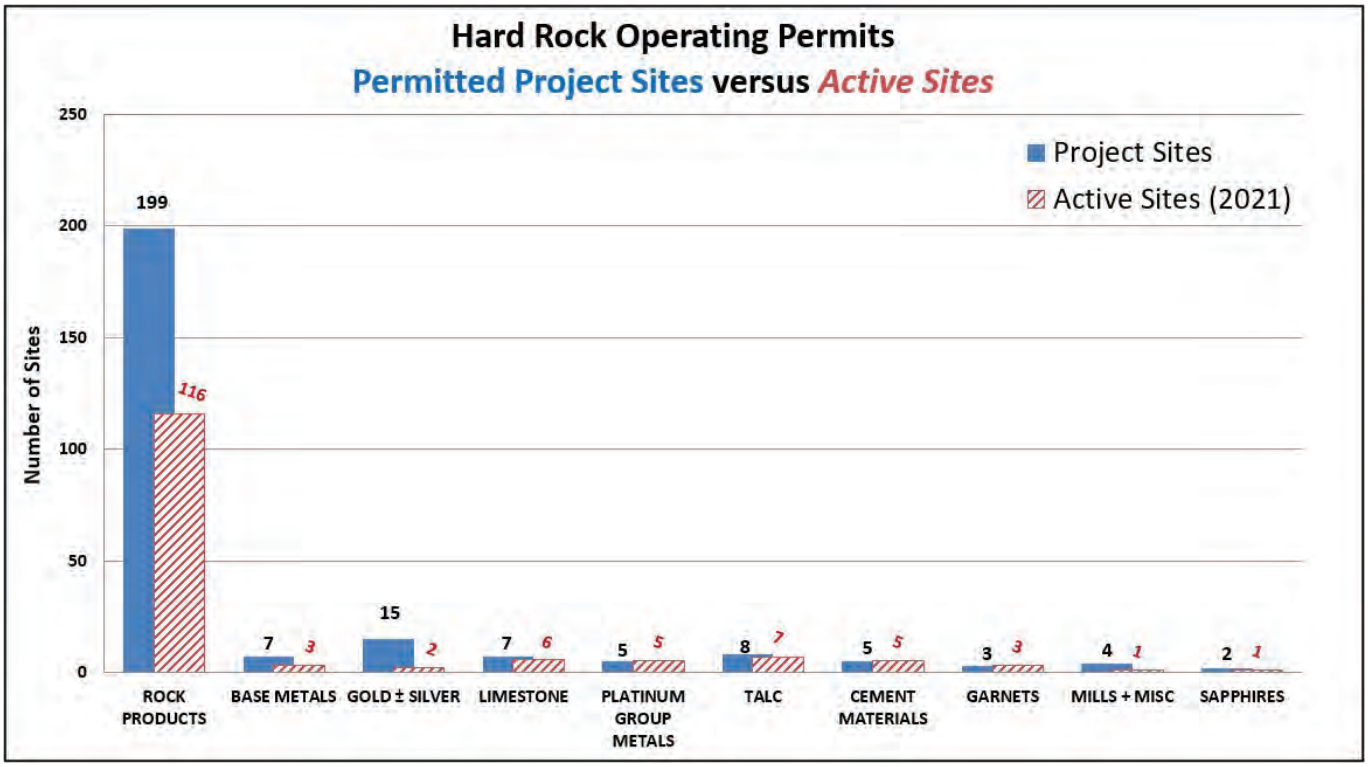

Figure 2. Distribution of Hard Rock Operating Permits by commodity. The project sites associated with a permit may include mine areas, product load-out facilities, processing sites, and/or disposal facilities that are not adjacent to the mine area. The project sites also reflect the number of multiple-site permits, which allow for more than one mining location under a single permit. Site activity is determined by the most recent site inspection and Annual Progress Report submitted by the permittee.

When comparing the number of hard rock mine operations that are currently active (i.e., generating mineral products, conducting construction or reclamation) or inactive, it is clear that rock product sites outnumber the industrial mineral and metal mines (fig. 2). Rock product operations often benefit from low barriers to entry for equipment and project design, relatively simple operation and reclamation plans, reduced potential for environmental impacts, and permitting actions that receive little public attention or litigation. Many of the metal mines in Montana are currently in care and maintenance status or in the process of final reclamation and closure. Many industrial mineral mines and rock quarries have amended their permits in recent years to extend production. Rock product operations continue to expand but they are also experiencing increased competition in many regions. Updates about some of the major developments at active operations and pending projects are included below.

Continental Mine Complex, Montana Resources, Butte (Cu, Mo, Ag)

Montana Resources in Butte continues to produce ore from the Continental Pit, while the overburden is being used as construction material around the site, particularly for raising the embankments of the tailings storage facility to a higher elevation. Copper concentrate is also produced from leach pad solutions, Berkeley Pit water, and Horseshoe Bend seepage at the Horseshoe Bend copper precipitation plant, and the Horseshoe Bend water treatment plant continues to treat a combination of sources for reuse in the concentrator and processing circuit.

Following the Final EIS and Record of Decision in 2020, an amendment was approved to raise the west embankment of the tailings storage facility to an elevation of 6,450 ft and expand the total storage capacity of the facility. Among other construction logistics, this expansion requires water management on the west side of the facility, to prevent potential degradation of groundwater beneath the nearby ridge from tailings pond seepage. The construction designs and geotechnical requirements were evaluated through a statutory process enacted in 2015, which requires the review and approval from a third-party Engineer of Record and Independent Review Panel, which consists of three experts in the field of tailings storage facilities. Construction of the facility expansion continued through 2021.

The groundwater at the mine is managed in accordance with Superfund requirements and not the mine operating permit, but there is overlap in the objectives for the sitewide water balance. Under the remedial action requirements for the Butte Mine Flooding Operable Unit, Montana Resources and other parties began pilot projects in 2019 to develop long-term management and treatment strategies for water in the Berkeley Pit and nearby groundwater. The water is currently being pumped into the process water circuit, which eventually discharges into the tailings impoundment. Water from the tailings pond is then conveyed to a new “Polishing Plant” facility which treats the water to applicable surface-water standards before being discharged. The water elevations in the Berkeley Pit and nearby compliance points have not increased since 2019, and as of August 2021, the total volume of the tailings pond continues to decrease, and approximately 4 billion gallons have been treated and discharged.

Golden Sunlight Mine, Barrick Gold Corp., Whitehall (Au, Ag)

Mining in the Mineral Hill Pit and the underground workings beneath the pit was suspended in November 2015 and April 2019, respectively. An underground expansion (“Apex”) to the north of Mineral Hill Pit was approved in 2018, but it was ultimately not constructed or developed. This also means that the milling and processing facility ceased operations and it no longer receives material brought in by third parties, which often originated from historic waste rock and tailings from across the area. The reclamation of rock disposal areas and other disturbances in the permit area has continued since production ceased (fig. 3), in addition to ongoing pit dewatering and other water management activities.

Following the Final EIS and Record of Decision in 2021, an amendment was approved for a tailings reprocessing project that would extend activity at Golden Sunlight by approximately 12 years. The proposed amendment application would allow GSM to excavate and reprocess tailings from the previously reclaimed Tailings Storage Facility-1 (TSF-1). This involves the construction of a repulping plant to resuspend the tailings in a slurry and then processing the tailings through a flotation system in the existing mill facilities. A fine gold

Figure 3. Various stages of reclamation and revegetation on the East Dump Complex at the Golden Sunlight Mine.

and sulfide concentrate would be produced, thus lowering the sulfide concentration (and potential reactivity) of the residual tailings that would be thickened and disposed as backfill in the Mineral Hill Pit. Tailings process solutions within the pit would be recycled to the mill circuit and groundwater would continue to be captured in the mine-working voids beneath the pit. The former TSF-1 footprint would be reclaimed to reflect pre-mining topography to support post-closure land uses for grazing, recreation, and wildlife habitat. The reprocessing of the tailings may also reduce the scale of long-term water treatment on site by eliminating discharge from TSF-1 and by reducing the flow and improving the quality of water pumped from the Mineral Hill Pit.

Stillwater Mine, Sibanye-Stillwater Ltd., Nye (Pt, Pd, Rh, Au, Cu, Ni)

Stillwater Mining Co. was acquired by Sibanye Gold Ltd. of South Africa in mid-2017, becoming Sibanye-Stillwater Ltd. Normal operations continued through 2021 at the Stillwater Mine near Nye. Capping of the Nye tailings storage facility is in progress. The facility is still used for water management, but all tailings are being disposed in the Hertzler Ranch tailings storage facility, which is about 5.5 mi northeast of the mine. The East Side Waste Rock Storage Area liner project has been completed through Stage 3 and will provide lined storage capacity for the next 12 to 15 months. Waste rock has been placed on liners since 2015 and Stage 4 of the project is scheduled for installation in summer 2022. A future amendment is anticipated to increase the crest height for the waste rock storage area and expand the capacity of the Hertzler tailings storage facility.

East Boulder Mine, Sibanye-Stillwater Ltd., McLeod (Pt, Pd, Rh, Au, Cu, Ni, Co)

Like the Stillwater Mine, the East Boulder Mine continued normal operations through 2021. Following the Final EA and Decision Document in 2021, an amendment was approved for the Stage 6 expansion of the tailings storage facility, which should provide storage capacity beyond 2030. A new amendment application is also currently under completeness review, which would authorize the construction of a new tailings storage facility ("Lewis Gulch") and a new waste rock storage area ("Dry Fork"). Both facilities would be constructed on liners, to manage any seepage through the waste materials. Following the application completeness review, DEQ and the United States Forest Service will conduct an environmental review for the new amendment and receive comments from the public and other stakeholders.

Troy Mine, Hecla Mining Co. (Cu, Ag) Closure

After acquiring the Troy Mine in 2015, Hecla Mining Co. (Hecla) continues to implement the reclamation plan by demolishing the mill and other surface structures, maintaining the pipeline to convey mine water to the impoundment, and by covering and vegetating other portions of the impoundment. An upcoming reclamation bond review will assess the eligibility for bond release for the areas that have been reclaimed.

Black Butte Copper Project, Sandfire Resources America Inc./Tintina Montana Inc. (Cu)

Following the Final EIS and Record of Decision in 2020, the final permit was issued for the Black Butte Copper Project, to the north of White Sulphur Springs. This underground mine project would develop the upper and lower Johnny Lee copper deposits through cut and fill methods to extract ore and backfill the completed stopes with cemented paste tailings. The surface facilities would include a lined impoundment that would contain cemented paste tailings and waste rock, storage ponds for process water and storm water collection, a water treatment plant, groundwater infiltration galleries for treated water discharge, a cement plant, and a mill facility with crushing and flotation capabilities. The development construction for the project was approved and bonded to occur in two phases. The first phase of construction took place in 2020 and 2021, although legal challenges to the project have not been resolved and a court ruling on motions for summary judgment is still pending (fig. 4).

Figure 4. Phase 1 construction of the Contact Water Pond facility at Black Butte Copper.

Yellowstone Mine, Magris Talc USA, Inc. (Talc)

In early 2021, the talc mine and mill facilities that were operated by Imerys Talc America, Inc. were transferred to a new permittee, Magris Talc USA, Inc. At the Yellowstone Mine south of Ennis, operations have continued under new management, with two phases of ore production within the South 40 Pit and the Phase 6 layback continuing to expose additional ore toward the north. Future mining phases will expand the pit toward the south and require the relocation of the onsite sorting facility. In September 2021, the final backfill and grading plan was authorized for the reclamation of the old North Main Pit by backfilling the pit with overburden, grading the area to promote runoff, and then placing soil and revegetating the disturbance.

Rock products, various companies

There are multiple operating permit applications and/or amendments that have recently been submitted to HRMS for rock product operations. These sites include Huppert Brothers Construction near Laurel, Glacier Stone Supply near Marion, and Montana Frontier Sandstone near Harlowton. More than 90 sites in northwest Montana were previously permitted for Southern Pine Plantations, LLC (formerly Plum Creek Timber Co. and Weyerhaeuser), but in 2021 a portion of those sites were transferred to Green Diamond Resource Co. and N5b Acquisitions, LLC (figs. 5, 6).

Figure 5. Angular rock products from a quarry near Harlowton, Montana Frontier Sandstone.

Figure 6. Shonkinite quarry near Fort Shaw, Shumaker Trucking and Excavating Contractors, Inc.

School of Mines at the College of Montana, Deer Lodge, 1888–1900

Anne Millbrooke

Historian, Bozeman, Montana

In January 1888 a School of Mines formally opened at the College of Montana in Deer Lodge. The first class of consisted of 12 students, including 1 from Michigan, another from the Dakota Territory, and 2 from Canada. Student Joseph T. Pardee was the son of the distinguished Philipsburg mining man J.K. Pardee, and student Albert Moog had been the first White child born in Silver Bow County. These young men were already studying mining engineering at the young college. This college had recruited a distinguished faculty from the best schools in the East. The School of Mines had no competition, as there was no other college, university, or mining school in the entire Montana Territory. In fact, the nearest competition for the new School of Mines were state mining programs at Golden City, Colorado, and Berkeley, California. The School of Mines operated successfully for several years, but the entire College of Montana struggled through hard times in the 1890s. In 1900 the College of Montana closed its doors. What happened? This is the story of the short-lived, yet significant, School of Mines (1888–1900) in the context of the College of Montana (1883–1916) and in the context of Montana transitioning from territory to state.

The lands of Montana came into the United States via the Louisiana Purchase of 1803 for lands east of the Continental Divide and via the Oregon Treaty of 1846 for lands west of the Continental Divide. Of course, there were Indigenous people here before those dates. Paleoindian remains from more than 10,000 years ago have been found at the Anzik archaeological site near the Crazy Mountains in central Montana, and many tribal peoples have occupied territory in what became the State of Montana: Arikara, Assiniboine, Bannock, Blackfoot (Niitsítapi), Chippewa, Cree, Crow (Absáalooke), Flathead, Gros Ventre (Aaniiih), Hidatsa, Kootenai, Little Shell Chippewa, Mandan, Northern Cheyenne, Pend d'Oreille, Salish, Shoshone, and Sioux. As the Louisiana Territory divided into smaller units, what became Montana bounced among territories. Eastern Montana was included in the Nebraska Territory that formed in 1854, then in Dakota Territory that formed in 1861, then in Idaho Territory that formed in 1863. Western Montana was part of the Oregon Territory that formed in 1848, then part of Washington Territory that formed in 1853, then part of Idaho Territory that formed 1863. Montana became a separate territory in 1864.

The Lewis and Clark Corps of Discovery had passed through Montana westbound in 1805 and eastbound the next year. Missionaries came. Fur traders came. But mining is what opened Montana to White settlement, with minor gold discoveries in the 1850s, then the Bannack boom in 1862, the gold rush to Alder Gulch in 1863, and subsequent strikes. Initially, the mining was placer for gold. That required low capital investment and thus eased entry for those seeking mineral wealth in the Mountain West. Merchants, farmers, and ranchers followed the miners, and the White population swelled. Alder Creek miners bought hydraulic mining to the territory. Silver mining began slowly and then, in the 1880s, boomed. Congress had passed the Bland–Allison Act in 1878 and thereby provided a silver subsidy in the form of government purchases of silver. Copper mining in Butte also boomed in the 1880s. Railroads arrived in the 1880s and provided transportation of ore to smelters and markets beyond the territory, and brought in equipment and supplies for the construction of mining infrastructure, notably smelters, within the territory. That was the context for establishing the first college and soon the first school of mines in Montana.

Montana Collegiate Institute

In January 1878, at the suggestion of Edwin H. Irvine, civic leaders of Deer Lodge decided it was time for Montana to have a college. Irvine had come to Montana in the early 1860s and engaged in mining and real estate. Colonel Lelander J. Sharp, an attorney, and William A. Clark, then of the banking house of Donnell, Clark & Larabie, liked Irvine's suggestion. These men acted immediately. They raised money and organized the Montana Collegiate Institute, the name suggested by Rev. M.N. Gilbert of the Episcopal Church. A preparatory

and transitional collegiate institute, rather than college *per se*, recognized the educational realities of the territory. The incorporators were Irvine, Sharp, Clark, and Philip E. Evans, John Y. Batterton, Charles P.H. Bielenberg, Hiram Knowles, James H. Mills, Thomas Stuart, and Howard H. Zenor. The board of directors elected officers: Irvine, president; Clark, vice-president; Stuart, secretary; and Zenor, treasurer. T.L. Napton, Colonel George W. Morse, and James H. Mills joined the board of directors later (New North-West, January 4, 1889; Edwards, 1907).

They acquired land for a campus. Acts of Congress and the Territorial Legislature had provided for townsites to be established through the preemption of public lands and recognition of existing private claims. An acre of land in each township could be set aside as a school site. A territorial act of 1869 finally addressed the needs for higher education by allowing planners to reserve up to 20 acres in a townsite for the future construction of a college or university. Communities platting townsites responded variously. Philipsburg had no unclaimed lands within its townsite, not even one acre for use as a school site; a local settler donated land for that town's school. Butte claimed a school site and reserved 20 acres for a college, but, rather than hold college land in trust until a college could be established, Butte sold the college land to raise funds for school construction. When formally platting the city of Deer Lodge in 1869, the community reserved and thereafter held 20 acres for a future college.

They recruited Clinton H. Moore, then principal of the Deer Lodge school, as president of the new institute. He had attended Kimball Union Academy and then Dartmouth College, both in New Hampshire, and he had been principal of the Lyndon Academy in Vermont before moving West for his health. Moore traveled East to buy equipment and hire staff. He employed Anna N. King of New Jersey to teach music and Grace Pike of Connecticut to teach languages. In Boston, he purchased "philosophical" apparatus, including a solar microscope, electrical machine, air pump, telescope, tellurian globe, and surveyor's implements. In Chicago, he purchased Henry L. Hay's architectural plans for a school building.

Construction was underway when the Prospectus of the Montana Collegiate Institute appeared in print that August. According to the prospectus, the Music Department offered instrument courses in piano, guitar, and organ, as well as voice lessons. There was a college preparatory course, a classical course of study leading to a diploma, and common English and business classes. The school year had three terms: a 15-week fall term, 14-week winter term, and 11-week spring term. Tuition for full-time students in either the preparatory or classical program was $18.75 each 10 weeks.

That fall the Montana Collegiate Institute opened in rented rooms. Three instructors—King, Moore, and Pike—taught a total of 32 students. Alas, the institute closed after that 1 year. Meanwhile, construction of the school building was completed. Made of locally quarried granite and bricks made in Helena, the building was made to house offices, classes, and laboratories. Irvine rented the new building and maintained a school there in 1879–1880. The staff consisted of Principal (Rev.) Wiley Mountjoy, and local teachers Fannie Hart in the literary department and Carrie Grimes in the music department. But debt from construction of the school building and a lack of funds for operations led to suspension of operations. Both the Collegiate Institute and Irvine's private school failed to thrive, or even survive. Nonetheless, the Montana Collegiate Institute created the first college campus, built the first college building, and inspired interest in higher education in Montana.

College of Montana

The vacant campus in Deer Lodge attracted the interest of the Presbytery of Montana, which transferred the assets and liabilities to a board of trustees in August 1882. The Territorial legislature the following March approved a college affiliated with the Presbyterian Church. The Presbyterian Church spread non-denominational Christian, Protestant education for both sexes in the West. It did so in part because a Christian education was necessary to prepare candidates for the ministry and missionary work and to prepare laymen and women for their services to the church. In the late 19th century the church had a College Board, and Boards of Home Missions, Foreign Missions, Sabbath-school Work, Church Erection, Ministerial Relief, Education (other than colleges and Sunday schools), and Freedmen. Synod by synod, the Presbyterians saw a need for Christian colleges. Princeton College, in New Jersey, was the pinnacle of Presbyterian education in the East, and Oberlin

College, in Ohio, was among the "Western Princetons." The states and territories west of the Mississippi River were of particular interest to the Board of Home Missions, and it was there that the church found a leader for the college to be established in Montana, Rev. Duncan James McMillan (fig. 1; Presbyterian Church, 1907).

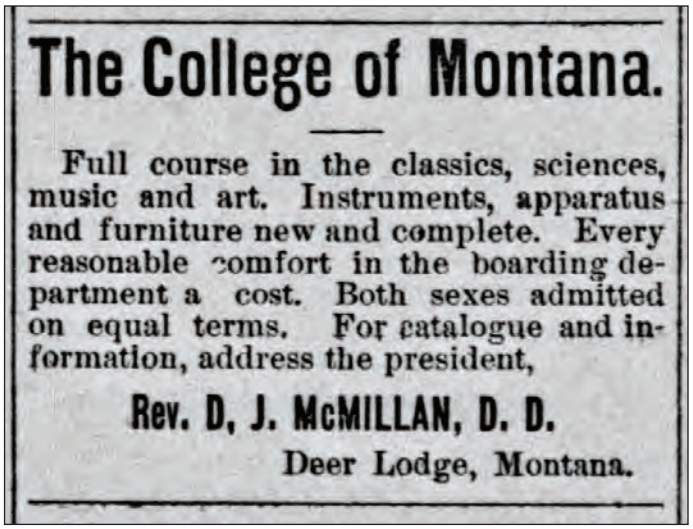
The College of Montana.

Full course in the classics, sciences, music and art. Instruments, apparatus and furniture new and complete. Every reasonable comfort in the boarding department a cost. Both sexes admitted on equal terms. For catalogue and information, address the president,

Rev. D, J. McMILLAN, D. D.
Deer Lodge, Montana.

Figure 1. Advertisement, 1883. This is the first advertisement that the College of Montana ran in newspapers in Montana Territory.

Born in Tennessee, McMillan was the fifth son of a minister. The family had moved to Illinois before the Civil War. Duncan was one of three McMillan boys who served in the Union Army, as did their father. McMillan was among the soldiers under the command of General William T. Sherman, who marched from Atlanta to the Atlantic Ocean. After the war McMillan attended Blackburn College in Carlinville, Illinois. The college became a university in name in 1869, the year before McMillan graduated. He received a both a Bachelor of Arts degree and Bachelor of Sacred Theology degree, and later a Master of Arts degree. He taught at a Presbyterian church in Illinois before his health prompted him to move west for the dry air of the Great Basin. Serving under the Board of Home Missions, he established schools in the Utah territory, for Protestants who lived among the Mormons, and his territory extended into what became Montana and Idaho. The Sanpete Valley was a center of his missionary work, and there in the community of Mount Pleasant he established the Wabash Academy in 1875. That same year he helped found the Salt Lake Collegiate Institute, a preparatory school that grew into Sheldon Jackson College in 1897 (and became Westminster College in 1902). In total, McMillan established over 30 mission schools, including 4 academies. To his credit, in the eyes of the church, Brigham Young denounced him as "an imp of perdition, a minion of Satan, a Presbyterian devil" (MacDougall, 1917). (Although many of the schools he founded in Utah closed in the early 20th century, the Wasatch Academy and Westminster College continue in operation.)

McMillan moved to Deer Lodge to take on the task of creating a Christian college there. He, J.K. Russel of Butte, and Eiko J. Groeneveld, also of Butte—all Presbyterian clergymen—constituted the first Board of Trustees of the planned college. They recruited to join them as incorporators of the college Samuel T. Hauser of Helena, a banker and business leader (soon to appointed governor of the territory); John F. Forbis, who had read law in the office of federal Judge Hiram Knowles and who had become a noted mining attorney; Ferd Kennett, whose home had been the site of weekly Presbyterian hymn singing in Philipsburg until a church was established there, and who was working at a bank in Helena at the time he became involved with the college (and who later became mayor of Missoula); and Rev. Dr. William A. Holliday, pastor of a Presbyterian Church in Brooklyn, New York, and thus in a position to aid with fundraising in the East.

The new College of Montana opened in September 1883 with about 30 students and 5 faculty. As was standard practice in Presbyterian education, both sexes were admitted on equal terms. There were four programs in which students could enroll: a 2-year preparatory course, a 3-year teacher training or "normal" course, a 4-year scientific course, or the traditional 4-year classical college course. College president Rev. McMillan taught ancient languages and the natural sciences. Arthur M. Mattoon taught mathematics and English, Nellie Hutchinson taught music, and Rev. Groeneveld taught German and natural sciences. Mrs. A.M. Mattoon worked in the preparatory department and served as matron. In all, 47 students studied at the college that first year. For the second year, the college added to the faculty Lillian Hudson to teach drawing and painting, and J.J. Robinson to teach Latin and vocal and instrumental music. M.A. Potter became the matron. That second year the college enrolled a total of 76 students. The college expanded again for its third year of operations. It added Kate Calvin, McMillan's wife, and James W. Rhodes to the music department, M.R. Patterson to the art department, and May Daken to the preparatory department. Eighty students enrolled that year. In the practice of the time, female faculty members had the title Miss or Mrs., or instructor, while male faculty were all professors.

A priority for the trustees was fundraising, first to eliminate the debt acquired with the assets from the collegiate institute, second to develop the college, and third to create an endowment. Trustee Rev. Holliday quickly proved useful. His wife was a daughter of wealthy businessman Alanson Trask, who had made his fortune in the shoe trade and who was a founder of the Equitable Life Assurance Society. Trask donated the money to retire the debt. In his honor, the college named its building Trask Hall. Fundraising continued and enabled the college to construct a power plant behind the college building, and then a dormitory building in 1885. The dormitory became the South or Gentlemen's Dorm in 1888 when the North or Ladies' Dorm was completed. The Ladies' Dorm included music classrooms and a gymnasium in the basement. Among the donors for these new buildings and an expanding faculty were Trask, W.H. Murray of Chicago, John A. Winslow of Poughkeepsie, New York, and Montana businessmen E.L. Bonner, S.E. Larabie, and Governor Hauser.

A.M. Mattoon, who had taught mathematics and English at the college since it opened in 1883 and whose wife had worked in the preparatory department, left Deer Lodge in 1886 for Bozeman, to become principal of the Presbyterian academy in Bozeman

In 1886, under McMillan's encouragement and fundraising, the College of Montana established a Department of Chemistry and Metallurgy and hired Chester F. Lee, a Princeton graduate, for the chair of chemistry and assaying. The college provided laboratory, furnaces, and everything necessary for that new department, in the basement of Trask Hall. Instruction in chemistry and metallurgy began that September. The plan was ambitious:

> "1. A condensed course in Assaying, requiring six hours per week for three months, in which will be taught assaying of gold, silver, lead and copper. This course will fit the student for the ordinary work of an assayer."
>
> "2. Special Course in Chemistry, Assaying and Mineralogy—requiring the student's exclusive time for one year. The year will be divided into two terms of five months each:
>
> 1st Term.—Qualitative Chemical Analysis, Mineralogy and Blowpiping.
>
> 2d Term.—Quantitative Analysis and Assaying in all its branches. This is a professional course, and is designed to prepare the student for all the work required of a Chemist and Assayer in the West."
>
> "3. The general course in Chemistry, Mineralogy, Assaying and kindred branches embraced in the Scientific Course as prescribed in the College Catalogue." (New North-West, August 20, 1886)

The department would also undertake assaying and chemical work for hire. Ten students, all male, completed the course in assaying that first year it was offered. Some sources date the founding of the School of Mines to this 1886 program, and some to the start of the fall term 1887 when the faculty were present (fig. 2). The school announced that the formal opening of the School of Mines occurred on January 5, 1888, when the required minimum of 10 students were enrolled and present for the new term; in fact, there were 12 students present (New North-West, January 27, 1888). Before that, developments were steps toward establishing a school of mines.

School of Mines

In 1888 the College of Montana opened its School of Mines with a faculty of 7 and an enrollment of 12 (fig. 3). The students were Samuel Clay Butcher of Spear Fish, Dakota; William Edward Coleman of Deer Lodge; Frederick Morse Ferrell of Charlotte, Michigan; John Fisher and William Fisher of Greenwood, Ontario, Canada; David Walker Hardenbrook of Deer Lodge; Robert Lee Kelley of Deer Lodge; Robert Alexander McArthur of Butte; Albert Moog of Stuart; Joseph Pardee of Philipsburg; Henry S. Reed of Deer Lodge; and William O'Neill of Deer Lodge (fig. 4). The college catalog for that year listed Reed and O'Neill as special students, meaning non-degree seeking.

McMillan was president of the School of Mines. Frank W. Traphagen, who had replaced Lee, was a native of Ohio. He had earned a doctorate from the Columbia School of Mines. He taught at the Staunton Military Academy in Virginia before moving to Deer Lodge to fill the position vacated by Chester Lee. Traphagen taught general and analytical chemistry, mineralogy, and physics. Augustus M. Ryon was born in New York City

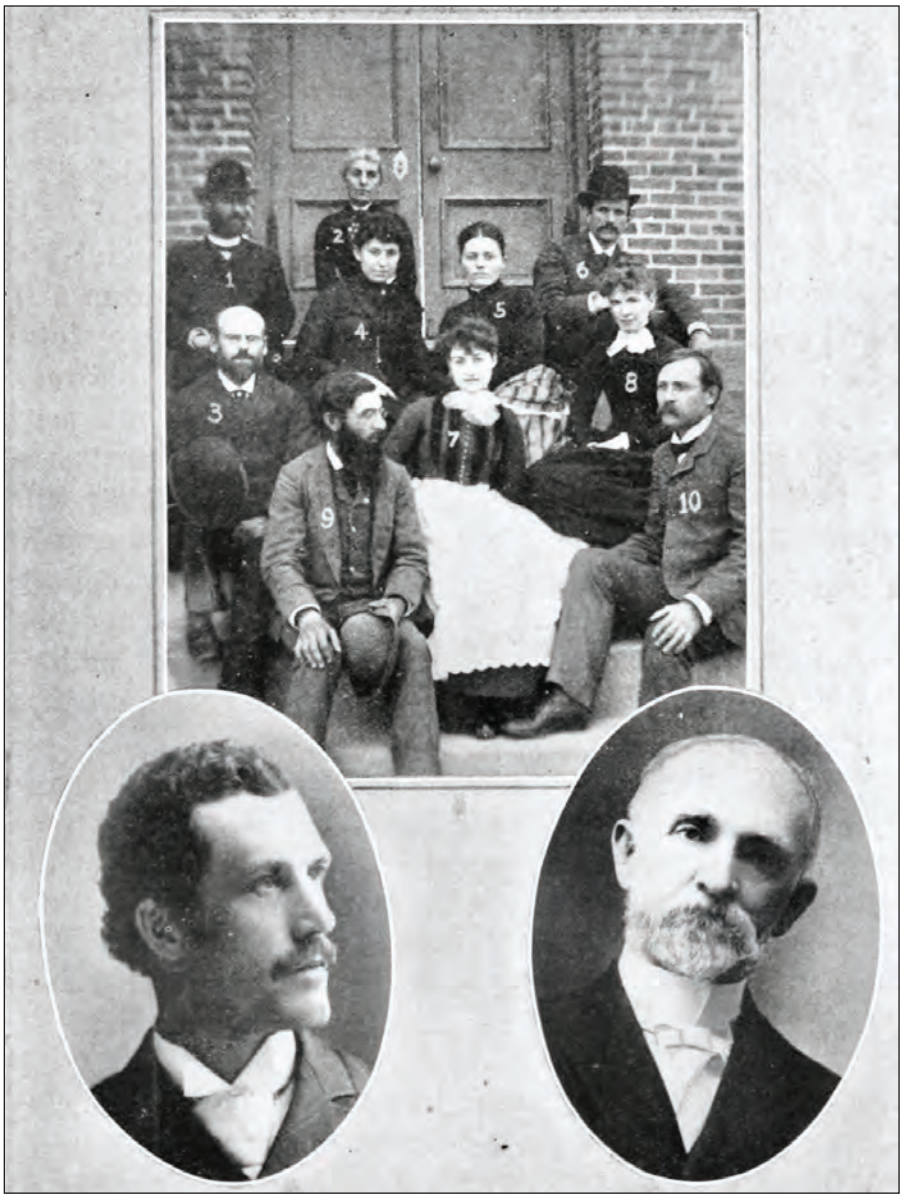

Figure 2. Mining Faculty, 1887. 1. Frank N. Notestein, 2. Mary B. Hill, 3. F.D. Kelsey, 4. Lizzie Woolfolk, 5. Lena Vaughn, 6. Theodore Brantly, 7. Lois Reat, 8. Kate Calvin, 9. Frank W. Traphagen, 10. Duncan J. McMillan, and overlay shows James Reid (left) and Albert B. Martin (right), two of the college presidents (Image from G. Edwards's article "Presbyterian Church History in Montana," in Contributions to the Historical Society of Montana, v. 6, 1907).

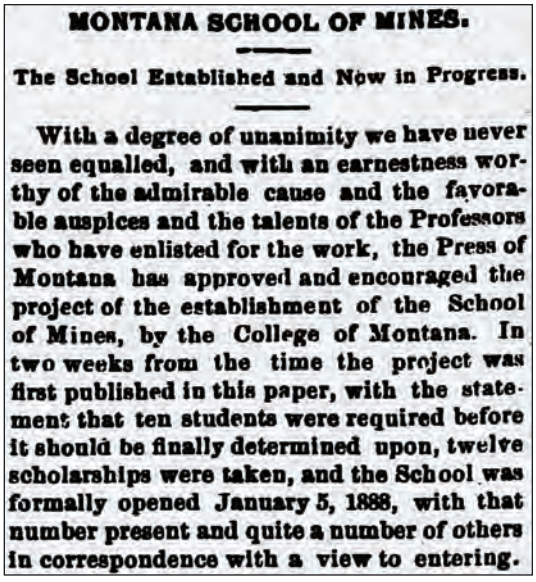

MONTANA SCHOOL OF MINES.

The School Established and Now in Progress.

With a degree of unanimity we have never seen equalled, and with an earnestness worthy of the admirable cause and the favorable auspices and the talents of the Professors who have enlisted for the work, the Press of Montana has approved and encouraged the project of the establishment of the School of Mines, by the College of Montana. In two weeks from the time the project was first published in this paper, with the statement that ten students were required before it should be finally determined upon, twelve scholarships were taken, and the School was formally opened January 5, 1888, with that number present and quite a number of others in correspondence with a view to entering.

Figure 3. Announcement, 1888. On January 5, 1888, the College of Montana opened its School of Mines. This excerpt from that announcement was printed in the local New North-West newspaper (January 27, 1888).

Figure 4. Faculty and second-year students in the School of Mines, 1889. Student Joseph T. Pardee is in the back, third from left. Professor Frank W. Traphagen is front right. Professor F.D. Kelsey is back, second head from right. (Photo 121, Pardee Family Papers, Mining Archives, Montana Bureau of Mines and Geology, Butte, Montana.)

and raised in New York and Connecticut. He completed a Bachelor of Science degree in Mining Engineering at Columbia. He worked as civil engineer for a few years before accepting a post at the College of Montana, where he taught civil and mining engineering and metallurgy. Frank N. Notstein taught mathematics, surveying, and astronomy. Theodore Brantly had graduated from Southwestern Presbyterian University in Clarksville and Cumberland University Law School in Lebanon, both in his home state of Tennessee. He taught mining law; he also taught Latin and Greek in the college. Lois A. Reat, taught drawing—until her marriage in 1891 to Brantly. Rev. Groeneveld taught German language, an important subject given the global influence of the Freiberg Mining School.

The School of Mines at the College of Montana reflected a national movement toward technical education in higher education (fig. 5). In the mid-19th century the leading institutions teaching mining, mining engineering, and metallurgy were in Europe, led by the German School of Mines at Freiberg in Saxony (established in 1766). A few Americans studied there each year; fewer studied at the French École des Mines in Paris (established in 1783) and even fewer at the British Royal School of Mines in London (established in 1851). American colleges began offering mining courses in the 1850s and granting mining degrees in the 1860s. The first separate School of Mines in this country opened at Columbia College in 1864. The success of the school, and the subsidies available as a result of the Morrill Land Grant College Act of 1862, spurred other colleges to establish mining schools: Massachusetts Institute of Technology in 1868, Lehigh University in 1870, Washington University in 1872, and University of Pennsylvania in 1874.

California and Colorado established western mining schools. California had established a mining program within a new Mining and Agricultural College in San Francisco in 1864. Mining was among the original courses of study when the new California State University began operations in Oakland in 1869, while university buildings were being constructed in Berkeley. The construction of the Colorado School of Mines had begun in 1869, as part of the denomination Jarvis Hall collegiate institute, established in Golden City by the Episcopal Church. The Territory of Colorado took over funding the School of Mines in 1870 and acquired the entire Episcopalian campus in 1874, by which time instruction had begun in mining, metallurgy, chemistry, civil engineering, and mechanical. The new Colorado School of Mines issued its first catalogue in 1874, which is often cited as the founding date. The first formal commencement was not until 1883. Despite a good building, well-equipped laboratories and classrooms, and faculty members who had trained at the mining schools of Europe, the Colorado School of Mines attracted few students in the 70s and 80s and, like the School of Mines in Deer Lodge, struggled through the hard times of the 1890s (Read, 1941).

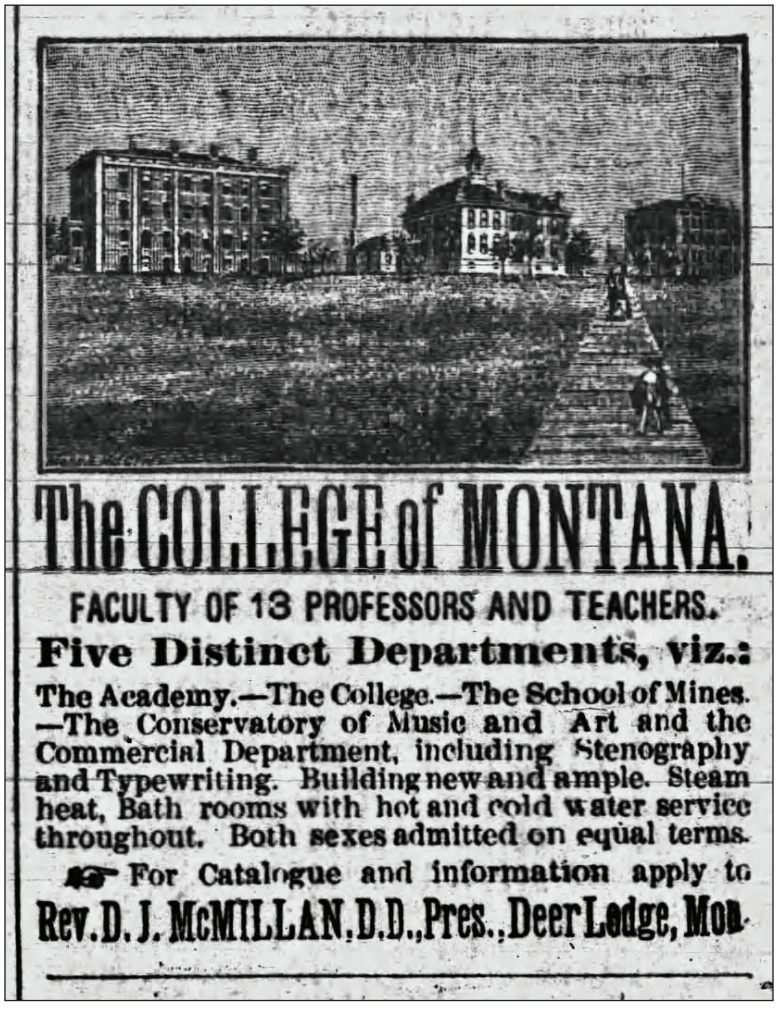

Figure 5. Advertisement, 1890. This advertisement includes the School of Mines that opened in 1888.

R.H. Richards (1887) of the Massachusetts Institute of Technology gave the presidential address at the 1886 meeting of the American Institute of Mining Engineers. He reported that there were only 15 schools in the United States that

offered a course of study in mining engineering. He defined engineer in general, "An engineer (Latin *ingenium*, signifying facility of invention, natural capacity) is a man who can efficiently utilize the materials of nature by means of the forces of nature." He explained that schools can teach in a short time what would require a much longer time to learn on the job. What mining schools need to do, he said, is combine theory and practice. That is done explicitly in the course of study outlined for the School of Mines established at Deer Lodge.

First-year mining students at the Montana School of Mines were required to take trigonometry, mensuration, analytical and descriptive geometry, general chemistry, qualitative analysis, mechanical drawing, and German language.

Seven of the first class students returned for the second year: Clay, the two Fishers, Hardenbrook, McArthur, Moog, and Pardee. Two students were in that year's freshman class: John Oliver Eaton of Brooklyn, New York, and George Robert Metlen of Red Rock, Idaho. Second-year students studied surveying, calculus, physics, crystallography, blowpiping, theoretical mineralogy, determinative mineralogy, zoology, botany, applied chemistry, mechanical drawing, and German. Both Traphagen and Ryon gave lectures on metallurgy. The topics covered during the second year included general principles, fuels, refractory materials, furnaces, iron, and steel. According to the college's Fifth Annual Catalogue for the Academic Year 1888–1889, Ryon also taught the practical course on drawing, covering for second-year students "grading, tinting, topographical drawing, conventional signs, perspective, shades and shadows, engineering construction drawing, machine construction drawing," as well as the preparation of bills of materials and strain sheets.

In addition to each year's prescribed courses for all mining students, there were summer assignments, including memoir writing, field work, and a senior thesis in mining engineering. As part of their general education, mining students were required to take at some point in their education U.S. history and general history, English grammar, composition, and rhetoric. French and Latin were optional. Students could also take electives. Pardee studied voice, which was taught by Nettie Birdsall. He also studied piano, taught by either Birdsall or Lizzie Woolfolk. This was not unusual. Three of his colleagues in the second-year class of the School of Mines also took vocal training (John Fisher, William Fisher, and Albert Moog), and both first-year mining students (John Eaton and George Metlen) took piano. Moog also played the violin. Music lessons meant sometimes performing in college concerts. Pardee and two other mining students also took the elocution course, taught by Miss Abbie Birdsall. Extracurricular activities were also popular. Pardee, for example, helped organize the Victor Lawn Tennis Club and served as its secretary. He helped prepare an ice skating rink, open to students and by fee to the public during hours not used by the students.

Third-year requirements included mechanics, engineering, properties of materials, practical mining, assaying, ore dressing, geology (the textbook was Joseph Le Conte's Elements of Geology: A Text-Book for Colleges and for the General Reader), chemical philosophy, chemical physics, mechanical drawing, and mining law. The fourth-year courses covered surveying, mechanical engineering, hydraulic engineering, kinematics of machinery, dynamics of machinery, mining engineering, qualitative analysis, mechanics and mill work, a project in metallurgy, mechanical drawing, and the senior thesis in mining engineering.

Of the first class of 12 students, 2 graduated in 1891: Robert McArthur and Al Moog. McArthur engaged in mining, homesteading, and ranching. Moog worked as a mining engineer, for a while affiliated with the Anaconda Copper Company. Joe Pardee transferred to the University of California in Berkeley for the last two years of his formal education. Walker Hardenbrook became a civil engineer; he caught typhoid while working on a job in Mexico and died in 1901.

At its peak, the College of Montana had five major projects. The Academy provided 2 years of preparatory studies. The College provided a 4-year course of classical studies. The School of Mines provided a 4-year scientific course of study and practice. The Conservatory provided customized instruction in art and music. The Commercial Department taught business courses, often in the evening.

Even in the decline that came in the hard times of the 1890s, the College of Montana supported its School of Mines. The School of Mines even shared the heading on the title page of the college catalog for 1894–1895. The college filled vacancies that opened in the program, and there was turnover in the mining faculty. H.M. Lane

taught mining and civil engineering in 1895–1896. In 1896 the college hired mining engineer E.H. MacDonald. A particularly prestigious recruit was William G. King, hired in 1898 as professor of chemistry and metallurgy. King had graduated from Western University in Cleveland, added a chemistry degree from Cooper Institute in New York, and did graduate work in chemistry at the Columbia School of Mines in New York. He taught chemistry at the Case School of Applied Sciences in Cleveland for 16 years. In Montana, in addition to teaching at the college in Deer Lodge, he worked as an assayer and chemist, including for the Parrot mine and Montana Ore Purchasing Company.

Decline in 1890s

The events of the 1890s conspired against the College of Montana. The frontier and open range closed. A global pandemic struck down at least one of the college students. Monetary policy shifted from bimetallism to the gold standard and closed the silver mines. The Panic of 1893 started a national depression that lasted for years. Departure of the founding president and fundraising difficulties forced a change in oversight of the college, and competition of various sorts arose. But the college and its School of Mines continued to provide strong instruction to students.

The Great Blizzards of 1886–1887 and 1887–1888, combined with White settlement, effectively closed the open range and thus reduced the great cattle herds of the West. The Oklahoma Land Rush of 1889 (and a lesser rush of 1893) were the last hurrah of the frontier. Conrad Kohrs, whose large ranch had relied upon the open range was based in Deer Lodge, served on the college's Board of Trustees The 1890 Federal Census reported a national population density of more than two people per square mile, although Montana had not yet reached that density. The historian Frederick Jackson Turner popularized the closing of the frontier with his 1893 thesis on the significance of the frontier in the nation's history. The nation was settled.

The Great Russian Flu Pandemic of 1890 came in three global waves between 1889 and 1894, with outbreaks of declining severity thereafter, and possibly as late as the flu resurgence in early 1900. Initially reported in the spring of 1889 in the Asian city of Bukhara, Russia (now in Uzbekistan), the disease spread rapidly as soon as it reached shipping and rail lines. In November 1889 the disease hit Moscow, Kiev, and Saint Petersburg. In December, Germany, France, and Great Britain, and even the United States, had cases.

By early January, influenza—also called catarrh or grippe—was epidemic in Montana. Choteau reported one-third of its residents sick with influenza. Cases flooded the railroad hospital in Missoula, 46 cases in 3 days, and many railroad workers in Billings were among the afflicted. Boulder closed its schools due to the number of students and teachers with influenza. "Never in the history of Bozeman has there been so much sickness at one time as at present," said one news account (Helena Independent, January 10, 1890). The fraternal Knights of Pythias in Anaconda reported a drain on funds due to nursing and funeral benefits paid during the pandemic. In Helena, influenza patients, some of whom acquired pneumonia as a complication, filled both St. John's and St. Peter's hospitals. The wife and son of former Governor Hauser were among the early stricken; both recovered. Also, the disease contributed to a lack of quorum that disrupted legislative sessions of both the Montana House and Senate.

The 1890 pandemic killed more than a million people out of a global population of approximately 1.5 billion. The one student death at the College of Montana that spring was attributed to a long bout of pneumonia; the school held a funeral service for the deceased student, Mabel Sedman of Virginia City (New North-West, Deer Lodge, April 11, 1890). Pneumonia was commonly listed as the immediate cause of death in influenza cases, though it was a complication of the flu. (Although the coronaviruses were not discovered until the 1930s, some scientists now suspect that the Russian flu of 1890 was a coronavirus with an animal, probably cow-, to-human zoonotic transmission; in fact, the neurological symptoms convinced some doctors at the time of pandemic, including some in Montana, that the disease was not influenza; Brüssow, 2021).

A shift in monetary policy was a leading cause of the economic disaster that struck Montana and the nation in 1893. Congress set early monetary policy in coinage acts. The Coinage Act of 1792 established the silver to gold exchange rate of 15:1 by weight of pure metal. The act of 1834 adjusted the exchange rate to 16:1. The act of 1853 debased silver by lowering the silver content of coins. Then the Coinage Act of 1873 abandoned bimet-

allism and stopped authorizing the use of silver dollars ("the Crime of '73"). Although the act did not outlaw silver coins, an economic depression followed. Over President Rutherford B. Hayes's veto, Congress passed the Bland–Allison Act of 1878 that arranged for government purchases of silver for minting silver dollars. The Sherman Silver Purchase Act of 1890 aided western silver mines, such as those in the Philipsburg and Deer Lodge areas. Under that act, the Treasury would buy 4.5 million ounces of silver a month at market rates, and pay via notes redeemable in either gold or silver. The silver mines and foreign countries sold their silver for gold, thus causing an outflow of gold from the Treasury. The mines of the West produced surplus silver, which deflated the price of silver, induced inflation, and continued to drain the nation's gold reserves. In an effort to halt both inflation and the drain of the gold reserves, Congress in special session finally repealed the Sherman Act in the fall of 1893, and the Bland–Allison Act was also repealed that year. But it was too late. Despite silver mines closing throughout the West, the gold reserves continued to fall. The nation entered a severe economic depression that lasted through a 1896 downturn. (Economical historians have described that Panic of 1893 as worse than the Great Depression of the 1930s.)

The mining West was hit particularly hard by the prolonged Panic of 1893. That dried up philanthropy from mining interests, just as the closing of the open range and the economic depression reduced donations from ranchers. Yet Montana remained a mining state, as late as 1895 producing more than four times as much mineral wealth as cattle shipments; farm products were the third largest economic resource. Widespread unemployment and inflation meant that few benefited from the wealth. The concentration of wealth in Butte among a few "copper kings"—William A. Clark, Marcus Daly, and F. Augustus Heinze—illustrates a nationwide problem at that time. This was the era of the "robber barons," of capitalists taking advantage of labor and public resources. Copper kings and robber barons, however, did make charitable contributions. Clark, a college trustee who also served as president of the board, made a generous donation to the college's Chemistry department in 1894, paid the college's entire deficit in 1896, and provided additional support thereafter (New North-West, October 12, 1894; Butte Miner, December 6, 1897).

Leadership changes affected fundraising and management. The College of Montana lost its founder when McMillan left in 1890, after 6 years as college president. He became the secretary of the Presbyterian Board of Home Missions. Competent replacements amid a nationwide economic depression were not as effective at fundraising as McMillan had been. James R. Reid became the college's second president and by default also the President of the School of Mines. Born in Canada, Reid was a naturalized citizen of the United States. He had studied at the University of Toronto, the Hamilton Collegiate Institute, and McGill University, where he earned his Bachelor's degree. He continued his studies at the Union Theological Seminary in New York and the Presbyterian College of Montreal, at the latter earning a master of divinity degree. He concluded his formal education at the University of Edinburgh in Scotland and with additional study at the Union Theological Seminary. He thus became a Presbyterian minister who presided over the College of Montana from 1890 to 1894. The trustees then recruited Rev. George F. Danforth from the East to preside over the college. He had been preaching in Hornellsville, New York. At the time, the local newspaper—always a college booster—noted that the College of Montana was a credit to Montana, in good financial shape, and well equipped for instruction in the classics, natural sciences, mining, engineering, chemistry, music, and art (New North-West, September 7, 1894; October 12, 1894). Danforth stayed one year, 1894-1895.

Rev. Dr. Albert B. Martin became the fourth president in 1895 and closed the school in 1900. Martin's parents were from Ireland. He was born in Pennsylvania. He came to Montana via positions in Kansas City, Fort Collins, and Central City and Black Hawk, Colorado. Martin remained as pastor of the Presbyterian Church in Deer Lodge for a couple of years and then moved to a church in Dillon. His friendship with W.A. Clark was beneficial for the college, which both men supported.

Amid the national depression, the Board of Home Missions of the Presbyterian Church decided to undertake no new work, and to suspend some work already in progress. That retrenchment affected Montana, where the Presbyterians had been the largest denomination. As of 1896, the Presbyterians had 33 churches in the state, but only 9 were self supporting, and other denominations were moving in where once Presbyterian missions would have served the growing population. Also, the Presbyterians had over 50 colleges and academies in the states

and territories. There just was not enough money to support all existing programs. Given the financial straits among the mines and large ranching operations around Deer Lodge, the Presbytery of Butte and the trustees of the College of Montana in September 1896 transferred oversight of the college to the Synod of Montana, away from local control.

Competition came from another college established in Montana, new mining programs throughout the West, the state institutions of higher education established in the new state of Montana, and even from county splitting. First, the College of Montana was no longer the only collegiate option available in Montana. Led by William Wesley "Brother Van" Van Orsdel, the Methodist Church approved a college in 1889 and laid the cornerstone for Montana Wesleyan College in the Prickly Pear Valley outside Helena in 1889; the college moved into Helena in 1899. The Butte Business College, established in 1890, proved popular with courses in shorthand, typewriting, bookkeeping, commerce, even commercial courses for miners, and general education courses (it remained in operation into 1975). The Helena Business College, established in 1883, and the younger Commercial College in Great Falls, established in 1894, had little impact on recruiting students for the College of Montana in Deer Lodge.

Other states and territories established colleges, courses in mining subjects, and schools of mines. The University of North Dakota opened in 1884 and added a School of Mines in 1891. South Dakota authorized construction of a School of Mines in 1885, completed the building in 1886, and opened in 1887. The University of Nevada moved to Reno in 1885, and there the next year it offered mining courses in a School of Mines. Founded in 1886, the University of Wyoming had a professor of geology who soon added mining courses, and the school hired a full-time mining professor in 1897. Established in 1889, the University of Idaho in 1893 added courses in mining and metallurgy and within a few years offered a degree in mining engineering. When the University of Arizona opened in 1891, it offered mining courses, but the School of Mines remained small through the decade. Washington State College at Pullman offered courses from the early 1890s onward, and the Oregon State Agricultural College at Corvallis announced a School of Mines in its 1899–1900 catalog. The University of Deseret in Salt Lake City awarded a few mining degrees in the 1890s. Statehood in 1896 enabled Utah to plan for a system of higher education, and in 1901 the legislature passed an act establishing a School of Mines that was fully organized and operational within the University of Utah by 1905 (Read, 1941).

The most serious competition for the College of Montana came from state colleges established in the 1890s, in particular the Montana Agricultural College established in 1893 and opened in that year in Bozeman, and the Montana State School of Mines, established in 1895 and opened in 1900 in Butte. Montana State College was established in 1893 and opened in 1895 in Missoula. Each state college received an endowment of tens of thousands of acres of land. Colleges and other state institutions went to communities as consolation prizes or "spoils of statehood," heavily influenced by the state capital selection process. In the state prison, Deer Lodge got a consolation prize rather than a spoil of statehood. It probably had not helped that during the campaign for the capital site, a proponent of Deer Lodge had said that "Helena is dying; she has sent for the priest," and then made a racial slur against that city (Anaconda Standard, November 2, 1894).

Under the congressional act of February 18, 1881, Congress granted 46,000 acres (72 sections) to Montana as an endowment for a state university. Once Montana achieved statehood in 1889, that university became a priority. But the location of state institutions became tokens promised in exchange for votes in the selection of a state capital site. The territorial capital had been at Bannack in 1864–1865, Virginia City in 1865–1875, and Helena since 1875. Montana became a state in 1889. Great Falls, Boulder, Bozeman, Butte, and Deer Lodge placed bids to become the state capital and lost in the end as the competition came down to Helena and Anaconda. Prominent in what became a fight for the state capital were the "copper kings." Supporting Helena, William Clark was currying favor for his U.S. Senate bid. Supporting Anaconda, Marcus Daly was promoting his smelter town. By vote in a hotly contested election in 1894, with claims of fraud before and after voting, Montana established Helena as its state capital.

Helena became the capital, and Missoula, Bozeman, and Butte got the main institutions of higher education, Dillon got the teacher's college, Miles City got the reform school, Twin Bridges got the state orphanage, Boulder got the state hospital, and Columbia Falls got the veterans home. Deer Lodge got the state prison. That

ended the dream for the College of Montana to became the foundation for the state system of higher education. Earlier the College had failed in its efforts to get legislative designation required to qualify for a federally funded agricultural research station. Now it failed to become the foundation, or even a part, of the state system of higher education.

The establishment of the state college system became a drain from the private college, drawing students, faculty, and donations away from Deer Lodge. The state draw also reached the board level. Instead of following his father on the board of trustees of the College of Montana, W.A. Clark, Jr., joined the board of the state School of Mines.

The new state institutions poached faculty from the College of Montana. After 5 years teaching in Deer Lodge, Traphagen left to teach the natural sciences at the new state Agricultural College in Bozeman, where he laid the scientific basis for what became Montana's sugar beet industry. Ryon, Professor of Engineering and Metallurgy, left to become the first president of that state college in Bozeman (1893–1894). Reid, who had become president of the College of Montana and of its School of Mines, followed Ryon to Bozeman and became the second president of that agricultural college (1894–1904). Even Army Lieutenant G.P. Ahern, of the 25th Infantry, who taught military science and tactics at the College of Montana, moved to Bozeman in 1897 to teach military courses there. The state School of Mines opened in 1900 with William G. King as its Professor of Chemistry and Metallurgy; he went to Butte directly from the college in Deer Lodge. Some faculty recruited by the College of Montana faculty went indirectly to state faculty jobs. MacDonald, for example, became Anaconda's city engineer between employment at the College of Montana and the Montana State School of Mines.

County splitting brought another form of competition as each new county focused on its own development and the college's "local," as in county, base shrank. When Montana became a territory in 1864, Deer Lodge County was one of the territory's original nine counties, and it encompassed the towns of Deer Lodge, Anaconda, Philipsburg, Butte, and the county seat of Silver Bow City. The next year the county seat moved to the town of Deer Lodge. Silver Bow County separated from Deer Lodge County in 1881 and established its county seat at Butte. Granite County split away in 1893 and chose Philipsburg as its seat. Deer Lodge County's seat moved to Anaconda in 1896, but the town of Deer Lodge became a county seat again in 1901 when Powell County left Deer Lodge County; Anaconda remained the county seat of Deer Lodge County and the town of Deer Lodge became the county seat of Powell County. This county splitting reflected the population growth of the area and meant less travel to and from government offices. With statehood in 1889, county splitting also increased local political influence because the state legislature was apportioned one senator per county.

As if the 1890s were not hard enough on the college, in June 1900 a hail storm hit the campus and broke 226 window panes.

Revived College and Mergers

Montana College opened in 1904, albeit not with a full college curriculum. Rather it was a "department school." It offered both high-school-level and college-level courses arranged by department, rather than arranged by grade, in order to meet the needs of each individual student. According to its catalog, the school offered academic classes to prepare a student to enter any college or university. It also offered courses of study to prepare a student to enter professional life without taking the time necessary for a college degree, such as normal courses to prepare students in 2 to 4 years to be teachers, a 3-year course in manual arts, an option to take electrical engineering in lieu of the third year of manual arts, a 2- or 3-year domestic science program to prepare females as homemakers, 1-year and 2-year options in business, and a 1-year course in oratory. In 1905 it added a practical course in assaying and a College of Music. (The name Montana College may have been chosen to reflect the new approach or to avoid confusion with what was then called the Agricultural College of Montana, which was the state college in Bozeman.)

L.T. Eaton was a professor and the president of the school. It published a 4-year curriculum. Eaton had been a county superintendent of schools in Iowa and then taught at the High Park College normal school in Des Moines, Iowa. Conrad Kohrs was president of the board of trustees, and S.E. Larabie, who had originally joined

the College of Montana board in the 80s, was a member of the new board.

The school was again operating as the College of Montana in 1906, under the continued leadership of Eaton (fig. 6). “The school that was dead is alive again,” proclaimed a college catalog. A few familiar names were among the college trustees, including S.E. Larabie of Deer Lodge, Theodore Brantly of Helena, and Rev. E.J. Groeneveld of Butte. Eaton proved successful in getting in pledges of money, so successful that he was lured away in 1908. He moved to Billings to organize a new school there, the Billings Polytechnic College. Rev. H.A. Fancher then became president of the College of Montana. He had been educated at the Union College and Auburn Seminary out East, and he had preached at Batavia, New York, for over a decade. The faculty of seven taught mathematics and engineering, Latin and history, English, science, Greek and German, commercial branches, piano, and pipe organ. L.E. Boner taught the engineering classes, but it was electrical engineering rather than mining engineering. Fern Renick, the science professor, and Helen Waugh, the English professor, had doctoral degrees.

There were other successes. There were over 130 students in 1908–1909, mostly Montana young people, also 3 from Nevada, 3 from Idaho, 1 from Canada, and 1 from Japan. Nine students graduated that spring. In an example from December 1913, the college dedicated a new gymnasium, with a swimming pool in the basement. But financial stability escaped the college.

In 1913 Great Falls businessmen explored the possibility of the College of Montana moving from Deer Lodge to Great Falls. That city had long expressed an interest in a university. In the late 1880s a Great Falls newspaper claimed that Great Falls was the most appropriate place in Montana for a university teaching mining, agriculture, and stock raising. When the College of Montana opened its School of Mines, the same newspaper said that the private school should be encouraged and that the future state of Montana should found its mining university at Great Falls. The trustees of the College of Montana considered the 1913 proposal to move the school. They decided instead to raise the endowment. That fundraising effort failed.

Fancher left in 1915 for a finance job at Whitman College in Washington. The history professor, Earl C. Parker, filled in until a new president could be hired. That new president was W.H. Hannum, just back from 30 years of missionary work in India. The financial pressures remained. Two students received degrees at the com-

Figure 6. Photo of the College of Montana, circa 1907. Completed in 1888, North Hall (on the left) had college parlors and music rooms on the first floors and rooms for 40 female students on the second and third floors. Built in 1878, Trask Hall was the original college building, and it had the offices, assembly hall, recitation rooms, and in the basement laboratories. The heating and lighting plant was the second building built on the campus. Opened in 1885, South Hall (on the right) had recitation rooms on the first floor and rooms for forty male students on the second and third floors. Dormitory basements were used for meetings, dining, and gymnasium. (Image is from G. Edwards, 1907, Presbyterian Church History in Montana, in Contributions to the Historical Society of Montana, v. 6.)

mencement in May 1916, and four received academic diplomas. Hannum then retired. He and his wife left for his hometown in Ohio. At the time Rev. Groeneveld, who had helped organize the college in 1883, was president of the board of trustees. When the college closed at the end of the spring term, the trustees still expressed optimism. But the college never reopened.

The Deer Lodge School District Number One bought the campus. It had the dormitory buildings dismantled in the 20s and 30s. Meanwhile, in 1923, the college trustees merged the College of Montana with Montana Wesleyan College in Helena. That merger created Intermountain Union College, based in Helena. An earthquake destroyed the Helena campus in 1935. Classes were temporarily held in Great Falls, but, rather than rebuild, the college moved to Billings, to space available on the campus of the Billings Polytechnic Institute. The two Billings institutions merged in 1947 and became Rocky Mountain College. Back in Deer Lodge, the school district had administrative offices in Trask Hall until 1979. Now Trask Hall and the modified gymnasium building of the long-gone College of Montana remain on College Hill, off College Street, in Deer Lodge (fig. 7).

Figure 7. Trask Hall, 2021.The first college building constructed in Montana is now an empty shell on College Hill, Deer Lodge, Montana. The building is listed on the National Register of Historic Places. (Photo by Anne Millbrooke.)

Conclusion

The short span of the School of Mines at Deer Lodge was actually not unusual; for example, Harvard had a short-lived School of Practical Mining and Geology in 1869–1874. While schools in the Mountain West generally struggled through the 1890s, enrollment in the mining college at the University of California in Berkeley boomed that decade. Pardee finished his studies as a special student there in 1891; there was not yet a system of transferring credits between universities so a degree would have required starting over as a freshman. Pardee then began his career as an assayer and miner. That was before he switched careers to geology.

The direct legacies of the College of Montana and its School of Mines were the example and the people. The college showed there was a need and it could be met in Montana. The people—both the faculty and the students—had productive lives after the college in Deer Lodge, Montana. Mining engineer Al Moog, federal geologist Joe Pardee, metallurgy professor W.G. King, college president J.R. Reid, and Montana chief justice Theodore Brantly are examples of individuals who went successfully from the College of Montana and its School of Mines into the world at large.

References

Brüssow, H., 2021, What we can learn from the dynamics of the 1889 ‘Russian flu’ pandemic for the future trajectory of COVID-19: Microbial Biotechnology, available at https://pubmed.ncbi.nlm.nih.gov/34464023/ [Accessed June 2021].

College of Montana, 1883–1908, Catalogues for first (1883-84), fourth (1886–87), fifth (1999–89) and sixth (1889–90) academic years, and for Montana College, 1905–06, and College of Montana, 1908-09, William K. Kohrs Memorial Library, Deer Lodge.

Edwards, G., 1907, Presbyterian church history in Montana: Contributions to the Historical Society of Montana v. 7, p. 290–444, and therein anonymous: The College of Montana, p. 384–388, https://catalog.hathitrust.org/Record/008696751?type%5B%5D=all&lookfor%5B%5D=008696751&ft=ft [Accessed June 2021].

MacDougall, D., ed., 1917, Scots and Scots' descendants in America, v. 1: New York: Caledonian Publishing Company, https://archive.org/details/scotsscotsdescen00macd/ [Accessed May 2021].

Newspapers printed in Deer Lodge, Anaconda, Butte, Bozeman, Great Falls, Helena, and Missoula, available at https://chroniclingamerica.loc.gov/ and https://www.newspapers.com/.

New North-west, 1889, The College of Montana, a glimpse of its history and an invocation for its future: January 4, 1889, p. 2, available at https://newspapers.com/image/171728008/ [Accessed April 2021].

Presbyterian Church in the U.S.A., College Board, 1907, Our Presbyterian colleges. Philadelphia: McCalla & Company for Presbyterian Church in the U.S.A., p. 108–109, available at https://www.google.com/books/edition/Our_Presbyterian_Colleges/2oVPAAAAYAAJ?hl/ [Accessed April 2021].

Read, T.T., 1941, The Development of mineral industry education in the United States: New York: American Institute of Mining and Metallurgical Engineers, available at https://archive.org/details/developmentofmin-00read/page/6/mode/2up/ [Accessed April 2021].

Richards, R.H., 1887, American mining schools: Transactions of the American Institute of Mining Engineers, v. 15, p. 309–340.

Anne Millbrooke (center) at the field trip to Elkhorn Ghost Town. Photo by Peter Larson.

Once Upon a Time in the West—There Was Federal Support for Mineral Exploration

Patrick Dawson

Author and Prospector, Billings, Montana

This paper contrasts the lack of government assistance for exploration and mining in the U.S. with the active programs of Canada and Australia.

For many prospectors and small miners in Montana, the 1950s and 1960s were a busy time. Their activity was encouraged—and, in some cases, aided—by the Department of Interior's experimental mission to assist prospectors and miners with mineral exploration and development (Chicago Tribune, 1953).

Initially inspired by the World War II urgency to find strategic and critical materials and uranium to help power the new Atomic Age and supply other military applications, the Defense Minerals Administration (DMA) was launched under the authority of the Defense Production Act (1950). Certain minerals, including asbestos, uranium, industrial diamonds, platinum group metals (PGMs), and iron ore were eligible for up to 90% federal participation. Gold and silver were not in the mix (USGS, 2016a).

DMA was joined in 1951 by the Defense Minerals Exploration Administration (DMEA), which focused on metals and mineral concentrates in short supply. For example, the DMEA in 1951 paid 75% of the $26,000 project cost to mining engineer Wade Lewis (fig. 1) to develop the new Free Enterprise uranium mine near Boulder, MT. Before that, Lewis leased the Elkhorn Mine (fig. 2) in the late 1940s and the ore he mined and shipped—with no subsidies—equaled about the same revenue he received later from the government for the Free Enterprise (just a coincidence).

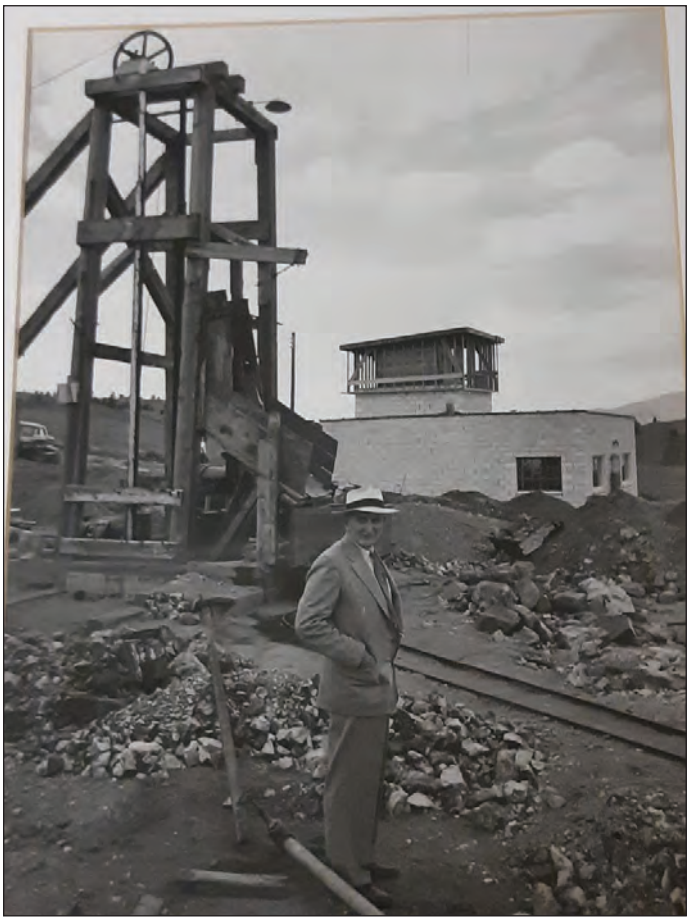

Figure 1. Mining engineer Wade Lewis, who discovered the uranium ore and developed the Free Enterprise Mine near Boulder, Montana.

In 1958, the Office of Minerals Exploration (OME) replaced and extended those programs to stimulate exploration for vital mineral raw materials. This time around, gold and silver were included. But, in order to be considered, applicants had to demonstrate their financial need by showing two letters from banks denying them loans for their mining projects.

This worked fine for underfunded prospectors, but left out the larger mining enterprises that were too flush with assets to meet the criteria. Under the previous regimen, several large operators had received assistance for their projects. As the U.S. Geological Survey history explains, "Another change restricted governmental participation in an OME exploration contract to $250,000, which eliminated large and expensive exploration projects, some of which had been notably successful under the DMEA program" (USGS, 2016a). That new rule, said William G. Mahoney of Butte of the Montana Mining Association, would require prospectors to sign a pauper's oath to get exploration funds (Daily Missoulian, 1958).

At the June 1958 Senate Interior subcommittee hearing considering extension of the program, mining industry spokesmen urged its preservation, and Interior Secretary Fred A. Seaton testified that federal mining

Figure 2. The Elkhorn Mine mill building circa 1950s (Credit: Elkhorn Mining Company).

assistance should be continued and expanded. “The greatest problems faced by the domestic mining industry today,” Seaton stated, “are the depletion of its easily accessible high-grade reserves, the substantially increased costs that go with the mining of low-grade ores, and the difficulties encountered in the search for and mining of more deeply buried ore deposits. Limited known world reserves, the strategic nature of these minerals and the heavy dependence of the Unites States on distant overseas sources for supplies underscore the desirability of making every effort to develop and maintain some production of these commodities from domestic sources.” The extension bill, sponsored by Montana Senator James E. Murray, quickly passed the House and Senate and was signed by President Dwight D. Eisenhower (Daily Missoulian, 1958).

For aspiring Montana prospectors and miners, the programs were hardly a free ride on a government gravy train. The U.S. Bureau of Mines and USGS field geologist examiners and auditors were diligent and rigorous in their scrutiny of applications and in their follow-up reviews. During the two decades of the programs, only 49 of 370 applicants in Montana made it to the first cut of funding (USGS, 2016a).

The OME program was active until 1974, when Congressional appropriations ended for all but administrative functions. The program was officially terminated in 1993. There has been no federal assistance for prospectors in Montana since 1969.

Meanwhile, in Canada, national, provincial, and territorial government assistance to prospectors and mining companies continues to this day. From Newfoundland and Labrador to the Yukon, grants and tax incentives are made annually to encourage mineral exploration and development (Natural Resources Canada, 2019).

According to a report by the Prospectors and Developers Association of Canada, for example, Newfoundland offers prospecting grants on Crown lands up to $6,000 (all amounts referring to Canada are in Canadian dollars) for traditional and grassroots prospecting, plus up to $6,000 for prospects to remote areas only accessible by helicopter or float plane (PDAC, 2019). Nova Scotia offers prospecting and exploration grants up to $20,000 to support early stage grassroots prospecting (PDAC, 2019).

New Brunswick’s Junior Mining Assistance Program provides up to 50% of project costs to a maximum of $100,000 per project, per year, to companies with no self-sustaining cash flow. The province’s Prospector Assistance Program funds prospectors with existing claims up to $15,000 (PDAC, 2019).

Quebec has established a fund capitalized at $1.2 billion to invest in mining and other non-renewable resources (PDAC, 2019).

Ontario offers prospector grants up to $85,000 to qualified prospectors with properties with high economic potential (PDAC, 2019).

To encourage exploration projects in remote areas, Manitoba offers a maximum of $200,000 per recipient per fiscal year (PDAC, 2019).

Saskatchewan's Targeted Mineral Exploration Incentive offers eligible explorers up to $50,000 per year to drill for base metals, precious metals, or diamonds in a defined geographic region (PDAC, 2019).

Northwest Territories incentivizes grassroots prospecting for hard rock and placer mining, and has a small miner program of $1 million to help small prospectors and corporate explorers. Designed to spur hard rock mining exploration activity at a time when investment in the sector languished, the 2020 incentives marked the sixth year in which the territorial government's Department of Industry, Tourism and Investment has handed out monetary assistance to members of the mining industry. From 2014 to 2018, the NWT Mining Incentives Program has invested roughly $3 million in NWT mineral exploration projects, which resulted in nearly $15 million in total spending from funded projects (North of 60 Mining News, 2021).

Yukon Territory also incentivizes grassroots prospecting for hard rock and placer mining. The Yukon Mineral Exploration Program provided for qualified prospectors to apply for up to $15,000 per year to cover basic operating expenses while searching for new mineral occurrences (PDAC, 2019).

Australia's aggressive support of its prospectors and miners (Reuters Commodities, 2017) coincides with its 2021 surpassing of China in gold production. China, also the biggest gold importer, had been the world's leading producer of gold since 2007, when it surpassed South Africa (Kitco News, 2021).

The Minerals Council of Australia issued a 2018 report that concluded, "The Federal Government's commitment to retaining an exploration incentive for junior explorers undertaking greenfields exploration through the Junior Minerals Exploration Incentive (JMEI) will help ensure that junior explorers without taxable income can claim exploration deductions and also stimulate greater exploration investment" (Investing News Network Australia, 2018).

In 2021, the JMEI announced it will contribute $100 million (Australian dollars) to extend the program four more years (Australian Taxation Office, 2021).

The government's Geoscience Australia states that it "aims to facilitate increased exploration expenditure in Australia by promoting both the benefits of exploring in Australia and the geoscience information available to reduce exploration risk." The agency goes on to explain that "Government funding, information and tools are available to help companies progress major critical minerals projects in Australia. We aim to grow Australia's emerging critical minerals sector by supporting innovation, attracting investment and exporting to new markets" (Minerals Council of Australia, 2019).

The U.S. is a net importer of strategic minerals and rare earth elements. Most of the metals-mining operations in the U.S. are owned by multinational corporations. Montana's PGM Stillwater-Sibanye for example, is a South African company.

Of the top gold-producing operations in the U.S., 64% are foreign (USGS, 2016b), and 83% of uranium mining or exploration companies in the U.S. are foreign-owned (World Nuclear Association, 2019; U.S. Energy Information Administration, 2019).

The U.S. government has recently awakened to the stark challenges of global competition for precious, strategic, and critical metals and rare earth elements. While Australia and Canada value the efforts of its grassroots explorers, the U.S. government has not offered assistance or incentives to small miners and prospectors for 50 years.

The new USGS Earth-Mapping Resources Initiative (E-MRI) program aspires to help mitigate future U.S. reliance on imports. Its data-gathering efforts should help, but federal aid to domestic, small, private miner exploration is, once again, glaringly obvious by its absence.

Interior Secretary Seaton's pronouncement in 1958 on the dire need for new U.S. mineral discoveries rings just as true today as it did back then, and poses a logical question: Do we need a 21st Century version of the Defense Production Act of 1950 that revives assistance to grassroots exploration?

References

Australian Taxation Office, 2021, Australia Junior Minerals Exploration Incentive, available at https://www.ato.gov.au/General/New-legislation/In-detail/Direct-taxes/Income-tax-for-businesses/Junior-minerals-exploration-incentive/ [Accessed February 2022].

Chicago Tribune, 1953, Interior Dept. U.S. giant with myriad duties, March 7, 1953, p. 5.

Daily Missoulian, 1958, Mineral exploration program included in Senate measure, June 10, 1958, p. 10.

Defense Production Act, 1950, Public laws–CHS, September 8, 1950, available at https://fraser.stlouisfed.org/title/defense-production-act-1950-6114/fulltext [Accessed February 2022].

Investing News Network Australia, 2018, Mining in Australia: Incentives and initiatives, July 29, 2018, available at https://investingnews.com.au/mining-in-australia-incentives [Accessed February 2022].

Kitco News, 2021, Australia usurping China to become world's top gold producer, August 30, 2021, available at https://www.kitco.com/news/2021-08-30/Australia-usurping-China-to-becomes-world-s-top-gold-producer-Surbiton-Associates.html [Accessed February 2022].

Minerals Council of Australia, 2021, Government investment in mining exploration will boost regions and create jobs, May 5, 2021, available at https://www.minerals.org.au/news/government-investment-mining-exploration-will-boost-regions-and-create-jobs [Accessed February 2022].

Mining Association of Canada, 2019, Canadian mining facts 2019: The state of Canada's mining industry, available at https://mining.ca/resources/reports/facts-and-figures-2019/ [Accessed February 2022].

Natural Resources Canada, 2019, Mineral exploration tax credit—Natural Resources Canada 2019, available at https://www.nrcan.gc.ca/science-and-data/21444 [Accessed February 2022].

North of 60 Mining News, 2021, Government offers more mining incentives—(Yukon Territory) January 1, 2021, available at https://www.miningnewsnorth.com/story/2021/01/01/news/government-offers-more-mining-incentives/6585.html [Accessed February 2022].

Prospectors & Developers Association of Canada (PDAC), 2019, 2019 Financial incentives for mineral exploration and prospecting in Canada, available at https://www.pdac.ca/docs/default-source/priorities/access-to-capital/flow-through-shares/compilation-of-financial-incentives-for-mineral-exploration-in-canada-may-2019.pdf [Accessed February 2022].

Reuters Commodities, 2017, Australia's new gold rush lures prospectors down under, November 29, 2017, available at https://www.reuters.com/article/us-australia-gold-kirklandlake/australias-new-gold-rush-lures-prospectors-down-under-idUSKBN1DU04F [Accessed February 2022].

U.S. Energy Information Administration, 2019, 2018 Domestic uranium production report, Washington DC, available at https://www.eia.gov/uranium/production/annual/archive/dupr2018.pdf [Accessed February 2022].

U.S. Geological Survey, 2016a, U.S. Geological Survey Data Series 1004: Historical files from Federal Government mineral exploration-assistance programs, available at https://pubs.usgs.gov/ds/1004/ds1004_ome.htm [Accessed February 2022].

U.S. Geological Survey, 2016b, Minerals Yearbook: Gold, p. 73, available at https://s3-us-west-2.amazonaws.com/prd-wret/assets/palladium/production/mineral-pubs/mcs/mcs2016.pdf [Accessed February 2022].

World Nuclear Association, 2019, U.S. Uranium Mining and Exploration, June 2019, available at https://world-nuclear.org/information-library/country-profiles/countries-t-z/us-uranium-mining.aspx [Accessed February 2022].

Deep Sediment-Hosted Porphyry Copper Deposits with Critical Mineral Potential and the Geochemical Relationship of Orbicular Actinolite Alteration to District Zoning and Oxidation by Carbonate Dissolution CO_2 Release

George H. Brimhall

Clementine Exploration LLC, Wise River MT and

Earth and Planetary Science, Emeritus Professor of Geology

University of California, Berkeley

Abstract

Deep syntectonic sediment-hosted porphyry copper deposits occurring within Sevier fold and thrust belt anticlines in Montana are structurally controlled and hydrodynamically confined. Hence, these porphyry systems can exhibit limited upward indicators of early high-temperature alteration, and little evidence for a clear porphyry to epithermal environment of mineralization. These characteristics are unlike similar porphyry mineral deposits found in plutonic and volcanic wall rocks in the Chilean Andes. These differences therefore require a modification of the porphyry copper model. A revised model for porphyry copper deposits is presented here for systems that form above the frontal Sevier thrust and interact with thick Paleozoic through early Triassic sedimentary platform sequences, often within anticlinal domes referred to here as "apex" exploration targets. Besides recognizing structural controls, the passive Atlantic-style margin platform sedimentary sequences in our model are considered as having great importance far surpassing the subordinate role ascribed to mere wall rocks in relation to later short-lived but ore-forming magmatic-hydrothermal systems. Instead, platform sediments with great lateral consistency and predictability are integral parts of a composite crustal-scale metallogenic system with depositional, erosional, and exposure features formed from Cambrian to Triassic time.

Varied well-known geological attributes of the sedimentary sequences affect and enhance ore deposition. Attributes of the evolved sedimentary system are incorporated into the porphyry copper ore genesis model as interdisciplinary knowledge, including sequence stratigraphy, global unconformities, paleo-karst, and basin evolution and redox cycling. Unprecedented opportunities emerge that support value-added metallic resources that expand the copper base to include rare earth elements (REEs) in Permian age phosphate deposits, and potential for Leadville, Colorado-style unconformity-related paleo-karst high-grade Cu-Ag vein and mantos replacement ore bodies. The acronym for the new modified model is termed the Deep Apex Sediment-Hosted Enhanced Resource, or the DASHER porphyry copper deposit (PCD) model. Putting REEs into a copper perspective shows that the *in situ* value of REEs in the Retort member of the Phosphoria formation in southwest Montana contains from about 0.3 to 1.25% copper value equivalent and the P_2O_5 phosphate contains about 1 to 1.5% copper value equivalent, indicating that REEs alone in the Phosphoria may locally double the value of contained base metals. Superimposed on these strata-bound mineral resources are magmatic-hydrothermal processes typical of traditional PCDs. The zoning pattern includes distal orbicular actinolite alteration, which was first recognized at Bingham Canyon, Utah and related to early high-temperature Potassic alteration. At the Clementine prospect, which is the type example of the DASHER PCD model, this actinolite orb zone occurs as a large 3 by 5 km ring pattern that dips outward, implying a high-level position. This Sevier-age (70.1 Ma) alteration ring surrounds and is coaxially aligned with the axial plane of a doubly plunging anticlinal dome. Along the apex of the anticline is a system of mineralized breccia vein gossans containing up to 3,700 ppm As, 2,300 ppm Sb, and 3,000 ppm Ba, with an exposed strike length of 1.5 km and a large elliptical zone containing barren breccias with two granitic plutons occurring on the east side. Since the sedimentary sequence at Clementine has 700 m of reactive Madison limestone and 180 m of carbonaceous Jefferson dolomite at depth, the full range of magma-derived metals is expressed in addition to the syngenetic REEs in the Phosphoria formation. In order to prove that the actinolite orbicular zone is in fact an integral part of the PCD system, a new chemical thermodynamic phase diagram is presented here in log fugacity CO_2/CH_4 vs log fugacity H_2S coordinates, showing the orbs in relation to

well-known mineral assemblages in the PCDs in relation to the sedimentary source rocks of basinal brines and hydrocarbons. Using sulfide, oxide, and alteration silicate mineral assemblages as guideposts, porphyry copper mineral assemblages form a definitive trend line along which the actinolite orbs plot, representing the outer and upper interaction zones with porous wall rock sedimentary formation pore fluids where actinolite forms within orbs by diffusion at the edges of advection with CH_4-dominated reduced fluids. This co-linearity of the orbs with the porphyry copper trend line and their location at the reduced end where granitic wall rock mineral buffers and sedimentary fluid sources converge proves the genetic linkage with early high-temperature porphyry copper mineralization, removing any doubt that mapped actinolite orb rings are indicative of potentially important porphyry copper mineralization. Furthermore, closed ring patterns coaxial with high Sb, As, and Ba veins serve as a powerful targeting tool. The phase diagram explains why carbonate-bearing sedimentary wall rocks exert a far stronger hydrolysis effect on hydrothermal fluids than volcanic and plutonic wall rocks. Acid attack of thick sections of carbonates produces CO_2 gas, which rapidly elevates the CO_2/CH_4 ratio and drives the fluid composition towards a higher oxidation state along the porphyry copper trend line from the chalcopyrite–pyrrhotite boundary up into the bornite and chalcocite fields along and past the edge of the granitic wall rock and actinolite buffer boundaries. Compared to volcanic-hosted PCDs, carbonate dissolution also broadens the array of minerals precipitated so that a fuller expression of the overall suite of metals being transported from the parental magma is made possible, including W, As, Sb, Ga, Te, Bi and Se. Furthermore, given the passive Atlantic style tectonic margin and related sequence stratigraphy of the Paleozoic age sediments, it is likely that four well-known unconformities may control paleo-karst along which high-grade Leadville, Colorado-style mantos and vein systems developed. As deep porphyry enhanced resource targets high-grade hypogene mantos may serve, along with the REEs and P_2O_5 in the Phosphoria as the critical value-added economic boost to copper grade previously offered by supergene enrichment, but without the need to strip and relocate the inevitable voluminous leached cap waste rocks. Taken as a whole, the DASHER PCD targets offer substantial new opportunities for discovery of domestic supply-chain-constrained critical and basic minerals. Given the range of traditional PCD mineralization, the enhanced resource character of the DASHER targets could support an unusual flexibility in utilization of underground space during the mine life cycle that minimizes the environmental footprint on the surface through back-filling of space by development and processing wastes. Over time, acceptance of the DASHER PCD model and innovations in underground mining might help soften if not transform the current negative attitudes about mining as a purely extractive industry and replace it with understanding and appreciation of ore deposits as the primary origination point for a sustainable energy future. Earning a social license for domestic mining starts with aspiring to transform social attitudes through making authentic progress in reimagining what the mine life cycle means.

Introduction

Knowledge of porphyry copper deposit genesis used in exploration today is based upon research in mines where the porphyritic parental intrusions encountered volcanic or plutonic wall rocks considered largely as a passive backdrop for mineralization (Lowell and Guilbert, 1970; Gustafson and Hunt, 1975; Seedorf and others, 2013; Sillitoe, 2010). However, exploration in Montana, with the expanse of the Sevier-age fold and thrust belt, requires consideration of the role of sediments in a new light. Therefore, this paper addresses six challenges in porphyry copper (PCD) exploration in terranes with abundant sedimentary rock formations: First, describing the regional geology of the Sevier-age fold and thrust belt of Montana in terms useful for exploration for deep sediment-hosted porphyry copper deposits. Second, updating the PCD model to incorporate structural and stratigraphic controls using the Clementine prospect as the type system. Third, devising new thermodynamic phase equilibria in the CO_2/CH_4-H_2S framework appropriate to explain fluid interaction with sedimentary as well as igneous mineral assemblages. Fourth, using these equilibria to rigorously prove and explain the association of orbicular actinolite alteration with early high-temperature porphyry copper zonation and Potassic alteration. Fifth, evaluating the opportunities for value-added metallic resources contained in the sediments including phosphate and rare earth elements (REEs), and finally, describing the potential for unconformity-related, paleo-karst high-grade Cu-Ag vein and mantos replacement ore bodies.

The common dissociation of magmatic-hydrothermal and stratiform ore deposits reflects in part a lack of a comparative geochemical framework, which depicts the composition of ore-forming fluids spanning both magmatic sources and hydrocarbon, brine, and meta-sedimentary fluids from which possible interrelationships might be discerned or discounted. Thus, without understanding how magma, sedimentary wall rocks, and sediment-derived fluids may comingle under certain geological circumstances, exploration for sediment-hosted PC deposits in the Sevier fold and thrust belt will remain poorly informed by geoscience and opportunities can be overlooked. This dichotomy is in part a hard-rock versus soft-rock division in geoscience education that persists in professional specialization within industrial sectors of materials (metals and mining) versus energy (oil and gas), thus largely divorcing ore genesis from petroleum geology, and even splitting science from engineering. However, today, clean sustainable green energy by decarbonization and electrification of the U.S. economy requires transformative solutions not limited by technical legacies imposed by historic scientific and engineering subdivisions. Newly mined critical and basic minerals, especially copper, are needed to support production of electric vehicles, semiconductor electronics, magnets, and lithium storage at an unprecedented level of demand. Petroleum geologists and geophysicists displaced as the shift towards carbon-zero energy advances have expertise and command of massive datasets synthesized by the American Association of Petroleum Geologists (AAPG) globally through corporate sharing of information and State and Federal partnerships, which are rare in mining. The wealth of soft-rock knowledge and expertise could synergize with the economic geology by helping to create unprecedented multidisciplinary exploration models of merit. The development of a domestic supply chain starts with raw materials produced sustainably with a transparency demanded by the necessity of earning a social license for mining through deep mine development with a minimal environmental footprint. We start here then presenting porphyry copper deposit exploration in Montana using an AAPG tectonic map based on a tectonically classified stratigraphic framework contained in the AAPG Correlation of Stratigraphic Units (COSUNA), widely used in petroleum exploration.

Regional Geology and Broad Controls on Mineralization

The AAPG tectonic map (fig. 1, next page) covers parts of Montana, Utah, and Colorado. In blue are platform sediments that formed on an expansive Atlantic-style passive tectonic margin (Dickinson, 1981). The sediments therefore correlate throughout the western U.S. and consist of recurrent depositional cyclic sequences of sandstone, shale, and limestone. The color patterns are deliberately vivid so as to highlight certain tectonic-stratigraphic units of central importance. Notice also that basement rocks below the platform sequence are shown in red, contrasting sharply with the use of red in economic geology to demark igneous rocks. Here such magmatic systems are shown in green. Larry Sloss worked throughout the western and eastern U.S. defining cratonic, onlapping mega sedimentary sequences that were named after the Indian tribes indigenous near where a sequence was best observed and defined by regional unconformities (Sloss and Laird, 1947; Sloss and Moritiz, 1951; Sloss, 1963. The cratonic sequence stratigraphy defined five intercontinental unconformities from oldest to youngest: the Sauk, Tippecanoe, Kaskaskia, Absoroka, and Zuni (Sloss and Laird, 1947; Sloss and Moritz, 1951; Sloss, 1967) shown in figure 1A. These unconformities result largely from global episodes of marine transgression and regression. Long intervals of non-deposition and erosion, shown as squiggly lines, are unconformities on which paleo-karst may have developed. The importance of recognizing these unconformities is historic and deserves acknowledgement here, where we apply this knowledge to exploration for metallic minerals. Recursive graphical elements such as unconformities are included in the following figures to develop the narrative linking interdisciplinary processes. The field of sequence stratigraphy was started by Larry Sloss, who worked at the Montana Bureau of Mines and Geology and Montana Tech for 7 years in the 1940s. Later, one of Sloss's graduate students at Northwestern University, Peter Vail, started the field of seismic stratigraphy (Vail and others, 1977a), from which global sea levels and eustatic curves over time have emerged (Vail and others, 1977b) while working for Exxon (Dott, 1992, 2014),

While the porphyry and vein ore deposits at Butte (shown as a red dot in fig. 1) are related to porphyritic magmas that intruded plutonic Butte Granite wall rocks shown in green, sediment-hosted deposits like Bingham Canyon formed where the intrusions invaded thick sedimentary sequences (represented here in light blue on fig. 1). At Bingham, the Mississippian-Missourian age Yampa and Highland limestones, which are in the middle

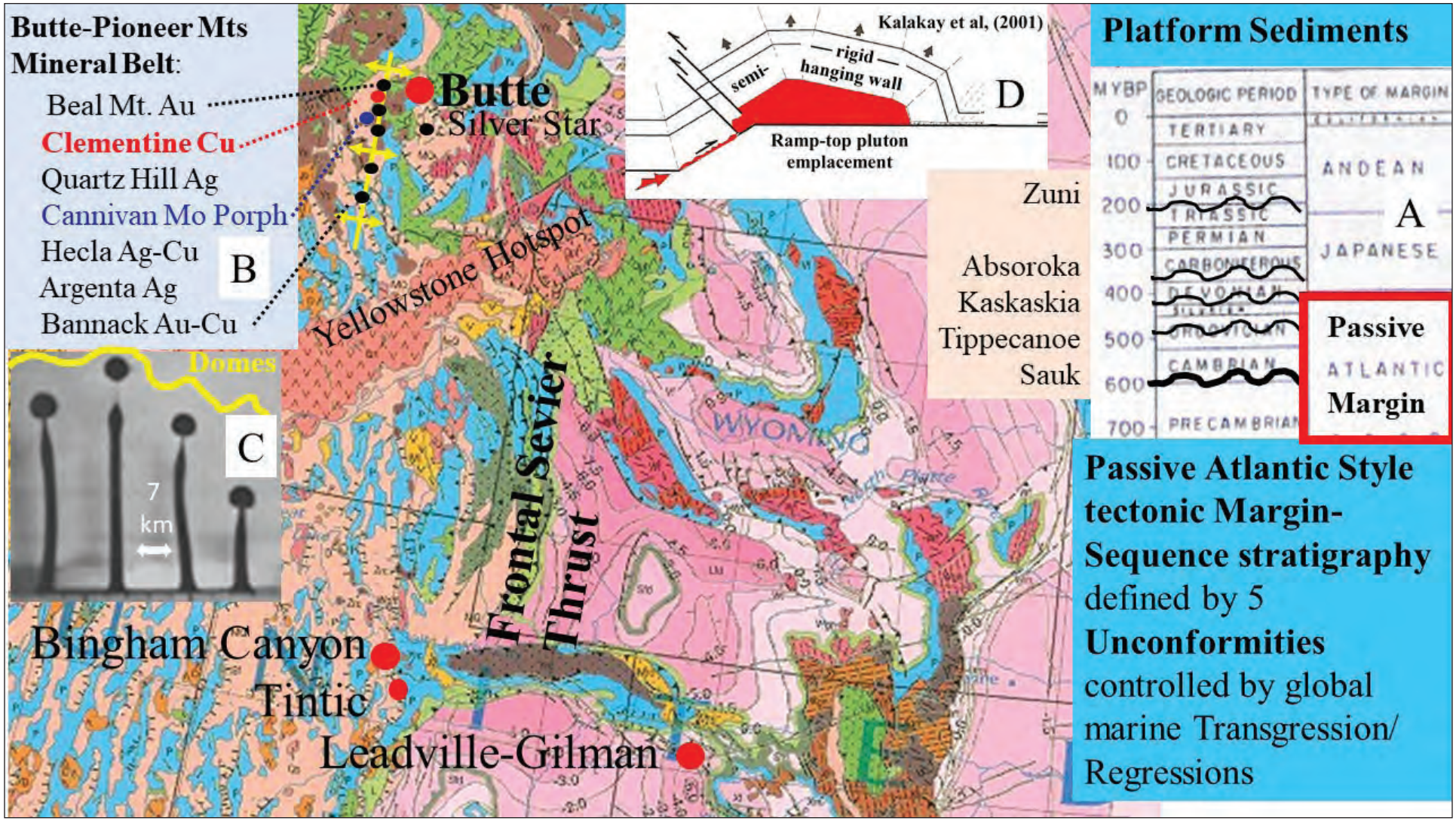

Figure 1. AAPG tectonic map based on COSUNA sections. North–south-trending blue patterns in lower left are due to east–west Basin and Range extension along listric faults. (A) Plate tectonic margin styles through time from Dickinson (1981) with intercontinental unconformities shown as squiggly black lines (Sloss and Moritiz, 1951; Sloss 1963) are the (C) 7 km average spacing between magma plumes. (B) The Butte–Pioneer Mountain mineral belt of Brimhall and Marsh (2017) and the position of the Clementine prospect in relation to known mining districts. (C) Rayleigh–Taylor gravitational instabilities forming magmatic plumes modeled by Bruce Marsh with an equal spacing of about 7 km. Each of the ore deposits in B form at structural domes, shown in yellow lines along the regional north–south-trending anticlinorium in B. (D) The idealized laccolith formed in the hanging wall of the frontal Sevier Thrust (Kalakay and others, 2001) where we assert that magmatic plumes ascended up the fault ramps.

part of the Oquirrh Group (locally called the Bingham Mine Group), were altered to *proximal* mineralized skarn up to a maximum distance of 400 m from the intrusion (Atkinson and Einaudi, 1978, fig. 7B). The pre-Tertiary structures interpreted by Atkinson and Einaudi (1978) to be bedding plane faults at the base of the Highland Boy limestone played an important role in determining the geometry of orebodies in the sedimentary rocks of the contact aureole of the Bingham Stock and in causing high concentration of sulfides. Alternatively, inspection of AAPG CONSUNA Charts Great Basin (GB; Oquirrh Mountains Column 26 and Central Wasatch Column 27 by Hintze and others, 1985) shows that the base of the Bingham Mine Group may, instead of being a bedding plane fault, be a regional unconformity that controlled fluid migration. An indisputable example of unconformities playing a role in mineralization are high-grade Cu-Ag veins, and *distal* carbonate replacement manto ores developed in aerially widespread super-unconformity paleo-karst carbonate aquifers as in the Leadville and Gilman districts of the Central Colorado mineral belt southeast of Bingham (Beaty and others, 1990; Sando, 1988). The top of the Leadville Limestone of Mississippian age is a super-unconformity shown in the AAPG CONSUNA Charts Central and Southern Rockies (CSR) (Kent and others, 1988; Piceance Basin Column 17 by Al Sanborn) on which high-grade mineralization developed in paleo-karst (De Voto, 1988) serving as permeable pathways that cross stratigraphy. Unlike igneous-hosted PCDs, sediment-hosted porphyry systems share a vast lateral continuity of the stratigraphy and regional unconformities, which implies that Cu-Ag vein and mantos systems developed in paleo-karst in Colorado can be expected in Montana.

In southwest Montana (shown in the northwest corner of fig. 1), the same Mississippian super-unconformity controlling mantos carbonate replacement ore deposition at Leadville, Colorado occurs and is shown in AAPG CONSUNA Charts Northern Rocky/Williston Basin (NRW; Ballard and others, 1983; Butte, Bozeman, SW Montana Column 9 by Susan Vuke). In figure 1B, a linear belt of geochemically varied intrusion-related (Au, Ag, Cu, W, and Mo) historic mining districts occurs and is listed as shown with Beal Mountain gold on the north to Bannack on the south. Brimhall and Marsh (2017) termed this the Butte Pioneer Mountains mineral belt. The regular spacing of these deposits is about 7 km through the Pioneer Mountains. Most of these districts are localized within dome structures and occur along a single north–south-trending regional anticlinorium of the frontal (easternmost) anticline of the Cordilleran fold and thrust belt of Sevier (Late Cretaceous) age, shown in yellow (Zen, 1988). We proposed a mechanism that explains the regular spacing of mining districts, a theme that has been fundamental in focusing our fieldwork leading to geological discoveries at Clementine (shown in red, fig. 1). From aerially extensive buoyant ribbon-like layers of magma presumably existing at depth along thrust fault flats, our calculations show diapiric ascent occurring at a regular spacing determined by Rayleigh–Taylor gravitational fluid (magmatic) instabilities (fig. 1C). Using our regional exploration model with both its regional structural and magma self-organizational aspects, Brimhall recognized a gap between the Beal Mountain and Quartz Hill Districts. Consequently, he focused fieldwork on the former Divide District, which had no prior history of metal production but occurs at a suggestive spacing with an associated anticlinal fold. Through digital mapping within a nappe window into the Lewis overthrust, Clementine Exploration LLC discovered a mineralized syntectonic frontal thrust fault-bend anticline consistent with the idealized east–west cross-section published by Kalakay and others (2001; fig. 1D; based upon earlier work Schmidt and others, 1990) as part of the Boulder Batholith mapping project of the U.S. Geological Survey. This model of syncompressional laccolith formation has been adopted for the Clementine prospect (shown in fig. 1B) within a linear belt of mining districts exposed at different erosion levels. On the north end, the surface at the Beal Mountain gold deposit is in Cretaceous age sediments of the Black Leaf Formation at a relatively high stratigraphic level. Clementine surface exposures extend from Black Leaf down to Mississippian age Madison. Quartz Hill through Bannack occur within older sedimentary formations. Syntectonic pluton emplacement raises the question of how to make room for magma in environments where crustal shortening, not extension, occurs on a regional scale. Finite element modeling (Nemcok and Henk, 2006) of an analogous fold and thrust belt explored for oil in the Western Carpathian Mountains of Romania showed the existence of an overall mean stress decrease inside the thrust sheet anticlines. Our interpretation asserts that in southwest Montana similar thrust sheet anticlines were also the loci of magma ascent, mineralization, and alteration processes in syncompressional environments at the top of frontal thrust ramps where “releasing steps” at ramp tops served as initial points of emplacement, subsequent pluton growth, and exceptional levels of chemical differentiation within underlying laccoliths.

Revision of the Porphyry Copper Model in the Sevier Fold and Thrust Belt

Consideration of the strong structural control on magma ascent and mineralization described above requires updating the paradigm used in porphyry exploration (fig. 2). This requires understanding features not yet well-known as a common part of the porphyry paradigm. Described here then is a revision of the tops of the porphyry copper model where the porphyry to epithermal transition might otherwise be expected (Sillitoe, 2010). Key to this revision is a distal type of early stage, high-temperature orbicular actinolite alteration shown diagrammatically here as green dots by Marco Einaudi, who along with Bill Atkinson, described the first occurrence of orbicular actinolite in diamond drill holes in the Carr Fork skarn area of the Bingham district in 1978. Since then orbicular alteration has been mapped in detail at the Clementine Prospect, and also noted at Escondida and El Hueso (Chile), Cajamarca (Peru), Morenci and Fortitude (USA), Cananea (Mexico), and Oyu Tolgai (Mongolia) (Marco Einaudi, oral commun.). Orbiclues are spherical to elliptical objects in three dimensions, often 1 to 2 cm in diameter. Orb zones are not orbicular granites nor miarolitic cavities, nor strange metamorphic effects. The orbs we have mapped at Clementine occur in the hanging wall anticline of the frontal Sevier Thrust. Since they dip outwards, we interpret them to be the Apex of a deep intact, uneroded porphyry Cu deposit. The location of orbicular alteration is shown diagrammatically in figure 2A, surrounding an ore-forming magma ascending from the top of a laccolith where magmatic water saturation occurs and drives advection fluid flow. The orb ring represents the outer edge of advective flow where radial diffusion becomes visible at crack tips and is hence mappable (Brimhall, 2018). Radiometric dating of hydrothermal titanite (70/7 +/- 1.3 Ma) was reported by Brimhall and Fanning (2019).

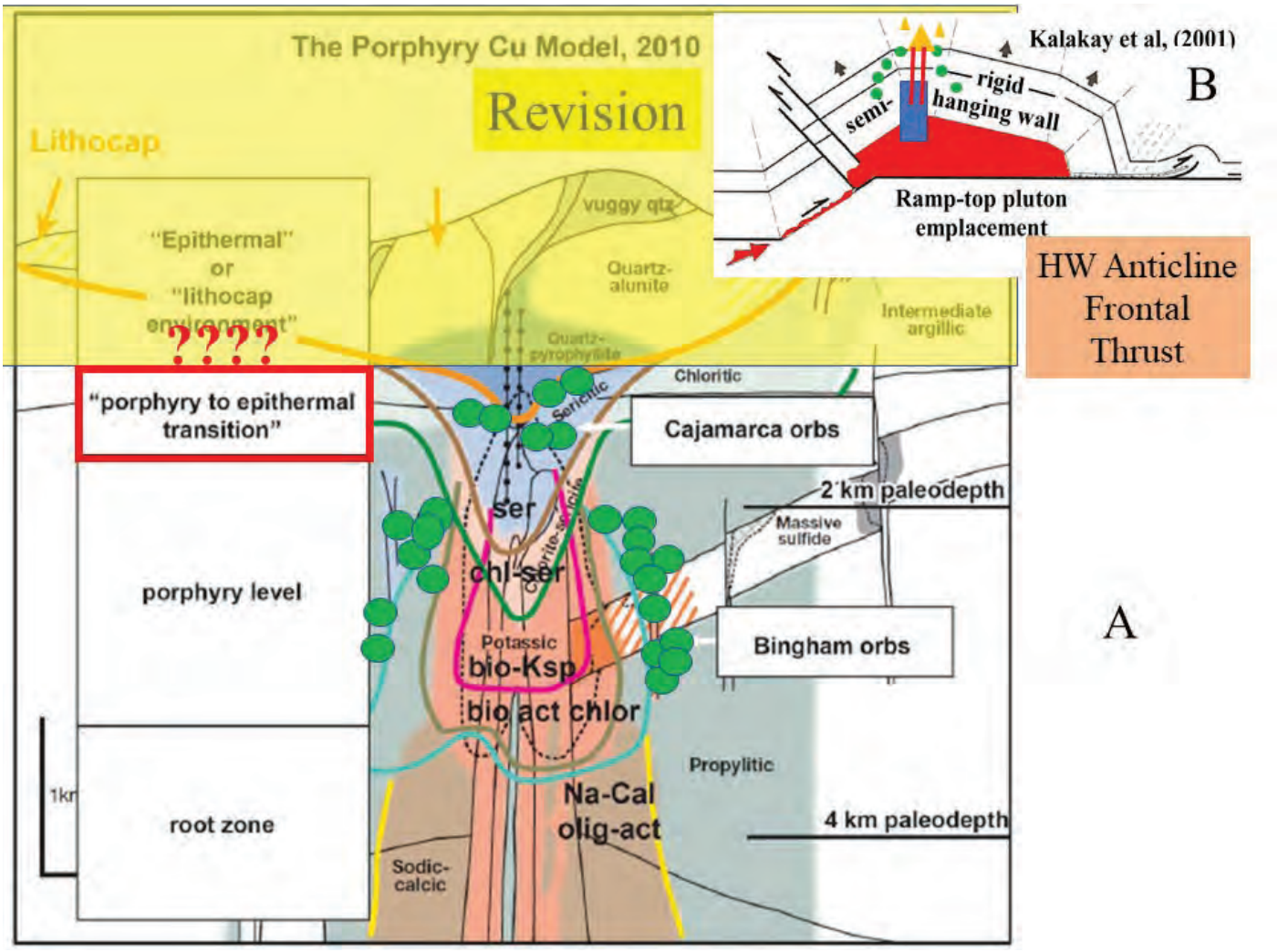

Figure 2. (A) Cross-section of porphyry copper model (fig. 6 in Sillitoe, 2010) with orbicular actinolite alteration at Bingham, Utah shown diagrammatically as green circles by Marco Einaudi (oral commun.). (B) Idealized cross-section of Kalakay and others (2001) with the proposed site of water saturation at the apex of a differentiated laccolith shown in blue, veins in red lines, and breccia in yellow triangles by Brimhall (this communication) with orbicular actinolite alteration shown as green dots.

Revisions of porphyry copper models used in exploration (Lowell and Guilbert, 1970; Gustafson and Hunt, 1975; John and others, 2010; Sillitoe, 2010) are necessary now for three reasons. First, adapting these models to a specific tectonic environment is necessary in order to reasonably estimate the likely vertical position of the present land surface within the mineralization-alteration column, since high degrees of rapid erosion (Dilles and Scarberry, this volume) are likely and porphyry deposits form over a 10-km range in depth of the emplacement (John and others, 2010; Seedorf and others, 2005). This vertical positioning estimate affects the estimates of mineral potential in grassroots, early stage, and advanced targets. Therefore, recognizing the PCD tops versus the bottoms is vital to exploring for deep mineralization systems with sound economic potential. Second, the poor discovery rate of the past decade of new grassroots PCD systems based on traditional field-based exploration methods has motivated the application of recently developed office-based technologies. According to Woodhead and Mathieu (2021), artificial intelligence (AI) has been touted as:

> "a disruptive technology that can be leveraged to reverse the current decline in discovery of quality resources. Part of this rationale stems from the belief that unrecognized or untested ore deposit signatures are likely to be present within the voluminous geoscience data that are now widely available to the public or, in some cases, reside in company archives. Artificial intelligence technologies provide an attractive way to cope with the multidimensional nature of exploration and increasingly large data sets that are routinely generated in the exploration process. In the view of the proponents of AI, this process offers the potential to quickly and efficiently extract, categorize, and analyze such data to identify the hidden signatures of ore deposits that are not readily revealed, or were missed, by conventional methods and thereby allow for more rapid testing of targets and, ultimately, an improved discovery rate."

Here, then, we caution that for AI to actually deliver on its promise, the geo-spatial PCD models into which voluminous multicomponent data is applied must be geologically accurate and relevant to specific tectonic regions to be explored. The USGS has long maintained regional studies vital in informing model development and assessment through AI: Hildenbrand and others (2000); Pearson and others, (1992); and Ruppel and others (1993). Third, deep underground mining of an enhanced resource combining PCD mineralization with bedded phosphorite with REEs and Leadville style high-grade veins and mantos provides transformational opportunities for re-imagining underground space utilization during the mine life cycle. Besides bulk mining methods of the main PCD ore body, selective mining could offer unprecedented advantages for mining REE and phosphate and stoping high-grade veins and mantos that create valuable open space for underground storage of development waste rock early in mine development. Processing wastes could be re-emplaced underground for rock support (Underground Engineering for Sustainable Urban Development, 2013).

Plan Map of the Clementine Prospect in Southwest Montana

Given the worldwide application of the Sillitoe (2010) PCD model over the past two decades of exploration, Brimhall (2018) raised the question as to what features, besides lithocaps, may prove to be effective guides to locating the porphyry copper hypogene mineralization center, particularly in the Sevier fold and thrust belt. Orbicular actinolite alteration offers new insight as it has been shown to occur not only at Bingham, Utah where it was discovered (Atkinson and Einaudi, 1978), but now also has been mapped regionally at the Clementine prospect in southwest Montana. By considering distal orbicular actinolite alteration as an early high-temperature zoning feature in both an early syntectonic Sevier age ore system at Clementine and Bingham, which formed after the Sevier orogeny, this alteration has been shown to define the outer edge of early advective fluid flow. This paper describes our fieldwork at the pre-deep pilot drilling phase to map and interpret extensive orbicular alteration as part of lateral and vertical zoning at the Clementine prospect, a possible new deep porphyry copper system in Montana. The intent is to develop within the porphyry copper paradigm new predictive mapping tools for better locating the edges and tops of hypogene hydrothermal fluid flow that has evaded many recent exploration efforts searching beneath lithocaps.

The Clementine prospect (fig. 3A) occurs between the southwest edge of the Boulder Batholith and the northernmost pluton of the Pioneer Mountains, the Big Hole River pluton. Actinolite–calcite–titanite-filled orb zones shown in circles demark a zone 3 by 5 km centered on the apex of a doubly plunging anticline where a vein breccia gossan system extends 1.5 km north–south, shown in figure 3 as thin red lines. The rock matrix be-

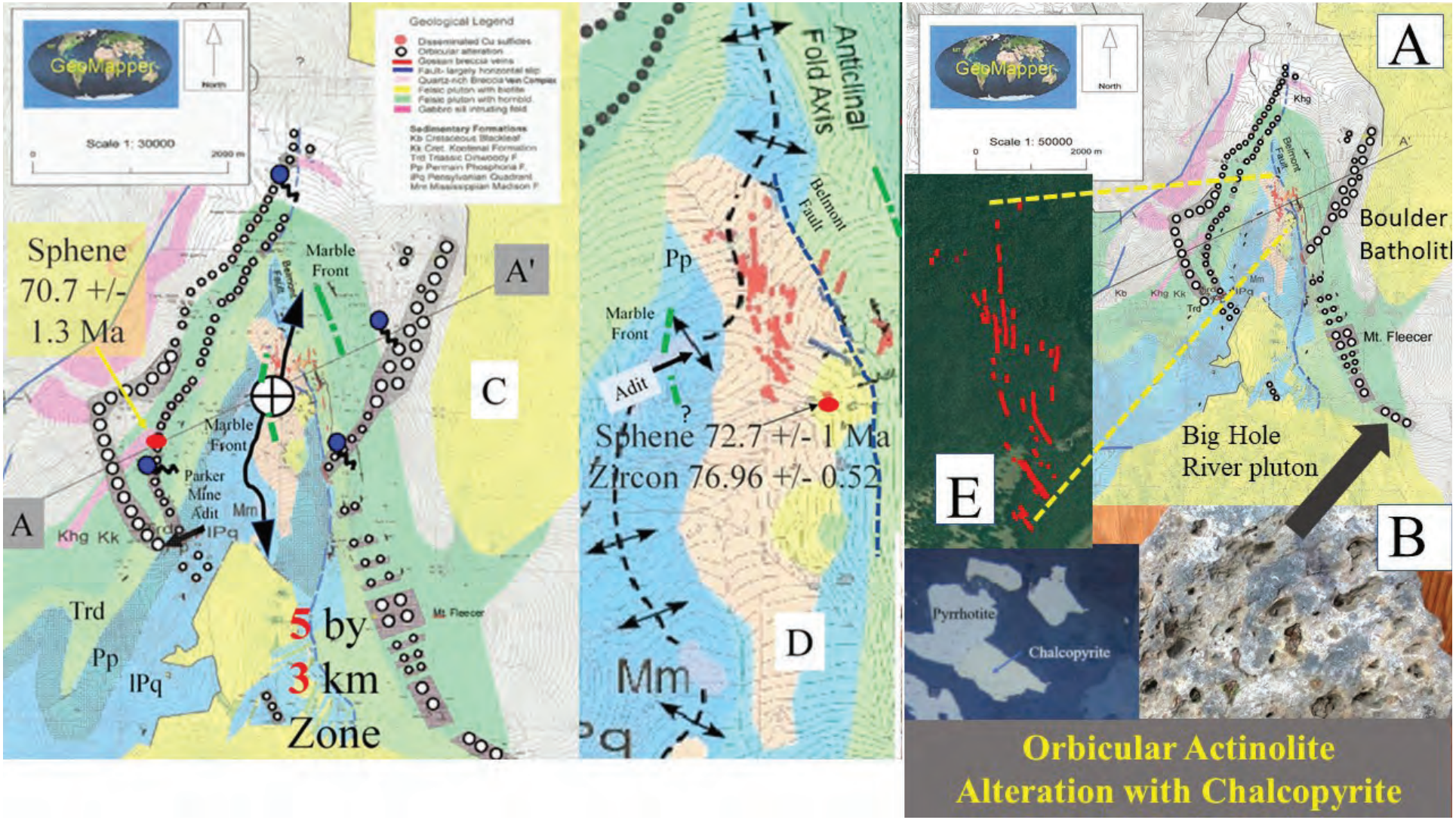

Figure 3. (A) Location of the Clementine prospect in southwest Montana between the southwest edge of the Boulder Batholith and the most northerly pluton of the Pioneer Mountains, the Big Hole River pluton. (B) Photograph of orbicular actinolite alteration shown in A with the insert showing chalcopyrite, pyrrhotite, and ilmenite between orbs zones. (C) Geological map showing the apex of the Clementine doubly plunging anticline co-axial with the surrounding actinolite orbicular rings and central zone containing a breccia vein gossan system shown in red (insert B in reflected light), 2.2-km-long elliptical zone containing barren breccias in pink, and two small plutons in yellow just east of horizontal bedding symbol. The marble front is shown in a thick green line (Sillitoe, 2010) on the east side of the anticline and a green line on the west side where it has been approximately located. It is important to note that the orbicular actinolite bands occur outside of the marble front, implying a lower temperature; yet actinolite growth is related to the early high-temperature potassic alteration expected at the deposit interior. A SHRIMP date on titanite in the orbs is shown. Blue circles are modern day springs. Cross section A–A' line trends northeast. (D) A blow-up of C with SHRIMP dates on the northern altered pluton. (E) An orthoimage of the central breccia vein gossan system mapped as red lines using digital mapping methods (Brimhall, 2018) in dense forest cover while using digital mapping methods and GeoMapper/PenMap software (Brimhall and Vanegas, 2001; Brimhall and others, 2002, 2006). Note that the breccia vein gossans are centrally located and co-axial with the outline of the orbicular actinolite zonation that defines an outer alteration ring (Brimhall, 2018; Brimhall and Fanning, 2019). Both the breccia vein gossans and orbicular alteration are mappable using digital field methods using 72-channel GNSS systems even under the densest forest canopy by combining American GPS and Russian GLONAS satellite coverage.

tween the actinolite–calcite–titanite orbs (fig. 3B) contains disseminated chalcopyrite, pyrrhotite, and ilmenite. Figure 3C shows the location of a SHRIMP radiometric age date on titanite from within an actinolite orb is 70.7 ± 1.3 Ma (Brimhall and Fanning, 2019). An enlargement of the orbicular ellipse elongated north–south (fig. 3C) shows that it is centered on and coaxial with a doubly plunging anticline. Modern-day springs that are commonly headwaters for spring creeks and mud holes are shown in blue circles with a squiggly tail. The area otherwise is remarkably dry and devoid of surface water except for late spring snowmelt runoff. Orbs define a key hydrodynamic boundary at the outer edge of early high-T hydrothermal convection and today control the aligned distribution of spring creeks. Springs and spring creeks are very rare hydrogeological features. The springs are not just random places where water flows out of the earth. The crest of the elliptical dome is centered on a 2.2-km-long elliptical zone shown in pick oriented north–south containing rock fragments of barren quartzite breccia and quartz rock flower. The marble front where the interface of dark bluish limestone is in contact with coarse-grained white marble is shown as green lines near the anticlinal crest symbol (Sillitoe, 2010, fig. 6). A further enlargement (fig. 3D) shows this anticlinal apex core area and the crest line of the anticline with a small area of Mississippian-age Lodge Pole Madison limestone near where the adit symbol is shown. Rocks on the adit mine dump contain wollastonite and marble. The marble front is shown as a dashed green line. Hence, given the observation of Meinert (1982) at Cananea, Mexico on the occurrence of wollastonite near the marble front suggests that the presence of wollastonite in marble implies prograde skarn formation at temperatures within the wollastonite stability field. Experiments by Greenwood (1967) show this temperature to be 400–450°C in fluids that are mostly H_2O with little CO_2. Shown as a swarm of red lines is a mineralized matrix breccia vein gossan system. The breccia vein gossans are not obvious continuously outcropping features but rather subtle individual samples mapped on the forest floor (fig. 3E) using 2.5-m accuracy GPS and GNSS-supported digital mapping systems described in Brimhall (2018). Only by connecting the dots of mapped vein gossan samples does their linear connectivity emerge and reveal the vein gossans as an organized system, clearly different from the barren rock breccias that occur randomly within the area (shown in pink in fig. 3D). The highest assay values of 34 vein gossan surface samples (in ppm) are: 861 Cu, 0.68 Ag, 60 Mo, 3,730 As, 2,030 Sb, 3,040 W, and 77 Ga. The breccia vein gossans are highly ferruginous, containing up to 32% Fe, reflecting a high pre-oxidation total sulfide content. Since W correlates highly with Fe (R = 0.79) and not with Ca (R = 0.23), the likely tungstate is ferberite ($FeWO_4$) rather than scheelite ($CaWO_4$), and no UV fluorescence has been observed. Ag, As, Sb, W, and Ga all correlate with Fe with R values of 0.68, 0.81, 0.97, 0.79, and 0.79, respectively, indicative of original sulfide host minerals. Ga correlates with W (R = 0.93), not Al nor Zn. Ge correlates with Ga (R = 0.78). Two small felsic plutons, each about 700 m in diameter, are shown in yellow (fig. 3). Two SHRIMP radiometric age dates on the northern pluton are shown. A hydrothermal alteration titanite gives an age of 72.7 ± 1 Ma and an older zircon age of 76.97 ± 0.52 Ma, indicating that this pluton was not the parent for the observed zoning pattern.

Permian Age Retort Member of the Phosphoria Formation

Given the fact that phosphate is now on the Critical Minerals list, one economically notable platform sedimentary wall rock formation occurring at Clementine is the Permian Age Retort member of the Phosphoria Formation, labeled Pp (shown in fig. 3C in blue with a faint stippled pattern that wraps around the anticline). The Phosphoria Formation occurs on both the west and east sides of the anticline, spanning a strike length of about 6 km. The thickness of the Phosphoria is usually less than 100 m.

Geological Cross-Section

A geological cross-section along line A–A' in figure 3C is shown in figure 4A based on surface geological mapping and formation thickness. Figure 4B shows the cratonic sequence stratigraphy defining five intercontinental unconformities from figure 1A. Actinolite–calcite orbs (fig. 4C), central vein gossan system, and an altered pluton are shown. Purple is a gabbroic sill. Four regional unconformities, each with possible paleo-karst that could have controlled formation of copper–silver mineralization, are shown as black squiggly lines. The marble front is shown as a green line. Inside the marble front proximal Cu skarn mineralization could occur, while outside the marble front distal Cu-Ag veins and carbonate replacement ore could occur. For scale, a pro-

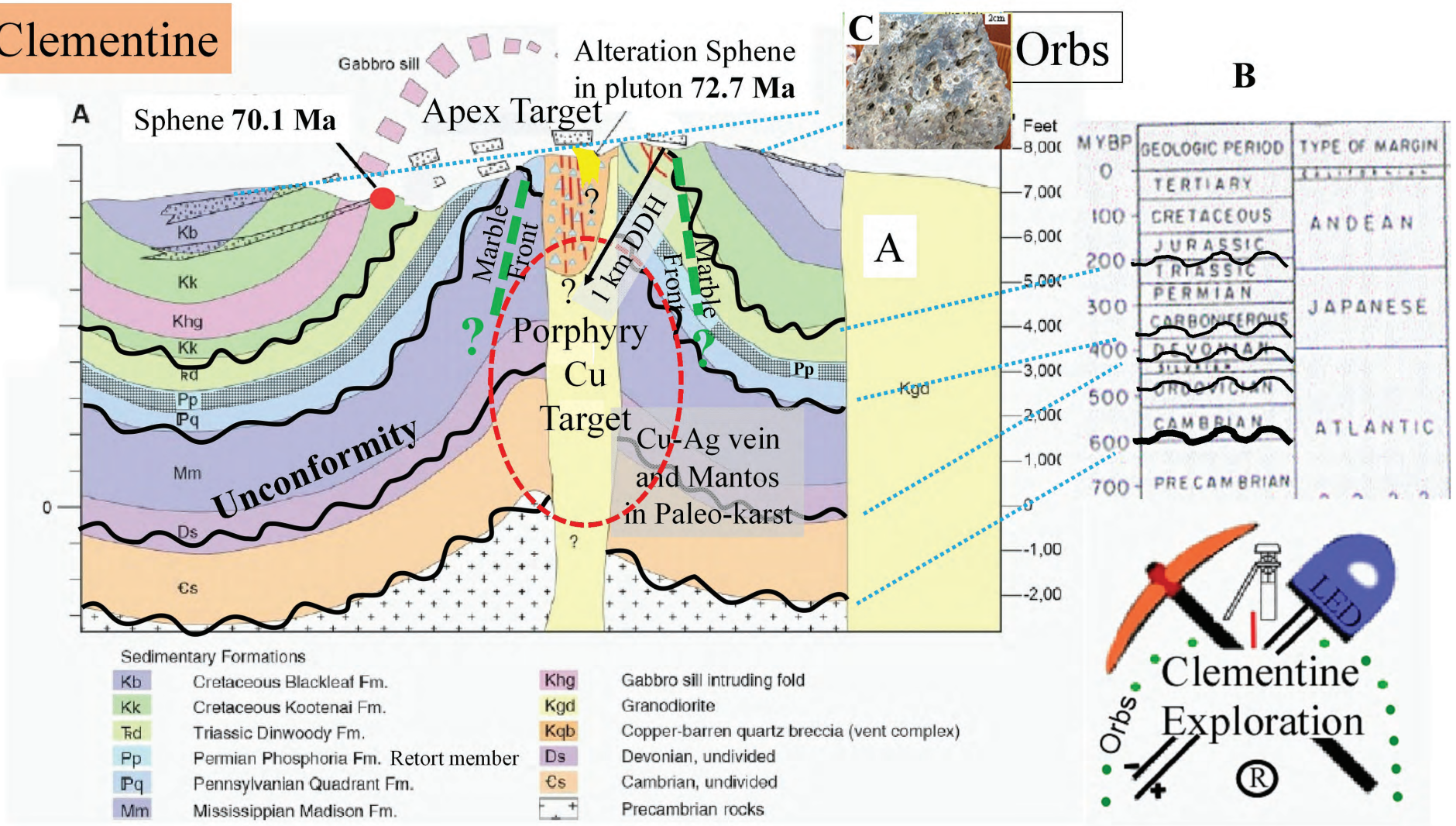

Figure 4. (A) Geological cross-section of the Clementine prospect anticline along line A–A' (fig. 3C) looking northward. The orbicular actinolite alteration is shown dipping outwards B. The central zone breccia vein gossans are shown as thin red lines. Four unconformities named in figure 1 are shown as squiggly black lines and shown in C. Paleo-karst is possible on all these unconformities. Within the near-field of the magmatic-hydrothermal system Leadville style Cu-Ag veins and mantos mineralization is possible. A proposed 1-km-long pilot diamond drill hole is shown into the apex target, probably deep enough to encounter the top of the Devonian Jefferson Formation.

posed 1-km-long drill pilot hole is shown. The Phosphoria formation (Pp) is shown with a stippled back pattern.

The local outward dip of the actinolite orbs is implied from the trace of the orb belts and how they intersect topography. These outward dips compared to the steep distal orb at Bingham imply that the present earth surface at Clementine is high in the mineralization system. This assertion is strengthened by the fact that the marble front (shown as a green line, fig. 4) can be found and mapped on the eastern-central side of the anticline. Alternatively, if what few limestone beds occur were all marble or skarn, the exposure level would be deeper in the higher-temperature part of the mineralization column. Therefore, we conclude that current topography exposes the upper parts of the Clementine mineralization system, not the mid-levels as at Cannivan Gulch nor the distal vein and mantos systems at Quartz Hill, Hecla, and Bannack. Besides Cu-Mo-Ag in the porphyry, vein, and mantos, additional metallic resources would add value to the composite system being explored.

Critical Mineral Occurrences at the Clementine Prospect

Several metals on the Critical Minerals list occur at Clementine, including As, Sb, W, and Ga in the mineralized matrix breccia vein system. In addition, the Permian age Phosphoria Formation presents an opportunity to add an important complement of valuable high-demand REEs, many of which are supply-chain-limited. The USGS has long maintained a programmatic research mission on phosphate resources in the U.S. (Hein and others, 2014) in support of production of inorganic fertilizer. Recently, Emsbo and others, 2015 and 2016 described significant REE potential occurring within the Perman age Phosphoria Formation as offering an alternative to imports of these chemical elements, which are vital to modern electronics and sustainable energy high-field-strength magnetic components and guidance systems. Most current phosphate mining in the Western Phosphate Field is done by open-pit methods in Idaho, where relatively high-grade phosphate rocks occur near the center of the Phosphoria Basin where the Guadalupian Series Roadian Stage Meade Peak member outcrops. In Montana, near the northern edge of the basin, the slightly younger Guadalupian Series Wordian Stage Retort Mountain member occurs and was mined underground east of the Pioneer Mountains at Maidenrock north of Melrose. REE consistency within a given time horizon makes both Phosphate and REEs reliable co-products (Emsbo and others, 2015). Emsbo and others (2015, 2016) show that contained REEs are entirely hosted in francolite and are nearly 100% recoverable using the same process currently used to acid leach and produce the world's phosphate supply. In addition, the REE content in even the lowest grade of these deposits exceeds the current value of the phosphate itself. At Clementine an adit with drifts in the Retort Member Phosphoria was made in the mid-1970s in Parker Creek (fig. 3C). The *in situ* value of the REEs can be put into a porphyry copper perspective using REE assays on grab samples from that Parker Creek mine dump and on the Retort Member data contained in the Supplemental Data in the Emsbo and others (2015) paper. The *in situ* value of REEs in the Retort member of the Phosphoria Formation in southwest Montana contains from about 0.3 to 1.25% copper equivalent and the P_2O_5 phosphate contains about 1 to 1.5% copper equivalent. While the Phosphoria Formation is not among the thickest platform sedimentary units, it is continuous, and with the REE suite it contains it offers economically important opportunities for selective underground mining.

Hypogene Enrichment and the Environmental Footprint

Exploration for deep porphyry copper deposits is motivated by several factors. First, grassroots discovery of new ore bodies has been a rarity in the past two decades, implying that most of the exposed systems have been discovered through traditional techniques. Such outcropping systems are exposed at their midsections in the vertical mineralization column, where relatively high sulfide content compared to their tops caused secondary supergene leaching and enrichment, creating enrichment blankets with Cu grades 2 to 5 times higher than the protore at depth (Brimhall and others, 1985a; Alpers and Brimhall, 1988, 1989). Traditionally, supergene enrichment by descending solutions provided an economic boost to the early stages of PCD mine development, making them feasible and mineable by open-pit mining methods. Today, however, environmental considerations, especially on public lands, require underground mining of deep ore bodies with a far smaller environmental footprint without generating voluminous waste rock piles from stripping leach cap waste. Consequently, a second factor motivating deep mining is that a far greater degree of selectivity in fragmenting and moving a

rock mass is possible than in mining supergene enriched systems. The economics of deep underground mining is enhanced if there are high-grade zones at depth that can be selectively mined to offset development costs. Fitting this requirement are hypogene (upward flowing solutions) that may have formed multiple high-grade ore bodies at depth in the form of proximal skarns, distal skarns, Leadville, Colorado-style veins and carbonate replacement mantos controlled by unconformities and paleo-karst, and sediment-hosted distal disseminated ores.

Proximity of Regional Unconformities with Paleo-Karst to Clementine

How close to the apex of the Clementine prospects do known paleo-unconformities with paleo-karst come? Should these features with sedimentary and eustatic origins actually occur nearby, then given the lateral continuity of sedimentary strata and unconformities, hypogene enrichment may occur in the apex anticlinal core strata at Clementine. Fortunately, a nearby exposure answers this conjecture. Only 8 km south of the Clementine apex zone, the top of the Mississippian Madison Group is exposed just west of the town of Dewey (fig. 5A). Here, the upper surface of the Madison has a reddish-orange-colored discoloration due to ancient oxidation below a 30-million-year-long exposure. The caverns are obvious proof that paleo-karst developed, then burial ensued during the subsequent Absaroka marine transgression. Figure 5B shows a diagrammatic sketch of the expected paleo-karst where Leadville and Gilman, Colorado-style high-grade Cu-Ag veins and mantos are expected at Clementine. Polymetallic Cu-Ag-Au vein and mantos ore bodies controlled by paleo-karst and evaporite solution on the Absoroka age unconformity on top of Mississippian Age Leadville limestone is analogous to the exposure of Mississippian Madison in Montana (fig. 5A). In the Leadville–Gilman belt, major porphyry systems occur, including Climax and Henderson Mo porphyries of the same general age range as the manto ore bodies.

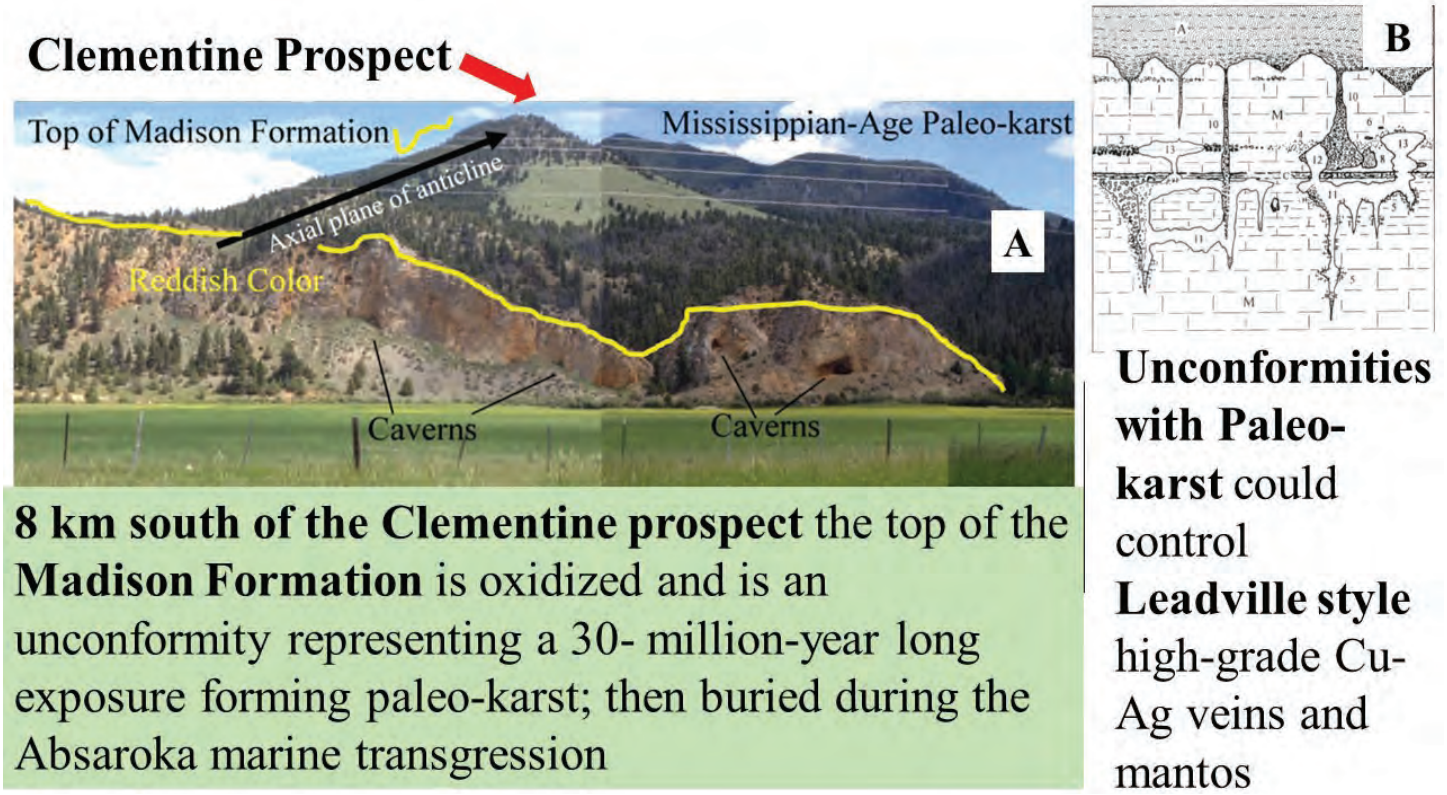

Figure 5. (A). Photograph looking north at Dewey, Montana across the Big Hole River showing the steep cliff face of the top of the exposed Mississippian Madison Group, shown as a yellow line. Reddish orange discoloration parallel to the surface of the upper formation contact is due to oxidation over a 30-million-year exposure when this surface was an unconformity. Below the unconformity surface are paleo-karst caverns. (B) Diagrammatic depiction of paleo-karst in cross-section where elsewhere in the Leadville–Gilman mining districts of Colorado, this same unconformity controlled high-grade vein and mantos replacement ore bodies.

Linking Geology with Geochemistry

Geological mapping at the Clementine prospect showed a zoning pattern similar to the Sillitoe (2010) porphyry copper model augmented with the orbicular actinolite alteration ring. The apical anticlinal dome at Clementine coaxial with the orbicular ring and central breccias vein gossan system clearly implies structural control on hydrothermal fluid flow by the Sevier age thrust and fold system consistent with the 70.7 Ma age. The McCartney Mountain stock, which intrudes the frontal fold and thrust zone east of the Pioneer Batholith and is about 30 km southeast of Clementine, has yielded a preliminary K-Ar date of 70 ± 1.5 m.y. (Ruppel and Lopez, 1984, from Brumbaugh, 1973, p. 48).

On a district scale, the orbicular alteration affects a wide variety of sedimentary lithologies within the Madison, Quadrant, Phosphoria, Dinwoody, Kootenai, and Black Leaf Formations, spanning an age from Mississippian through Cretaceous. While orbicular actinolite alteration was described long ago by Atkinson and Einaudi (1978) and noted in many porphyry copper deposits since then, the Clementine prospect appears to offer the first district-scale mapped pattern to date. Therefore, we feel it useful to understanding porphyry copper genesis broadly speaking to clarify and develop further linkages among the geology, orbicular actinolite alteration, and the overall geochemistry of the Clementine mineralization within the framework of known PCD mineral assemblages. In particular, it is vital to establish how the orbicular actinolite orb assemblages actually relates genetically to well-known porphyry copper mineral assemblages, including potassic alteration, and to granitic magmatic sources of early high-temperature hydrothermal fluids and rock buffers. Simultaneously, it is important to ascertain how orbicular actinolite alteration relates to the sedimentary wall-rock packages in the orbs that have developed.

Hydrocarbons in the Sevier Orogen

The Sevier orogenic belt and associated foreland basins include well-known hydrocarbon source rocks and reservoirs within structural traps (Ruppel and Lopez, 1984; Lageson and Schmidt, 1994). Considering also the sequence stratigraphy, unconformities, and paleo-karst where Leadville, Colorado-style replacement mantos are expected at Clementine, discerning possible geochemical relationships between actinolite orbs and mantos is important. An important clue about copper mineralized stratabound mantos in both sedimentary and volcanic rocks in north-central Chile comes from Zentilli and others (1997), where mantos contain a variety of hydrocarbons and over-mature bitumen. In order to quantify relationships of actinolite orbs with porphyry copper ore systems and stratabound copper mantos with hydrocarbons, chemical thermodynamic principles were applied to discern mineralogical relationships in the CO_2/CH_4-H_2S fluid–rock interaction framework.

Chemical Phase Equilibria

In the interest of integrating hydrothermal ore genesis with sedimentary basin evolution including hydrocarbons, a new chemical thermodynamic phase diagram of CO_2/CH_4 vs H_2S was generated by the author that compares oxidation and sulfidation states of magmatic-hydrothermal and sediment-hosted ore deposits in relation to granitic rock buffers and the sedimentary source rocks of basinal brines, hydrocarbons, and graphitic metasediments. Phase diagrams typically used to describe porphyry copper deposits cannot show hydrocarbon species, as the common coordinate axes are sulfur and oxygen fugacity without any provision for organics with carbon and hydrogen, and hence offer less than an integrated representation of sediment-hosted ore assemblages.

Equilibrium phase diagrams have long served as powerful interpretive tools for understanding the significance of recurring mineral assemblages in hydrothermal ore deposits. Holland (1959) developed the log fS_2 vs log fO_2 coordinate framework for the Fe-O-S system, which Meyer and Hemley (1967) expanded by using sulfide mineral assemblages as signpost markers demarking pathways of fluid evolution over time in relation to wall-rock alteration buffer assemblages determined petrographically and verified experimentally. Einaudi (1977) applied these phase diagrams to the Cerro de Pasco ore deposit of Peru. Brimhall (1980) added the biotite–potassium feldspar–Fe oxide buffer of potassic wall-rock alteration and showed the position of diverse early high-temperature porphyry copper systems. While log fS_2 and log fO_2 variables contributed much to advanc-

ing understanding porphyry copper ore genesis, their fugacity values are vanishingly small in magnitude and hence are not themselves major constituents in the ore-forming fluids. In the interest of representing equilibria in terms of more abundant aqueous and gas species in nature, Brimhall (1980) developed a phase diagram with log a(Fe^{2+}/a^2Cu^+) versus log fH_2S gas, which has the distinct advantage of using variables directly involved in sulfide precipitation and copper leaching (fig. 6). At different log fH_2S values serial cross-sections of log fO_2 vs log a (Fe^{2+}/a^2Cu^+) depicted the three-dimensional volumes of chalcopyrite, bornite, chalcocite, covellite, pyrite, and pyrrhotite in relation to the biotite–potassium feldspar–Fe oxide oxygen fugacity buffer (fig. 7). Recently Mernagh and Bastrakov (2013) developed the diagram of log f CO_2/CH_4 vs log fH_2S coordinates around the magnetite–pyrrhotite–pyrite assemblage, making it possible to study vapor-rich fluid inclusions using Raman spectroscopy to estimate H_2S concentrations directly.

In the present study coordinate axes of log f CO_2/CH_4 vs log f H_2S are selected again in figure 8 so that: (1) equilibria involving hydrocarbons can be added, (2) minerals formed from fluids derived from sedimentary host rocks can be depicted in the same space as magmatic-hydrothermal ore deposits, and finally (3) the relative abundance of CO_2, CH_4, and H_2S gases inferred from fluid inclusions in different types of ore-forming systems become evident in the coordinate space chosen. An advantage of using log fH_2S gas with a range of -4 to +2 in figures developed below, which is far higher than the values of log fS_2 (-5 to -8), signifies that H_2Sgas is among the abundant species in the natural systems. Furthermore, from an equilibrium of $H_2S_{gas} = H_2S_{aqueous}$ we show that $H_2S_{aqueous}$ is a major reduced sulfur species in ore-forming solutions from which sulfides precipitate. In so doing, a comparative phase diagram emerges here in which a wide spectrum of ore deposit types can be plotted

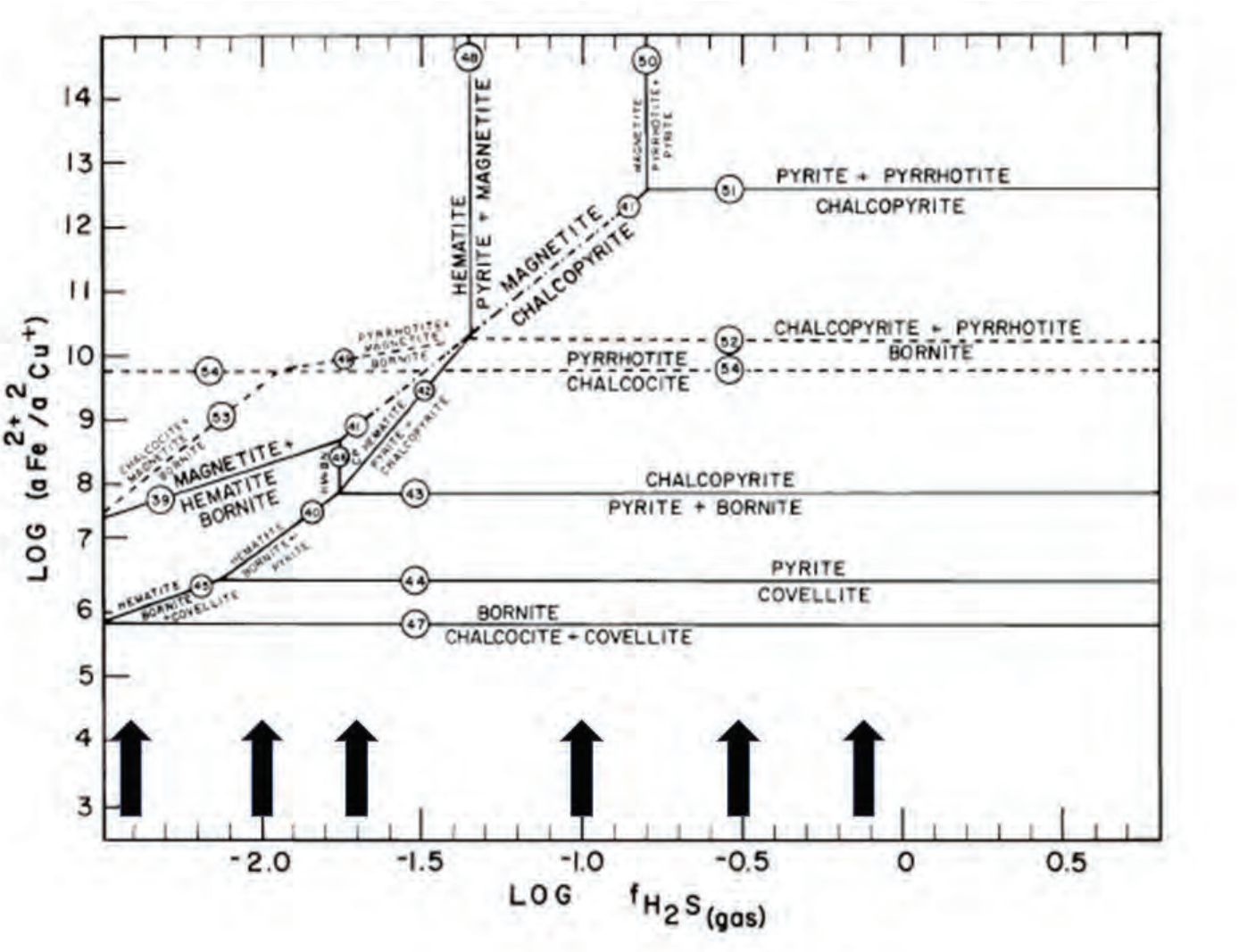

Figure 6. Mineral triple points from Brimhall (1980), figure 4, with black arrows at values of H2S for serial cross sections in figure 7.

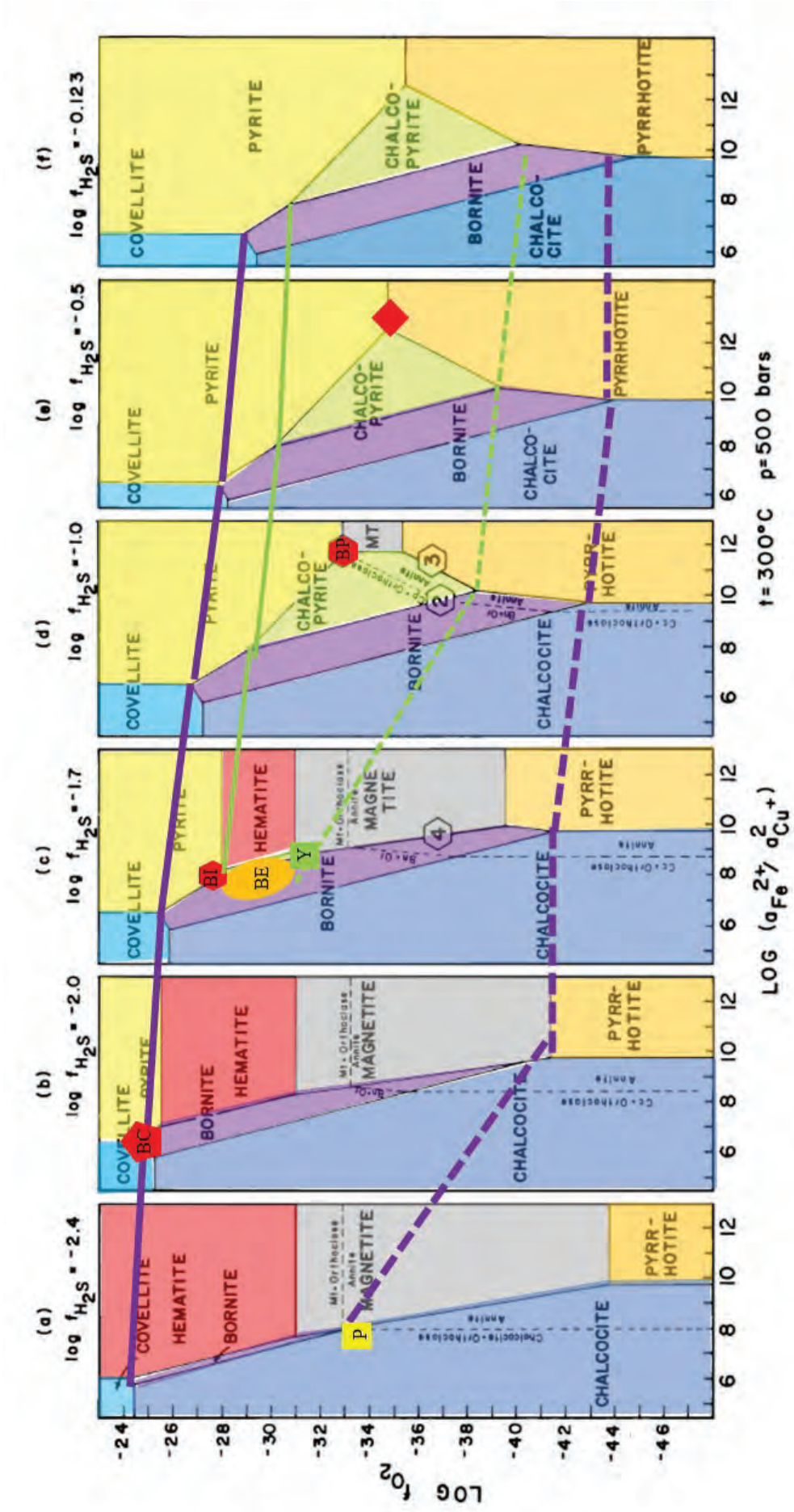

Figure 7. Serial cross-sections at different values of H2S showing the stability fields of chalcopyrite, pyrite, pyrrhotite, bornite, chalcocite, and covellite. The granite redox buffer is shown in a thin dashed line (annite–orthoclase). Mineral assemblages of porphyry copper deposits are shown: early stage Butte as red octagon (BP), intermediate zone (BI), and central zone late stage as red pentagon (BC). Pyrrhotite locked in pyrite at Butte and El Salvador Chile as red diamond. Porphyry copper assemblages from table 4 of Einaudi and others, 2003 are shown as: early chalcopyrite–bornite without pyrite or magnetite at Bingham as orange ellipse (BE). Panguna is shown in a yellow square (P) and Yerington in a green square (Y). In solid green is the trace of the high oxidation edge of chalcopyrite with the low oxidation state dashed. In solid purple is the trace of the high oxidation edge of bornite with the low oxidation state dashed. These four lines are shown in figure 9 for reference.

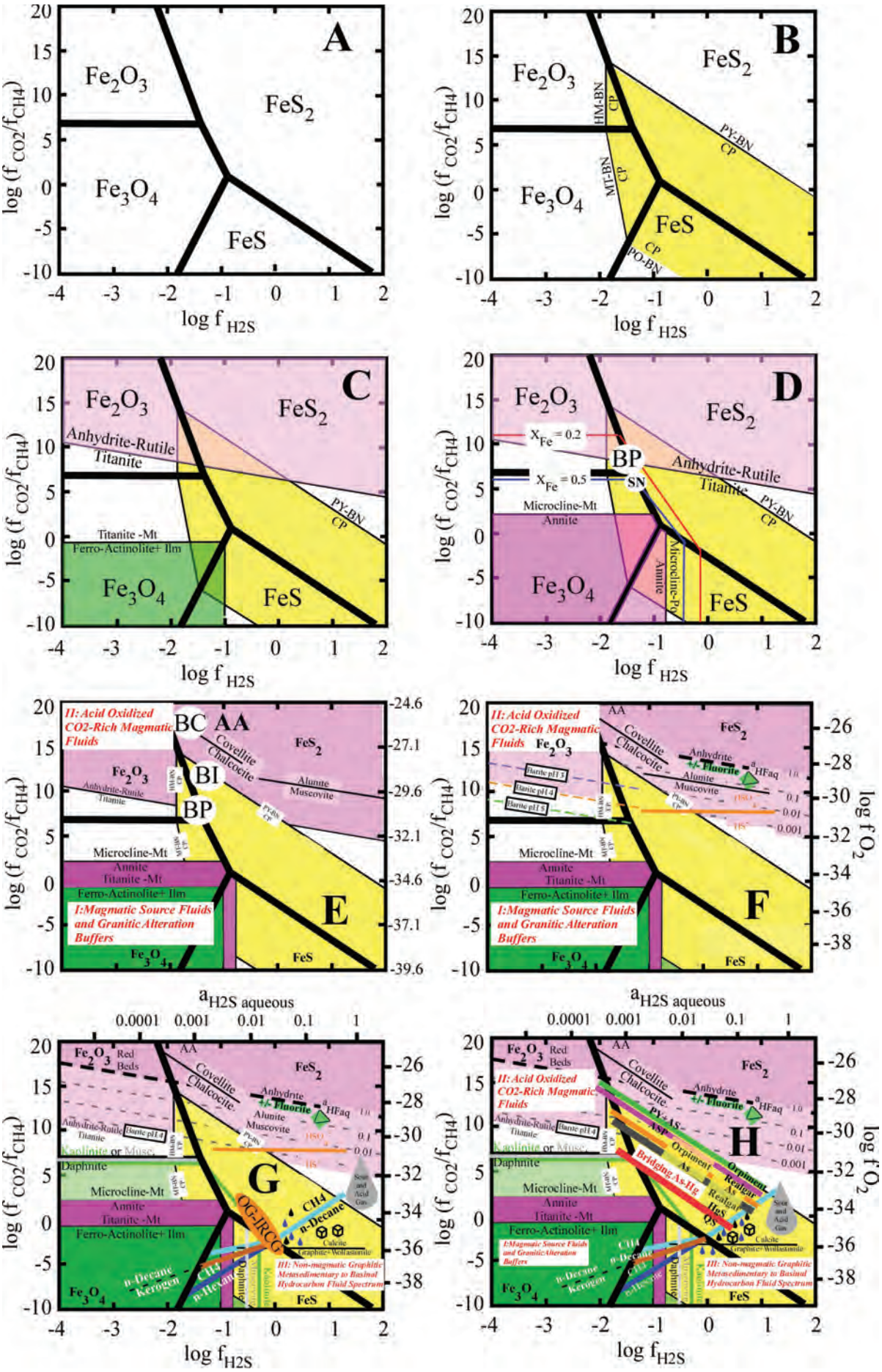

Figure 8: caption on adjoining page.

and assessed for involvement of multiple source fluids including magmatic-hydrothermal fluids, highly oxidized meteoric fluids and evaporites, and reducing sediment-derived connate basinal brines and hydrocarbons. The diagram helps to quantify geological interpretations about external fluid derivation and hypothesized mixing presented previously in schematic models of porphyry copper and related deposits (Taylor, 1974; Sheppard and Taylor, 1974; Dilles and Einaudi, 1992; Runyon and others, 2018; and Zentilli and others, 1997).

Methods

Mineral–Solution–Gas Equilibria Stoichiometry

In complex multicomponent systems, knowing which minerals occurring in rocks represent equilibrium mineral assemblages is essential to meaningful modeling and constitutes a problem to which many alternative approaches exist (Lanari and Duesterhoeft, 2019, p. 36–38). Here, rather than perform forward theoretical modeling using Gibbs Free Energy minimization (Wood, 1987), we rely on natural field and microscopic observations of well-known recurrent mineral assemblages that have been studied in ore deposits worldwide for over a century and constitute well-tested empirical features of the ore deposit models used successfully in mineral exploration (Meyer and Hemley, 1967; Hemley and others, 1980; Lowell and Guilbert, 1970; and Gustafson and Hunt, 1975). For each mineral assemblage selected, the stoichiometry of each reaction must be computed defining the reaction coefficient mole numbers for each reactant and product including CO_2, CH_4, H_2S, and H_2O. Rather than present only the final phase diagram, which is complex, the thermodynamic relations supporting different parts of the diagram are presented in stepwise stages so that the final diagram can be more readily understood (figs. 8A–8H), and readers seeking to verify and reproduce the equilibria can more easily do so. Since the coordinate axes have been deliberately chosen as log f CO_2/CH_4 vs log f H_2S, specific requirements guide how the stoichiometric coefficients are determined.

The rules developed here in determining the stoichiometric reaction coefficients are as follows: (1) conserve the number of moles of Fe and Cu in solid minerals, (2) set the coefficient of H_2S the same as the moles of S contained in sulfides, (3) in reactions where a chemical element like sulfur is oxidized, as in the formation of a sulfate-bearing mineral such as alunite, place CO_2 on the opposite side of the reaction to conserve electrons, and (4) solve three simultaneous linear equations describing conservation of mass of H, O, and C, where (5) the number of moles of CO_2 equals the number of moles of CH_4. Stipulation (3) stems from considering the oxidation (loss of electrons) of carbon in methane to form CO_2 as oxygen gas is reduced (gain of electrons) to oxide in water, whereby a total of 8 electrons are transferred and must be conserved ($C^{-4}H^{+}_4 + 2O^0_2 = C^{+4}O^{-2}_2 + 2H^{+}_2O^{-2}$). Specifically, when C^{-4} is oxidized to C^{+4}, a loss of 8 electrons, while 4 O^0 are reduced to 4 O^{-2}, which is a gain of 8 electrons, sum to zero, thus conserving electrons. Stipulation (5) is necessary in order to compute log (f_{CO2}/f_{CH4}) as the y-axis in the phase diagram, which requires that CO_2 and CH_4 occur on opposite sides of each reaction and that their stoichiometric coefficients are identical but of opposite sign. An example illustrates the algebraic solutions. Consider the hematite–pyrite phase boundary in figure 8A, where thick black lines define stability fields of pyrite, magnetite, hematite, and pyrrhotite. The defining reaction is shown in equation 1, where *l*, *m*, and *n* are the desired stoichiometric coefficients of CO_2, CH_4, and H_2O, respectively, having con-

Figure 8. Construction sequence of reaction equilibria lines at temperature of 300°C. (A) Boundaries for the hematite, magnetite, pyrite, and pyrrhotite. (B) Stability field of chalcopyrite shown in yellow. (C) Stability field of ferro-actinolite surrounded by titanite and either magnetite or pyrrhotite, shown in green with the field of anhydrite shown in pink. (D) Stability annite component of biotite surrounded by microcline, pyrite, or pyrrhotite shown in purple expanded by the influence of magnesium substitution for iron expressed as mole fraction Fe. BP and SN represent the compositions of biotites in the Butte pre-Main Stage and Sierra Nevada batholith, respectively. (E) Shows the nested fields of ferro-actinolite and annite representing I. Magmatic source fluids and granitic alteration buffers. The locations of mineral assemblages of the Butte Intermediate (BI) and Central Zones (BC) representing II. Acid-oxidized CO_2-rich magmatic fluids. (F) Fluorite–anhydrite equilibria are shown at different values of HF aqueous up to a value of 1.0. Location of barite at different values of pH. (G) Kerogen (brown), hexane (dark blue), and decane (light blue) siderite equilibria representing fluids derived from sedimentary source rocks host petroleum, gas mixtures, basinal brines, and graphitic metasedimentary fluids under reducing, CH_4 -rich conditions. (H) Bridging the sedimentary fluid source spectrum and porphyry copper/IOCG trend is a family of parallel equilibria involving quicksilver, cinnabar, arsenic, orpiment, realgar, and arsenopyrite along which basinal $H2_S$-rich petroleum/brines comingle with oxidized heated magmatic fluids. From low to high H_2S values, these bridging reactions demark hot spring Hg-Au, including the McLaughlin and Culver Baer deposits in California and Carlin Au in Nevada.

served Fe in hematite and pyrite and then set the coefficients of H_2S to a value of 4 since 2 moles of pyrite has 4 moles of S.

$$Fe_2O_3 + 4H_2S + lCO_2 = 2FeS_2 + mCH_4 + nH_2O. \quad (1)$$

Conservation of the number of moles of H, O, and C is given by equations 2, 3, and 4, respectively.

$$8 = 4m + 2n, \quad (2)$$
$$3 + 2l = n, \text{ and} \quad (3)$$
$$l = m. \quad (4)$$

Solving equations 2, 3, and 4 simultaneously gives $l = m = 0.25$ and $n = 3.5$, as shown in equation 5.

$$Fe_2O_3 + 4H_2S + 0.25CO_2 = 2FeS_2 + 0.25CH_4 + 3.5H_2O. \quad (5)$$

Notice that the rules stated above are followed since CO_2 and CH_4 are on opposite sides of the reaction and that their stoichiometric coefficients are both 0.25. Notice also that there are 2 moles of Fe in both Fe_2O_3 and $2FeS_2$. Finally notice that there are 4 moles of S in both $4H_2S$ and $2FeS_2$.

Example of Equilibrium Expressions

With the activity of H_2O set to 1 for simplicity, the equilibrium constant for equation 5 is given in equation 6 as:

$$K = \frac{f_{CH4}^{0.25}}{f_{CO2}^{0.25}} \frac{1}{f_{H2S}^{4}} \quad (6)$$

Taking logarithms yields a linear equation for the magnetite-pyrite phase boundary in equation 7

$$\log \frac{fCO2}{fCH4} = -16 \log f_{H2S} - 4 \log K \quad (7)$$

The value of log K is computed as 3.826 as described below yielding a linear equation in the general form of $y = a_o + a_1x$ as given in Eq. 8 where the y-intercept is -15.305 and the slope is negative 16.

$$\log \frac{fCO2}{fCH4} = -15.305 - 16 \log f_{H2S} \quad (8)$$

Chemical Thermodynamic Calculations

The phase diagram has been computed here using thermodynamic equilibrium constants at 300°C and 50 MPa showing mineral-solution-gas reactions within CO_2/CH_4-H_2S gas fugacity coordinates. These physical conditions have been chosen so as to serve as a comparative reference condition for quantitatively describing mineral–solution–gas equilibria within porphyry copper deposits, orbicular actinolite alteration, and high-temperature oil field hydrocarbons. Once the reaction stoichiometry have been determined using the linear algebraic methods above, equilibrium thermodynamic calculations have been made using three software packages: CHNOSZ (Dick, 2019) for equilibria involving organic species and GEOPIG (Windman and Shock, 2008),

which are based on use of the SUPCRT92 package of Johnson and others (1992) developed at the University of California, Berkeley, incorporating advances in internal consistency in the database (Helgeson and others, 1978, 1998). SUPCRTBL (Zimmer and others 2016) was also used, and is based on the data contained in Holland and Powell (2011). Here, internal consistency of the thermodynamic data used has been checked by running the same chemical reaction in different computer programs.

Recurrent Mineral Assemblages

Recurrent sulfide–oxide–silicate mineral assemblages are well known in the ore deposit classes chosen for this study and in fact are an integral part of the genetic models of porphyry copper deposits and many other types of ore deposits. The reason for recurrent mineral assemblages lies in chemical thermodynamic equilibrium. In fact, recurrent mineral assemblages are proof that natural hydrothermal processes over time tend towards a state of equilibrium. Since Fe, O, and S are abundant chemical elements in ore deposits, the phase boundaries shown in figure 8A as heavy dark black lines exert a powerful buffering influence on the paths taken by ore-forming solutions seeking equilibrium. Mineral assemblages that typify several world-class ore deposits, including Butte, Montana, are plotted in the figures as they are developed in order to illustrate the use of the phase equilibria.

Chalcopyrite Stability Field

The stability field of chalcopyrite is shown in figure 8B in yellow. Chalcopyrite stability is central to understanding this phase diagram. Notice in particular that chalcopyrite has an extensive stability field situated astride the stability fields of hematite, magnetite, pyrite, and pyrrhotite, which are the most common ore-related Fe-minerals in nature. Note, however, that the chalcopyrite stability field does not occur at values of log fH_2S below -1.8, as discussed in Brimhall (1980), where detailed serial cross-section diagrams span wide ranges of log fH_2S and log aFe^{2+}/a^2Cu+, thus depicting three-dimensional volumes of sulfides in figures 6 and 7 contained therein. In figure 7 the extremities of the chalcopyrite field trace out the low and high limits of oxygen fugacity expressed here as log f CO_2/CH_4. Below log fH_2S values of -1.8, there is insufficient reduced aqueous sulfide to form chalcopyrite, although the more copper-rich but sulfur-poor sulfide bornite is stable. In the pyrite field, chalcopyrite is surrounded by bornite and in the hematite field chalcopyrite is surrounded by bornite. Similarly, in the magnetite field chalcopyrite in surrounded by bornite alone, and in the pyrrhotite field, chalcopyrite is surrounded by bornite.

Wall-Rock Alteration Mineral Assemblages

Common hydrothermal wall-rock alteration assemblages are readily depicted using the algebraic procedures described above. Here we show where in the diagram actinolitic and potassic alteration occurs in relation to magnetite, hematite, pyrite, pyrrhotite, and chalcopyrite. Since most hydrothermal amphiboles and biotite occur in solid solution containing iron, magnesium, and other elements, we show these phases as their iron-end members and then illustrate how incorporation of magnesium changes the phase relations using ideal site mixing in annite–phlogopite solid solutions (Brimhall and Crerar, 1987; Ague and Brimhall, 1987, 1988).

Ferro-actinolite, titanite (sphene), anhydrite, and rutile stability fields are depicted in figure 8C with the field of ferro-actinolite plus ilmenite being shown in dark green, surrounded by titanite (sphene) in both the magnetite and pyrrhotite fields. Substitution of Mg^{2+} for Fe^{2+} causes the actinolite field to expand outward so its upper right-hand corner extends into the pyrite field. The equilibria of titanite, anhydrite, and rutile is shown as occurring at high values of CO_2/CH_4 within the hematite and pyrite fields. The stability field of anhydrite is shown in pink. Titanite–anhydrite–rutile stability is important in understanding oxidizing conditions in porphyry copper deposits and is often related to biotitization of hornblende (Roberts, 1973, 1975; Brimhall and others, 1985b; Brimhall and Crerar, 1987).

The annite and microcline stability fields are shown in figure 8D, with the field of annite shown in purple surrounded by microcline plus magnetite, pyrite, or pyrrhotite. The stability field of annite expands outwards with substitution by Mg^{2+} for Fe^{2+} as the mole fraction annite (X_{Fe}) decreases from 1.0 to 0.5 and expands even more to a more fraction annite to 0.2 for highly Mg-rich hydrothermal biotites characteristic of potassic al-

teration in the porphyry copper deposits, which are both phlogopitic and highly enriched in F^- (Brimhall and others, 1985; Brimhall and Crerar, 1987; John and others, 2010) compared to common igneous biotites of the Sierra Nevada batholith "SN" (Ague and Brimhall, 1987, 1988a,b). Notice that the biotite boundary for X_{Fe} equal to 0.5 is near the triple point magnetite–pyrite–hematite and the titanite–anhydrite–rutile equilibria. The early high-temperature porphyry copper pre-Main Stage assemblage at Butte, Montana shows hornblende in the Butte granite wall rock that has been biotitized (Roberts, 1973, 1975), sphene has been converted to rutile, and anhydrite is shown plotted as a circle as "BP" although it formed at even higher temperatures (Brimhall, 1973, 1977) near 650°C. The high-Mg hydrothermal biotites are also fluorine-rich. Fluorination by late-stage magmatic volatiles is the cause of the oxidation and increase in log (f_{CO2}/f_{CH4}; Brimhall and Crerar, 1987). Brimhall (1979) and Brimhall and Ghiorso (1983) described hypogene copper leaching of the pre-Main Stage mineralization as the source of copper in the Main Stage veins.

The muscovite–alunite boundary occurs at the high levels of log (f_{CO2}/f_{CH4}) where anhydrite is stable and titanite (sphene) is unstable as shown in figure 8E. Finally at the highest levels of log ($f\,CO_2/f\,CH4$), the chalcocite–covellite boundary occurs typical of advanced argillic alteration (Brimhall, 1980). Notice in figure 8E that along the righthand edge of the figure, values of log fO_2 are shown that are calculated from the equilibria given in equation 9, for which the log K is -69.102 and the conversion of log (f_{CO2}/f_{CH4}) to log $f\,O_2$ is given in equation 10.

$$CO_2 + 2H_2O = CH_4 + 2O_2, \text{ and} \qquad (9)$$

$$\log fO_2 = -34.551 + 0.5 \log (f\,CO_2/f\,CH_4). \qquad (10)$$

The advanced argillic alteration assemblage with chalcocite and covellite represents the highest f_{CO2}/f_{CH4} and fO_2 states in porphyry ore deposits under hydrothermal conditions. The Main Stage mineral assemblage of the Central Zone of the Butte mining district in Montana (Meyer and others, 1968; Guilbert and Zeihen, 1964) is represented by point "BC" where covellite and chalcocite occur with advanced argillic wall-rock alteration (AA) with alunite (Khashgerel and others, 2008). In figure 8E notice the label in red: "I: Magmatic Source Fluids and Granitic Alteration Buffers," which applies to the lower left corner of the phase diagram. In contrast, notice in the upper left corner in red: "II: Acid Oxidized CO_2-Rich Magmatic Fluids." While oxygen is obviously a strong oxidant, it is not the strongest—a characteristic exceeded only by fluorine, which is the most electro-negative element in the Periodic Table. Consequently, the highly oxidizing advanced argillic assemblage (AA) often includes traces of fluorine-bearing minerals including fluorite (CaF_2), Zunyite ($Al_{13}Si_5O_{20}(OH,F)_{18}Cl$), and topaz ($Al_2SiO_4(F,OH)_2$) (Guilbert and Zeihen, 1964) and has cuprous sulfide ($Cu^{+1}S$) in equilibrium with covellite, cupric sulfide ($Cu^{2+}S$). The source of the fluorine in minerals of the advanced argillic assemblage is most likely the fluor-phlogopite in the district-scale Potassic alteration zone associated with the pre-Main Stage mineralization, which was dissolved and replaced by voluminous sericitic alteration during the Main Stage event.

The fluorite stability field in relation to anhydrite is expressed in equation 11, which has a log K equal to -13.473.

$$CaF_2 + H_2S + CO_2 + 2H_2O = CaSO_4 + 2HFaq + CH_4. \qquad (11)$$

Unlike that of anhydrite, the stability field of fluorite depends upon an additional variable, log a_{HF} aqueous, as shown in equation 12:

$$\log (f_{CO2}/f_{CH4}) = 13.473 - \log fH_2S + 2\log a_{HFaq} \qquad (12)$$

Figure 8F shows the bottom edge of the fluorite stability field for log a_{HFaq} values from 0.001 to the highest possible value of 1.0, where HFaq would be the dominant species in the ore-forming fluid rather than water. The iso-activity line for HSO_4^- and HS^- is shown in orange. Above this line oxidized sulfate dominates and below this line reduced sulfide occurs. Notice that high values of HFaq are within the HSO_4^- field well above the HS^- field relative to the iso-activity line shown in orange. Barite, like fluorite, has a stability dependent upon several factors, including pH and Ba^{2+} in solution. Here barite is shown for an assumed barium concentration of 100 ppm (Candela and Piccoli, 2005) for pH values of 3, 4, and 5, showing that barite, a mineral containing sulfate, plots within the HSO_4^- field where fluorite is also stable.

Hydrocarbon Reactions

Helgeson and others (2009) published a comprehensive chemical and thermodynamic model of oil generation in hydrocarbon source rocks that included thermodynamic data for solid, liquid, and gaseous hydrocarbons. Using this data, Dick (2019) created a new user computer interface called CHNOSZ that runs in R, which is an online computing environment for statistical computing and graphics. CHNOSZ computes equilibria involving organic species, consistent with the thermodynamic data of the SUPCRT92 package (Johnson and others, 1992), making it possible here to integrate into one phase diagram, organic phase equilibria with traditional inorganic species and thereby explore the possible oxidation–reduction–sulfidation relationships between different major ore-forming systems and sedimentary source rock organics and brines. While thermodynamic data in Helgeson and others (2009) does not include all the organic species identified by chromatography in ore deposits such as those described by Peabody and Einaudi (1992) or Peabody (1993), several common and geologically important species are included. In particular we compute phase relationships for mature kerogen ($C_{128}H_{68}O_7$), n-hexane (C_6H_{14}), and n-decane $C_{10}H_{22(l)}$ using the same algebraic methods discussed above that conserve moles of carbon, hydrogen, and oxygen, although the calculations are more difficult given the high molecular weights of the organic species. Figure 8G shows the phase boundary between mature kerogen and n-decane (eq. 13), n-hexane and methane (eq. 14), and n-decane and methane (eq. 15) in the presence of siderite and pyrrhotite or pyrite as in equation 16.

$$C_{128}H_{68}O_7 + 118FeS + 63\,CO_2 + 221H_2O = C_{10}H_{22}g + 63CH_4 + 118\,H_2S + 118\,FeCO_3, \quad (13)$$

$$C_6H_{14} + 6FeS + 8.5\,H_2O + 4.75CO_2 = 4.75\,CH_4 + 6FeCO_3 + 6\,H_2S, \quad (14)$$

$$C_{10}H_{22(l)} + 10FeS + 14.5\,H_2O + 7.75CO_2 = 7.75\,CH_4 + 10FeCO_3 + 10\,H_2S, \text{ and} \quad (15)$$

$$C_{10}H_{22(l)} + 10FeS_2 + 19.5\,H_2O + 5.25CO_2 = 5.25\,CH_4 + 10FeCO_3 + 20\,H_2S. \quad (16)$$

High values of H_2S fugacities are referred to as “sour” gas in the petroleum industry and reach levels as high as 40 percent of the gas phase (Gong, and others, 2014). CO_2-rich gas is referred to as “acid” gas. Both extreme gas concentrations are shown diagrammatically in figure 8G in a gray bubble. In the sour gas region where the log H_2S gas values are around 1.2, the activity of aqueous of H_2S (not log) can be calculated from the equilibrium constant for the equilibria of H_2S_{gas}=$H_2S_{aqueous}$, which is -1.568. Therefore, although the log H_2S gas fugacity is about 1.2, the log activity of aqueous H_2S is much lower, with a value of -0.368 or an activity of 0.42, implying that the associated fluid is still aqueous but with a high aqueous H_2S concentration. The scale of a $H_2S_{aqueous}$ is plotted along the top of figure 8G.

Chlorite–Muscovite–Kaolinite Reactions

Notice that these organic phase boundaries above intersect the annite–microcline boundary in the lower-left corner of the diagram in the pyrrhotite and magnetite fields typical of reduced granitic rocks. Surrounding the

granitic rock buffer, several other silicate mineral buffer reactions involving chlorite, muscovite, and kaolinite are important in sedimentary source rock environments and also as hydrothermal alteration reactions, but at higher values of log f CO_2/CH_4 and lower values of H_2S fugacities than in sedimentary environments. Phase boundaries for the Fe-end member chlorite (daphnite) with the clay mineral kaolinite are shown in light green and with muscovite in gray. Chlorite precipitation may inhibit quartz infilling pore and cracks and thereby maintain and enhance permeability in deeply buried sandstones (Worden and others, 2020) from which pore fluids may escape that become ore-forming non-magmatic brines.

Calcite–Graphite–Wollastonite Reaction, Orogenic Gold Deposits, and the Source of Water

Intersecting both the organic phase reactions and the daphnite to muscovite or kaolinite reactions is an equilibria involving calcite–graphite–wollastonite, shown in the lower right corner of figure 8G cutting the pyrite–pyrrhotite phase boundary. This assemblage of pyrite–pyrrhotite with graphite and wollastonite reflects the interpreted upper limit of orogenic gold deposits (Tomkins and Grundy, 2009) and the computed log f CO_2/CH_4 vs log f H_2S coordinates of both the Missouri gold deposit in Western Australia (Mernagh and Bastrakov, 2013) and the mineral assemblage in the "Reduced" porphyry copper–gold deposits described by Rowins (2000), labeled in figure 8G as "OG-IRCG." Finally, notice that in the lower right corner of figure 8G, a new label is shown in red: "III: Non-magmatic Graphitic Metasediment to Basinal Brine Hydrocarbon Fluid Spectrum."

Mercury–Arsenic Mineral Equilibria: Geochemical Bridge Pathways to Sediment-Hosted Ore Deposits

In figure 8H, equilibria involving sulfide minerals containing Hg and As (quick silver, cinnabar, realgar, elemental arsenic, orpiment, and arsenopyrite) form a family of parallel lines with a negative slope connecting two disparate stability fields: "III: Non-magmatic Graphitic Metasedimentary fluids and Basinal Brine Hydrocarbon Fluid Spectrum" and "II: Acid Oxidized CO_2-Rich F-Rich Magmatic Fluids." The implications of the Hg-As mineral reaction lines are obvious and powerful. These equilibria with quicksilver, elemental arsenic, realgar, orpiment, and arsenopyrite bridge a large geochemical space transitional between petroleum source rocks and epithermal veins with reduced (HS^-) sulfur species where gold transport occurs with magmatic-hydrothermal systems (Hofstra and Cline, 2000). These equilibria involving Hg and As minerals provide a family of reaction pathways buffered by coexisting As and Hg minerals connecting sediment-derived fluids with magmatic sources of heat and aqueous fluids, thus making interactivity of disparate metallogenic systems inevitable when and where geological proximity and permeable pathways develop.

Results

Assembly of the chemical thermodynamic reactions for sulfide, oxide, silicate alteration mineral, and organic petroleum liquids and gases shown in figures 8A–8H are assembled in figure 9. Most importantly, three distinct end member fluid compositions contributing to ore deposition are shown in red text: "I: Magmatic Source Fluids and Granitic Alteration Buffers" (lower left), "II: Acid Oxidized CO_2 and F- rich Magmatic Fluids and/or Meteoric water," and "III: Non-magmatic Basinal Brine Hydrocarbon Fluid Spectrum" (lower right).

Porphyry Copper Deposits

In figure 9 several key mineral assemblages of the district-scale zoning of the Butte mining district in Montana described in Meyer and others (1968) are depicted and labeled: "Butte Trend" shown with a diamond checkboard trend. Red ellipse "BP" represents the early high-temperature pre-Main Stage porphyry copper mineralization at Butte, Montana (Brimhall, 1977) at the triple point of magnetite–pyrite–hematite with chalcopyrite near the Mg-rich biotite–microcline granite buffer and the triple point magnetite–pyrite–chalcopyrite shown in Brimhall (1980, fig. 5). Here, potassic alteration involves biotitization of the hornblende of the Butte Granite forming a Mg-rich hydrothermal biotite (Robert, 1973,1975; Brimhall, 1977; Brimhall and others, 1985; Brimhall and Crerar, 1987) coexisting with rutile and anhydrite shown along the lower edge of the anhydrite stability field, shown in pink. "BI" represents the Butte Intermediate Zone (Meyer and others, 1968; Guilbert and Zeihen, 1964) with high-grade Main Stage copper veins consisting of chalcopyrite–pyrite and chalcopyrite–bornite veins with sericitic alteration envelopes that locally destroyed the granitic wall-rock buffer and allowed the

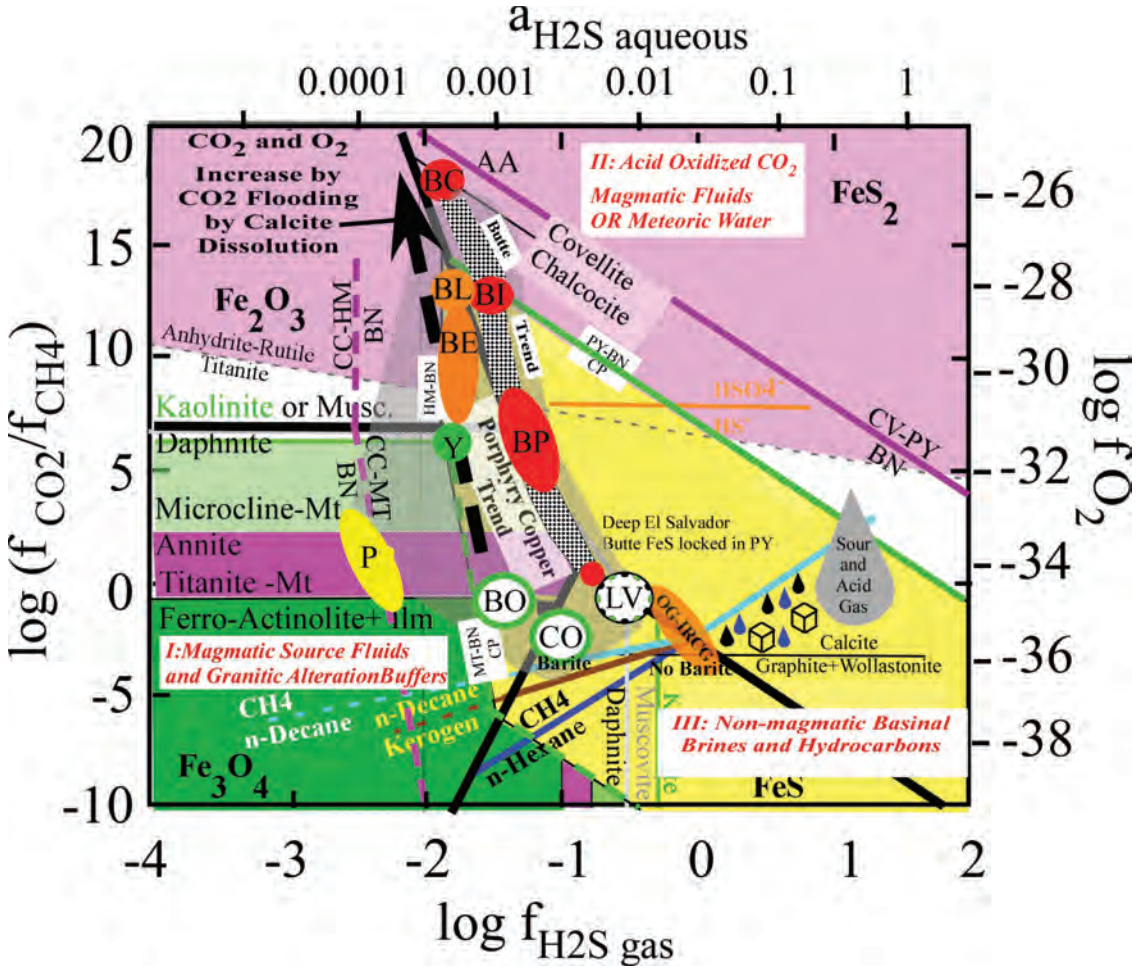

Figure 9. Color patterns are as follows: dark green represents actinolite, purple represents biotite, and light green represents chlorite in granitic magmas and related hydrothermal wall-rock alteration mineral assemblages defining reducing, low H2S conditions. Pink represents anhydrite either as a hydrothermal mineral or in evaporite sediments. Black oil droplet and cubes represent the hydrocarbon and salt brines emanating from sedimentary basin source rocks by diagenesis and maturation of organic carbon. Notice that these symbols occur near brown (kerogen) and blue (n-decane and n-hexane to methane) equilibria for petroleum products. Porphyry copper deposits shown in stipples define a nearly vertical band in which the Butte pre-Main Stage (BP), Intermediate Zone (BI), and Central Zone (BC) with covellite–chalcocite and advanced argillic alteration (AA) and alunite occur, forming the Butte Trend line, shown as a diamond checkerboard pattern. Other porphyry Cu deposits shown are Yerington (Y) and Panguna (P). Orbicular actinolite alteration at the Bingham Mine in Utah (BO) and the Clementine Prospect in Montana (CO) are shown as circles with a green rim and fall on the stippled porphyry copper trend line. Barite at Clementine proves that it is related to an oxidizing parent magma like Bingham, not a reducing magma as in the equi-granular orogenic gold-reduced cooper gold systems (OG-IRCG). The heavy black arrow depicts the effect of carbonate dissolution at depth, which drives up the CO_2/CH_4 ratio and the O_2 fugacity upwards along the granitic wall-rock and actinolite buffers, causing the sulfide mineral assemblages to evolve from pyrrhotite–chalcopyrite to chalcopyrite–bornite to bornite–chalcocite.

f CO_2/f CH_4 to rise by five orders of magnitude and the f O_2 by two orders of magnitude with incursion of meteoric water (Sheppard and Taylor, 1974). Point “BC” represents the Central Zone at Butte, Montana (Meyer and others, 1968; Guilbert and Zeihen, 1964), consisting of chalcocite–covellite–pyrite with advanced argillic alteration, often with alunite and pervasive sericite alteration that completely destroyed the buffer capacity of the Butte Granite (Brimhall, 1980). Using early mineral assemblages shown in table 4 from Einaudi and others (2003), “Y” for Yerington represents chalcopyrite–bornite–magnetite assemblages; “BE” and “BL” are for Bingham Canyon, Utah early and late sulfide assemblages. Shown as “BO” is distal orbicular Mg-rich actinolite alteration, first described by Atkinson and Einaudi (1978) in the Carr Fork area of the Bingham porphyry copper deposit. Such orbs have also been recognized at three deposits in Chile: Caspiche, La Escondida, and El Hueso; Cajamarca in Peru; Morenci and Fortitude Copper Canyon in the U.S.; Cananea in Mexico; and Oyu Tolgoi in Mongolia (Marco Einaudi, written commun.,2019). Finally, “CO” represents distal and high-level orbicular actinolite alteration with chalcopyrite, pyrrhotite, ilmenite, titanite (sphene), and actinolite at the Clementine Prospect, Montana (Brimhall, 2018; Brimhall and Fanning, 2019), mapped over a 2 by 6 km zone centered on a vein gossan system. Since Clementine has barite in sulfide assemblages, it is clear that the parental magma is

oxidizing, not reduced. Considering these data points together with geochemical evolution paths, porphyry copper mineral assemblages form a clear evolutionary trend line positioned along the hematite–pyrite and magnetite–pyrite boundaries, which coincides with a granitic wall-rock and potassic alteration buffer with Mg-rich biotite. Once oxidizing fluids interact with the early-stage mineral assemblages, the granitic rock buffer is outrun by sericitic alteration and the system evolves upwards in the diagram, where CO_2 dominates in meteoric fluids. In contrast, the reduced end of the trend has equal CH_4 and CO_2 fugacities and H_2S up to 10 times higher where distal orbicular actinolite alteration forms by diffusion at crack tips occurring along the edges of advection in porous wall-rock sediments (Brimhall, 2018). Here, rather than buffering by the potassic alteration assemblages, buffering is by ferro–actinolite–titanite–pyrrhotite.

Reaction Mechanism of Carbonate Sections of Wall Rocks on Cu and Critical Mineral Expression

Carbonate-bearing sedimentary wall rocks exert a far stronger hydrolysis effect on hydrothermal fluids than volcanic and plutonic wall rocks. Magma-derived acid attack of thick sections of carbonates produces CO_2 gas which rapidly elevates the CO_2/CH_4 ratio (eq. 9) and drives the fluid composition towards a higher oxidation state, as shown with the black arrow in figure 9 along the porphyry copper trend line. Both the Mississippian Madison (Mm) and Devonian (Dm) formations, with a combined thickness of 1,000 m (figs. 3, 4), served as external sources of CO_2 to the magmatic–hydrothermal system, forming a large open geochemical system. While the distal edges of a DASHER PCD has orbicular alteration at the base of the black arrow under a relatively low oxidation state, acid attack of the carbonate formations elevated the CO_2/CH_4 ratio and O_2 substantially from the chalcopyrite–pyrrhotite boundary up into the bornite and chalcocite fields along the edge of the granitic wall-rock and actinolite buffer boundaries. Compared to volcanic-hosted PCDs, carbonate dissolution also broadens the array of minerals precipitated so that a fuller expression of the overall suite of metals being transported from the parental magma is made possible including W, As, Sb, Ga, Te, Bi, and Se. It is possible also that dissolution of dolomite releases magnesium, which extends the solid solution range of hydrothermal biotite towards higher oxidation states and more copper-rich sulfides.

CO_2 Release by Limestone Dissolution, Causing Bornite Occurrence in Early Stage Porphyry Copper Deposits

Figure 9 illustrates an important difference between porphyry copper deposits developed entirely within plutonic wall rocks as at Butte, Montana and systems developed in wall-rock sequences containing major thicknesses of carbonates such as Bingham, Utah; Yerington, Nevada; El Salvador; Chile; Potrerillos, Chile; and Clementine, Montana. At Bingham, Utah the early sulfide assemblage with bornite and chalcopyrite (without pyrite or magnetite) is shown at point “BE” in an orange ellipse and the early bornite–chalcopyrite–magnetite assemblage at Yerington “Y” is shown in green, in contrast to the early assemblage of chalcopyrite–pyrite–magnetite at Butte “BP” in red, which lacks bornite (fig. 9). The consequence of the presence of bornite correlates with higher copper grade early stage ore assemblages than in deposits lacking early bornite as at Butte. This has a major impact on the concentration of gold as it substitutes for copper in early sulfides. Later sulfide assemblages involve incursion of meteoric water forming the intermediate “BI” and “BC” Butte Central Zone high sulfidation state assemblages with advanced argillic alteration and the Bingham “BL” late-stage chalcopyrite with pyrite (Marco Einaudi, written commun.). In summary, while admixture of oxidizing meteoric water may extend the oxidation trend considerably, the starting point with respect to the presence or absence of bornite may instead reflect incursion of CO_2-rich gases released from limestones at depth undergoing dissolution. Furthermore, while the redox state of parental magmas plays a role, the presence of a reactive carbonates in the wall-rock stratigraphic section also plays a determinative role in setting the early sulfide assemblage, copper, and gold grades.

Reduced “porphyry” copper–gold deposits described by Rowins (2000) are viewed by Einaudi and others (2003) as being more accurately classed with gold deposits related to reduced granites (e.g., Thompson and Newberry, 2000). Also reduced skarns often occur in clastic sedimentary sequences. The new phase equilibria offered here help explain these observations. Given the common pyrrhotite–pyrite–chalcopyrite sulfide assemblage, their reduced character, and the absence of barite or anhydrite, it is inferred here that a more accurate

name for these systems is reduced intrusion-related copper–gold deposits where the ore-forming fluid may have been derived from metasedimentary wall rocks and convected by heat from the cooling pluton as a sheeted quartz vein system without the local pluton being the dominant source of metals itself, as in porphyry copper deposits. Similarly, the orogenic gold systems may have derived their fluids from metasedimentary wall rocks as metamorphic fluids. Both ore types are labeled here as "OG-IRCG" and are shown in orange (fig. 9). These systems do not fall along the porphyry copper trend but are rather displaced to higher values of H_2S. The carbonate veins lacking sulfate minerals (anhydrite and barite) and methane-rich fluid inclusions and H_2S vapor phase are consistent with this conclusion (Mernagh and Bastrakov, 2013).

CO_2 Release by Limestone or Dolomite Dissolution, Causing Volume Change and Mineralized Breccia Formation

Unlike the normal hydrolysis reactions in PCDs when wall-rock minerals such as plagioclase are altered to sericite or clay minerals *in situ*, when acids dissolve calcite or dolomite, the release of CO_2 causes a very different result: the creation of gas-filled cavities. The potential for deformational mass transfer becomes highly likely (Brimhall and others, 1992). In contrast to water saturation, when porphyritic magmas saturate with water and explode, causing hydrofracturing and transferring the metals from the magma to the hydrothermal fluid, when carbonate minerals dissolve and release a gas phase that is less dense and more compressible than water, the volume change may be negative as void space is created. The potential for brecciation then becomes significant, but with a different mechanism than with typical hydrothermal breccias: collapse rather than explosion. This may explain both the breccia types at Clementine: the mineralized matrix vein breccia system and the earlier barren breccias. The apparent difference is the timing when the fugitive CO_2 gas phase intermingles with the ore-forming hydrothermal fluid. Given the difference in compressibility between CO_2 and water, it is possible that when gas-rich cavities form by carbonate dissolution, they affect the behavior of water in the nearby magma. If the pressure is lowered, then water saturation could be induced in the magma, thus extracting the metals via an escaping hydrothermal fluid. The resultant highly deformed rock mass would be dominated by brecccias to the extent that any hydrothermal breccia formed where water escaped the magma could be obliterated. Similarly, the stockwork of veinlets formed by hydrofracturing may be less well developed or absent. At Clementine, the mineralized matrix vein breccias occurred within throughgoing fractures that formed a vein system that extends for over 1 km. It is possible at depth, however, that the sulfide mineralization is not vein-controlled but instead is more distributed and massive, constituting the matrix between rock fragments.

Hydrothermal Fluid Characteristics

By considering hydrocarbon equilibria along with inorganic mineral assemblages, the phase relations in the CO_2/CH_4-H_2S coordinate system provide a powerful comparative framework for discerning genetic interrelationships expressed within a three-component fluid source mixing model. On one side of the triangle are the chemical evolution trajectories of porphyry copper deposits expressing their origin in granitic magmas, but eventually outrunning their influence as carbon dioxide flooding and sericitization destroys buffer mineral assemblages as oxidation by meteoric water or end-stage magmatic fluids increases the CO_2/CH_4 ratio by 15 orders of magnitude and the oxygen fugacity by 7 orders of magnitude. Sediment-hosted porphyry copper deposits extend this range downward by early high-temperature interactions with surrounding sedimentary wall rock, where diffusion-controlled growth of orbicular actinolite alteration forms and defines the outer edge of advective fluid flow. The CO_2/CH_4 ratio attending orb growth is 0.01 (log = -2), so CH_4 is about 99% and CO_2 is about 1%. Since the orbicular actinolite orb zones are mapped outside the marble front where the temperature was about 400 to 450°C, orbs represent the outer edge of the early high-temperature magmatic hydrothermal phase of PCD growth before incursion of CO_2-rich meteoric water with lower temperatures. Thus, if orbs grew under relatively high temperatures not much below 400°C, it raises questions as to the nature of the pore fluids before mineralization.

Hydrocarbon–Magmatic–Hydrothermal Fluid Mixing

Given the proximity of actinolite orbs and the spectrum of hydrocarbon equilibria derived from basin diagenesis as shown in figure 9, it is possible in some PCD environments for liquid and/or gaseous hydrocarbons generated by maturation of sedimentary organics in source rocks to have migrated into the same domal structure trap/reservoirs where later PCD magmatic/hydrothermal processes occurred. In such cases the apex PCD target environment would have been primed for interaction of hydrocarbons and magmatic–hydrothermal fluids (Zentilli and others, 1997; Ozdemir and Palabiyik, 2019). Comingling of hydrocarbon-rich fluids and hydrothermal fluids could have a spectrum of consequences from oil-filled vacuoles similar to those at the Culver Baer mercury mine in the Coast range, California (Peabody and Einaudi, 1992; Peabody 1993) or degraded bitumen in association with chalcocite, chalcopyrite, and bornite as at El Soldado, Chile (Zentilli and others, 1997), where petroleum occupied the host rock porosity before copper mineralization. At Clementine a central soil anomaly of Hg may be suggestive of such an interplay of hydrocarbons and magmatic–hydrothermal fluids evident in the proximity of the cinnabar–liquid mercury equilibria to the Clementine orb gas composition.

Conclusions

The deep apex sediment-hosted enhanced resource or the DASHER PCD model is presented here, combining PCD mineralization containing Cu, Ag, Sb, As, W, and Ga with earlier sedimentary phosphate with REEs and unconformity-related paleo-karst controlling high-grade Leadville, Colorado-style veins and Cu-Ag mantos since the same Mississippian age unconformity occurs in Montana and Colorado. This DASHER model includes multiple metals on the Critical Minerals list and phosphate. Since the sedimentary sequence at Clementine has 700 m of reactive Madison Limestone and 180 m of carbonaceous Jefferson dolomite at depth, the full range of magma-derived metals may be geochemically expressed in addition to the syngenetic REEs in the Phosphoria Formation. Domestic production of critical and basic minerals from DASHER PCDs could help reduce supply chain vulnerabilities.

However, the occurrence of REEs in the Phosphoria Formation highlights areas of overlapping mineral right laws, as phosphate is leasable while the metals are locatable. The high U content of the Phosphoria provides a means of mapping phosphate using aerial radiometric surveys.

Using chemical thermodynamic principles, a new equilibrium phase diagram proved that distal orbicular actinolite alteration is an integral part of PCD genesis and can be used reliably to help in targeting PCDs. By combining bulk and selective underground mining of the enhanced resource during the mine life cycle, innovative space utilization could minimize the environmental footprint on the surface. Regions where selective mining of phosphate occurs could be used as back-fill zones for development waste rock and flotation and phosphate leach plant gypsum products. Underground mining is primed for innovations in carbon-free electrification and use of autonomous vehicles. Over time, acceptance of the DASHER PCD model and innovations in underground mining might help soften if not transform the current negative attitudes about mining as a purely extractive industry and replace it with understanding of ore deposits as the primary origination point for a sustainable energy future.

Acknowledgments

The 2009 paper by late Harold Helgeson and associates, “A chemical and thermodynamic model of oil generation in hydrocarbon source rocks,” is a milestone in organic geochemistry and provided the chemical thermodynamic data necessary for this study to integrate organic and inorganic species with ore deposit geochemistry. Special gratitude is expressed to Jeff Dick, who patiently guided the first author in the use of his CHNOSZ computing software platform to perform thermodynamic calculations of equilibrium constants for reactions involving organic species and biomolecules included in the Helgeson and others (2009) paper. Kathy Ehrig’s thoughtful discussion significantly improved the fluid mixing interpretation. Marco Einaudi kindly helped to improve the clarity of presentation of the sulfide assemblages of porphyry copper deposits. A review by Alan Boudreau improved the clarity of this paper. Poul Emsbo shared his knowledge of REEs with the author, which is much appreciated. Jay Ague brought to the first author’s attention program SUPCRTBL for thermodynamic modeling, developed by Chen Zhu as a modification of SUPCRT program of the Helgeson Group and also in discussion of CO_2-driven oxidation processes. The author thanks his colleagues in Clementine Exploration for

their abiding interest and support, including Mary Jane Brimhall, Doug Fuerstenau, Ray Morley, Dan Kunz, Ed Rogers, Bruce Marsh, Abel Vanegas, Christ Lewis, and Tim Teague.

References

Ague, J.J., and Brimhall, G.H., 1987, Granites of the batholiths of California: Products of local assimilation and regional-scale crustal contamination: Geology, v. 15, p. 63–66.

Ague, J.J., and Brimhall, G.H.,1988, Regional variations in bulk chemistry, mineralogy, and the compositions of mafic and accessory minerals in the batholiths of California: Geological Society of America Bulletin, v. 100, p. 891–911.

Alpers, C.N., and Brimhall, G.H., 1988, Middle Miocene climatic change in the Atacama Desert, northern Chile: Evidence from supergene mineralization at La Escondida: Geological Society of America Bulletin, v. 100, p. 1640–1656.

Alpers, C.N., and Brimhall, G.H., 1989, Paleohydrologic evolution and geochemical dynamics of cumulative supergene metal enrichment at La Escondida, Atacama Desert, northern Chile: Economic Geology, v. 84, p. 229–255.

Atkinson, W., and Einaudi, M.T., 1978, Skarn formation and mineralization in the contact aureole at Carr Fork, Bingham, Utah: Economic Geology, v. 75, p. 1326–1365.

Ballard, W.W., Bluemle, J.P., and Gerhard, L.C., coordinators, 1983, Northern Rockies/Williston Basin correlation chart, *in* Correlation of stratigraphic units of North America: Tulsa, Oklahoma, American Association of Petroleum Geologists, 1 sheet.

Beaty, D., Landis, G., and Thompson, T., eds., 1990, Carbonate-hosted sulfide deposits of the central Colorado mineral belt: Economic Geology Monograph 7, 417 p.

Brimhall, G.H. Jr., 1973, Mineralogy, texture, and chemistry of early wall rock alteration in the deep underground mines and Continental area, *in* Miller, R.N., ed.,Guidebook for the Butte field meeting of the Society of Economic Geologists: Society of Economic Geologists Guidebook, Anaconda Company, Butte, Montana, p. H1–H5.

Brimhall, G.H., 1977, Early fracture-controlled disseminated mineralization at Butte, Montana: Economic Geology, v. 72, p. 37–59.

Brimhall, G.H, 1979, Lithologic determination of mass transfer mechanisms of multiple stage porphyry copper mineralization at Butte, Montana: Vein formation by hypogene leaching and enrichment of potassium-silicate protore: Economic Geology, v. 74, p. 556–589.

Brimhall, G.H., 1980, Deep hypogene oxidation of porphyry copper potassium-silicate protores: A theoretical evaluation of the copper remobilization hypothesis: Economic Geology, v. 75, p. 384-409.

Brimhall, G.H., 2018, Orbicular alteration at the porphyry copper prospect of southwest Montana: Defining the edges of advective flow in the porphyry copper paradigm: Montana Bureau of Mines and Geology Special Publication 120, p. 71–84.

Brimhall, G.H., and Crerar, D.A., 1987, Ore fluids: Magmatic to supergene, *in* Thermodynamic modeling of geological materials: Minerals, fluids and melts, I. Carmichael and H. Eugster, eds.: Mineralogic Society of America Reviews in Mineralogy, v. 17, ch. 10, p. 235–321.

Brimhall, G.H., and Fanning, M., 2019, Supporting the transition to deep porphyry copper exploration: SHRIMP U/Pb radiometric dating of titanite ($CaTiSiO_5$) in the distal and superjacent orbicular alteration zone of the Clementine prospect, southwest Montana: Montana Bureau of Mines and Geology Special Publication 121, p. 117–132.

Brimhall, G.H., and Ghiorso, M.S., 1983, Origin and ore-forming consequences of the advanced argillic alteration process in hypogene environments by magmatic gas contamination of meteoric fluids: Economic Geology, v. 78, p. 73–90.

Brimhall, G.H., and Marsh, B.D., 2017, Nature of the mineralization and alteration mapped at the Clementine porphyry copper prospect in the northern Pioneer Mountains of southwest Montana: Unpublished Abstract, Montana Bureau of Mines and Geology.

Brimhall, G.H., and Vanegas, A., 2001, Removing science workflow barriers to adoption of digital geological mapping by using the GeoMapper universal program and visual user interface, *in* Soller, D.R., ed., Digital Mapping Techniques ’01—Workshop proceedings: U.S. Geological Survey Open-File Report 01-223, p. 103–114, available at http://pubs.usgs.gov/of/2001/of01-223/brimhall.html [Accessed January 2022].

Brimhall, G.H., Alpers, C.N., and Cunnigham, A.B., 1985a, Analysis of supergene ore-forming processes and ground water solute transport using mass balance principles: Economic Geology, v. 80, p. 1227–1256.

Brimhall, G.H., Agee, C., and Stoffregen, R., 1985b, Hydrothermal conversion of hornblende to biotite: Canadian Mineralogist, v. 23, p. 369–379.

Brimhall, G.H., Chadwick, O.A., Lewis, C.J., Compston, W, Williams, I.S., Danti, K.J., Dietrich, W.E., Power, M.E., Hendricks, D., and Bratt, J., 1992, Deformational mass transport and invasive processes in soil evolution, Science, v. 255, p. 695–702.

Brimhall, G.H., Vanegas, A., and Lerch, D., 2002, GeoMapper Program for paperless field mapping with seamless map production in ESRI ArcMap and GeoLogger for drill-hole data capture: Applications in geology, astronomy, environmental remediation and raised relief models, *in* Soller, D.R., ed., Digital Mapping Techniques’02—Workshop proceedings: U.S. Geological Survey Open-File Report 02-370, p 141–151, available at http://pubs.usgs.gov/of/2002/of02-370/brimhall.html [Accessed January 2022].

Brimhall, G.H., Dilles, J., and Proffett, J., 2006, The role of geological mapping in mineral exploration in wealth creation in the minerals industry: Special Publication 12, Anniversary Publications of the Society of Economic Geologists, p. 221–241.

Brumbaugh, D.S., 1973, Structural analysis of the complexly deformed Big Hole River area, Madison, Beaverhead, and Silver Bow Counties, Montana: Bloomington, Ind., Indiana University, Ph.D. thesis, 96 p.

Candela, P.A., and Piccoli, P. M., 2005, Magmatic processes in the development of porphyry-type ore systems: Economic Geology 100th Anniversary Volume, v. 25–38.

De Voto, 1988, Late Mississippian paleokarst and related mineral deposits, Leadville Formation, central Colorado: Paleokarst, N.Y., Springer-Verlag, p. 278–305.

Dick, Jeffrey M., 2019, CHNOSZ: Thermodynamic calculations and diagrams for geochemistry: Frontiers in Earth Science, available at https://doi.org/10.3389/feart.2019.00180 [Accessed January 2022].

Dickinson, W., 1981, Plate tectonics and the Continental Margin of California, *in* The geotectonic development of California, Rubey Volume: Englewood Cliffs, N.J., Prentice Hall, p. 1–18.

Dilles, J.H., and Einaudi, M.T., 1992, Wall-rock alteration and hydrothermal flow paths about the Ann-Mason porphyry copper-deposit, Nevada—a 6-km vertical reconstruction: Economic Geology, v. 87, p. 1963–2001.

Dott, Robert H. Jr., 1992, Eustasy: The Historical ups and downs of a major geological concept: Geological Society of America Memoir 180, 83–91.

Dott, Robert H. Jr., 2014, Rock Stars: Lawrence L. Sloss and the sequence stratigraphy revolution: GSA Today, March, p. 24–26.

Einaudi, M.T., 1977, Environment of ore deposition at Cerro de Pasco, Peru: Economic Geology, v. 72, p. 893–924.

Einaudi, M.T., Hedenquist, J., and Inan, E., 2003, Sulfidation state of fluids in active and extinct hydrothermal systems, Giggenbach Volume, Simmons, S.F., ed.: Society of Economic Geologists and Geochemical Society Special Publication 10, p. 285–313.

Emsbo, P., McLaughlin, P. I., Breit, G.N., du Bray, E.A., and Koenig, E.A., 2015, Rare earth elements in sedimentary phosphate deposits: Solution to the global REE crisis?: Gondwana Research, v. 27, p. 776–785.

Emsbo, P., McLaughlin, P. I., du Bray, E.A., Anderson, E.A., Vandenbroucke, T.R., and Zielinski, R.A., 2016, Rare Earth elements in sedimentary phosphorite deposits: A global assessment: Reviews in Economic Geology, v. 18, ch. 5, p. 101–113.

Gong, D., Huang, S., Wu, W., Yu, C., Fang, C., and Liu, D., 2014, Characteristics of gas compositions in giant gas fields of China: Energy exploration and Exploitation, v. 32, p. 635–656.

Greenwood, H., 1967, Wollastonite: Stability in H_2O-CO_2 mixtures and occurrence in a contact-metamorphic aureole near Salmo, British Columbia, Canada: American Mineralogist, v. 52, p. 1669–1680.

Guilbert, J.M., and Zeihen, G.L., 1964, The mineralogy of the Butte district, Montana: Montana Bureau of Mines and Geology Open-File Report 268, 38 p.

Gustafson, L.B., and Hunt, J.P., 1975, The porphyry copper deposit at El Salvador, Chile: Economic Geology, v. 70, p. 857–912.

Hein, J., Perkins, R., and McIntyre, 2014, Evolution of thought concerning the origin of the Phosphoria Formation, western U.S. phosphate field, *in* Hein, James R., ed.. Handbook of exploration and environmental geochemistry, v. 8, Hale, M., series ed.: Amsterdam, Elsevier, p. 19-42.

Helgeson, H.C., Delany, J.M., Nesbitt, H.W., and Bird, D.K., 1978, Summary and critique of the thermodynamic properties of rock-forming minerals: American Journal of Science, v. 287-A, p. 1–229.

Helgeson, H.C., Owens, C.E., Knox, A.M., and Laurent, R., 1998, Calculation of the standard molal thermodynamic properties of crystalline, liquid, and gas organic molecules at high temperatures and pressures: Geochimica Cosmochimica Acta, v. 62, p. 985–1081, doi: 10.1016/S0016-7037(97)00219-6

Helgeson, H.C., Laurent, R., McKenzie, W.F., Norton, D.L., and Schmitt, A., 2009, Chemical and thermodynamic model of oil generation in hydrocarbon source rocks: Geochimica Cosmochimica Acta, v. 73, p. 594–695, doi: 10.1016/j.gca.2008.03.004

Hemley, J.J., Montoya, J.W., Marinenko, J.W., and Luce, R.W., 1980, Equilibria in the system Al_2O_3-SiO_2-H_2O and some general implications for alteration/mineralization processes: Economic Geology, v. 75, p. 210–228.

Hildenbrand, T.G., Berger, B.R., Jachens, R.C., and Ludington, S.D., 2000, Regional crustal structures and their relationship to the distribution of ore deposits in the Western United States, based on magnetic and gravity: Economic Geology, v. 95, p. 1583–1603.

Hintze, L.F., 1985, Great Basin correlation chart, *in* Correlation of stratigraphic units of North America: Tulsa, Oklahoma, American Association of Petroleum Geologists.

Hofstra, A., and Cline, J., 2000, Characteristics and models for Carlin-type gold deposits: Society of Economic Reviews, v. 13, p. 163–220.

Holland, H.D., 1959, Some Applications of thermochemical data to problems of ore deposits.stability relations among the oxides, sulfides, sulfates, and carbonates of ore and gangue metals: Economic Geology, v. 54, p. 184-233.

Holland, T., and Powell, R., 2011, An improved and extended internally consistent thermodynamic dataset for phases of petrological interest, involving a new equation of state for solids: Journal Metamorphic Geology, v. 29, p, 333–383.

John, D.A., Ayuso, R.A., Barton, M.D., Blakely, R.J., Bodnar, R.J., Dilles, J.H., Gray, F., Graybeal, F.T., Mars, J.C., McPhee, D.K., Seal, R.R., Taylor, R.D., and Vikre, P.G., 2010, Porphyry copper deposit model, ch. B, *in* Mineral deposit models for resource assessment: U.S. Geological Survey Scientific Investigations Report 2010–5070–B, 169 p.

Johnson, J., Oelkers, E., and and Helgeson, H., 1992, SUPCRT92: A software package for calculating the standard molal thermodynamic properties of minerals, gases, aqueous species, and reactions from 1 to 5000 bar and 0 to 1000°C: Computers and Geoscience, v. 18, no. 7, p. 899–947.

Kalakay, T., John, B., and Lageson, D., 2001, Fault-controlled pluton emplacement in the Sevier fold-and-thrust belt of southwest Montana, USA: Journal of Structural Geology, v. 23, no. 6-7, p. 1151–1165.

Kent, H., Couch, E., and Knepp, R., 1988, Southern and central Rockies, *in* Correlation of stratigraphic units of North America: Tulsa, Oklahoma, American Association of Petroleum Geologists.

Khashgerel, B., Kavalieris, I., and Hayashi**,** K., 2008, Mineralogy, textures, and whole-rock geochemistry of advanced argillic alteration: Hugo Dummett porphyry Cu–Au deposit, Oyu Tolgoi mineral district, Mongolia: Mineralia Deposita, v. 43, p. 913–932.

Lageson, D., and Schmidt, J., 1994, The Sevier orogenic belt of the western United States: Recent advances in understanding its structural and sedimentologic framework: Mesozoic Systems of the Rocky Mountain Region, USA, AAPG Data Pages, p. 27–64.

Lanari, P., and Duesterhoeft, E., 2019, Modeling metamorphic rocks using equilibrium thermodynamics and internally consistent databases: Past achievements, problems and perspectives: Journal of Petrology, v. 60., no. 1, p. 19–56.

Lowell, J.D., and Guilbert, J., 1970, Lateral and vertical alteration-mineralization zoning in porphyry ore deposits: Economic Geology, v. 65, p. 373–408.

Meinert, L., 1982, Skarn, manto, and breccia pipe formation in sedimentary rocks of the Cananea mining district, Sonora, Mexico: Economic Geology, v. 77, p. 919–949.

Mernagh, T.P., and Bastrakov, E.N., 2013, An evaluation of hydrogen sulfide in orogenic gold fluids and the uncertainties associated with vapor-rich inclusions: Geofluids, v. 13, p. 494–505.

Meyer, C., and Hemley, J.J., 1967, Wall rock alteration, *in* Barnes, H.L., ed., Geochemistry of hydrothermal ore deposits: N.Y., Holt, Rinehart, and Winston, p. 166–232.

Meyer, C., Shea, E., Goddard, C., and staff, 1968, Ore deposits at Butte, Montana, *in* Ridge, J.D.,ed., Ore deposits of the United States 1933–1967, The Graton-Sales Volume: N.Y., American Institute of Mining, Metallurgical, and Petroleum Engineers, v. 2, p. 1363–1416.

National Research Council, 2013, Underground engineering for sustainable urban development: Washington, DC, The National Academies Press, 221 p., doi: https://doi.org/10.17226/14670.

Nemcok, M., and Henk, A., 2006, Oil reservoirs in foreland basins charged by thrust belt source rocks: Insights from numerical stress modelling and geometric balancing in the West Carpathians: Geological Society London Special Publications v. 253, no. 1, p. 415–428.

Pearson, R., Trautwein, C., Ruppel, E., Hanna, W., Rowan, L., Loen, J., and Berger, B., 1992, Mineral resource assessment of the Dillon 1° x 2° quadrangle, Idaho and Montana: U.S. Geological Survey Circular 1077, 14 p.

Ozdemir, A., and Palabiyik, Y., 2019, Significance of relationships between hydrocarbons and metallic ore deposits in oil and gas exploration: Part II. Copper deposits: Ankara, Turkey, Conference Proceedings.

Peabody, C., 1993, The association of cinnabar and bitumen in mercury deposits of the California Coast Ranges, *in* Parnell, J., and others, eds., Bitumens in ore deposits: Berlin, Springer-Verlag, p. 178–209.

Peabody, C., and Einaudi, M., 1992, Origin of petroleum and mercury in the Culver Baer cinnabar deposit, Mayacmas District, California: Economic Geology, v. 87, p. 1078–1103.

Roberts, S.A., 1973, Pervasive early alteration in the Butte district, Montana, *in* Miller, R.N., ed., Guidebook for the Butte field meeting of the Society of Economic Geologists: Society of Economic Geologists Guidebook, Anaconda Company, Butte, Montana, p. HH1–HH8.

Roberts, S.A., 1975, Early hydrothermal alteration and mineralization in the Butte district, Montana: Harvard University, Ph.D. dissertation, 157 p.

Rowins, S.M., 2000, Reduced porphyry copper-gold deposits: A new variation on an old theme: Geology, v. 28, no. 6, p. 491–494.

Runyon, S., Nickerson, P., Seedorff, E., Barton, M., and Mazdab, F., 2018, Sodic-calcic family of alteration in porphyry systems of Arizona and adjacent New Mexico: Economic Geology, v. 114, p. 745–770.

Ruppel, E.T., and Lopez, D., 1984, The thrust belt in southwest Montana and east-central Idaho: U.S. Geological Survey Professional Paper 1278, 41 p.

Ruppel, E.T., O'Neill, J.M., and Lopez, D.A., 1993, Geologic map of the Dillon 1° x 2° quadrangle, Idaho and Montana: U.S. Geological Survey Miscellaneous Investigation Series 1803-H.

Sando, W.J., 1988, Madison Limestone (Mississippian) Paleokarst: A geologic synthesis: Paleokarst, N.Y., Springer-Verlag, p. 256–277.

Schmidt, C., Smedes, H., and O'Neill, M., 1990, Syncompressional emplacement of the Boulder and Tobacco Root Batholiths (Montana-USA) by pull-apart along Old Fault Zones: Geological Journal, v. 25, no. 304, p. 305–318.

Seedorff, E., Dilles, J., Proffett, J., Einaudi, M., Zurcher, L., Stavast, W., Johnson, D., and Barton, M., 2005, Porphyry deposits: Characteristics and origin of hypogene features: Economic Geology 100th Anniversary Volume, p. 251–298.

Sheppard, M.F., and Taylor, H.P., Jr., 1974, Hydrogen and oxygen isotope evidence for the origins of water in the Boulder batholith and Butte ore deposits, Montana: Economic Geology, v. 69, p. 926–946.

Sillitoe, R., 2010, Porphyry copper systems: Economic Geology, v. 105, no. 1, p. 3–41.

Sloss, L., 1963, Sequences in the cratonic interior of North America: Gcological Society of America Bulletin, v. 74, p. 93–114.

Sloss, L., and Laird, W.M., 1947, Devonian system in central and northwestern Montana: Bulletin of the American Association of Petroleum Geologists, v. 31, no. 8, p. 1404–1430.

Sloss, L., and Moritz, C.A., 1951, Paleozoic stratigraphy of southwestern Montana: Bulletin of the Society of Petroleum Geologists, v. 35, no. 10, p. 2135–2169.

Taylor, H.P. Jr., 1974, The application of oxygen and hydrogen isotope studies to problems of 1035 hydrothermal alteration and ore deposition: Economic Geology, v. 69, p. 843–883.

Thompson, J.F.H., and Newberry, R.J., 2000, Gold deposits related to reduced granitic intrusions: Reviews in Economic Geology, v. 13, p. 377–400.

Tomkins, A., and Grundy, C., 2009, Upper temperature limits of orogenic gold deposit formation: Constraints from the granulite-hosted Griffin's Find Deposit, Yilgarn craton: Economic Geology, v. 104, pp. 669–685.

Underground Engineering for Sustainable Urban Development, 2013, The National Academies Press, 221 p.

Vail, P.R., and Mitchum, R.M., 1977a, Seismic stratigraphy and global changes of sea level, Part 1: Overview, *in* Payton, C.E., ed., Seismic stratigraphy—Applications to hydrocarbon exploration: AAPG Memoir 26, p. 51–52.

Vail, P.R., Mitchum, R.M., Todd, R.G., Widmier, J.M., Thompsom, S., Sangree, J.B., Bubb, J.N., and Hailelid, W.G., 1977b, Seismic stratigraphy and global changes in sea level, *in* Payton, C.E., ed., Seismic stratigraphy—Applications to hydrocarbon exploration: AAPG Memoir 26, p. 49–212.

Windman, T., and Shock, W., 2008, A web-based interactive version of SUPCRT92: Computers & Geosciences, v. 90, part A, May 2016, p. 97–111.

Wood, B.J., 1987, Thermodynamics of multicomponent systems containing several solid solutions, *in* Carmichael, I.S.E. and Eugster, H.P., eds., Thermodynamic modeling of geological materials: Minerals, fluids and melts: Mineralogical Society of America, Reviews in Mineralogy, v. 17, p. 71–95.

Woodhead, J., and Mathieu, L., 2021, Harnessing the power of artificial intelligence and machine learning in mineral exploration—Opportunities and cautionary notes: SEG Discovery, October, p. 19–31.

Worden, R.H., Griffiths, J., Wooldridge, L.J., Utley, J.E.P., Lawan, A.Y., Muhammed, D.D., Simon, N., and Armitage, P.J., 2020, Chlorite in sandstones: Earth-Science Reviews, v. 204, doi: 10.1016/j.earsci-rev.2020.103105.

Zentilli, M., Munizaga, F., Graves, M., Boric, R., Wilson, N., Mukhopadhyay, P., and Snowdon, L., 1997, Hydrocarbon involvement in the genesis of ore deposits: An example in cretaceous stratabound (manto-type) copper deposits of central Chile: International Geology Review, v. 39, p. 1–21.

Zen, E-An, 1988, Bedrock geology of the Vipond Park quadrangle: U.S. Geological Survey Bulletin 1625, 49 p.

Zimmer, K., Zhang, Y., Peng, L., Yanyan, C., Guanru, Z., Mehmet, D., and Zhu, C., 2016, SUPCRTBL: A revised and extended thermodynamic dataset and software package of SUPCRT92: Computers & Geosciences, v. 90, part A, p. 97–111.

The Montana Tunnels open pit mine. Photo by Peter Larson.

Mining History and Mineralogy of the Black Pine Mine, Granite County, Montana

Michael J. Gobla

Engineer, U.S. Department of the Interior, Bureau of Reclamation, Denver, Colorado

Introduction

The Black Pine mine is located 10 mi northwest of Philipsburg in sections 16, 17, and 21, T. 8 N., R. 14 W., in the John Long Mountains in Granite County, Montana. Discovered in 1882, the Black Pine mine, also called the Combination mine, produced 5.62 million oz of silver. In the 1980s the mine produced excellent crystals of cerussite, hübnerite, pyrite, quartz, and tetrahedrite and became a prolific source of rare minerals, which occur mostly as microcrystals. A total of 80 different mineral species have been identified as occurring at the Black Pine mine. The mine is the type locality for three new minerals: auriacusite, joëlbruggerite, and philipsburgite.

Geology

The deposit occurs in the Mount Shields Formation of the Belt Supergroup metasediments. There are four veins—the Upper, Tim Smith, Combination, and Onyx veins—that were emplaced along low-angle thrust faults (Waisman, 1992). The igneous source for the vein formation is not known but is suspected to be a buried intrusion. There are intrusive stocks located a few miles to the east and north, but these are too far away to have caused the formation of the Black Pine veins. Initial mining produced minor amounts of ore from all four veins, but during the first year of mining it became evident that only the Combination vein had significant quantities of rich silver ore.

Mining History

Mining claims were staked in 1882 by Aeneas McAndrews in a new mining district called Black Pine. The initial production was in November 1885, when 400 tons of ore were shipped to the Hope mill in Philipsburg. The test shipment yielded a small profit and demonstrated the value of the mine. This action resulted in more prospecting and claim staking in the area and attracted the attention of investors. James A. Pack leased the claims for $25,000 and on October 6, 1886, the Black Pine Mining Company was incorporated with J.M. Merrill of Butte as president, William P. Shryock of St Louis as vice president, Joseph H. Harper of Butte as secretary and treasurer, and James A. Pack as superintendent and manager, along with Frederick W. Flint, Ralph B. Wallace, and Aeneas McAndrews. A mining town called Black Pine (after the Black Pine Mining Company) was established in 1887.

The new company acquired 15 claims and began work in December 1886 with a crew of 13 men. The main shaft was on the Oxide claim. The shaft was 150 ft deep and about to commence ore production when the shaft house burned down in June 1887. This put the company in a difficult financial situation while they were trying to complete construction of a 10-stamp mill. The shaft house was rebuilt, and the mill began operations on July 12, 1887 with 17 men employed at the mine and 11 in the mill (fig. 1).

The Black Pine Mining Company shipped five bars containing 900 oz of silver in August but did not pay wages to the miners or pay any of its bills. There also were four more bars of silver bullion and several

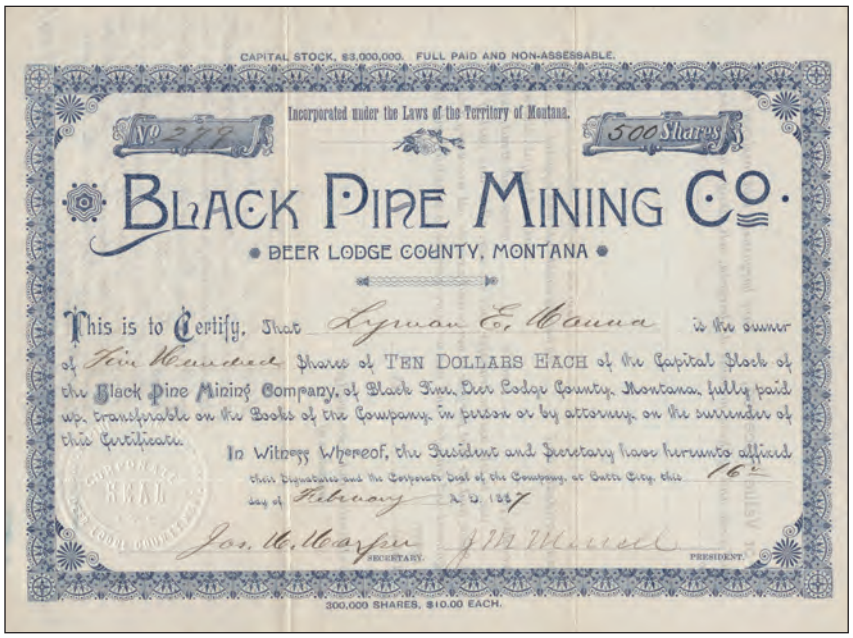
CAPITAL STOCK, $3,000,000. FULL PAID AND NON-ASSESSABLE.

Incorporated under the Laws of the Territory of Montana.

No 378 500 Shares

BLACK PINE MINING CO.

DEER LODGE COUNTY, MONTANA

This is to Certify, That Lyman E. Wanna is the owner of Five Hundred Shares of TEN DOLLARS EACH of the Capital Stock of the Black Pine Mining Company, of Black Pine, Deer Lodge County, Montana, fully paid up, transferable on the Books of the Company, in person or by attorney, on the surrender of this Certificate.

In Witness Whereof, the President and Secretary have hereunto affixed their Signatures and the Corporate Seal of the Company, at Butte City, this 16th day of February A. D. 1887

Jos. H. Harper SECRETARY. J. M. Merrill PRESIDENT.

300,000 SHARES, $10.00 EACH.

Figure 1. Stock certificate issued by the Black Pine Mining Company in February 1887 (Michael Gobla collection).

hundred pounds of amalgam in the mill about to be processed for shipment. This angered the workers; since the mill was finally producing silver bullion, they believed it was time to start paying wages and the debts of the company. Thirty-six people filed suit in September and the property was seized by the Sheriff to be sold at auction on October 8, 1887. The property was purchased by Charles D. McLure, who was the former superintendent of the Hope mill. At the time, McClure was making a fortune in silver from his development of the Granite mine near Philipsburg. McLure was able to attract investors to form a new mining company. On December 30, 1887 the Combination Mining and Milling Company was incorporated by C.D. McLure, E.H. Wilson, H. Williams, C.W. Goodale, Ed Maule, J. Harper, A.H. Barrett, and Patrick Talent (fig. 2). John M. Long was put in charge as superintendent of the mining operation. Long was a miner from the Comstock who was in charge of several mines in Butte when the company hired him.

Figure 2. Stock certificate issued in 1896 by the Combination Mining and Milling Company, which operated the Black Pine mine, Granite County (Michael Gobla collection).

Initially, $41,000 worth of stock was subscribed. With this cash the company paid its bills and resumed operations at the mine in January 1888. Although the mine, mining district, and the town were all named Black Pine, McLure changed the names to Combination in honor of his new company. The company would not hire anyone that drank alcohol, nor allow it to be sold in the town. As a result, bars and gambling houses became established above the town to the north just beyond the company-owned land.

Figure 3. Illustration of the Black Pine mill, Granite County (Weitfle, 1891).

The mill was expanded to 20 stamps and resumed operation by June 1888. On the last day of August 1889, there was a devastating fire that burned the shaft house, the C.E. Miller store, the boarding house, several residences, and a large area of the adjacent forest. The damage was $6,000, but insurance only covered $2,500 of it. The facilities were rebuilt, and the operation was resumed. The holdings eventually grew to 52 patented and 5 unpatented lode claims, and 15 patented mill site claims. Profitable operations allowed for an expansion of the mill to 30 stamps in 1891 (figs. 3, 4; Volin and others, 1952).

The mine closed July 1, 1893 due to the silver crash, putting 130 people out of work. The mine was reopened a short time later on a smaller scale and continued operations until 1897, when the

Figure 4. Illustration of the town of Black Pine; in 1890 the population was 100 people (Weitfle, 1891).

operations became unprofitable and the company went into debt. From initial operations in 1885 to closure in 1897, a total of 2,185,000 oz of silver and 1,411 oz of gold was produced from approximately 100,000 tons of ore (Walker, 1960).

The property was sold on May 11, 1900 to pay the company's debt of $40,000. In 1916, C.D. McClure increased his ownership of the Combination company to 95% by trading his partial ownership in the Granite Mountain–Bimetallic mines for Combination stock. He later acquired complete ownership of the property, but he died in 1918 heavily in debt.

The Black Pine Leasing Company installed a steam hoist in May 1919 and began pumping out the mine. William, the son of Charles McClure, was involved with the effort, which exposed some rich ore. In 1922 the property was sold, but the McLure family fought this and eventually acquired clear title to the mine. The mine was operated by Willian R. McLure on a small scale and later by the Hecla Mining Company, but Hecla declined to purchase the mine. In 1931 the McLure family defaulted on a mortgage and the mine was sold to Herbert Fay, who then sold it to Walter L. Pope and J.F. Harrington.

In May 1932, three people from the McLure family, along with some Seattle investors, formed Black Pine Mines, Inc., which purchased the property and erected a 200 ton/day mill. Operations resumed, but by 1935 the operation was no longer profitable. There were changes in capitalization and the company name was changed to Black Pine Silver Mines, Inc. Ownership transferred to Mr. August Buschmann of Seattle, who was a major investor in the company. In 1936 the property was purchased by a company called Combination Silver Mines, Inc., and it was active until about 1942 with Black Pine Silver Mines, Inc. as a major stockholder. Mr. Buschmann had been loaning the company money, and in 1940 he foreclosed. He took title in 1941 and the Black Pine Silver Mines, Inc. and Combination Silver Mines, Inc. were dissolved. The Montana Climax Corporation purchased the property from Mr. Buschmann for $150,000 in 1959 and they operated the mine in 1964.

Inspiration Development Company, a subsidiary of Inspiration Consolidated Copper Company, leased the mine in 1970 and purchased the property in 1974. Starting in April 1974, a 1,000 ton/day underground mine was developed by Inspiration under the name Black Pine Mining Company. It was mined by the room and pillar method from 1974 until 1980, when it closed due to low silver prices. It soon reopened and was worked full time to 1988, and then intermittently until the mine closed in 2000. The last operation of the mine was by the American Smelting and Refining Company, who purchased the mine in 1990 and mined lower grade ore as

silica flux for the East Helena smelter (fig. 5). A total of $17.3 million was provided for site reclamation by the Montana Environmental Trust Group, LLC, which was established to oversee the resources from the ASARCO bankruptcy settlement.

Figure 5. The Black Pine mine as it appeared in 2003. This waste rock pile was a popular collecting locality after the mine closed.

The modern mine produced ore averaging 5.7 oz of silver per ton with copper, lead, and zinc being recovered in the mill concentrate. The total mine production is 5,622,000 oz of silver, 3,000 oz of gold, 10,678,000 lbs of copper, along with some lead and zinc (Spanski, 2004). In 2005, ASARCO filed for bankruptcy and the Montana Environmental Trust took over ownership of the property. In 2016 the State of Montana began site reclamation. The project removed 400,000 yd^3 of tailings and waste rock, which was placed into an onsite repository. Unfortunately, a major source of rare minerals was lost with the removal and burial of the waste rock pile (figs. 6, 7).

Mineralogy

The unusual mineralogy of the Black Pine mine was recognized shortly after mining began, when Dr. Richard Pearce identified the presence of hübnerite and pseudomalachite in specimens recovered from the mine (Hillebrand, 1884). The mine also won an award for its copper ore and pyrite displayed at the 1893 World's Fair in Chicago. Little attention was given to the mineralogy until the mine reopened in 1974. Unusual minerals were encountered, and specimens were taken to Mr. Lester Zeihen at the Montana Bureau of Mines and Geology in Butte for identification by X-ray diffraction analysis. The mine began producing the world's best veszelyite crystals, which because of their beauty were sought out by mineral museums and collectors throughout the world (fig. 8). By the mid-1980s, Mr. Zeihen had identified 33 minerals, including numerous rare arsenate species. A green mineral with a unique x-ray pattern was found. Further work would result in the naming of a

Figure 6. Photograph from the Montana DEQ showing the construction of the waste repository where the mill tailings and waste rock were buried.

Figure 7. The Black Pine Mine waste-rock pile has been removed as shown in this photograph of the site taken in 2021.

Figure 8. An exceptional thumbnail specimen of veszelyite crystals (2.1 x 2.1 cm) from the Black Pine mine, Granite County, from the Alan Young collection (photograph by Jeff Scovil).

new species called philipsburgite (Pecor and others, 1985). Investigation of the deposit led to two master's theses being written, one studying the geology and mineralogy (Waisman, 1985), and one studying the paragenetic relationships, zoning, and mineralogy (Zeihen, 1985).

As the academic studies began, crystal specimens of many different minerals such as azurite, brochantite, hübnerite, philipsburgite, pyrite, Japan-law twin quartz, and tetrahedrite began appearing in Butte rock shops. Because of the size of the crystal pockets, most of the specimens were thumbnail (1 in) size specimens. Butte mineral dealer Duane Johnson signed a contract with the mining company in the 1980s to recover crystal specimens, which he sold at the Denver, Tucson, and several of the Montana mineral shows. Specimens were also recovered by the miners.

Continued study included the discovery of two more new minerals to science: auriacusite and joëlbruggerite, which were collected from a rock pile outside the mine by John Dagenais of Vancouver, British Columbia, in the spring of 1993. Specimens from the deposit continue to be studied. With a total of 80 different mineral species, including 3 type minerals, the Black Pine mine is a world-class mineral locality. The mine closed in 2000, and since then the site has been reclaimed, thus ending the supply of specimens from the mine. An alphabetical list describing the 80 known minerals from the Black Pine mine follows:

Acanthite Ag_2S

Acicular acanthite microcrystals associated with small grains of native silver have been collected from the waste rock dump.

Adamite $Zn_2AsO_4(OH)$

The cuprian variety of adamite occurs as emerald green diamond-shaped microcrystals with pale green terminations, perched on quartz in association with bayldonite (Zeihen, 1985).

Aikinite $PbCuBiS_3$

A tentative identification was made using optical properties and microprobe results. Aikinite was observed as subhedral prismatic grains in a few polished sections in association with tetrahedrite (Zeihen, 1985).

Anglesite $Pb(SO_4)$

Anglesite occurs as massive coatings on altered galena and as small, colorless prismatic spear-shaped crystals, and as tabular prisms similar in appearance to cerussite forms (Zeihen, 1985).

Arsenbrackebuschite $Pb_2(Fe^{3+},Zn)(AsO_4)_2(OH,H_2O)$

A specimen of aesenbrackebuschite from the Black Pine mine is reported on the mindat website as being in the collection of J. Dagenais.

Arsentsumebite $Pb_2Cu(AsO_4)(SO_4)(OH)$

Initially reported as tsumebite found in only two specimens (Zeihen, 1985). Rare as green microcrystals

(Waisman, 1992). Additional specimens were found but analysis showed they are arsentsumebite, not tsumebite (Jensen and Nikischer, 2012). It occurs as pale green platy microcrystals in rosette-like groups, and small, pale lime-green globular coatings on quartz and as overgrowths on mimetite or duftite.

Arthurite $CuFe^{3+}_2(AsO_4)_2(OH)2•4H_2O$

A rare occurrence as microcrystals (Waisman, 1985, 1992).

Auriacusite $Fe^{3+}Cu^{2+}(AsO_4)O$

The Black Pine mine is the type locality for this new mineral, which is an iron-containing mineral of the olivenite group (Piilonen and others, 2010). It was collected from a rock pile outside of the mine by John Dagenais. Auriacusite occurs as golden yellow to yellow-brown needles and fibrous mats lining small vugs in quartz and coating quartz crystals. The needles are tiny, being only 1 to 2 μm thick, by 5 μm wide, by 100 μm (0.1 mm) long, so it would be easy to overlook even when examining samples with a microscope. It is associated with brochantite, pyrite, and tetrahedrite. The mineral is named for the Latin “auri” meaning golden yellow and “acus” meaning needle. Co-type specimens are no. 6234 in the Mineral Sciences Department, Natural History Museum Los Angeles County, California, USA, and no. CNMMC 86090 in the Canadian Museum of Nature, Ottawa, Canada (Mills and others, 2010a).

Aurichalcite $(Zn,Cu)_5(CO_3)_2(OH)_6$

Rarely found as pale blue microcrystals in vuggy quartz, on chrysocolla, and as spherical aggregates on hemimorphite (fig. 9; Zeihen, 1985; Waisman, 1985, 1992).

Figure 9. Acicular microcrystals of aurichalcite (3 mm long needles in a 1 cm wide field of view) on quartz with a cluster of hemimorphite at left, Black Pine mine (Michael Gobla collection).

Azurite $Cu_3(CO_3)_2(OH)_2$

As crystalized crusts, stubby prismatic microcrystals, and rosette-like microcrystal aggregates on quartz, often associated with malachite, brochantite, and chrysocolla (fig. 10; Waisman, 1985, 1992).

Baryte $Ba(SO_4)$

Baryte occurs rarely as colorless transparent to white translucent plate-shaped microcrystals (Zeihen, 1985). A specimen from this locality is in the Montana Bureau of Mines and Geology Mineral Museum collection (no. 16050).

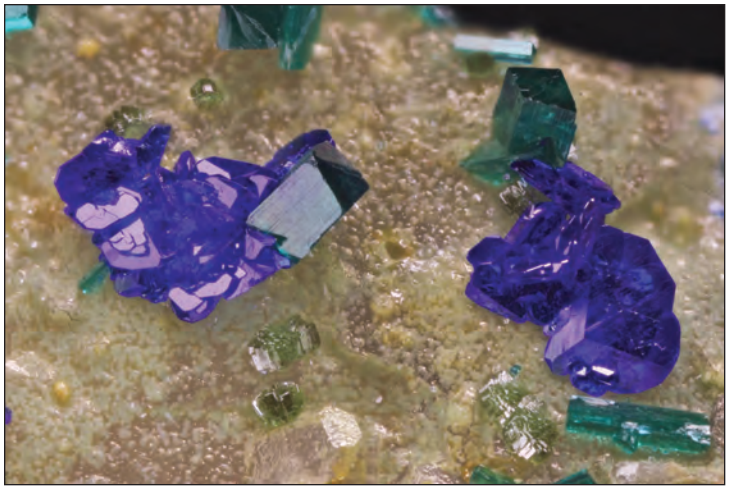

Figure 10. Blue (0.3 x 0.5 mm) aggregates of azurite microcrystals with dark green (0.2 to 0.4 mm long) brochantite microcrystals, Black Pine mine (Michael Gobla collection).

Bayldonite $Cu_3PbO(AsO_3OH)_2(OH)_2$

As bright-green microcrystals (flattened rhombs) and as crusts coating other minerals (Waisman, 1985, 1992). It is fairly common at the mine; it can be confused with duftite (Jensen and Nikischer, 2012). Bayldonite often forms coatings and encrustations on mimetite microcrystals; less commonly the mimetite is partly to completely dissolved away, leaving hollow forms (perimorphs) after mimetite. In more intensely altered specimens the mimetite is both encrusted by bayldonite, and the mimetite is partly to completely replaced by bayldonite, such as the specimen shown in figure 11.

Figure 11. Bayldonite after mimetite, Black Pine mine (Michael Gobla collection). The crystals vary from 0.08 to 0.35 mm wide; the field of view is 5.0 mm wide.

Beudantite $PbFe^{3+}{}_3(AsO_4)(SO_4)(OH)_6$

Yellow-brown pseudocubic microcrystals of beudantite occur in vugs formed in partly dissolved tetrahedrite (figs. 12, 13; Zeihen, 1985; Waisman, 1985, 1992). Beudantite is associated with scorodite and other rare arsenates (Jensen and Nikischer, 2012).

Bornite Cu_5FeS_4

Microscopic grains of bornite occur as inclusions in tetrahedrite (Waisman, 1985).

Boulangerite $Pb_5Sb_4S_{11}$

Silver-colored needles of boulangerite up to 2 mm long occur in massive white quartz showing alteration to stibiconite (Jensen and Nikischer, 2012).

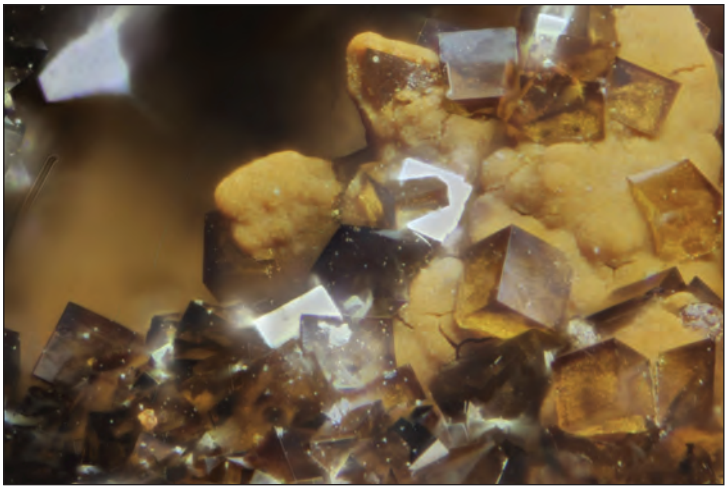

Figure 12. Beudantite (0.1 mm) microcrystals, Black Pine mine (Michael Gobla collection).

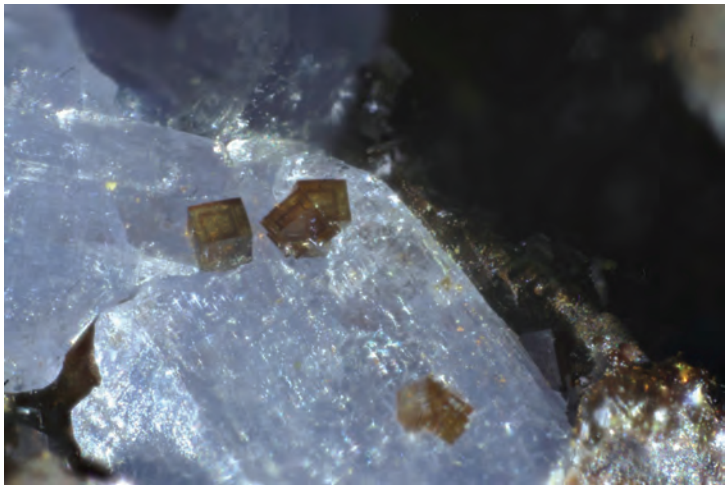

Figure 13. Color-zoned 0.1 mm microcrystals of beudantite on blue scorodite, Black Pine mine (Michael Gobla collection).

Brochantite $Cu_4(SO_4)(OH)_6$

Common as crusts and as prismatic and tabular microcrystals of great beauty. Brochantite is often associated with azurite and tetrahedrite (fig. 14; Zeihen, 1985; Jensen and Nikischer, 2012).

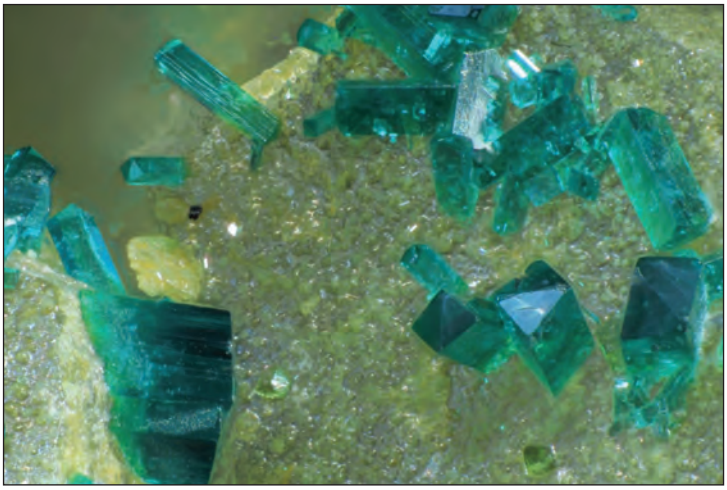

Figure 14. Green (0.2 to 0.4 mm long) microcrystals of brochantite, Black Pine mine (Michael Gobla collection).

Carminite $PbFe^{3+}_2(AsO_4)_2(OH)_2$

Rare occurrence in vuggy tetrahedrite as red to orange needle-shaped microcrystals and radiating aggregates to 0.5 mm (Jensen and Nikischer, 2012).

Cerussite $Pb(CO_3)$

Colorless, white, and pale yellow crystals up to 2 cm (Waisman, 1985; Jensen and Nikischer, 2012). A single vug produced over 200 crystals that were embedded in clay (Waisman, 1992).

Chalcanthite $Cu(SO_4)•5H_2O$

Glassy, blue-botryoidal clumps to 1 mm with brochantite (Jensen and Nikischer, 2012).

Chalcocite Cu_2S

Commonly observed in polished sections as rims on tetrahedrite and replacing sphalerite and galena along grain boundaries (Zeihen, 1985). Chalcocite forms sparkling microcrystalline crusts coating corroded tetrahedrite (Jensen and Nikischer, 2012).

Chalcopyrite $CuFeS_2$

Chalcopyrite occurs as inclusions in pyrite, quartz, sphalerite, and tetrahedrite (Zeihen, 1985; Waisman, 1985, 1992).

Chrysocolla $(Cu_{2-x}Al_x)H_{2-x}Si_2O_5(OH)_4 \bullet nH_2O$

Common throughout the mine as crusts on quartz and as small masses. Foil-like seams of native silver occur in some of the deep blue chrysocolla (Zeihen, 1985).

Clinoclase $Cu_3(AsO_4)(OH)_3$

Rare occurrence as blue diamond-shaped microcrystals in vugs with azurite, limonite, or chrysocolla (Zeihen, 1985; Waisman, 1992; Jensen and Nikischer, 2012).

Connelite $Cu_{36}(SO_4)(OH)_{62}Cl_8 \bullet 6H_2O$

Connelite was rarely encountered as a post-mining alteration product forming less than 0.1 mm electric blue spheres with a fibrous texture and associated with blue langite microcrystals on corroded tetrahedrite (Jensen and Nikischer, 2012).

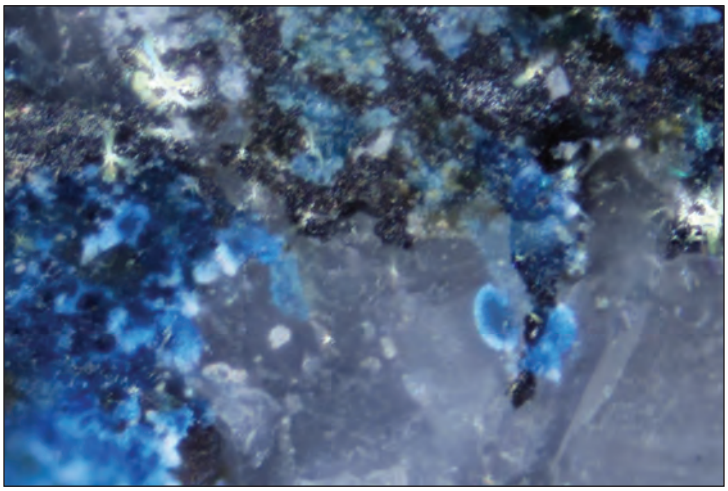

Figure 15. Connelite forms blue hemispherical (0.1 mm) aggregates of acicular microcrystals, Black Pine mine (Michael Gobla collection).

Copper Cu

Uncommon as thin films coating cuprite, as arborescent groups, rare as wires, and as microcrystals including spike-shaped spinel twins (Zeihen, 1985; Waisman, 1992; Jensen and Nikischer, 2012).

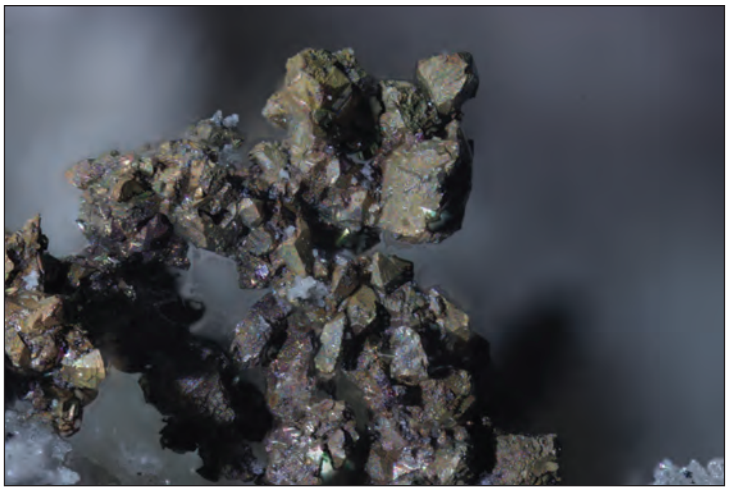

Figure 16. Copper (0.3 to 1 mm) microcrystals, Black Pine mine (Michael Gobla collection).

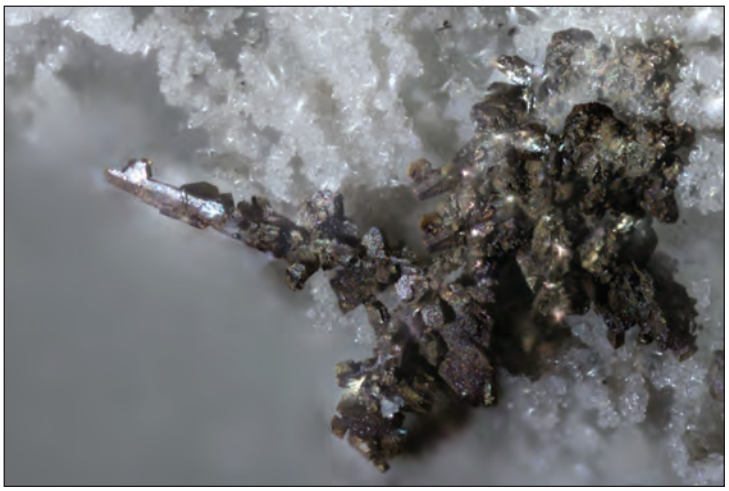

Figure 17. Copper microcrystals exhibiting a 1.5-mm-long spinel twin form, Black Pine mine (Michael Gobla collection).

Corkite $PbFe^{3+}_3(SO_4)(PO_4)(OH)_6$

Corkite occurs rarely at the Black Pine mine as thin crusts comprised of minute microcrystals (Waisman, 1992). The MBMG Mineral Museum collection includes two specimens of corkite from this locality that were purchased from the Excalibur Mineral Company (no. 12987, and no. 12988 with pseudomalachite).

Cornwallite $Cu_5(AsO_4)_2(OH)_4$

As deep green botryoidal coatings and spheres in association with clinoclase and olivenite (Jensen and Nikischer, 2012).

Covellite CuS

Observed in polished sections as rims replacing tetrahedrite, galena, sphalerite, aikinite, and luzonite (Zeihen, 1985).

Cuprite Cu_2O

Uncommon, as microcrystals, cubes, octahedrons, filaments (chalcotrichite variety), globular crusts, as thin coatings encrusting small dendritic sheets of native copper (Waisman, 1992), as microcrystals on gartrellite (Jensen and Nikischer, 2012), associations include chrysocolla and malachite.

Figure 18. Cuprite microcrystals fill a vug in quartz specimen with overall size of 4.8 x 3.8 cm, Black Pine mine (Michael Gobla collection).

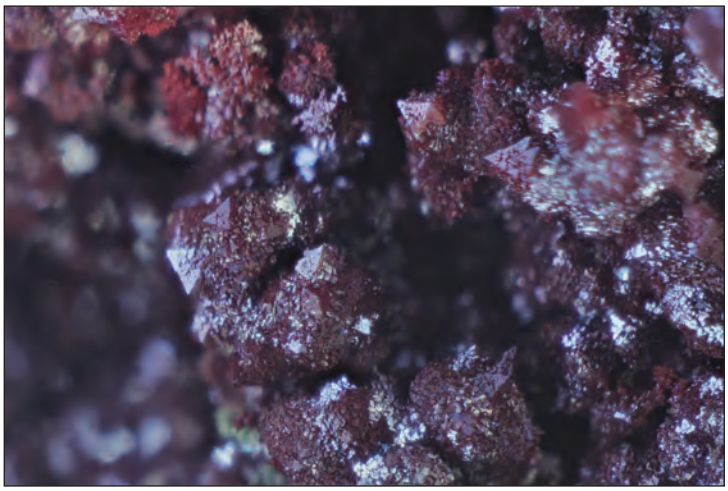

Figure 19. Cuprite forms aggregates of (0.15 mm) octahedral microcrystals, Black Pine mine (Michael Gobla collection).

Devilline $CaCu_4(SO_4)_2(OH)6•3H_2O$

As pale sky-blue micaceous flakes on altered tetrahedrite in association with brochantite and serpierite (Jensen and Nikischer, 2012).

Duftite $PbCu(AsO_4)(OH)$

Rare as green to gray-green to olive-green globular coatings on quartz, radiating sprays of lath-like microcrystals, and as dipyramids. It is sometimes associated with azurite (Zeihen, 1985; Waisman, 1985, 1992; Jensen and Nikischer, 2012).

Dugganite $Pb_3Zn_3(TeO_6)(AsO_4)_2$

Rare as pale purple to blue hexagonal, barrel-shaped, and tabular microcrystals collected by John Dagenais. Analysis is required to distinguish this mineral from joëlbruggerite and kuskite (Mills and others, 2009).

Freibergite $Ag_6[Cu_4Fe_2]Sb_4S_{13-x}$

Freibergite was reported to occur (Waisman, 1992) but probably is not present at the Black Pine mine. Freibergite forms a solid solution with tetrahedrite where silver substitutes for some of the copper in tetrahedrite. Past practice was to label any silver-bearing tetrahedrite as freibergite. Later mineralogical

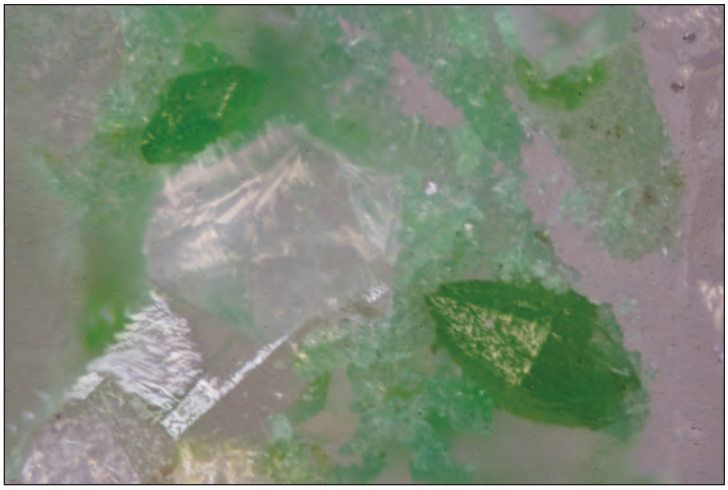

Figure 20. Duftite microcrystals on quartz (largest crystal is 0.3 mm long), Black Pine mine (Michael Gobla collection).

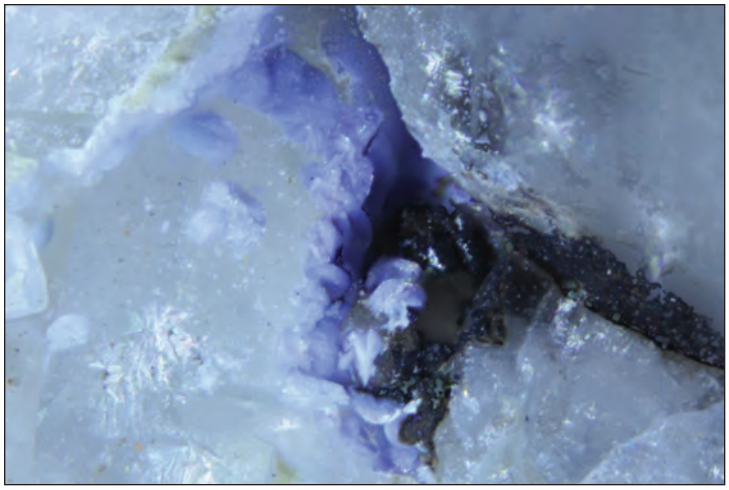

Figure 21. Dugganite (0.1 mm) microcrystals on quartz, Black Pine mine (Michael Gobla collection).

study determined that at least 4 of the possible 6 silver atoms must be present for the mineral to be freibergite; specimens with a lower silver content are more properly labeled as tetrahedrite (Moëlo and others, 2008). A later investigation of many crystal specimens from this mine did not identify any freibergite (Jensen and Nikischer, 2012). All of the specimens in the study were found to be either tetrahedrite or tennantite but did not contain enough silver to be freibergite. Unless a specific analysis shows otherwise, mineral specimens labeled freibergite from the Black Pine mine should be relabeled as tetrahedrite.

Galena PbS

Galena occurs as small crystals with sphalerite on quartz. The galena is associated with the highest grades of ore in the mine and it contains traces of Se and Te (Waisman, 1985). Galena was recovered as an ore of lead and silver.

Gartrellite $PbCuFe^{3+}(AsO_4)_2(OH) \cdot H_2O$

Rare as yellow to pale green crystalline botryoids (Jensen and Nikischer, 2012).

Goethite FeO(OH)

Goethite occurs as replacements of the sulfides along fractures (Zeihen, 1985), as thin crusts, and as pseudomorphs after small crystals of pyrite (Waisman, 1985, 1992).

Gold Au

As a component in the pyrite, individual grains have not been observed (Zeihen, 1985).

Gypsum $Ca(SO_4) \cdot 2H_2O$

Gypsum is rare in occurrence. It forms small transparent needles coating quartz in association with philipsburgite and mimetite (Waisman, 1992). It was observed in two specimens, as microcrystals on beudantite, and as a vug filling in corroded tetrahedrite ore with crystals to 3 mm (Jensen and Nikischer, 2012).

Hematite Fe_2O_3

Reddish brown coatings and crusts on quartz.

Hemimorphite $Zn_4(Si_2O_7)(OH)_2 \cdot H_2O$

As white earthy coatings on quartz and tabular crystals (Zeihen, 1985), colorless to pale blue crystal aggregates, and one deep blue crystal group was found (Waisman, 1985, 1992).

Hübnerite $Mn(WO_4)$

Reddish brown crystals of hübnerite were initially reported from the Combination (Black Pine) mine in association with pseudomalachite (Pearce, 1900). Hübnerite is abundant at the Black Pine mine and many fine specimens have been recovered (Walker, 1960). The crystals are mostly frozen in a quartz matrix, but they also occur as free-standing crystals on quartz (Waisman, 1992). The crystals are around 3 cm long but up to 8 cm in some cases (Zeihen, 1985). Some of the hübnerite crystals are corroded and altered, and on close inspection a few of these show pseudomorphic replacement. Some crystals are partly replaced by alteration to stoltzite and a few complete pseudomorphs of stoltzite after hübnerite have been found.

Figure 22. Hübnerite crystal on quartz with a single crystal of pale pink rhodochrosite at the bottom center of the specimen (2.5 x 1.3 cm), Black Pine mine (Michael Gobla collection).

Jarosite $KFe^{+3}_3(SO_4)_2(OH)_6$

It occurs as pale yellow-brown fine-grained coatings on quartz crystals (Jensen and Nikischer, 2012).

Joëlbruggerite $Pb_3Zn_3Sb^{5+}As_2O_{13}(OH)$

The Black Pine mine is the type locality for this new trigonal arsenate mineral (Mills and others, 2008). It is very rare, occurring as pale purple-blue prismatic and barrel-shaped microcrystals up to 50 μm typically on prisms of mimetite (Mills and others, 2009). Dugganite and kuskite are related species that form a solution series with joëlbruggerite. Analysis is required to distinguish these species from one another. Associated minerals include azurite, beudantite, chalcocite, duftite, dugganite, kuskite, and pseudomalachite. The mineral is named after a Swiss-Australian mineralogist named Joël Brugger for his contributions to mineralogy. Co-type specimens are no. G32400 in the Department of Mineralogy, South Australian Museum, and a microprobe mount, specimen no. CMNMC 86061 in the Mineral Sciences Division, Canadian Museum of Nature, Ottawa, Canada.

Kipushite $(Cu)_6(PO_4)_2(OH)_6 \cdot H_2O$

Some mineral specimens from the Black Pine mine, labeled as philipsburgite, have been identified by infrared spectra to be kipushite (Braithwaite and Ryback, 1988; Robinson and King, 1990). Kipushite occurs as bright green spherical aggregates of transparent microcrystals coating quartz in association with colorless tapering prismatic crystals of phosphatian mimetite, yellow earthy “bindheimite” (oxyplumboroméite), and an unidentified mineral forming tiny blue-green translucent spherules. The kipushite specimens showed a slight arsenate content. The mineral association is different from that of the original find of philipsburgite that occurs with mimetite. Analysis is required to distinguish kipushite from philipsburgite; therefore, it is not known how many of the “philipsburgite” specimens from Black Pine are actually kipushite. There is a specimen of kipushite in the MBMG Mineral Museum collection (no. 18218).

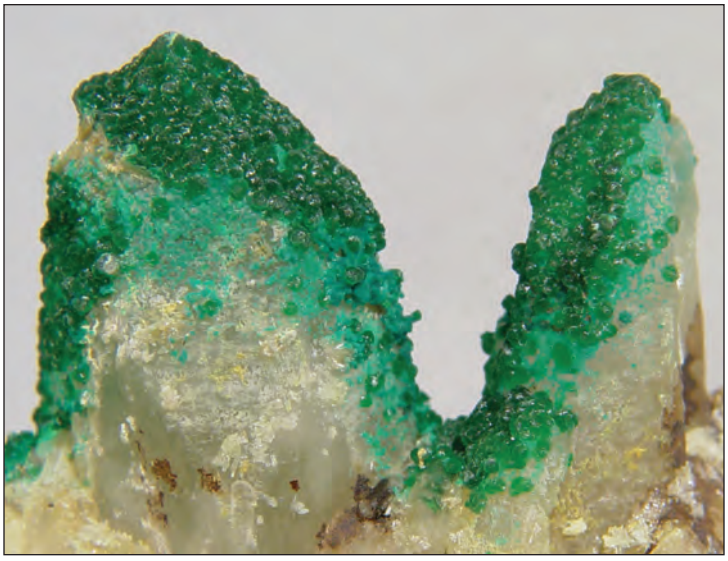

Figure 23. A presumed specimen of kipushite based on its association with small blue spheres (possibly chrysocolla), 2.4 x 1.7 cm overall specimen size, Black Pine mine (Michael Gobla collection).

Kuksite $Pb_3Zn_3TeO_6(PO_4)_2$

A single specimen collected in July 1993 by John Dagenais from a rock pile outside of the mine contained a 2.5 cm vug in quartz containing kuksite crystals. The kuksite occurs as rosette-like aggregates of pale green transparent hexagonal crystal plates about 0.5 mm in size found in association with tiny 0.8 mm azurite crystals. Other associations include malachite, pseudomalachite, chalcocite, beudantite-corkite, duftite, dugganite, and Joëlbruggerite. Kuksite forms a solid solution with dugganite and Joëlbruggerite, and analysis is required to distinguish between these species (Mills and others, 2010b).

Langite $Cu_4(SO_4)(OH)_6 \cdot 2H_2O$

Langite occurs as an alteration product forming prismatic and three-rayed “star” twin transparent deep blue microcrystals to 0.5 mm on joint surfaces and in vugs of corroded tetrahedrite in association with pale tan acicular mimetite and rarely with connellite and wroewolfite (Jensen and Nikischer, 2012)

Libethenite $Cu_2(PO_4)(OH)$

Rare as blue green botryoids and spherulites, which are difficult to distinguish from pseudomalachite (Zeihen, 1985).

Linarite $CuPb(SO_4)(OH)_2$

Rarely found in the mine as microcrystals to 0.2 mm on anglesite, and as inclusions in anglesite crystals (Jensen and Nikischer, 2012).

Figure 24. Linarite (0.5 mm crystal) with colorless anglesite microcrystals, Black Pine mine (Michael Gobla collection).

Luzonite Cu_3AsS_4

As intergrowths with grains of tetrahedrite (Zeihen, 1985).

Malachite $Cu_2(CO_3)(OH)_2$

Malachite commonly occurs as botroydal coatings, radiating needles, and small masses to 2 cm on quartz (Zeihen, 1985; Waisman, 1985, 1992; Jensen and Nikischer, 2012).

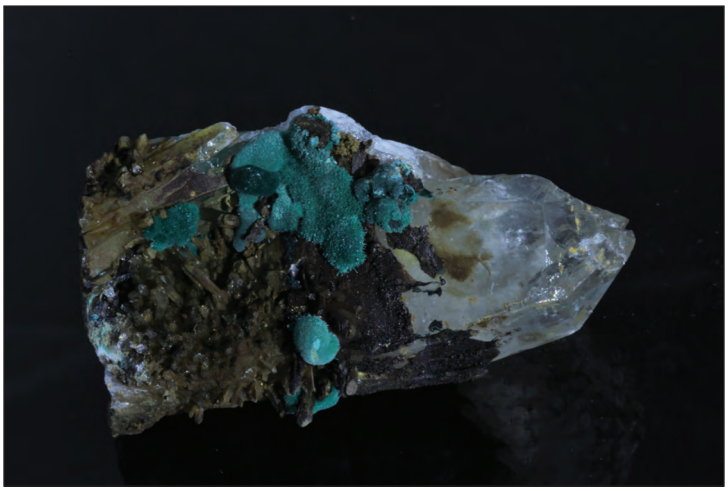

Figure 25. Malachite hemispherical aggregates on quartz (5.1 x 2.6 cm), Black Pine mine (Michael Gobla collection).

Mawbyite $PbFe^{3+}_2(AsO_4)_2(OH)_2$

Rarely found as red scalenohedral “dogtooth”-shaped microcrystals about 0.2 mm long (Jensen and Nikischer, 2012). Later, specimens with “sword”-shaped microcrystal sprays were identified in vuggy altered tetrahedrite and are some of the finest known examples of this mineral species. Associations include scorodite, segnitite, and beudantite.

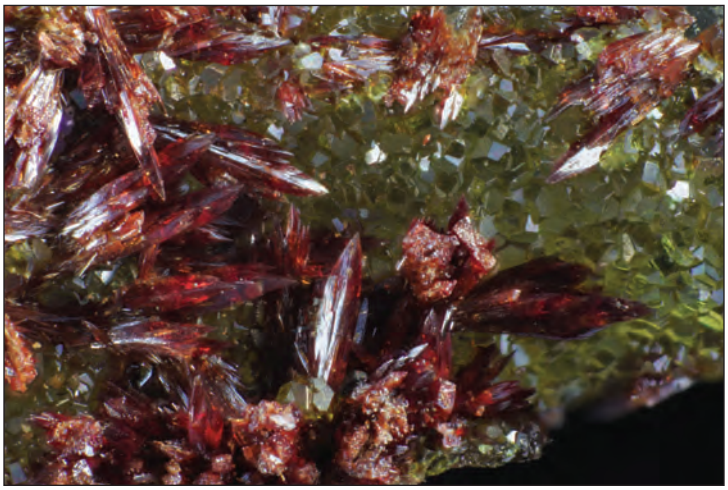

Figure 26. Mawbyite forms red (0.4 mm long), spear-shaped microcrystals with segnetite, Black Pine mine (Michael Gobla collection).

Mimetite $Pb_5(AsO_4)_3Cl$

Prolific amounts of prismatic, brown specimens from this locality that were labeled by mineral dealers as “pyromorphite” are actually mimetite (Jensen and Nikischer, 2012). Mimetite occurs as needle-shaped to barrel-shaped hexagonal crystals and microcrystals that can be colorless, white, yellow, pale tan, to brown. In some specimens bayldonite forms as coatings (perimorphs), hollow casts (epimorphs), and replacements (pseudomorphs) after mimetite/pyromorphite.

Figure 27. Mimetite (0.2 mm long) crystals on quartz (6.1 x 5.0 cm overall size), Black Pine mine (Michael Gobla collection).

Murdochite $Cu_{12}Pb_2O_{15}Cl_2$

Rare, only a few specimens known, as sparse tiny black microcrystals on hemimorphite (Jensen and Nikischer, 2012).

Olivenite $Cu_2(AsO_4)(OH)$

Initially a single specimen of olive-green microcrystals forming plates in a cockscomb form similar to marcasite was found (Zeihen, 1985). Years later a few more finds were made of needle-shaped microcrystals in radiating sprays (Waisman, 1992; Jensen and Nikischer, 2012).

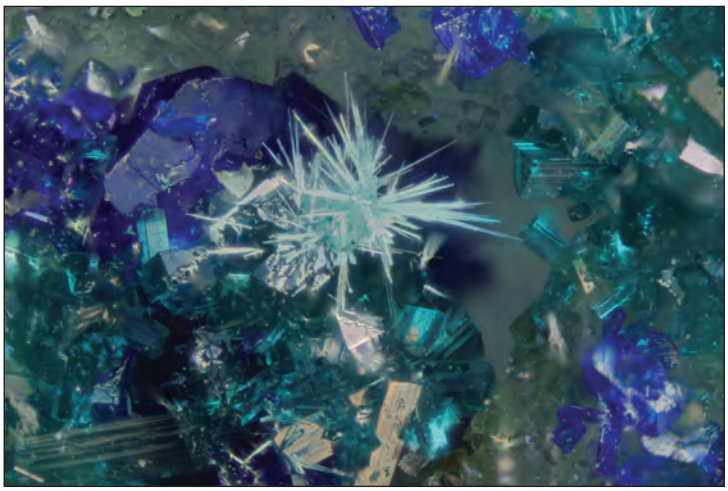

Figure 29. Needle-shaped microcrystals of olivenite (0.7 mm wide aggregate of olivenite) occur with azurite and brochantite, Black Pine mine (Michael Gobla collection).

Figure 28. Olivenite acicular microcrystals (0.7 mm long), Black Pine mine (Michael Gobla collection).

Oxyplumboroméite Pb_2Sb_2O7

Common as earthy coatings and crusts due to the alteration of tetrahedrite (Zeihen, 1985; Waisman, 1992; Jensen and Nikischer, 2012).

Pharmacosiderite $KFe^{3+}_4(AsO_4)_3(OH)_4 \cdot 6\text{-}7H_2O$

Initially found as a single boulder on the ore dump as yellow-green pseudocubic microcrystals to 0.5 mm (Zeihen, 1985). It is of rare occurrence at the mine in vugs in altered tetrahedrite (Waisman, 1992; Jensen and Nikischer, 2012).

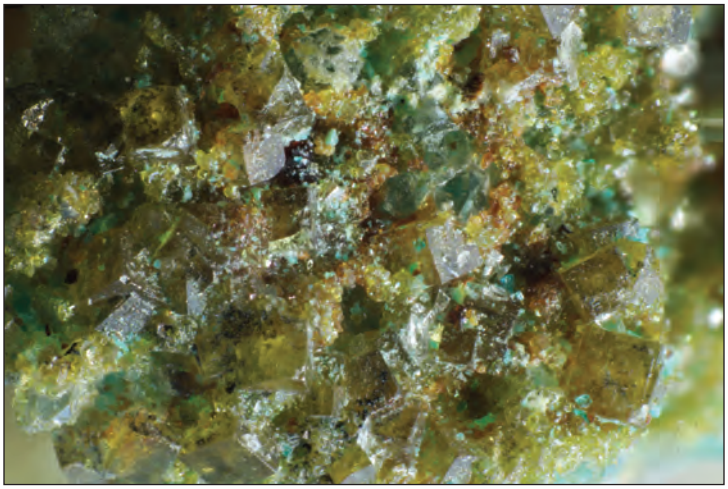

Figure 30. Pharmacosiderite microcrystals (crystal at lower right is 0.4 mm), Black Pine mine (Michael Gobla collection).

Philipsbornite $PbAl_3(AsO_4)(AsO_3OH)\ (OH)_6$

Mustard-yellow-brown crusts and coatings on quartz (Nikischer, 2004; Jensen and Nikischer, 2012).

Philipsburgite $Cu_5Zn(AsO_4)(PO_4)(OH)_6 \cdot H_2O$

Spherical aggregates of deep green microcrystals were identified as a new mineral from the Black Pine mine in the Combination district, Granite County, in 1985 (Peacor and others, 1985). It was named by Lester Zeihen, who first recognized it as a new mineral, for the town of Philipsburg. Type specimens were placed in the Smithsonian Institution in Washington D.C. and in the Royal Ontario Museum in Toronto. It occurs as lustrous deep emerald green spherical coatings on bayldonite, and quartz. Under high magnification, the individual spheres are seen to be composed of aggregates of intergrown monoclinic curved prismatic crystals with chisel-shaped terminations. The termination ends of the individual microcrystals project up out of the spherical mass. The aggregates of crystals in the spherical masses are not pure philipsburgite. X-ray analysis found that they typically contain minor to moderate amounts of bayldonite in the aggregates along with the philipsburgite.

The excellent crystallization distinguishes specimens of this mineral from green-colored pseudomalachite that also occurs at this mine. The crystalline nature does not distinguish the spherical aggregates from kipushite, which also occurs at the Black Pine mine in green spherical crystalline aggregates (Braithwaite and Ryback, 1988). Philipsburgite and kipushite are isostructural forming a solid solution with arsenate substituting for phosphate. It is not known what percentage of the "philipsburgite" specimens recovered from the Black Pine mine are mislabeled and are kipushite; however, it is suspected that kipushite may be common. There is a distinct difference in the reported mineral associations. Philipsburgite was reported to occur with pale yellow mimetite and bayldonite (arsenate minerals), while kipushite was reported to occur with colorless phosphatian mimetite, yellow earthy bindhemite, and tiny blue-green translucent spheres of an unidentified mineral.

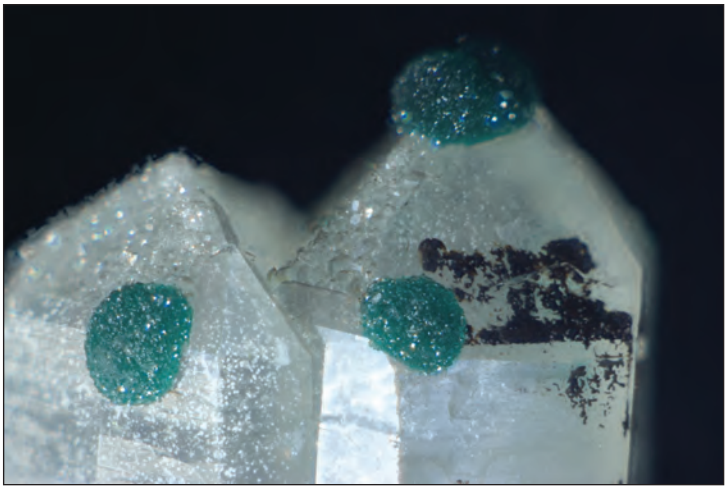

Figure 31. Philipsburgite forms green (1 mm diameter) hemispherical aggregates of microcrystals on quartz, Black Pine mine (Michael Gobla collection).

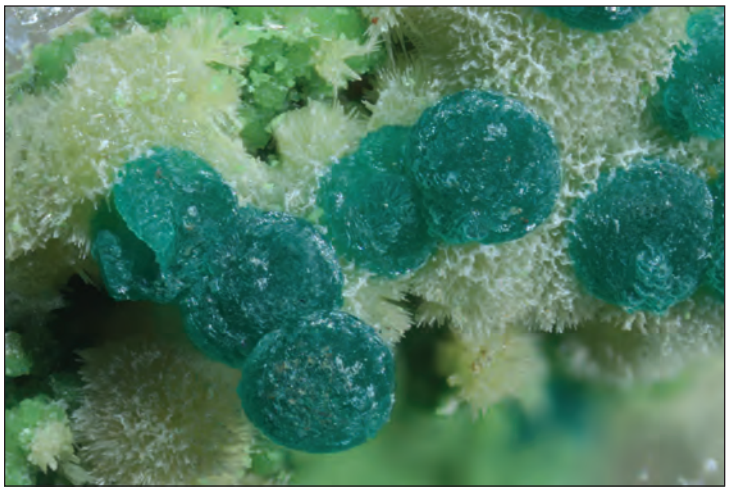

Figure 32. Philipsburgite forms green (0.7 mm diameter) spherical aggregates of acicular microcrystals with pale yellow mimetite, Black Pine mine (Michael Gobla collection).

Pseudomalachite $Cu_5(PO_4)_2(OH)_4$

Common as coatings and small dark green to blue-green spheres and crusts on quartz (Hillebrand, 1884; Zeihen, 1985; Waisman, 1985, 1992; Jensen and Nikischer, 2012). A specimen in the MBMG Mineral Museum collection (no. 12987) is associated with corkite.

Pyrite FeS_2

Pyrite is common as masses and crystals in the vein quartz. The crystals typically form pyritohedrons from 2 to 10 cm across. The larger specimens form as single crystals not attached to matrix (Waisman, 1985, 1992). The pyrite contains from 0.27 to 0.33 wt.% arsenic and is strongly anisotropic (Waisman, 1985, 1992; Zeihen, 1985).

Pyrolusite MnO_2

Black coatings of pyrolusite occur commonly throughout the mine (Zeihen, 1985; Waisman, 1985, 1992).

Pyromorphite $Pb_5(PO_4)_3Cl$

Rare as white to brown needle-shaped crystals. Most of the brown crystals are actually mimetite (Jensen and Nikischer, 2012). Some small white crystals with a bright orange fluorescence in long-wave ultraviolet light have been found (Robbins, 1985).

Quartz SiO_2

Quartz forms the massive vein filling that hosts the other minerals at the mine (Zeihen, 1985). Milky to colorless prismatic crystals occur throughout the mine. The mine is remarkable for the prolific amount of quartz crystals that it has produced. Most of the rare minerals from this locality are encrusted on small quartz crystals; some of these encrusted crystals form aesthetic specimens.

Single crystals are more common than groups of prismatic crystals and they vary from short stubby crystals to long slender prisms. The crystals, which average around 5 to 10 cm in length, are mainly the milky quartz variety with some transparent zones towards the crystal terminations. The transparent rock crystal variety of quartz occurs less commonly at the mine. A few large milky quartz crystal groups have been recovered.

In some cavities over 10% of the quartz crystals are in the form of Japan-law twins, and complex multiple twins consisting of a main crystal with twins projecting from the side have also been found (Waisman, 1992). The Japan-law twins are small (rarely over 4 cm), and most are uneven with one side of the twin typically being much larger than the other.

Quartz crystals with mineral inclusions have also been found including crystals of rhodochrosite in quartz, hübnerite in quartz, a quartz scepter with a single wire of silver, and commonly examples of quartz microcrystals with tetrahedrite inclusions have been recovered. One specimen, a Japan-law twin microcrystal that contains so many tetrahedrite inclusions that it appears to be black was recovered. Quartz crystals with 1 mm pyrite crystal inclusions in the tips of the crystals have also been found (Waisman, 1992).

Figure 33. Quartz Japan-law twin (5.7 x 3.2 cm) showing unequal lengths of the quartz prisms which is typical for the Black Pine mine (Michael Gobla collection).

Figure 34. Quartz crystal aggregate with a Japan-law twin (at right) showing equal lengths of the quartz prisms that is rarely found at the Black Pine mine (Michael Gobla collection). The overall specimen size is 4.3 x 4.1 cm.

Figure 35. Quartz scepter (25 x 9 mm), which is a rare form of quartz at the Black Pine mine (Michael Gobla collection). This specimen, formerly from the Chris van Laer collection, contains an inclusion of a silver wire in the head of the scepter.

Rhodochrosite $Mn(CO_3)$

Rhodochrosite is a rare constituent of the mineral deposit. A small quantity of light-pink colored rhombohedral crystals, typically 1 to 4 mm in size, and rosettes on quartz, were recovered from the mine. Some specimens are associated with small crystals of hübnerite and less commonly with galena.

Figure 36. Rhodochrosite forms small (2.5 mm) pale pink rhombohedral crystals on quartz (4.3 x 3.1 cm), Black Pine mine (Michael Gobla collection).

Figure 37. Rhodochrosite crystals on quartz (2.4 x 2.2 cm), Black Pine mine (Michael Gobla collection).

Rosasite $CuZn(CO_3)(OH)_2$

Rare as blue microscopic globular encrustations (Waisman, 1992).

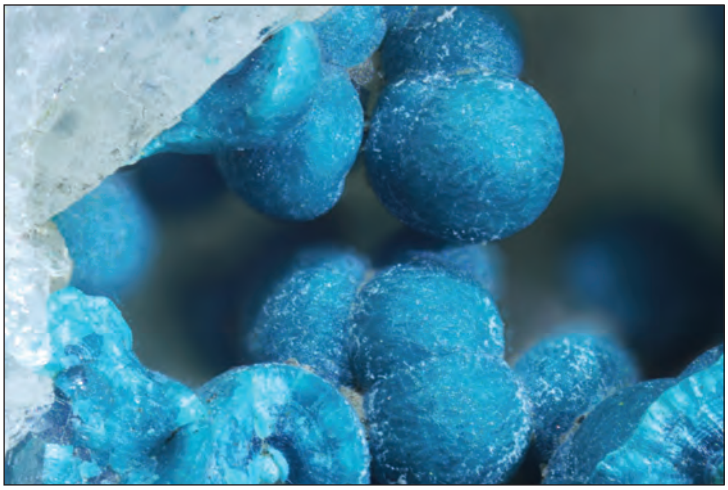

Figure 38. Rosasite microspheres (1 mm diameter spheres) on quartz, Black Pine mine Michael Gobla collection).

Scheelite $Ca(WO_4)$

Rare as grains and small masses in quartz (Jensen and Nikischer, 2012).

Scorodite $Fe^{3+}(AsO_4)\cdot 2H_2O$

Rare as greenish coatings, and as pale to medium blue transparent to translucent microcrystals in vuggy corroded tetrahedrite (Zeihen, 1985; Waisman, 1992; Jensen and Nikischer, 2012).

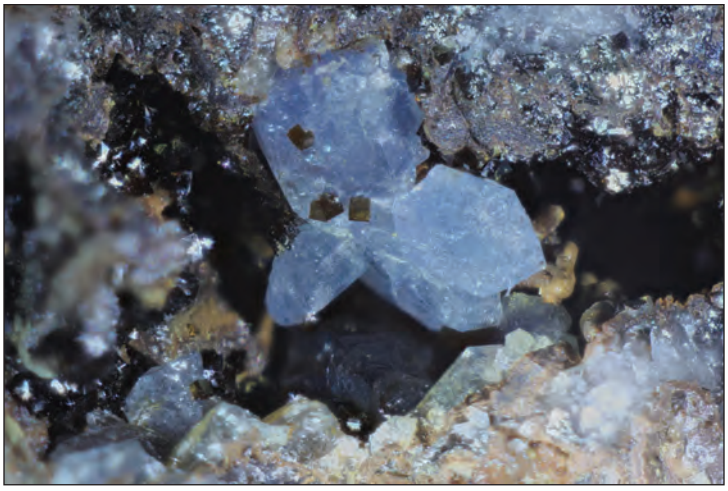

Figure 39. Blue scorodite microcrystals (0.5 mm long) with aggregates of tiny (0.01 mm) honey-colored beudantite microcrystals, Black Pine mine (Michael Gobla collection).

Segnitite $PbFe^{3+}_3(AsO_4)(AsO_3OH)(OH)_6$

It occurs as yellow-green coatings on quartz and rarely as transparent microcrystals up to 0.15 mm in diameter (Nikischer, 2004; Jensen and Nikischer, 2012).

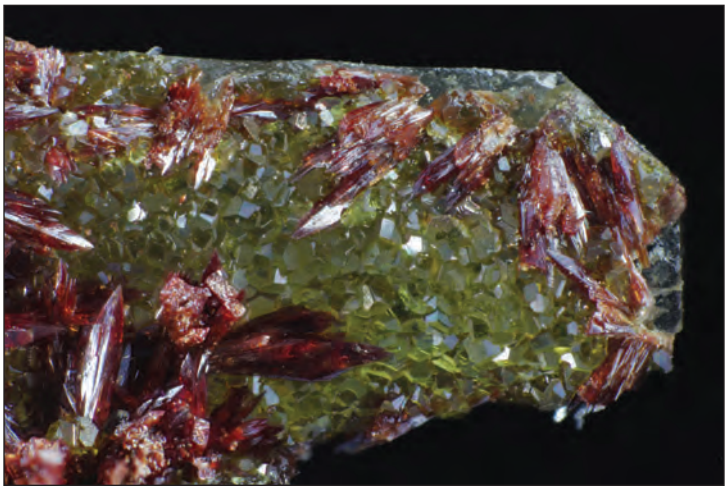

Figure 40. Yellow-green segnetite (0.08 mm diameter) microcrystals with red mawbyite microcrystals (0.4 mm long), Black Pine mine (Michael Gobla collection).

Serpierite $Ca(Cu,Zn)_4(SO_4)_2(OH)_6 \cdot 3H_2O$

Sky blue grains comprised of fibrous crystals associated with brochantite and devilline (Jensen and Nikischer, 2012).

Silver Ag

Silver occurs as foil-like thin films in deep blue chrysocolla, as coatings on fractures in and on crystal surfaces of tetrahedrite, rare as microcrystals in vugs, and in a few instances as wires (Zeihen, 1985; Waisman, 1985, 1992; Nikischer, 2020).

Sphalerite ZnS

A minor ore mineral associated with galena. Small green to dark brown crystals, usually under 2 mm in size, occur associated with galena (Zeihen, 1985; Waisman, 1985, 1992).

Stibiconite $Sb^{3+}Sb^{5+}2O_6(OH)$

Found as spongy-brown pseudomorphic replacements of tetrahedrite crystals (Zeihen, 1985; Waisman, 1992; Jensen and Nikischer, 2012). The MBMG Museum has a specimen from the Black Pine mine (no. 5153).

Stolzite $Pb(WO_4)$

As colorless to tan blocky pseudocubic crystals, it often partly replaces hübnerite, and a few complete pseudomorphs after hübnerite have been found. It rarely forms as platy and pyramidal crystals similar to wulfenite forms. It fluoresces a bright white color under short-wave ultraviolet light (Zeihen, 1985; Waisman, 1992).

Figure 41. Stoltzite (2 to 3 mm) crystals on quartz, Black Pine mine (Michael Gobla collection).

Strashimirite $Cu_4(AsO_4)_2(OH)_2 \cdot 2.5H_2O$

Rare as light green to blue-green needle-shaped microcrystals often forming hemisphere-shaped aggregates to 6 mm in association with azurite, brochantite, chrysocolla, malachite, mimetite, and olivenite (Jensen and Nikischer, 2012).

Stromeyerite AgCuS

A tentative identification using optical properties and microprobe results. As microscopic grains along fractures replacing tetrahedrite (Zeihen, 1985).

Tennantite $Cu_6[Cu_4(Fe,Zn)_2]As_4S_{13}$

As massive vein filling in quartz and as crystals, it was mined as an ore mineral. Both tennantite and tetrahedrite occur, but tennantite is far less abundant (Zeihen, 1985).

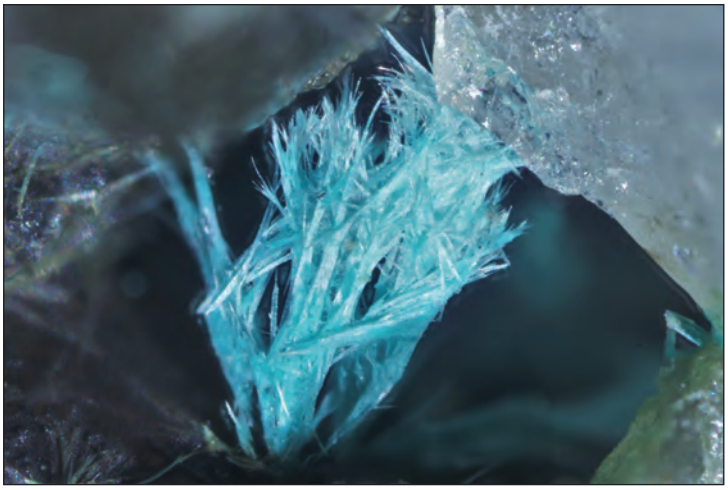

Figure 42. Strashimirite forms up to 1.5-mm- long feather-like blue microcrystals, Black Pine mine (Michael Gobla collection).

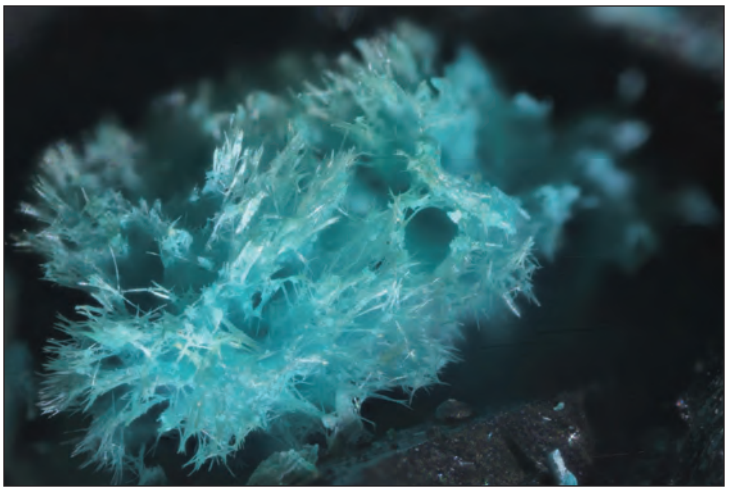

Figure 43. Strashimirite in a hemispherical aggregate (1.8 mm wide) of microcrystals, Black Pine mine (Michael Gobla collection).

Tetrahedrite $Cu_6[Cu_4(Fe,Zn)_2]Sb_4S_{13}$

The principal ore mineral at the mine, it occurs as massive filling in quartz veins, as euhedral crystals and as inclusions in quartz crystals (Zeihen, 1985). Analysis of several samples show that the composition of the crystals is near the division between tetrahedrite and tennantite and that both minerals occur at the mine (Jensen and Nikischer, 2012). The mine has produced several thousand fine crystal specimens of tetrahedrite, mostly as thumbnail size specimens. The crystals are typically 1 to 3 cm in size, found as loose crystals or perched on quartz crystals. Some larger cabinet specimens have been recovered, but the pockets were rarely large enough to produce such specimens. One museum specimen with a huge crystal of tetrahedrite was recovered from the mine.

Figure 44. Tetrahedrite crystal (12 x 8 mm) on quartz, Black Pine mine (Michael Gobla collection).

Theisite $Cu_5Zn_5(AsO_4)_2(OH)_{14}$

Rare as micaceous pale green microcrystals to 2 mm in quartz fractures associated with azurite, cuprian adamite, philipsburgite, and pseudomalachite (Jensen and Nikischer, 2012).

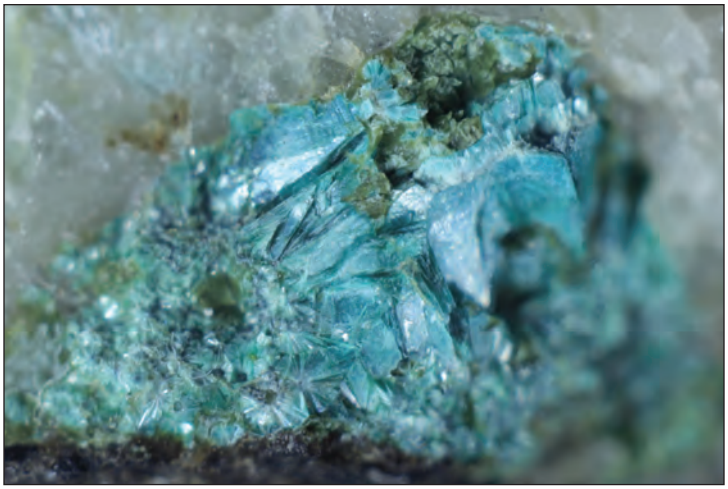

Figure 45. Theisite forms a blue-green mica-like (5 x 3 mm) aggregate on quartz, Black Pine mine (Michael Gobla collection).

Torbernite $Cu(UO_2)_2(PO_4)_2 \cdot 12H_2O$

Tiny pale green platy microcrystals with brochantite microcrystals on chrysocolla (only 5 specimens found) were identified by Tony Nikischer in 2021 (Nikischer, 2021).

Veszelyite $Cu_3(PO_4)(OH)_3 \cdot 2H_2O$

Small crystals and microcrystals of veszelyite on quartz, considered to be the world's finest for the species, were recovered from the mine (Zeihen, 1985). The color varies from blue in the blocky-shaped crystals to a dark blue (nearly black) seen in spear-shaped crystals; larger crystals are almost black in color. It is often associated with bayldonite and chrysocolla, (Waisman, 1985, 1992; Jensen and Nikischer, 2012).

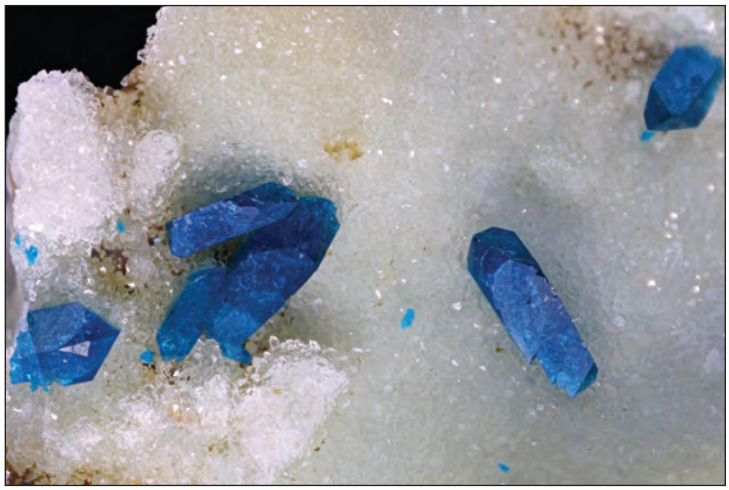

Figure 46. Veszelyite (1.2 to 2.3 mm long) blocky prismatic microcrystals on quartz, Black Pine mine (Michael Gobla collection).

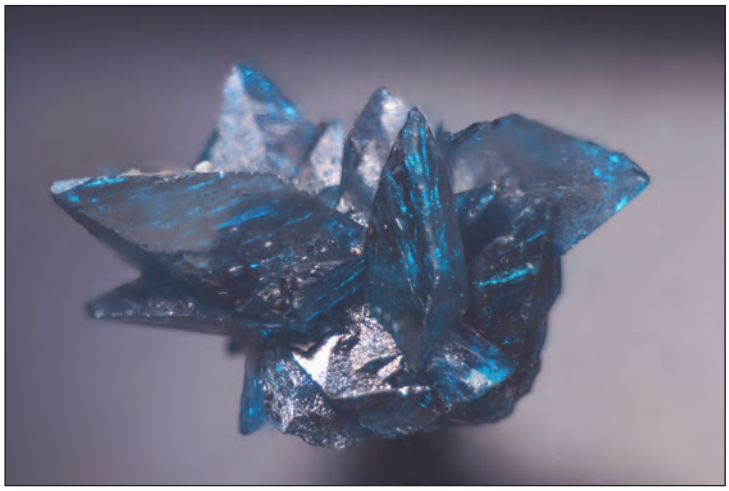

Figure 47. Veszelyite in the form of spear-shaped microcrystals (4.8 x 3.8 mm), Black Pine mine (Michael Gobla collection).

Wroewolfeite $Cu_4(SO_4)(OH)_6 \cdot 2H_2O$

Rare as blue striated prismatic microcrystals (Jensen and Nikischer, 2012).

References

Braithwaite, R.S.W., and Ryback, G., 1988, Philipsburgite from the Caldbeck Fells and kipushite from Montana, and their infrared spectra: Mineralogical Magazine, v. 52, p. 529–533.

Hillebrand, W.F., 1884, Mineralogical notes: Proceedings of the Colorado Scientific Society, v. 1, p. 118.

Jensen, M., and Nikischer, T., 2012, Some notes on the mineralogy of the Black Pine Mine, Granite County, Montana: Mineral News, v. 28, no. 6, p. 1–10.

Mills, S.J., Groat, L.A., and Kolitsch, U., 2008, Te, Sb, and W mineralization at the Black Pine mine, Montana, Poster presented at the 18th Annual V.M. Goldschmidt Conference, Vancouver, Canada, July 13–18, 2008: Abstract in Geochemistry Cosmochemistry Acta, v. 72, Special Supplement 12S, p. A632.

Mills, S.J., Kolitsch, U., Miyawaki, R., Groat, L.A., and Poirier, G., 2009, Joëlbruggerite, $Pb_3Zn_3(Sb^{5+},Te^{6+})As_2O_{13}(OH,O)$, the Sb^{5+} analog of dugganite, from the Black Pine mine, Montana: American Mineralogist, v. 94, p. 1012–1017.

Mills, S.J., Kampf, A.R., Poirier, G., Raudsepp, M., and Steele, I.M., 2010a, Auriacusite, $Fe^{3+},Cu^{2+}AsO_4O$, the first M^{3+} member of the olivenite group, from the Black Pine mine, Montana, USA: Mineralogy and Petrology, v. 99, no. 1–2, p. 113–120.

Mills, S.J., Groat, L.A., and Kolitsch, U., Housley, R.M., and Raudsepp, M., 2010b, The crystal chemistry and crystal structure of kuksite, $Pb_3Zn_3Te^{6+}P_2O_{14}$, and a note on the crystal structure of yafsoanite, $(Ca,Pb)_3Zn(TeO_6)_2$: American Mineralogist, v. 95, no. 7, p. 933–938.

Moëlo, Y, Makovicky, E., Mozgova, N.N., Jambor, J.L., Cook, N., Pring, A., Parr, W., Nickel, E.H., Graeser, S., Karup-Moller, S., Balic-Zunic, T., Mumme, W.G., Vurro, F., Topa, D., Bindi, L., Bente, K., and Shimizu, M., 2008, Sulfosalt systematics: A review: Report of the sulfosalt sub-committee of the IMA Commission on Ore Mineralogy: European Journal of Mineralogy, v. 20, p. 7–46.

Nikischer, T., 2004, A “new” discovery of philipsbornite and segnitite: Mineral News, v. 20, p. 1–2.

Nikischer, T., 2020, Native silver from the Black Pine mine, near Philipsburg, Granite Co., Montana: Mineral News, v. 36, no. 8, p. 9–10.

Nikischer, T., 2021, Torbernite discovered at Black Pine mine, near Philipsburg, Granite County, Montana: Mineral News, v. 37, no. 6, p. 8.

Peacor, D., Dunn, P., Ramik, R.A., Sturman, B.D., and Zeihen, L.G., 1985, Philipsburgite, a new copper zinc arsenate hydrate related to Kipushite from Montana: Canadian Mineralogist, v. 23, p. 255–258.

Piilonen, P.C., Poirier, G., Ercit, T.S., Rowe, R., and Tait, K.T., 2010, New mineral names: American Mineralogist, v. 95, p. 1594–1600.

Robbins, M., 1985, Fluorescent forum; fluorescence in pyromorphite and other lead apatites: Rocks and Minerals, v. 60, no. 6, p. 293–296.

Robinson, G.W., and King, V.T., 1990, What’s new in minerals, Montana: Mineralogical Record, v. 21, p. 483–484.

Spanski, G.T., 2004, Inventory of significant mineral deposit occurrences in the headwaters project area in Idaho, western Montana, and extreme eastern Oregon and Washington: U.S. Geological Survey Open-File Report 2004-1038, 13 p.

Volin, M.E., Roby, R.N., and Cole, J.W., 1952, Investigation of the Combination silver-tungsten mine, Granite County, Montana: U.S. Bureau of Mines Report of Investigations 4914, 26 p.

Waisman, D., 1985, Geology and mineralization of the Black Pine Mine, Granite County, Montana: Missoula, University of Montana M.S. Thesis, 66 p.

Waisman, D., 1992, Minerals of the Black Pine Mine, Granite County, Montana: Mineralogical Record, v. 23, no. 6, p. 477–483.

Walker, D.D., 1960, Tungsten resources of Montana: Deposits of the Philipsburg Batholith, Granite and Deer Lodge Counties: U.S. Bureau of Mines Report of Investigations 5612, 55 p.

Weitfle, C., 1891, Views of Granite, Philipsburg and vicinity: Granite, Montana, Chas. Weitfle, 16 p.

Zeihen, G.D., 1985, Paragenetic relationships, zoning, and mineralogy of the Black Pine mine, Granite County, Montana: Tucson, University of Arizona M.S. Thesis, 103 p.

Elkhorn ghost town and the Boulder River Valley from Elkhorn Peak. Photo by Joel Dietrich.

Depth of Emplacement of the Boulder Batholith, and Implications for Sevier Tectonic Shortening and Exhumation

John H. Dilles[1] and Kaleb C. Scarberry[2]

[1]*College of Earth, Ocean & Atmospheric Sciences, Oregon State University, Corvallis, Oregon*
[2]*Montana Bureau of Mines and Geology, Butte, Montana*

Introduction

The Boulder Batholith of western Montana was emplaced between ~82 and 75 Ma and lies principally in the hinterland, or hanging wall, of the late Cretaceous Sevier fold and thrust belt along the eastern Rocky Mountain front (fig. 1). We discuss both published (Houston and Dilles, 2013) and recently obtained electron microprobe compositional data for hornblende to obtain barometry estimates of the pressure of crystallization for the Butte Granite unit of the Boulder Batholith, and granitic intrusions of the western Pioneer Batholith in Montana. Hornblende from the Butte Granite of the Boulder Batholith (90% of samples) is compositionally unzoned, and the analyzed rims are co-crystallized with biotite, quartz, and K-feldspar, and therefore their compositions reflect the pressure of last pluton crystallization and not some greater pressure. The hornblende barometry method (e.g., Anderson and Smith, 1995; Mutch and others, 2016) yields pressure of crystallization (±0.5 kb) estimates of approximately 2 kb (corresponding to ~6–9 km depth) for samples collected from the northern Boulder Batholith south and southeast of Helena, and the southern Boulder Batholith between Butte and Whitehall. Samples from the western Pioneer Batholith (fig. 1) have relatively large errors and likely slightly greater depths of about 10–15 km. The Boulder Batholith in most cases intrudes along its roof the slightly older and ~3-km-thick Elkhorn Mountains Volcanics (EMVs; ~86–82 Ma; Klepper and others, 1957; Olson and others, 2016). The depth of emplacement estimates presented here include a distributed suite of samples from the eastern intrusive contact between the Butte Granite and EMV roof rocks (fig. 1). Consequently, the depth estimates based on hornblende barometry of 6 to 9 km differ greatly from the maximum stratigraphic thickness of 3–5 km of the roof or cover rocks.

EMV Regional Stratigraphic Relationships

The EMVs erupted ~86 to 83 Ma, and prior to emplacement of the early intrusions of the Boulder Batholith (~82 to 79 Ma) and the Butte Granite at ~76 Ma (summary in Olson and others, 2016; Reed and Dilles, 2020). The EMVs include a lower member of andesite and dacite lavas, a middle member of rhyolitic ignimbrites and other pyroclastic rocks, and a thin upper member of volcaniclastic sedimentary rocks and ignimbrites. The described total thickness of sections range up to 3 km (fig. 2) and composite thicknesses of correlated sections may be as much as 5 km (Smedes, 1966; summary in Scarberry and others, 2020).

Cretaceous Deformation in Western Montana

The zone of late Cretaceous Sevier (thin-skinned) shortening deformation lies along the eastern flank of the Rocky Mountain Front from the Canadian border southward to Helena and Whitehall, but farther south bifurcates into the more westerly Sevier belt and the easterly Laramide basement-cored uplifts of the Beartooth Mountains and Wyoming. Folds and local thrust faults deform the EMVs, which commonly have gentle (0–40°) dips and are deformed into open folds with north–south axes. East-vergent thrust faults are locally exposed on the flanks of the Boulder Batholith and locally place Paleozoic and Mesozoic (Jurassic–Cretaceous) sedimentary rocks over EMVs. The batholith post-dates and truncates these thrust faults. In the Wolf Creek quadrangle north of Helena, the 80–74 Ma volcanic and volcaniclastic rocks of the Two Medicine Formation were thrust-imbricated and folded prior to deposition of the Adel Mountain Volcanics between 74.7 and 73.7 Ma, which are in turn locally cut by younger thrust faults with minor offset (Harlan and others, 1988).

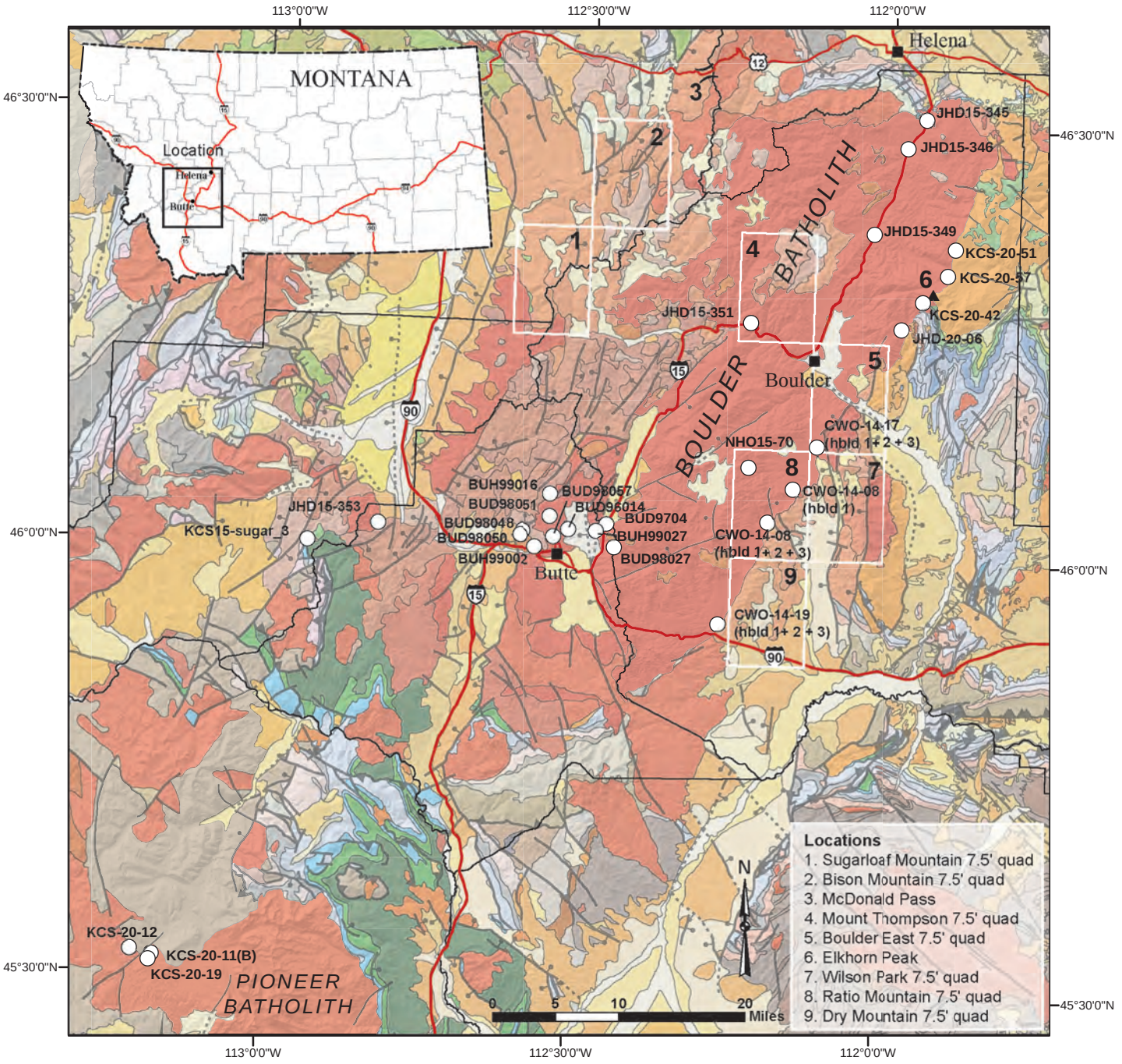

Figure 1. Regional geology of the Boulder and Pioneer Batholiths in southwestern Montana showing hornblende barometry sample locations (white circles) and 7.5' quadrangles mapped since 2013. Late Cretaceous Elkhorn Mountains Volcanics and other Cretaceous volcanic deposits (shown in orange) are exposed on the flanks of Late Cretaceous plutons (red).

Implications for Depth of Pluton Emplacement in Western Montana

A plausible explanation for the 6–9 km depth of emplacement of the currently exposed upper part of the Boulder Batholith is that these granitoids were emplaced into a thrust-imbricated, folded and thickened section of Elkhorn Mountain Volcanics. In other words, the EMV and locally Paleozoic sedimentary rocks may have been thrust atop EMV sections, and this process effectively doubled the EMV thickness immediately prior to batholith emplacement. The timing of shortening must therefore be in a narrow time window (<1–5 Ma) between eruption of the Elkhorn Mountain Volcanics and emplacement of the Boulder Batholith.between 81 and 76 Ma (du Bray and others, 2012). Although the data are more limited for the western Pioneer Batholith, the granitic samples yield greater depths (~10–15 km) and are commonly weakly deformed as seen by local gneissic and schistose textures. Consequently, the amount of exhumation is greater than for the Boulder Batholith.

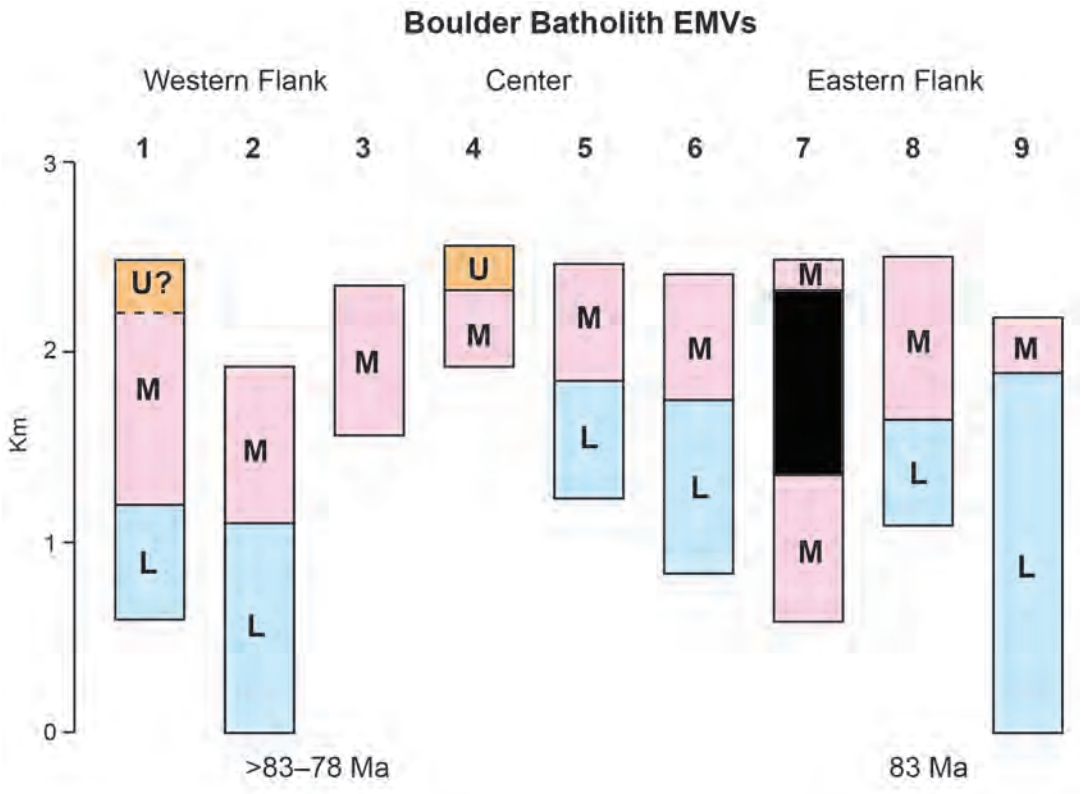

Figure 2. Schematic representation of Elkhorn Mountains Volcanics sections described in recent geologic mapping projects and other field studies (summary in Scarberry and others, 2019a,b). U, upper member; M, middle member; L, lower member. 80 Ma gabbroic sill (black)

Hornblende barometry studies of the Butte Granite at Butte (fig. 1) suggest that it was exhumed from ~6–9 km depth to ~2–5 km depth between ~66 Ma and 62 Ma, and continued exhumation brought rocks to the surface prior to deposition of the base of the Lowland Creek Volcanics at ~52 Ma (Houston and Dilles, 2013). These relationships suggest that Sevier shortening extended from ~80 Ma to 74 Ma and possibly to <62 Ma, and that exhumation was largely accomplished after Boulder Batholith magmatism ceased at 76 Ma. As normal faulting occurred synchronously with eruption of the Lowland Creek Volcanics in the Butte district, some of the post-62 Ma exhumation may have been partly driven by normal faulting and associated increases in topography.

References Cited

Anderson, J.L., and Smith, D.R., 1995, The effects of temperature and fO2 on the Al-in-hornblende barometer: American Mineralogy, v. 80, p. 549–559.

du Bray, E.A., Aleinikoff, J.N., and Lund, K., 2012, Synthesis of petrographic, geochemical, and isotopic data for the Boulder Batholith, southwest Montana: U.S. Geological Survey Professional Paper 1793, 39 p.

Harlan, S, Geissman, J., Lageson, D., and Snee, L., 1988, Paleomagnetic and isotopic dating of thrust-belt deformation along the eastern edge of the Helena salient, northern Crazy Mountains basin, Montana: Geological Society of America Bulletin, v. 100, p. 492–499.

Houston, R.A., and Dilles, J.H., 2013, Structural geologic evolution of the Butte district, Montana: Economic Geology, v. 108, no. 6, p. 1397–1424.

Klepper, M.R., Weeks, R.A, and Ruppel, E.T., 1957, Geology of the southern Elkhorn Mountains, Jefferson and Broadwater Counties, Montana: U.S. Geological Survey Professional Paper 292, 82 p., doi: https://doi.org/10.3133/pp292.

Mutch, E.J.F., Blundy, J.D., Tattitch, B.C., Cooper, F.J., and Brooker, R.A., 2016, An experimental study of amphibole stability in low pressure granitic magmas and a revised Al in hornblende geobarometer: Contributions to Mineralogy and Petrology, v. 171, p. 85, doi: 10.1007/s00410-016-1298-9.

Olson, N.H., Dilles, J.H., Kallio, I.M., Horton, T.R., and Scarberry, K.C., 2016, Geologic map of the Ratio Mountain 7.5′ quadrangle, southwest Montana: Montana Bureau of Mines and Geology EDMAP-10, scale 1:24,000.

Reed, M., and Dilles, J., 2020, Ore deposits of Butte, Montana, *in* Metesh, J.J., and Gammons, C.H., eds., Geology of Montana—Special Topics: Montana Bureau of Mines and Geology Special Publication 122, v. 2, 41 p.

Scarberry, K.C., Gammons, C.H., and Kallio, I.M., 2019a, Field guide to the geology and metallic mineral deposits along the eastern contact between the Boulder Batholith, the Elkhorn Mountains Volcanic Field, and Cretaceous–Paleozoic sedimentary rocks: Northwest Geology, v. 48, p. 97–108.

Scarberry, K.C., Coppage, E.L., and English, A.R., 2019b, Field guide to the geology and metallic mineral deposits along the western contact between the Boulder Batholith and the lower and middle members of the Elkhorn Mountains Volcanic Field: Northwest Geology, v. 48, p. 97–108.

Scarberry, K.C., Yakovlev, P.V., and Schwartz, T.M., 2020, Mesozoic magmatism in Montana, *in* Metesh, J.J., and Vuke, S.M., eds., Geology of Montana—Geologic History: Montana Bureau of Mines and Geology Special Publication 122, v. 1, 30 p.

Smedes, H.W., 1966, Geology and igneous petrology of the northern Elkhorn Mountains, Jefferson and Broadwater Counties, Montana: U.S. Geological Survey Professional Paper 510, 116 p., doi: https://doi.org/10.3133/pp510.

Kaleb Scarberry on block of marble just below Elkhorn Peak. Photo by Joel Dietrich.

Temporal Relations between the Boulder Batholith and Elkhorn Mountains Volcanics, Western Montana: "The Nature of Batholiths" Revised

K. Lund and J.N. Aleinikoff

U.S. Geological Survey, Denver, Colorado

Introduction

The Boulder Batholith and Elkhorn Mountains Volcanics, western Montana (fig. 1), served as a model for an influential paper on "The Nature of Batholiths" (Hamilton and Myers, 1967). This paper presented a persistently classic geologic model for coeval and cogenetic volcanic and plutonic rocks. A companion paper further developed the assertion that the Boulder Batholith, and by inference many other intrusive bodies, is less than 5 km thick (Hamilton and Myers, 1974). Combined, these papers presented a model for a thin plutonic layer in the crust that was overlain by its own volcanic ejecta (fig. 2). Despite being disputed (Klepper and others, 1971, 1974), the model of Hamilton and Myers (1967) has dominated assumptions for the Boulder Batholith region as well having been a template for such systems in the geologic literature more broadly. Although both the batholith and Elkhorn Mountains Volcanics were recognized as Late Cretaceous, methods to determine crystallization ages (which provide comparable emplacement and extrusion ages) were not available at the time of original studies. The isotopic ages, presented herein, provide the details to document the temporal relations and, therefore test, the genetic framework for the different parts of this igneous province.

Setting

The geologic details for both Boulder Batholith and Elkhorn Mountains Volcanics and for derivative genetic and geometric models came from the many detailed studies published by the U.S. Geological Survey. Those studies defined, mapped, and provided geochemical and preliminary age data for individual plutons of the batholith; determined map units in the Elkhorn Mountains Volcanics; and mapped the structure of the older country rocks. The studies were ultimately compiled into a geologic map of the region (fig. 1; Smedes and others, 1988; digital version in du Bray and others, 2009).

The Late Cretaceous Boulder Batholith occupies about 4,000 km^2 in southwest Montana. About 70 percent of the batholith is composed of the voluminous Butte Granite at the heart of the body (fig. 1). The rest of the batholith is composed of more than a dozen individually named intrusions that are contiguous with the Butte Granite. The smaller plutons are more compositionally diverse and include granodiorite, monzogranite, plus minor syenogranite and a mafic complex. Preliminary (K/Ar) ages were acquired for the main plutons of the batholith (Tilling, 1974). The batholith plutons intruded a thick succession of folded Mesoproterozoic Belt Supergroup, Paleozoic cratonic-basin sedimentary rocks, Late Cretaceous volcanic rocks, and Mesozoic orogenic-basin sedimentary rocks.

The Late Cretaceous Elkhorn Mountains Volcanics field covers about 8,000 km^2 in the area surrounding and above rocks of the batholith. They originally covered a significantly larger area (Smedes, 1967). The Elkhorn Mountains Volcanics are informally subdivided into three members, including (1) lower member that is a 760- to 1,520-m-thick succession of rhyodacitic and trachyandesitic tuff, tuff breccia, and subordinate flows and thin welded-tuff; (2) middle member that is as much as 2,290 m thick of rhyolitic welded tuff, crystal and lithic tuff, and less abundant volcanic breccia; and (3) upper member that is a more than 610-m-thick succession of volcaniclastic and pyroclastic rocks (Smedes, 1967; Scarberry and Yakevlev, 2018). Details from mapping in the best preserved parts of the field indicate the presence of eroded roots belonging to several calderas (Smedes, 1973; Watson, 1986; Rutland and others, 1989; Olson and others, 2016). The Elkhorn Mountains Volcanics unconformably overlie, and are folded with, the older sedimentary rocks.

The volcanic pile and the older sedimentary rocks were intruded by many named and unnamed "satellite" stocks and small plutons, which although exposed in the vicinity of the batholith, are separated from it by ex-

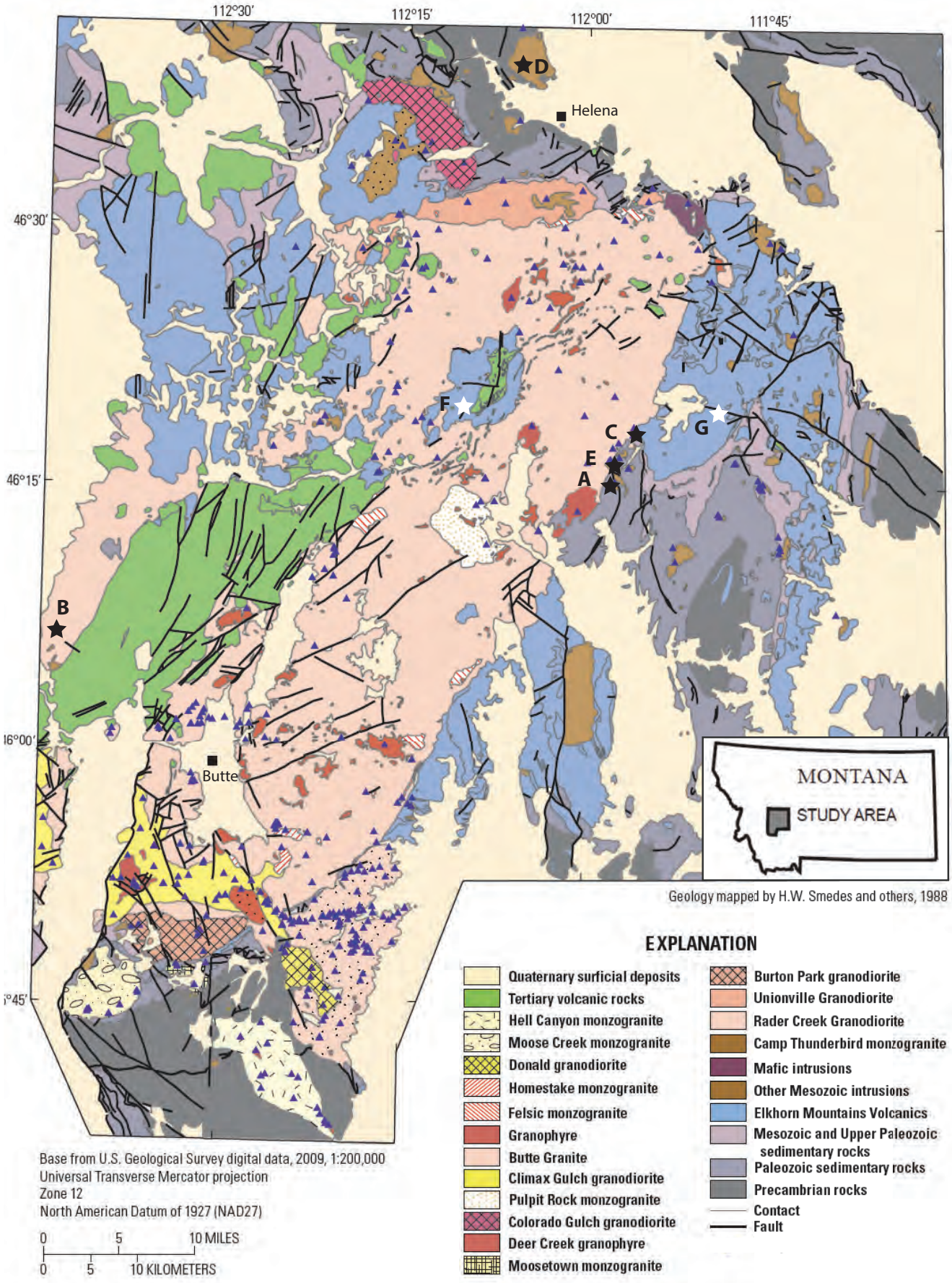

Figure 1. Generalized geologic map of plutonic units of the Boulder Batholith, western Montana (du Bray and others, 2009, from Smedes and others, 1988). Blue triangles, locations of geochemical data from du Bray and others, 2009, 2012); white stars, locations for dated samples of Elkhorn Mountains Volcanics; black stars, locations for dated samples of satellite plutons; letters refer to samples detailed in table 1.

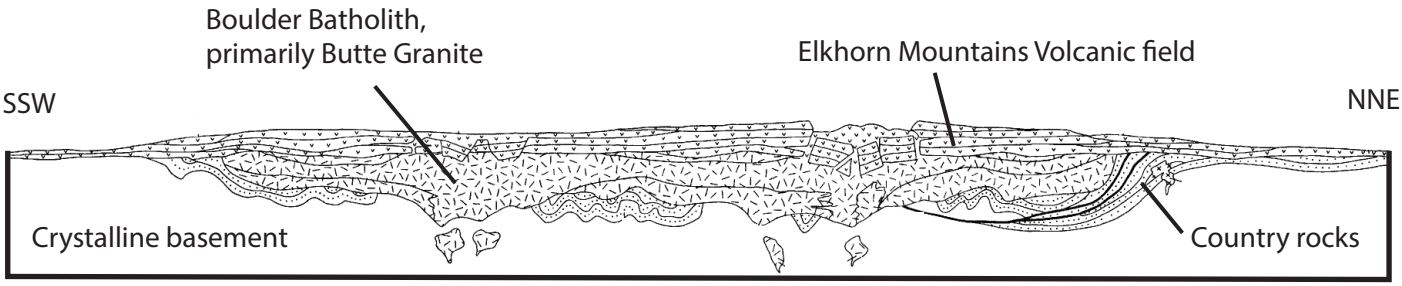

Figure 2. Model for the Boulder Batholith from "The Nature of Batholiths" (Hamilton and Myers, 1967).

posures of sedimentary or volcanic rocks (fig. 1). The satellite plutons exposed west and north of the Boulder Batholith include several large granite, granodiorite, and syenite plutons. East of the batholith there are also many smaller granodiorite to diorite plutons.

Previous Models for Boulder Batholith and EMV

The Boulder Batholith and Elkhorn Mountains Volcanics, being both Late Cretaceous and co-located, have long been considered to be coeval and cogenetic. The most widely publicized model describes (1) the volcanic rocks as a crust floating atop thin magmatic source bodies which are "in effect a gigantic mantled lava flow," (2) the volcanic and plutonic rocks as "contemporaneous and consanguineous," and (3) the plutons as having "crystallized beneath covers consisting largely of their own volcanic ejecta" (Hamilton and Myers, 1967, 1974). Based on the assumptions from that model, several geochemical and petrogenetic studies have directly related evolution of plutonic compositions to specific members of the volcanic section. In these studies, the lower volcanic member is linked with early more mafic plutons and most of the middle and upper volcanic members are linked with the younger more granitic plutons, primarily with the Butte Granite (Watson, 1986; Rutland and others, 1989; Ihinger and others, 2011).

The geologists involved in the original detailed mapping disputed much of that model, rejecting both that the batholith was less than 5 km thick and that the volcanic rocks were a cogenetic floating cap. As geologists who mapped most of the batholith and the volcanic units, Klepper and others (1971, 1974) combined geophysical and geologic evidence that modelled thickness of 10–20 km for the batholith (see references therein; Schmidt and others, 1990). More recent three-dimensional modeling interpreted the batholith as 7 km thick in thinner areas with two roots as deep as about 15 km (Berger and others, 2011). Based on geologic relations from their mapping, Klepper and others (1971) presented evidence that the volcanic rocks were folded with older country rocks before intrusion of the Butte Granite; thus, in agreement with much earlier descriptions (Weed, 1912). Their mapping also showed that, in several locations, the Butte Granite intruded into and cut out all members of the Elkhorn Mountains Volcanics section (Klepper and others, 1971); other studies reported hornfels metamorphism in the volcanic rocks near the granite contacts (Weed, 1912; O'Neill and others, 2004).

Geochronology

To test the diverse interpretations and petrogenetic models, we initiated an isotopic dating program for Elkhorn Mountains Volcanics members and satellite plutons to add to our earlier dating of the Boulder Batholith and northern satellite plutons (Lund and others, 2002, 2018; du Bray and others, 2012).

Existing geochronologic data for the Elkhorn Mountains Volcanics were limited; however, K/Ar ages on hornblende showed that volcanism began about 80 Ma (K/Ar data, as recalculated and summarized by Tysdal, 2000) and fossils associated with distal and presumably cogenetic volcanic rocks as well as from the volcaniclastic upper volcanic member show that volcanism continued until about 73 Ma (Robinson and others, 1968). This span in ages for the volcanism has been supported by more recent preliminary data (Ihinger and others, 2011; Olson and others, 2016).

The SHRIMP U-Pb emplacement ages for the plutons that form the Boulder Batholith produced the oldest age for a pluton at 80.7 Ma and the youngest at 73.7 Ma, with 14 plutons in the 78–74 Ma range. The Butte Granite produced two distinctly different ages of about 74.7 Ma in the north and 76.9 Ma in the south (Lund and

others, 2002). Although separate intrusions have not been mapped in the Butte Granite, the statistically distinct ages suggest that the two deeper roots identified in the Berger and others (2011) reinterpretation of geophysical data may have been the feeders for two discrete intrusive centers for rocks mapped as Butte Granite.

Five new SHRIMP U-Pb zircon ages for satellite plutons and ages for the lower and middle members of the Elkhorn Mountains Volcanics (table 1, fig. 3), in addition to our previously published emplacement ages for plutons of the batholith, provide constraints on interpretive magmatic relations. For the satellite plutons, 74.9-Ma diorite east of the batholith is about the same age as the younger batholith plutons, 75.8-Ma granitic granophyre west of the batholith is intermediate in age between the two dates for the Butte Granite, and 78.3-Ma granodioritic granophyre east of the batholith is about the same age as older plutons of the batholith (table 1, fig. 1). With the ages of the Boulder Batholith spanning 81–75 Ma, this group of new ages show that several satellite plutons both east and west of the batholith were coeval with it. Similar results were determined for previously dated satellite plutons exposed north of the batholith (du Bray and others, 2012). Alternatively, the new data for the 87.3-Ma Scratchgravel Hills syenite satellite north of the batholith and for the 88.6-Ma below Elkhorn townsite granodiorite east of the batholith (fig. 1, table 1) indicate that these satellite plutons are about 8 m.y. older than the oldest Boulder Batholith plutons. The SHRIMP U-Pb zircon ages indicate that lower and middle members of the Elkhorn Mountains Volcanics are 84.9 Ma and 83.3 Ma, respectively (fig. 1, table 1).

Table 1. SHRIMP U-Pb ages for selected satellite plutons and for volcanic members of the Elkhorn Mountains Volcanics, western Montana.

Satellite Plutons			
A	Mouth of Turnley Creek	Diorite	74.9 ± 1.3 Ma
B	Dry Cottonwood Creek	Granitic granophyre	75.8 ± 1.5 Ma
C	Windy Point	Granodioritic granophyre	78.3 ± 1.7 Ma
D	Scratchgravel Hills	Syenite	87.3 ± 1.4 Ma
E	Below Elkhorn town	Granodiorite	88.6 ± 2.1 Ma
Elkhorn Mountains Volcanics			
F	Big Chief Creek	Middle member	83.3 ± 1.8 Ma
G	Bomar Spring	Lower member	84.9 ± 1.6 Ma

Note. Locations shown by letters in figure 1. Isotopic data presented in Aleinikoff and Lund (in prep.).

Discussion

The new ages verify that the Elkhorn Mountains Volcanics and Boulder Batholith were not coeval. The pre-Boulder Batholith ages acquired for the Elkhorn Mountains Volcanics are corroborated by geologic relations that indicate that the volcanic rocks were folded with Mesoproterozoic to Mesozoic sedimentary country rocks before intrusion of the 77-Ma Butte Granite (fig. 1; Klepper and others, 1971; although the contact was subsequently also faulted). The ages are further supported by geologic evidence in the central northern part of Butte Granite exposures where (1) the Butte Granite intruded across all members of the Elkhorn Mountains Volcanics section (Becraft and others, 1963) and (2) Elkhorn Mountains Volcanics were contact metamorphosed near contacts with the Butte Granite (O'Neill and others, 2004).

The summary plot for the geochronologic data demonstrates that Boulder Batholith plutons and many satellite plutons were of the same generation (fig. 4). The plot also shows, however, that other satellite plutons are about 8 m.y. older than the batholith plutons. With respect to the Elkhorn Mountains Volcanics, the results indicate that Elkhorn Mountains volcanism initiated more than 2.5 m.y. after the early satellite plutons but more than 4 m.y. before emplacement of the oldest Boulder Batholith plutons and the bulk of the satellite plutons (fig. 4). The statistically valid gaps between the early satellite plutons and those of the batholith as well as between the known, dated plutons and the main volcanism of the Elkhorn Mountains Volcanics are significant enough to generally consider these as distinct magmatic events.

Revisiting this famous example of inferred cogenetic volcanics and plutons indicates a span of 7 m.y. between extrusion of the Elkhorn Mountains Volcanics and emplacement of the Butte Granite, although the granite was modeled as the underlying magma chamber and main source for the Elkhorn Mountains Volcanics.

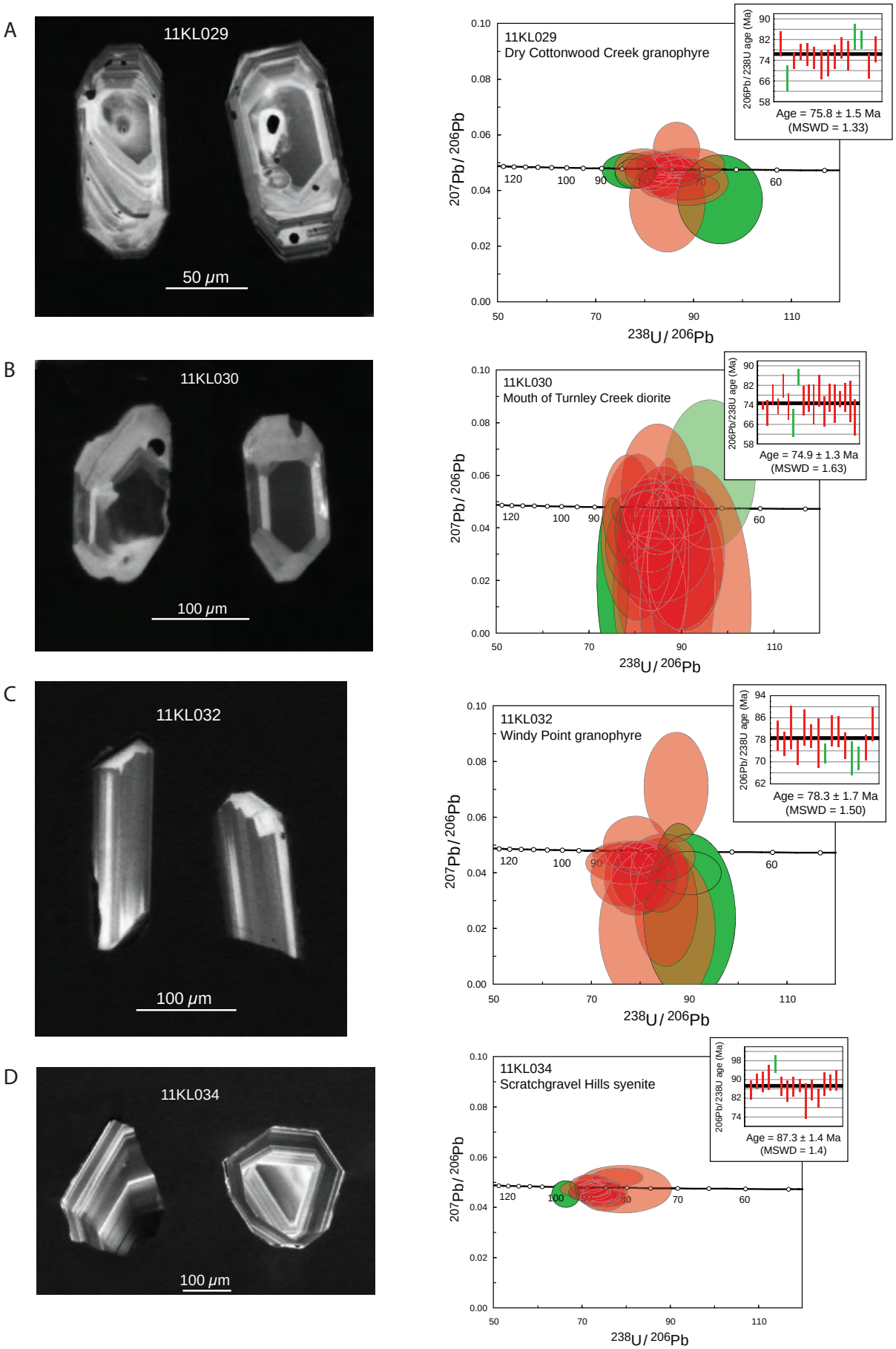

Figure 3. Results of SHRIMP U-Pb zircon geochronology of selected satellite plutons and of volcanic members of the Elkhorn Mountains Volcanics. Cathodoluminescence images of representative zircon grains from each sample shown on left and matched with Tera–Wasserburg concordia plots and weighted averages for the selected $^{206}Pb/^{238}U$ ages for each sample shown on right. Data summarized in table 1; sample locations shown in fig. 1. See Aleinikoff and Lund (2022) for data details.Parts E–G on following page.

E

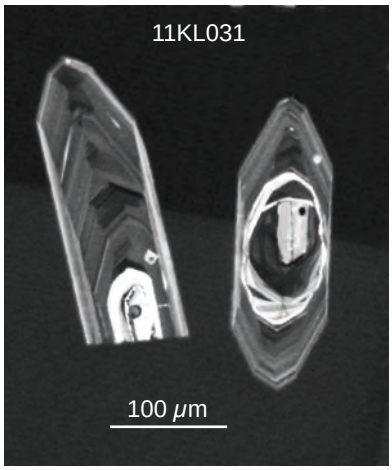

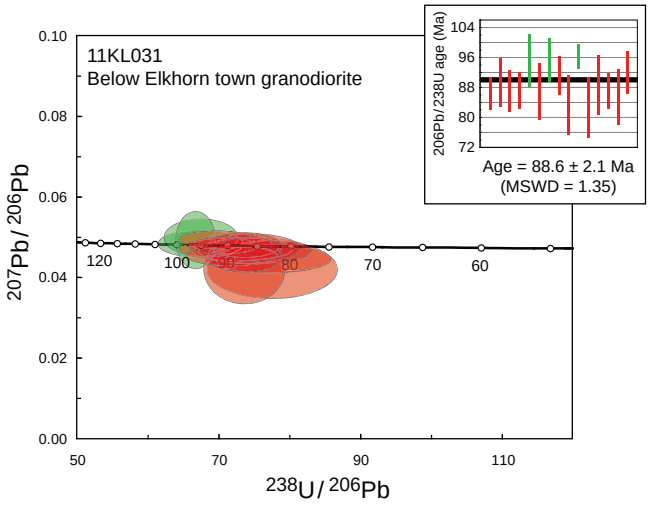

F

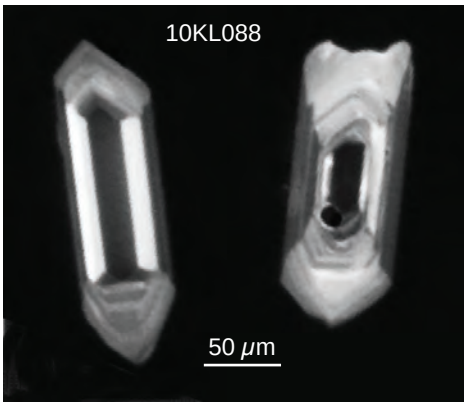

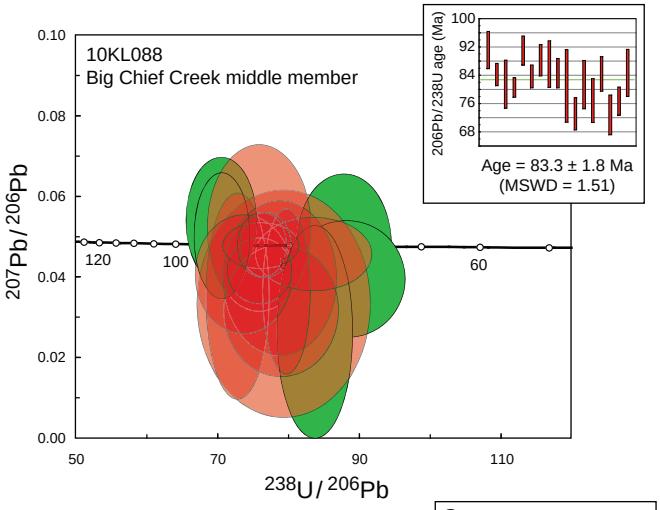

G

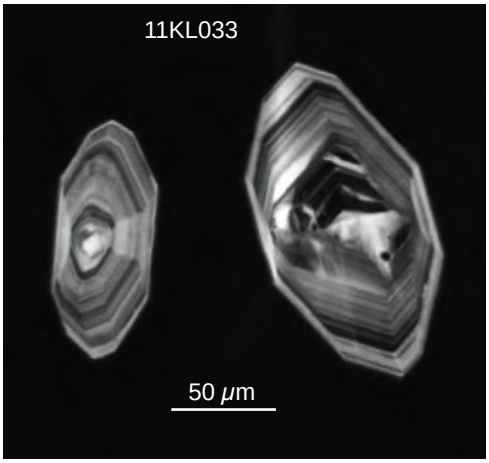

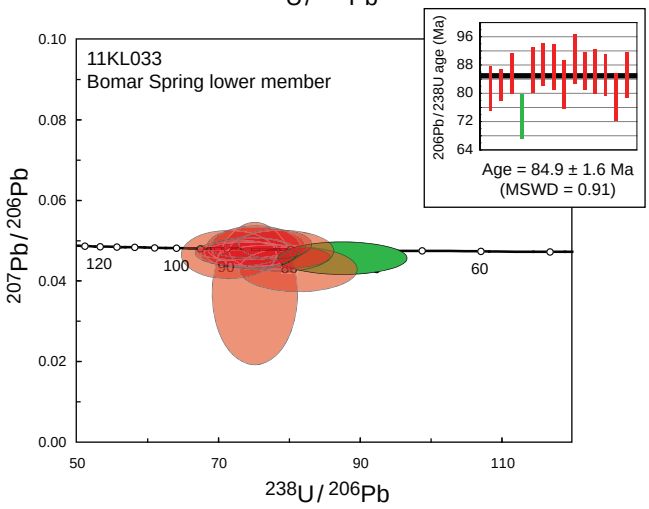

Figure 3 (cont.). Parts E–G. Caption on previous page.

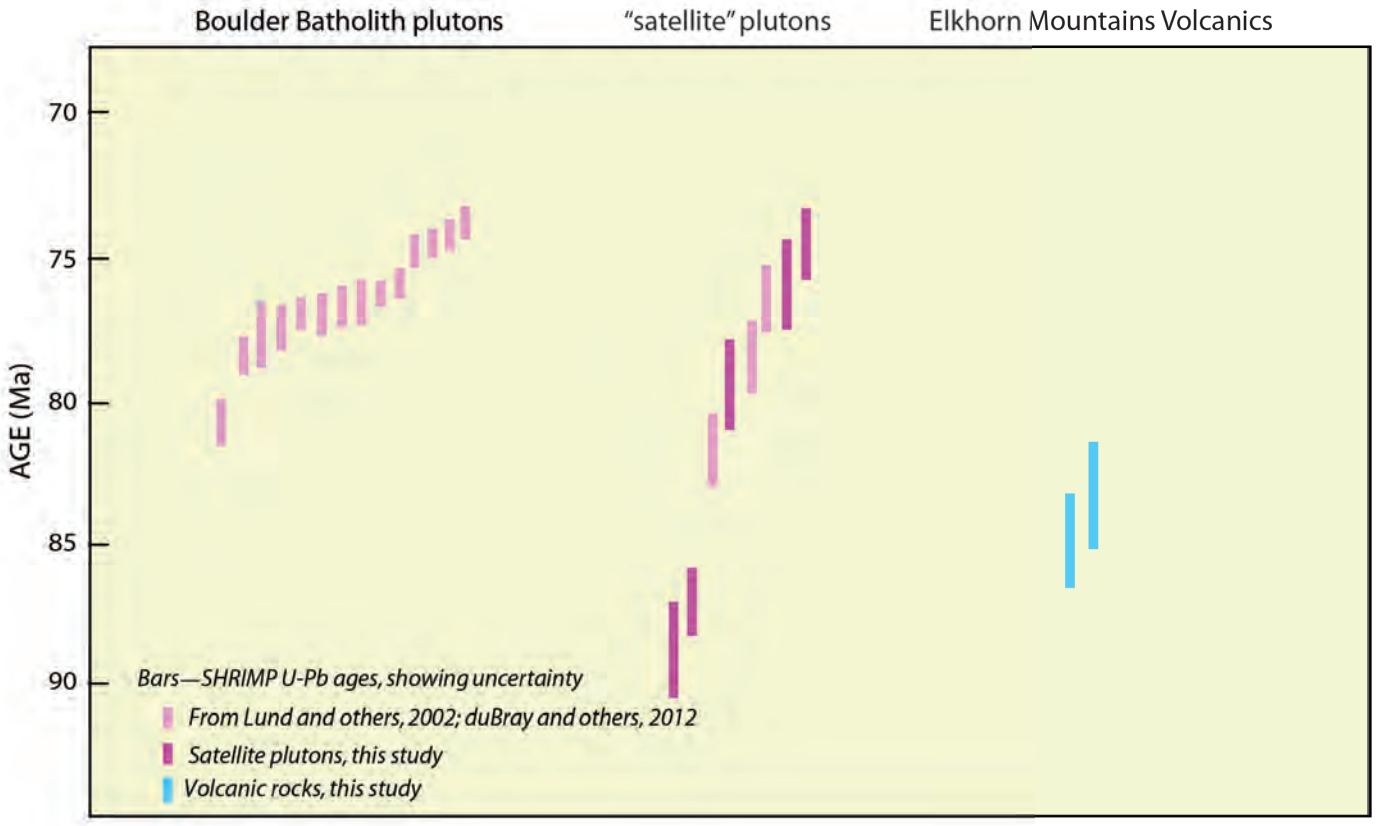

Figure 4. Summary of ages for Boulder Batholith plutons, satellite plutons, and Elkhorn Mountains Volcanics.

Thus, the volcanic and plutonic rocks did not have the same source magma. They were not the "contemporaneous and consanguineous" intrusive and extrusive system of Hamilton and Myers (1967). Our data confirm the statement of Klepper and others (1971), "Convincing examples of extrusive or quasi-extrusive thin batholiths must be sought elsewhere."

An interesting result of the dating is that the Elkhorn Mountains Volcanics eruptions occurred during an apparent gap in emplacement of known, dated plutons (fig. 4). The data show that, although it is possible that there may be yet-undated, small satellite plutons coeval with the EMV, there are no large plutons coeval with them. It is possible that the source of EMV was not centered over the Boulder Batholith, that the Butte Granite destroyed evidence for a hypothetical earlier and somewhat deeper plutonic system related to the Elkhorn Mountains Volcanics, or that the Elkhorn Mountains Volcanics did not have a significant intrusive equivalent. The resolution of these questions requires further research in the region.

References Cited

Aleinikoff, J.N., and Lund, K., in prep., SHRIMP U-Pb geochronologic data for zircon from the Elkhorn Mountains Volcanics and selected satellite plutons in the Boulder Batholith region, western Montana: U.S. Geological Survey Data Release, doi: https://doi.org/10.5066/P968GSXM.

Becraft, G.E., Pinckney, D.M., and Rosenblum, S., 1963, Geology and mineral deposits of the Jefferson City quadrangle, Jefferson and Lewis and Clark Counties, Montana: U.S. Geological Survey Professional Paper 428, 101 p.

Berger, B.R., Hildenbrand, T.G., and O'Neill, J.M., 2011, Control of Precambrian basement deformation zones on emplacement of the Laramide Boulder Batholith and Butte mining district, Montana, United States: U.S. Geological Survey Scientific Investigations Report 2011-5016, p. 29, available at https://pubs.usgs.gov/sir/2011/5016/ [Accessed January 2022].

du Bray, E.A., Lund, K., Tilling, R.I., Denning, P.D., and Dewitt, E.H., 2009, Geochemical database for the Boulder Batholith and its satellitic plutons, southwest Montana: U.S. Geological Survey Data Series 454, p. 19, available at http://pubs.usgs.gov/ds/454 [Accessed January 2022].

du Bray, E.A., Aleinikoff, J.N., and Lund, K., 2012, Synthesis of petrographic, geochemical, and isotopic data for the Boulder Batholith, southwest Montana: U.S. Geological Survey Professional Paper 1793, p. 46, http://pubs.usgs.gov/pp/1793 [Accessed January 2022].

Hamilton, W., and Myers, W.B., 1967, The nature of batholiths: U.S. Geological Survey Professional Paper 554-C, 30 p.

Hamilton, W., and Myers, W.B., 1974, The nature of the Boulder Batholith of Montana: Geological Society of America Bulletin, v. 85, p. 365–378.

Ihinger, P., Mahoney, J.B., Johnson, B.R., Kohel, C., Guy, A.K., Kimbrough, D.L., and Friedman, R.M., 2011, Late Cretaceous magmatism in southwest Montana: The Boulder Batholith and Elkhorn Mountains Volcanics: Geological Society of America Abstracts with Programs, v. 43, p. 647.

Klepper, M.R., Robinson, G.D., and Smedes, H.W., 1971, On the nature of the Boulder Batholith of Montana: Geological Society of America Bulletin, v. 82, p. 1563–1580.

Klepper, M.R., Robinson, G.D., and Smedes, H.W., 1974, Nature of the Boulder Batholith of Montana—Discussion: Geological Society of America Bulletin, v. 85, p. 1953–1960.

Lund, K., Aleinikoff, J.N., Kunk, M.J., Unruh, D.M., Hodges, W.C., du Bray, E.A., O'Neill, J.M., and Zeihen, G., 2002, SHRIMP U-Pb and $^{40}Ar/^{39}Ar$ age constraints for timing of mineralization in the Boulder Batholith, Montana: Economic Geology, v. 97, p. 241–267, doi: https://doi.org/10.2113/97.2.241.

Lund, K., McAleer, R.J., Aleinikoff, J.N., Cosca, M.A., and Kunk, M.J., 2018, Two-event lode-ore deposition at Butte, USA: $^{40}Ar/^{39}Ar$ and U-Pb documentation of Ag-Au-polymetallic lodes overprinted by younger stockwork Cu-Mo ores and penecontemporaneous Cu lodes: Ore Geology Reviews, v. 102, p. 666–700, doi: https://doi.org/10.1016/j.oregeorev.2018.05.018.

Olson, N.H., Dilles, J.H., Kallio, I.M., Horton, T.R., and Scarberry, K.C., 2016, Geologic map of the Ratio Mountain 7.5' quadrangle, southwest Montana: Montana Bureau of Mines and Geology EDMAP 10, scale 1:24,000, available at https://mbmg.mtech.edu/pdf_edmap/ed-10_RatioMtn.pdf [Accessed February 2022].

Robinson, G.D., Klepper, M.R., and Obradovich, J.D., 1968, Overlapping plutonism, volcanism, and tectonism in the Boulder Batholith region, western Montana: Geological Society of America Memoir 116, p. 557–576.

Rutland, C., Smedes, H.W., Tilling, R.I., and Greenwood, W.R., 1989, Volcanism and plutonism at shallow crustal levels—The Elkhorn Mountains Volcanics and the Boulder Batholith, southwestern Montana: International Geological Congress, 28th, Washington, D.C., Field Trip Guidebook T337, p. 16–31.

Scarberry, K.C., and Yakovlev, P.V., 2018, An overview of Mesozoic magmatism in Montana: Montana Bureau of Mines and Geology Special Publication 120 p. 57–62.

Schmidt, C.J., Smedes, H.W., and O'Neill, J.M., 1990, Syncompressional emplacement of the Boulder and Tobacco Root batholith (Montana-USA) by pull-apart along old fault zones: Geological Journal, v. 25, p. 305–318.

Smedes, H.W., 1967, Geology and igneous petrology of the northern Elkhorn Mountains, Jefferson and Broadwater counties, Montana: U.S. Geological Survey Professional Paper 510, 116 p.

Smedes, H.W., 1973, Regional setting and general geology of the Boulder Batholith, Montana: Society of Economic Geologists, Butte Field Meeting, p. A1–A6.

Smedes, H.W., Klepper, M.R., and Tilling, R.I., 1988, Preliminary map of plutonic units of the Boulder Batholith, southwestern Montana: U.S. Geological Survey Open-File Report 88-283, scale 1:200,000.

Tilling, R.I., 1974, Composition and time relations of plutonic and associated volcanic rocks, Boulder Batholith region, Montana: Geological Society of America Bulletin, v. 85, p. 1925–1930.

Tysdal, R.G., 2000, Revision of Cretaceous Slim Sam Formation, Elkhorn Mountains area, Montana: U.S. Geological Survey Professional Paper 1601-B, p. B1–B8.

Watson, S.M., 1986, The Boulder Batholith as a source for the Elkhorn Mountains Volcanics southeast quarter of the Deerlodge 15' quadrangle, southwestern Montana: University of Montana, Missoula, Mont., Master's Thesis, 113 p.

Weed, W.H., 1912. Geology and ore deposits of the Butte district, Montana: U.S. Geological Survey Professional Paper 74, 262 p.

Marble contact with the Elkhorn Mountains Volcanics near Elkhorn Peak. Photo by Stan Korzeb.

Joel Dietrich (center) at the field trip to Elkhorn Ghost Town. Photo by Peter Larson.

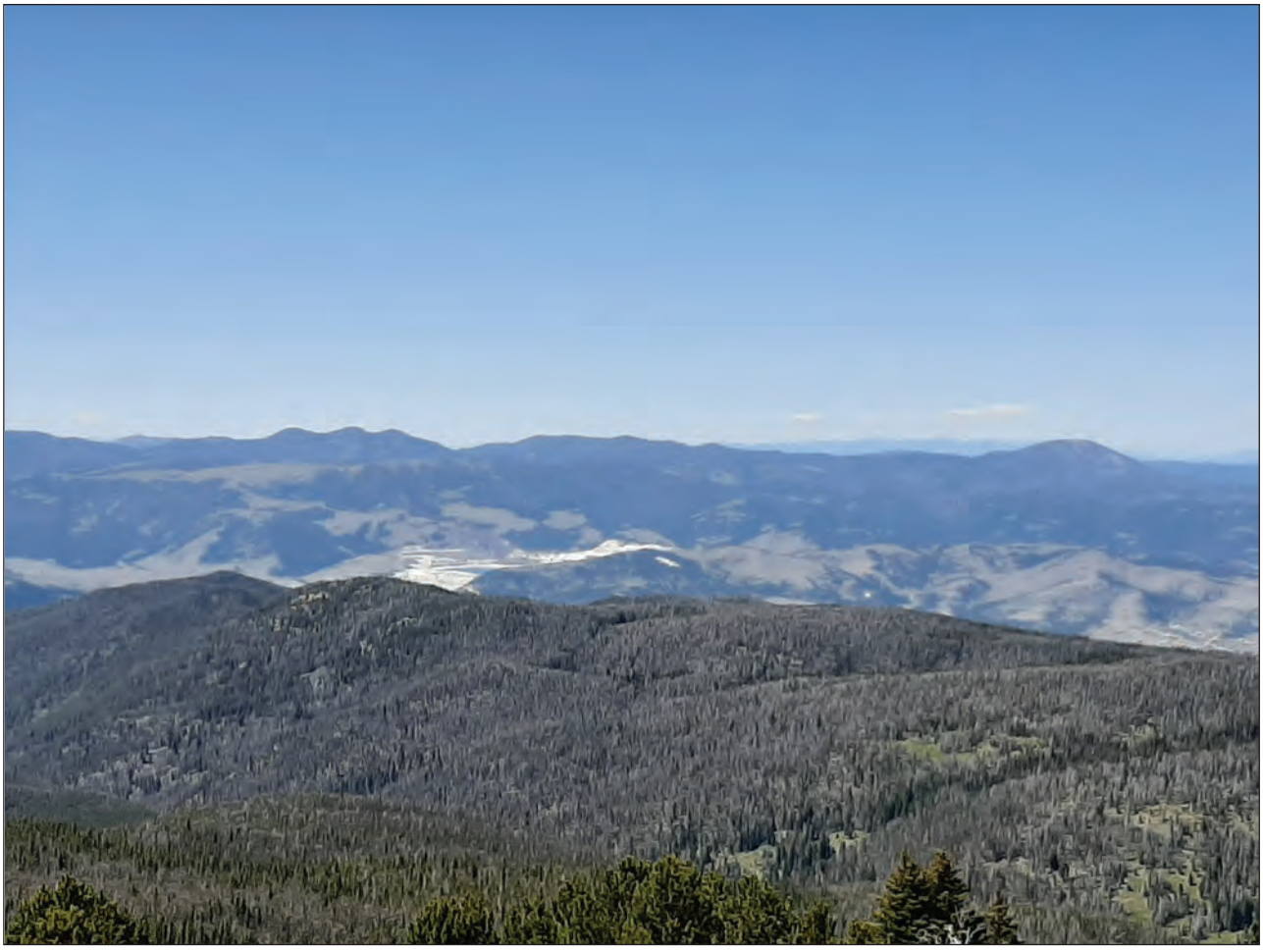

Montana Tunnels from Elkhorn Peak. Photo by Joel Dietrich.

Structural Analysis Reveals Wrench-Fault Controls of Vein Systems and Defines a New Ore Resource in the Radersburg District

C.B. Byington

Owner and Manager, Millenium Geoscience Consulting, Holistic Mines Group, and Crow Creek Mining Company

The Radersburg (aka Cedar Plains or Crow Creek) mining district is located approximately 90 highway kilometers southeast of Helena, Montana. The district produced in excess of 10,109 kg of gold (325,000 oz Au) with an average tenor of 26.4 g/tonne Au (0.77 opt Au), and is also credited with an additional 8,087 kg of silver (260,000 oz) and small amounts of copper, lead, and zinc (Klepper and others, 1971).

Techniques used in this study include Integrated Structural Analysis, statistical analysis of geometric fracture orientations, detailed structural field mapping, and paleo-stress field and paleo-kinematics determinations, and the development of a decline exposing the Arroyo and Revenue veins. These techniques were integrated with detailed satellite imagery defining associations of historic workings and placer relationships. Acquired or Crow Creek Mining-generated databases include soil survey geochemistry, aeromagnetics survey, multi-company drill hole cross-sections, maps and assay reports, petrographic and alteration mapping, transmitted-light microscopy, and mill tailings analysis.

Geometric-driven structural modeling and statistical analysis of measured fractures combined with innovative techniques in satellite analysis and detailed geologic mapping and sampling revealed a sinistral-dominated wrench fault system, herein named the Cedars Fault. The Cedars Fault system is at least 12 km in width (at Radersburg) and appears to be over 100 km in length, continuing from the Canyon Ferry reservoir southward to Virginia City, Montana. It also appears to be responsible for much of the intense folding of sediments in the southeastern Elkhorn Mountains. The Cedars system fractures cut an intrusive complex of three late Cretaceous(?) intrusive bodies including a pyrite-rich, gold-bearing, quartz-granitoid (Kq), a weakly porphyritic monzonite (Km), and an early porphyritic diorite (Kd), as well as Paleozoic sediments and Cretaceous Elkhorn Mountains Volcanics. Yet-to-be-sampled endoskarned diorite and exoskarned sediments are also present as large bodies. One fire assay sample of “cleaned” Kq contained 1.13 g Au per tonne (0.033 opt Au), confirming that Au occurs in the pyrite of the intrusive rock as well as along the fractures.

Two strands of the Cedars wrench system, the Spring and Crow Creek Faults, clearly control the veins of the Radersburg district, producing sympathetic extension fractures hosting most of the veins along with antithetic conjugate fractures that also host a few veins. Within the Radersburg district the extension fractures and the less common antithetic fractures occur in clusters producing three distinct vein swarms. One of the fracture swarms accounts for the Keating/Ohio area veins, and another for the Black Friday/Iron Age area veins, both of which are now incompletely mined out. A third unexplored vein swarm, herein called the Revenue vein system, is the largest of the three, and has received only superficial exploration, most of which was in the form of 1-m-deep prospect pits with two 8-m-deep shafts at the distal ends. The main Revenue vein and associated strands as mapped average about 100 m apart.

The Revenue vein system, clearly responsible for nearly all of the placer Au, has received little exploratory work beyond the surficial prospect pits of the earliest prospectors. This system is composed of at least five closely spaced large veins and many smaller veins developed as extension fractures between two strands of the Cedars Fault system, herein named the Spring and Crow Creek Faults. This new (to recent workers) vein system is explored to a maximum depth of 6 m by only two shafts separated by 1.6 km of strike length along the Revenue vein. Sixteen fire assay samples taken from dumps and outcrops representing the Revenue vein and its parallel strands along a 1.6-km strike length average 7 g Au per tonne (0.204 oz Au per ton), with the highest value being 27.9 g Au per tonne (0.814 opt Au). Inexplicably there is no known drill testing of the Revenue veins.

old-bearing veins along the Cedars Fault continue for 7.5 km while Au veining along the Revenue system is over 2.3 km in length. This structurally driven discovery is significant in that a NI 43-101 compliant Resource for the district's unmined veins calculated 38,655 kg Au in the Measured category, 81,446 kg Au in the Indicated category, and 47,194 kg in the Inferred category, totaling 167,295 kg Au (5.4 million oz Au, *in situ*, district wide). The NI 43-101-compliant Resource for Crow Creek Mining's 100% controlled newly discovered veins indicates 15,725 kg Au in the Measured category, 13,778 kg Au in the Indicated category, and 7,130 kg in the Inferred category, totaling 36,634 kg Au or about 1.18 million oz Au (*in situ*). All Resource calculations referenced here used a conservative 17–25% payability, a 1-m width, and a 300-m total depth, along with a discounted grade of 24.01 g Au/tonne (0.7 opt Au). Numerous specific gravity measurements were made to determine a precise tonnage factor.

Factors favoring production include:

1. High-grade Au veins (average production grade = 26.41 grams Au/tonne) in close proximity (~100 meters average separation) and with near-surface vein apexes and with an excellent depth projection of well beyond 300 m,
2. Ability to use all cyanide extraction techniques on underground ores,
3. Good metallurgy (reported 85+% gravimetric-only recovery in the 1860s–1920s, and 85–92% vat leach-only extraction with amalgamated ores in late 1980s),
4. Two nearby (<3 km) mills, one of which is currently permitted and operational,
5. A nearby (~500 m) high-voltage (500 kV) electrical power source,
6. Very encouraging diamond drill results in the Keating vein area, including wall-rock intercepts such as 3.4 g/tonne Au along 32 m, 3.8 g/tonne Au along 29 m, or 3.1 g/tonne Au along 30.5 m,
7. Good environmental and political reviews in various reports (no mine effluent in district, adjacent Bureau of Land Management's (BLM) OHV park, widespread historic placer disturbance, abundant patented land, and BLM-administered federal oversight),
8. Host rock with good geotechnical characteristics (i.e., stopes from late 1800s still accessible in early 1950s), and high vein density (up to six large veins within a 400-m width along the untested Revenue vein system),
9. Good logistics (maintained asphalt highway access with last 2 km of gravel road, and railroad siding at 16-km distance),
10. Encouraging gold-bearing strike continuity shown by Revenue vein dump-sample results (1.6 km of Revenue vein and splays strike length averaging 7 g Au per tonne (0.204 oz Au per ton), and
11. Good working relationship with State and Federal oversight agencies.

A New Look at the Sapphire-Bearing Yogo Lamprophyre Dike

Tracey Cotterell and John Ridley

Department of Geosciences, Colorado State University, Fort Collins, Colorado

The Yogo lamprophyre dike in the Paleogene Central Montana Alkaline Province (CMAP) is Montana's only known significant primary resource of gem- and industrial-grade sapphires (Berg, 2009). It has been mined in surface pits down to about 20 m, and in two underground mines down to about 100 m. The dike is a member of the dense cluster of alkaline intrusions in the Little Belt Mountains and forms a steeply dipping intrusion with local gaps, splays, and steps, approximately 7 km long and up to 6 m wide. The dike cuts shallowly dipping massive limestones of the upper Madison Group and the overlying clastic sedimentary rocks of the lower Big Snowy Group (Dahy, 1988; Gauthier, 1995). The Yogo dike is geochemically and petrographically unique among the alkaline intrusions of both the Little Belt Mountains and the broader CMAP as a carbonate-bearing, silica-poor, phlogopite- and clinopyroxene-bearing but olivine poor, lamprophyre with an analcime-rich matrix and abundant xenoliths and carbonate-bearing ocelli (fig. 1). It has been classified as ouachitite, a biotite-rich monchiquite, a class of ultramafic lamprophyre containing "forsteritic olivine, diopsidic pyroxene, various amphiboles and phlogopite in a matrix of similar minerals with primary carbonates and feldspathoids" (Streckeisen, 1979), although it doesn't share all characteristics of ouachitite at the type locality (Meyer and Mitchell, 1988).

The sapphires are rounded to platy megacrysts (fig. 1), in many cases with microscopic reaction rims of spinel against the ouachitite matrix. A number of ultimate sources of the sapphires have been proposed: they are either xenocrysts, picked up from a corundum-bearing lithology in the underlying metamorphic Archean crust or upper mantle, or are products of peritectic reactions between the lamprophyre melt and Al-rich xenoliths of the lower crust (e.g., Palke and others, 2018). Here we report on three areas of new results on the dike:

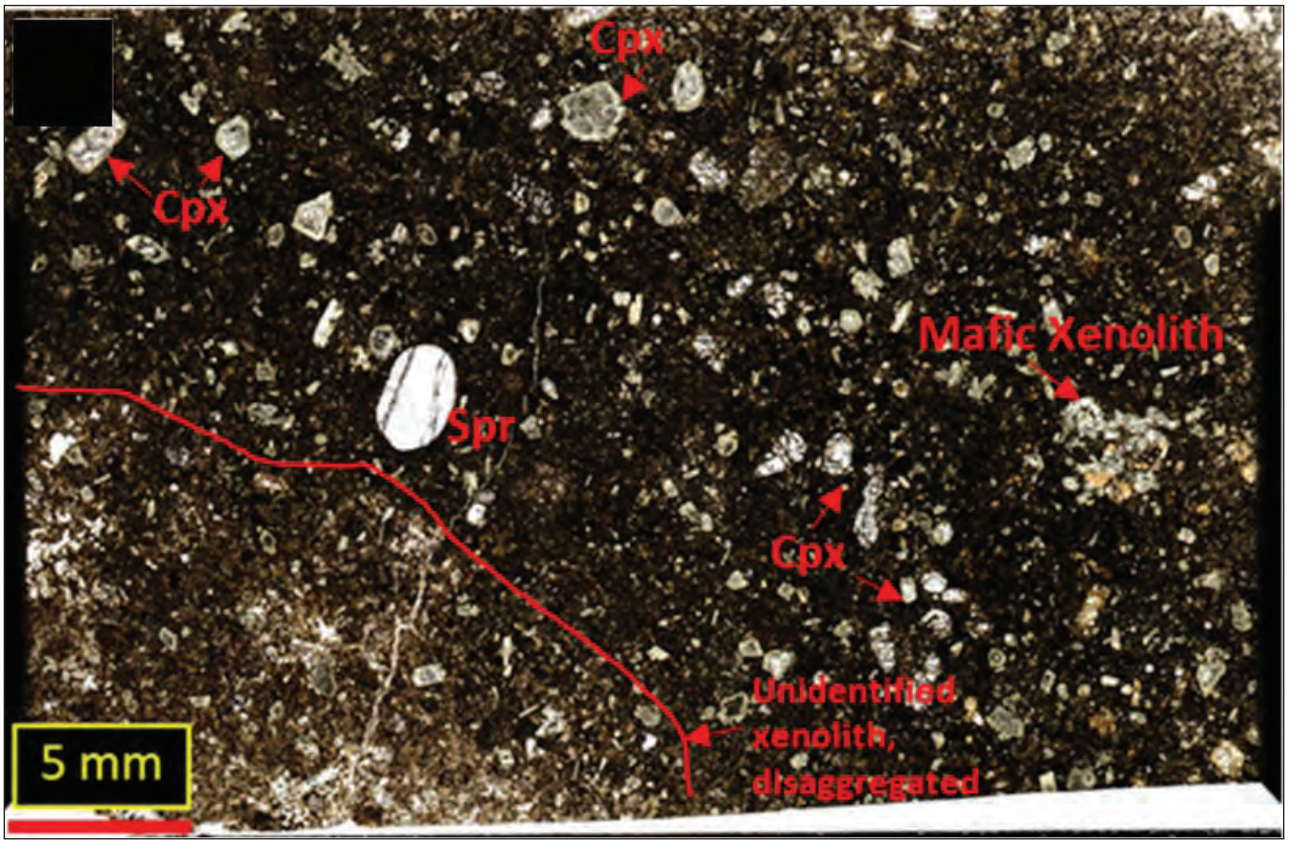

Figure 1. Large-area polarized light photomicrograph of a Yogo ouachitite sample with xenoliths, a rounded sapphire megacryst, and clinopyroxene phenocrysts, in a matrix of fine-grained phlogopite, clinopyroxene, analcime, and feldspathoids.

(1) greater variability of geochemistry and petrography than previously recognized; (2) interpretation of the nature and origins of xenoliths in the dike, and; (3) interpretation of the importance of Paleozoic karst on the structures of the dike and that some lamprophyre-bearing breccias are peperite, that is, a rock formed by mingling of coherent magma with unconsolidated wet sediment (e.g., Skilling and others, 2002).

Previous studies suggested from field relations that there were multiple phases of penecontemporaneous intrusion in the dike (e.g., Dahy, 1988). Two phases are distinguished here based on relatively subtle but consistent differences in both geochemistry and petrography. The contact between the two is sharp, but is not marked by chilling or remelting. Lamprophyre 1, for instance, is relatively FeO- and LREE-poor and Al_2O_3-rich compared to lamprophyre 2. Lamprophyre 2 has less biotite, more clinopyroxene, a significantly greater abundance of largely pseudomorphed olivine, few carbonate-rich ocelli, and a glassy as opposed to analcime- and feldspathoid-dominated matrix. As trace-element geochemistry implies that the two phases are petrogenetically related, they were thus presumably pulses within a single intrusive event. Both phases are sapphire-bearing.

Xenoliths are common throughout the lamprophyres, as they can be in many alkaline basaltic dykes. Xenoliths are of scientific interest as probes of components of the underlying crust and upper mantle, and in the case of the Yogo dike, for interpretation of potential sources of the sapphires, irrespective of whether these are xenocrystic or peritectically grown. The abundant and pervasive xenoliths at Yogo range in size from 1 to 40 mm, are generally rounded and often embayed, and are mineralogically and texturally very varied (Berger and Berg, 2002). Most have mineralogically distinct reaction rims a few millimeters wide against the host lamprophyre. The xenoliths can be classified based on mineralogy and textures in hand specimen as ultramafic (largely pyroxenite or biotite–pyroxenite), mafic (pyroxene–feldspar), granitic, quartz vein, calc-silicate, and metasedimentary. Petrographically it is observed that, in addition to the formation of reaction rims, most xenoliths have been strongly metasomatically altered throughout. The mineral assemblages of many xenoliths overlap those typical of fenites, with amphibole and calcite, and in some cases K-feldspar. For instance, K-feldspar has replaced plagioclase in the interior of one mafic clast and has reaction rims of blue muscovite and chlorite. Granitic clasts, and to a lesser extent mafic clasts, have been partially melted and typically have worm-like patches of glass between quartz and feldspars. Spot analyses of clast geochemistry by pXRF gives a range of element ratios, such as Zr:Ti and Cr:Ti, which likely remain invariant during alteration or weathering (Hallberg, 1984), confirming the interpretation of a range of xenolith rock types. Although some clasts have element ratios that correspond to the interpretation of rock type based on mineralogy, the dominant clast types have ratios corresponding to “dacite” and have higher concentrations, in particular of Zr, than all common rock types. The dacitic chemistry implies that many clasts are derived from crystalline lower crust or from Belt Group clastic metasediments. The strength of metasomatism in the xenoliths, and the presence of melt in granitic and mafic clasts, support the suggestion of Palke and others (2018) that corundum was a product of reactions with inclusions or along the contacts of the intrusion. No xenolith with corundum has been observed in this study. The range of xenolith rock types makes it difficult to constrain the rock type that either released the corundum to the magma or in which corundum was formed.

Because of its effect on the ease of sapphire extraction from the host rock, portions of the Yogo dike that have been softened by weathering have been the focus of mining. Breccias have also been sought after ores, but the geological reasons for their richness have not been investigated. The productive breccias along the length of the dike are those in which lamprophyre is included as generally scattered, strongly weathered blebby clasts from a few to tens of centimeters across and wispy thin dikes between clasts and matrix of the Madison Group massive limestones and Big Snowy Group siltstones. The weathered lamprophyre may have different colors (gray-green, red, or yellow), but is recognizable by the presence of bright green weathered pyroxene phenocrysts. This type of breccia is interpreted here to be a product of intrusion into karst.

Karst structures are widespread in the Madison Group in and around Yogo, are very similar to those described regionally in the Madison Group, and include dolines, spires, and sediment cones. As has been interpreted regionally (e.g., Sando, 1974), the Paleozoic, immediately post-depositional age of much of the karst is implied by the concentration of dolines along the upper contact of the Madison with the Big Snowy Group. Breccias are common and can be divided into monomict, which are generally consolidated and have clasts only

of the host limestone, and polymict, which are typically loose and are composed of a mixture of limestone and siltstone clasts. Transitions are recognized downwards and laterally from crackle- to mosaic- to rubble-karst breccias.

Lamprophyre clasts and dikelets are in all cases found in semi-consolidated polymict breccias which, in some instances, constitute a sediment cone in a karst breccia (fig. 2). There is very limited petrographic evidence of thermal or mechanical interaction between the lamprophyre and other clasts of the host breccias. There are no quench textures. Adjoining limestone is unrecrystallized, although there may be thin calcite veins along the dike–limestone contacts. The lamprophyre-bearing breccias were previously interpreted as post-intrusive karst breccias or syn-intrusive diatremes. However, in view of the textures and field relations observed in the current study, we reinterpret them as peperites (Skilling and others, 2002). The limited thermal interaction of magma and sediment is typical of peperite where a vapor film insulates the magma from the sediment. Peperite most typically forms where mafic lavas extrude over wet sediments, but could have formed at Yogo where magma intruded into and interacted with preexisting unconsolidated karst breccias in the Madison Group.

The strong weathering of lamprophyre clasts in breccias that are interpreted as sediment cones is presumably the result of meteoric water infiltrating preferentially through karst fractures, openings, and unconsolidated sediment fill. This interpretation, and the observation underground of localized strong weathering of the dike to at least the depths of mining of about 100 m, imply that karst structures and their permeability may be important controls on where the dike can be effectively mined.

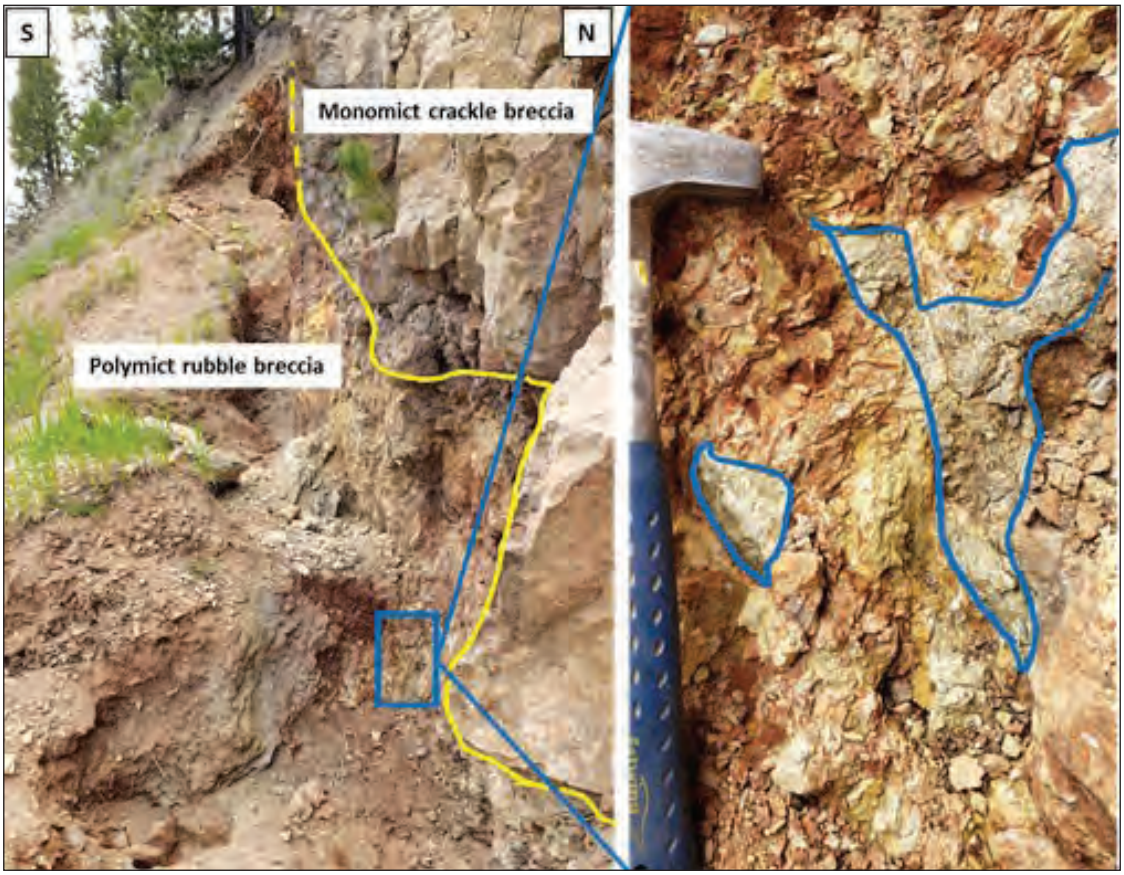

Figure 2. Polymict rubble breccia included wispy clasts of weathered lamprophyre, – as outlined in the right-hand frame. The breccia is along the strike of the Yogo dike and contains a monomict crackle breccia of massive Madison Group limestone overlying and adjacent to a semi-consolidated polymict breccia a few meters wide that has limestone, red siltstone, and lamprophyre clasts in a similar composition matrix and is interpreted as a sediment cone.

References

Berger, A.L., and Berg, R.B., 2002, Montana sapphires and speculation on their origin, *in* Scott, P.W., and Bristow, C.M., eds., Industrial minerals and extractive industry geology: Geological Society of London, p. 199–204.

Berg, R.B., 2009, Montana sapphires: Past, present, and future: Northwest Geology, v. 38, p. 7–18.

Dahy, J.P., 1988, The geology and igneous rocks of the Yogo sapphire deposit and the surrounding area, Little Belt Mountains, Judith Basin County, Montana: Montana College of Mineral Science and Technology, M.S. Thesis, 92 p.

Gauthier, G., 1995, Mineralogy, geochemistry, and geochronology of the Yogo Dike sapphire deposit, Montana: University of British Columbia, M.S. Thesis, 280 p.

Hallberg, J.A., 1984, A geochemical aid to igneous rock type identification in deeply weathered terrain: Journal of Geochemical Exploration, v. 20, p. 1–8.

Meyer, D.O.A., and Mitchell, R.H., 1988, Sapphire-bearing ultramafic lamprophyre from Yogo Gulch, Montana: A ouachitite: Canadian Mineralogist, v. 26, p. 81–88.

Palke, A.C., Wong, J., Verdel, C., and Avila, J.N., 2018, A common origin for Thai/Cambodian rubies and blue and violet sapphires from Yogo Gulch, Montana, USA?, American Mineralogist, v. 103, p. 459–479.

Sando, W.J., 1974, Ancient solution phenomena in the Madison Limestone (Mississippian) of north-central Wyoming: Journal of Research of the U.S. Geological Survey, v. 2, p. 133–141.

Skilling, I.P., White, J.D.L., and McPhie, J., 2002, Peperite: A review of magma-sediment mingling: Journal of Volcanology and Geothermal Research, v. 114, p. 1–17.

Streckeisen, A., 1979, Classification and nomenclature of volcanic rocks, lamprophyres, carbonatites, and melilitic rocks: Recommendations and suggestions of the IUGS Subcommission on the Systematics of Igneous Rocks: Geology, v. 7, p. 331–335.

East Coeur D'Alene Mining District, Mineral County, Montana: Production History, Structural Controls, and Renewed Exploration of Mesothermal Silver–Base Metal Veins

Bruce Cox and Ted Antonioli

Principals of Silver Trend Mines LLC, Missoula, Montana

Introduction

Silver and base metal deposits of the Coeur d'Alene mining district extend from the "Silver Valley" of Shoshone County, Idaho about 70 mi eastward into Mineral and Missoula Counties, in a narrow belt along the Osburn and Ninemile fault zones. The Coeur d'Alene trend is one the world's greatest producers of silver, rivaling the great silver mining districts of Mexico and Bolivia. Silver Trend Mines LLC (herein abbreviated STMLLC) owns exploration-stage properties in Montana's East Coeur d'Alene mining district covering historic mines named (west-to-east) Tarbox, Meadow Mountain, Black Traveler, and Prosperity (fig. 1). These mines exhibit geologic structures, wall-rock alteration, and vein minerals typical of major producers in the Idaho part of the district, but have not been explored or developed to depths that have historically yielded much higher ore grades.

History of Mining in the East Coeur D'Alene District

Tarbox and Meadow Mountain

The Tarbox Mining Company and the Mineral King Mining Company developed these mines from 1886 to 1952; workings included the 1,000-ft-deep Tarbox shaft and winze (fig. 2) with over 4,000 ft of underground workings and several satellite mine adits. American Smelting and Refining Company (ASARCO) and Sunshine Mining Company optioned the property in the 1950s and 1960s, performing surface exploration and rehabilitation of the shaft levels. In the 1980s, Resource Enterprises, Inc., a Canadian junior company, optioned the property and others now held by STMLLC. The Tarbox shaft collar and waste rock dumps have been reclaimed.

Black Traveler

The following paragraph on Black Traveler history is condensed from regional newspaper articles dated 1891–1913 and from abandoned mines files of the Montana Department of Environmental Quality. The principal Black Traveler and Saltese Consolidated veins were discovered in the 1880s by W.G. Lucas or O.S. Roof and operated into the 1930s by the Black Traveler Copper Mining Company. In 1939, Roof's successor and former partner conducted the last known underground development, which was reported to have intercepted "good copper" while extending the previous workings. ASARCO produced a geologic map of the principal surface workings in 1965. Resource Enterprises, Inc. controlled the property in the 1980s; they mapped the trend of the surface gossan and drilled one core hole that fell short of the targeted vein.

Prosperity

The Prosperity mines are part of the Keystone Mining District (formerly Carter Mining District) and were apparently discovered around 1889. Fred Wilson, Jr. and family began operating in upper Keystone Gulch in 1945 under the name of Prosperity Mines, Inc. The Wilsons developed several adit workings and one shaft on the "Blue" or "Cabin" vein trend. Jerry Major acquired the property and sank an 80-ft shaft (or deepened the existing shaft), developed crosscuts from the shaft, built a 50 ton/day mill on site and defined two ore shoots before abandoning the project. Various other parties conducted sporadic work prior to 2000.

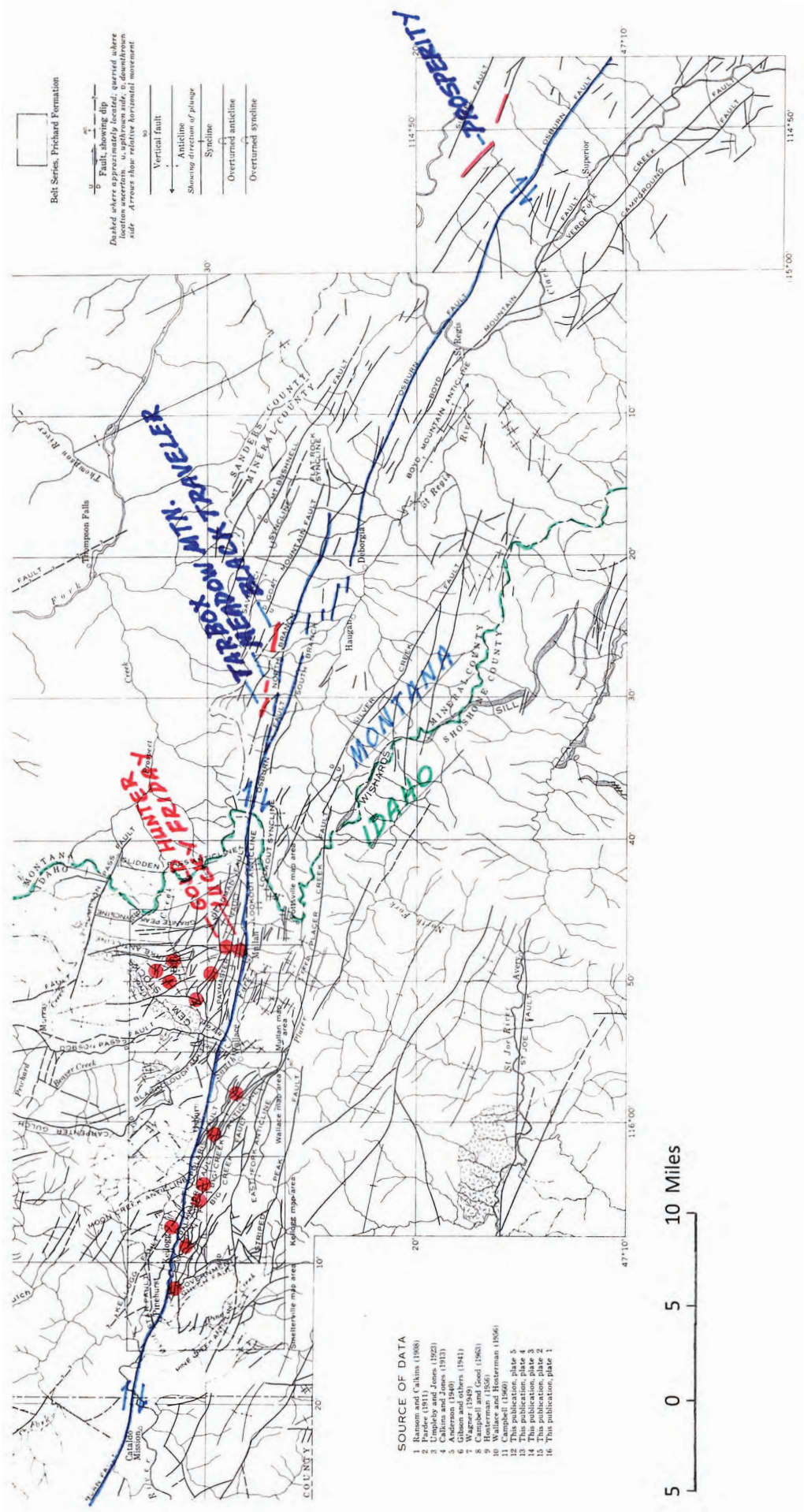

Figure 1. Geologic structure map of the Coeur d' Alene Mining District, Idaho and Montana. Silver Trend Mines LLC's properties are labeled in blue. Red dots are the central Coeur d' Alene district's major producers (each > 1,000,000 tons and >10,000,000 oz silver). The blue strand crossing west-to-east is the Osburn fault zone. Map modified from Hobbs and others, 1965, plate 9.

Figure 2. Tarbox mine, shaft headframe. Photo taken approximately 1900. From archive of Mineral County Historical Society, Superior, Montana.

East Coeur D'Alene District Geology

The East Coeur d'Alene mines are underlain by Proterozoic Belt sedimentary rocks, predominantly quartzites, argillites, and calcareous siltites of the Revett, St. Regis, and Wallace Formations. The NW-trending Osburn Fault and its Montana counterparts dominate the local structural and topographic grain and are the overriding ore control features (see fig. 1). Mesothermal vein deposits in western Montana are isotopically similar to veins in Idaho's Silver Valley and are likely to persist to great depth. Coeur d'Alene veins that have apex strike length greater than a few hundred feet typically extend into the subsurface for several thousand feet.

Tarbox/Meadow Mountain

The Tarbox and Meadow Mountain (TAMM) vein system bears striking resemblance to the apex iron oxide gossan of the Gold Hunter veins (figs. 3A, 3B), which Hecla Mining Company has been mining for decades at Mullan, Idaho from 4,900 to 7,000 ft below surface. The TAMM vein system comprises three or more WNW-trending discrete veins within prominent shears traceable by surface exposures of veining and iron oxide gossan for over 4,500 ft.

The Tarbox mine hosts a reported 200,000 ton resource, averaging 2.4 oz Ag per ton, 4.5% Pb, and 7% Zn with higher grades in the deeper levels and one drift section assaying up to 8% Cu (Mining Review, 1918). Gossanous shears and sulfide veins are exposed in an open cut and trenches northwest from the Tarbox shaft. Recent samples of these exposures by Hecla Mining Company and Silver Trend geologists yielded assay values up to 6.2 oz Ag/ton and 6.4% Pb.

The Meadow Mountain mine was developed by shallow trenches and short adits that expose sections of the 60° south-dipping gossanous shear. A 1937 Sunshine Mining Company memorandum describes an examination of the underground workings and notes six samples with assay values ranging from 0.1 to 1.9 oz Ag/ton and trace to 3.2% Pb.

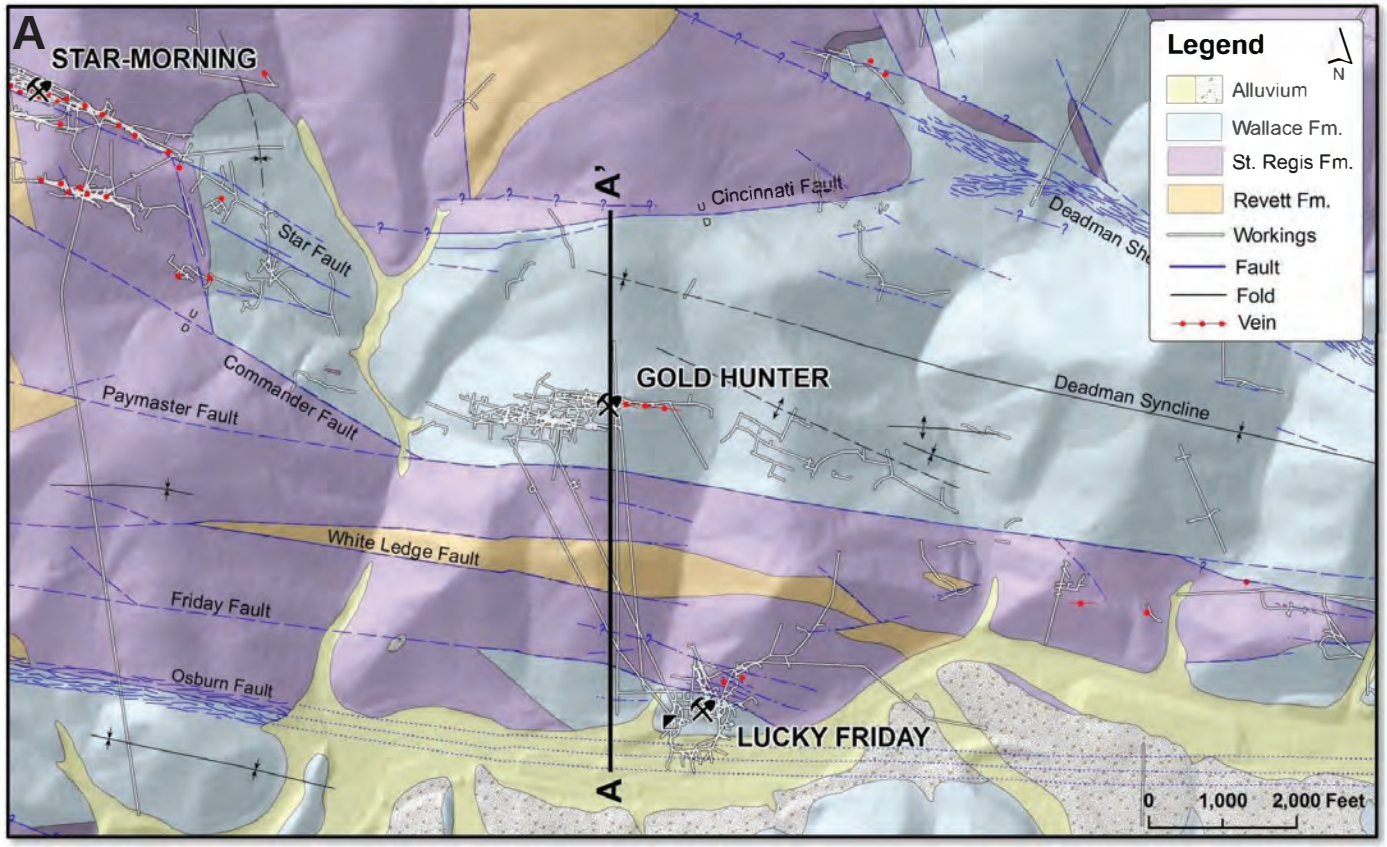

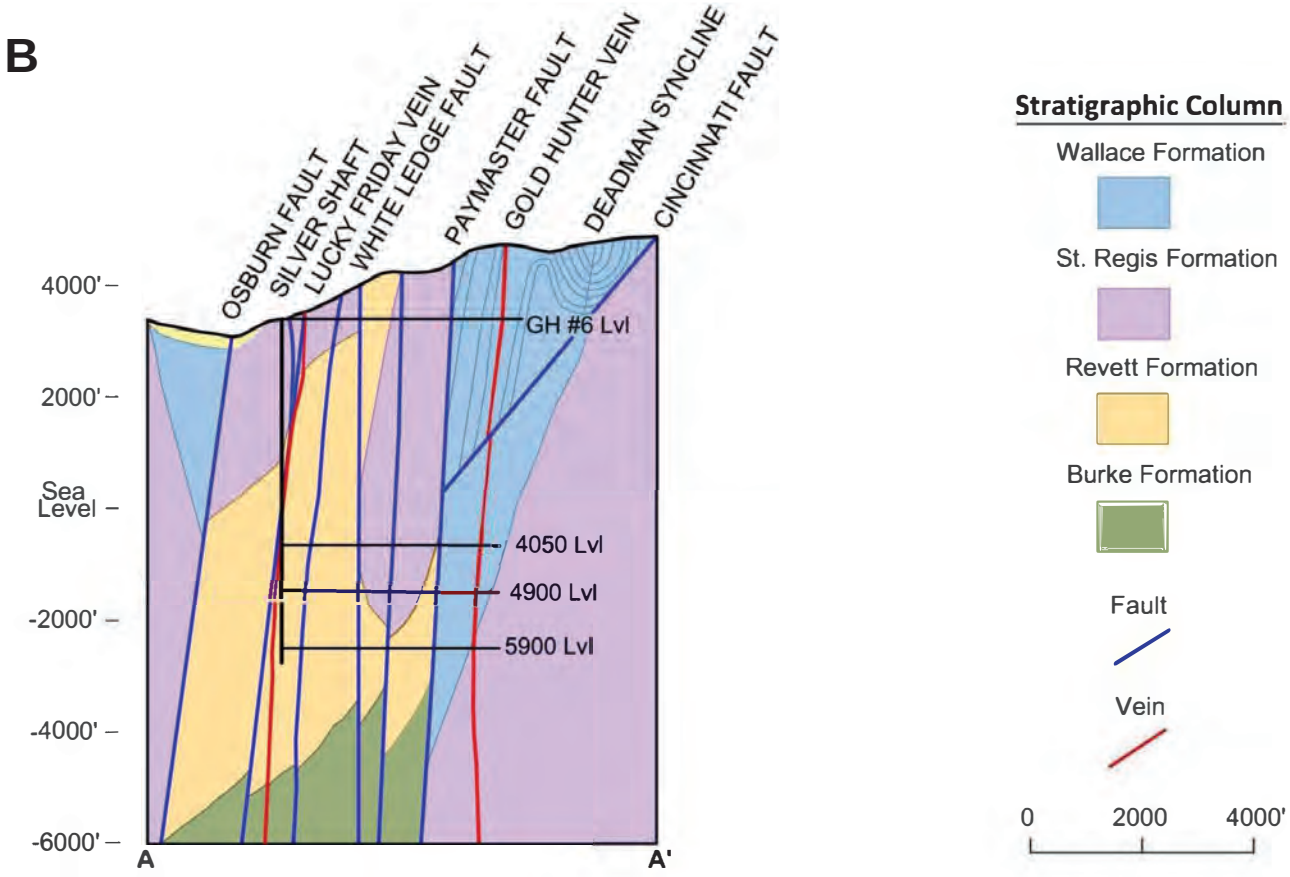

Figure 3. Gold Hunter vein system at the Lucky Friday Mine, Mullan, Idaho: (A) plan view of the mine area showing surface geology and (B) schematic cross-section through the center of the mine workings showing principal faults and veins. Note that the "Gold Hunter Vein" is a series of eight mineable veins, most of which extend at least 8,000 ft below the surface. Figures used with permission of Nick Furlin, Hecla Mining Company.

Black Traveler Geology

Two shear zones capped by iron oxide gossan are exposed by outcrops, float, and mine workings for 3,000 ft on a WNW strike through the center of the Black Traveler claims (fig. 4). Each shear/gossan is greater than 50 ft wide with local minor offsets across north-trending faults. Recent geologic mapping and sampling confirms the location of two principal veins noted in the historic newspaper reports: the Black Traveler vein and "North" vein. Data from a recent VLF-resistivity survey and review of historic records together suggest that the principal vein is dipping 90° or steeply south, opposite of the targeted direction of the 1984 drill hole.

Twenty-two samples were taken from surface vein exposures by Sunshine Mining Company, U.S. Borax and Minerals Exploration Company during the 1970s and 1980s. Six of these yielded assay values greater than 1.3 oz Ag/ton and 2.2% Cu; the highest grade sample carried 2.6 oz Ag/ton and 16.1% Cu. Vein grades ranging 3.5 to 22 oz Ag/ton and 9 to 75% Cu are noted in the historic newspaper articles.

Prosperity

The Iron Mountain mine (fig. 5), located 3 mi SE from the Prosperity Group, is the working model for Prosperity targets. Iron Mountain was the district's most productive mine, in continuous production from 1909 to 1930 and averaging 6 oz Ag per ton plus significant Pb and Zn credits; the deepest level was 2,200 ft below surface, about half the depth of major silver producers in the main Coeur d'Alene district.

Recent geologic mapping and sampling by Silver Trend and data from previous operators document a well-mineralized Prosperity shear fault system that has continuous strike expression for greater than 2 mi and appears to contain multiple parallel or *en echelon* veins along the axis of the Keystone syncline. Reconnaissance level soil sampling confirms the continuity of the alteration envelope and distinctly anomalous Ag, Pb, and Mn values along the principal vein. Vein structures dip steeply south or southwest and are hosted by siltites that display local intense shearing and phyllitic overprint. Ore minerals include: argentiferous galena, tetrahedrite,

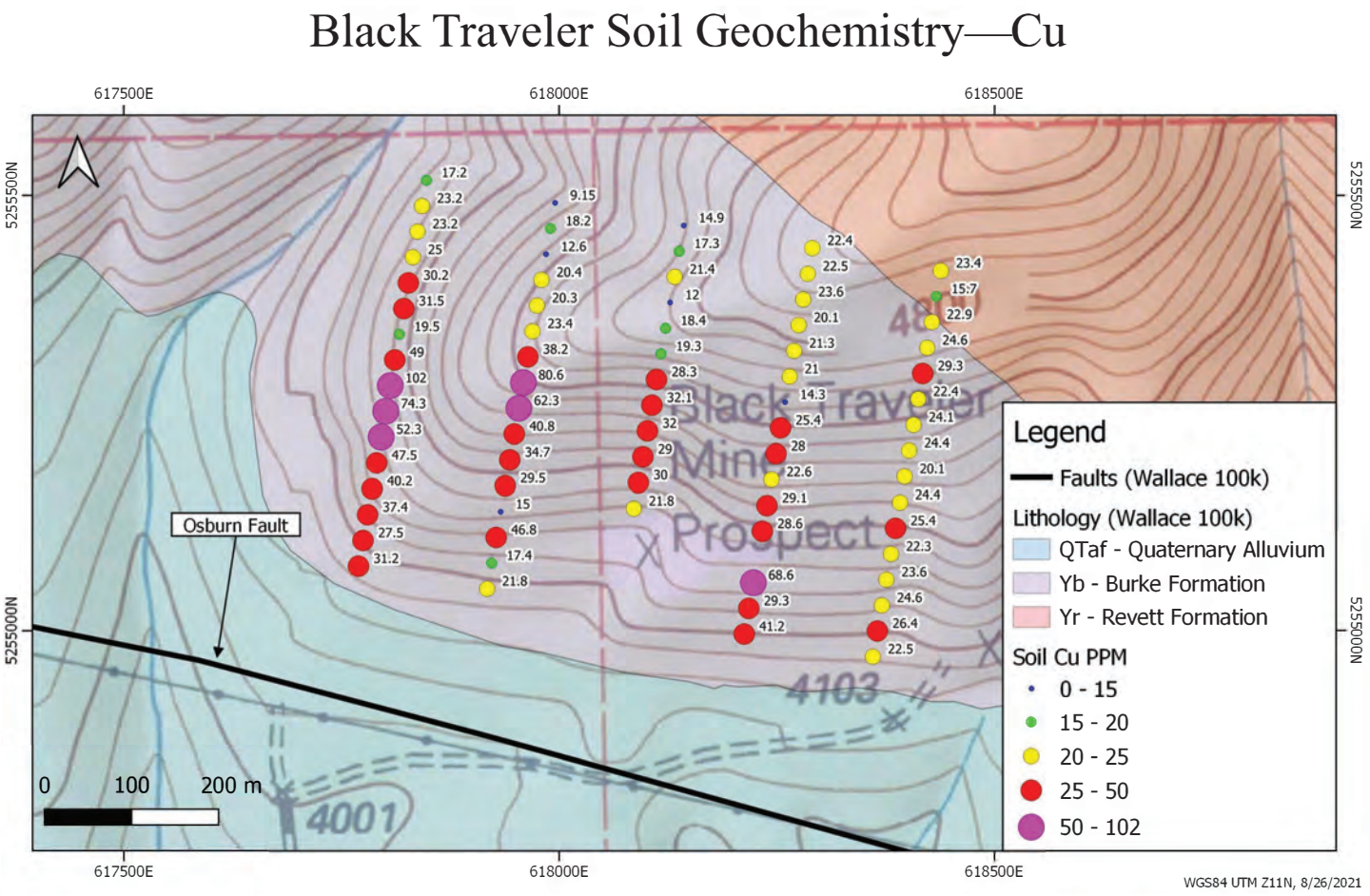

Figure 4. Black Traveler surface geology and 2021 soil geochemistry. Note proximity of the Osburn fault zone.

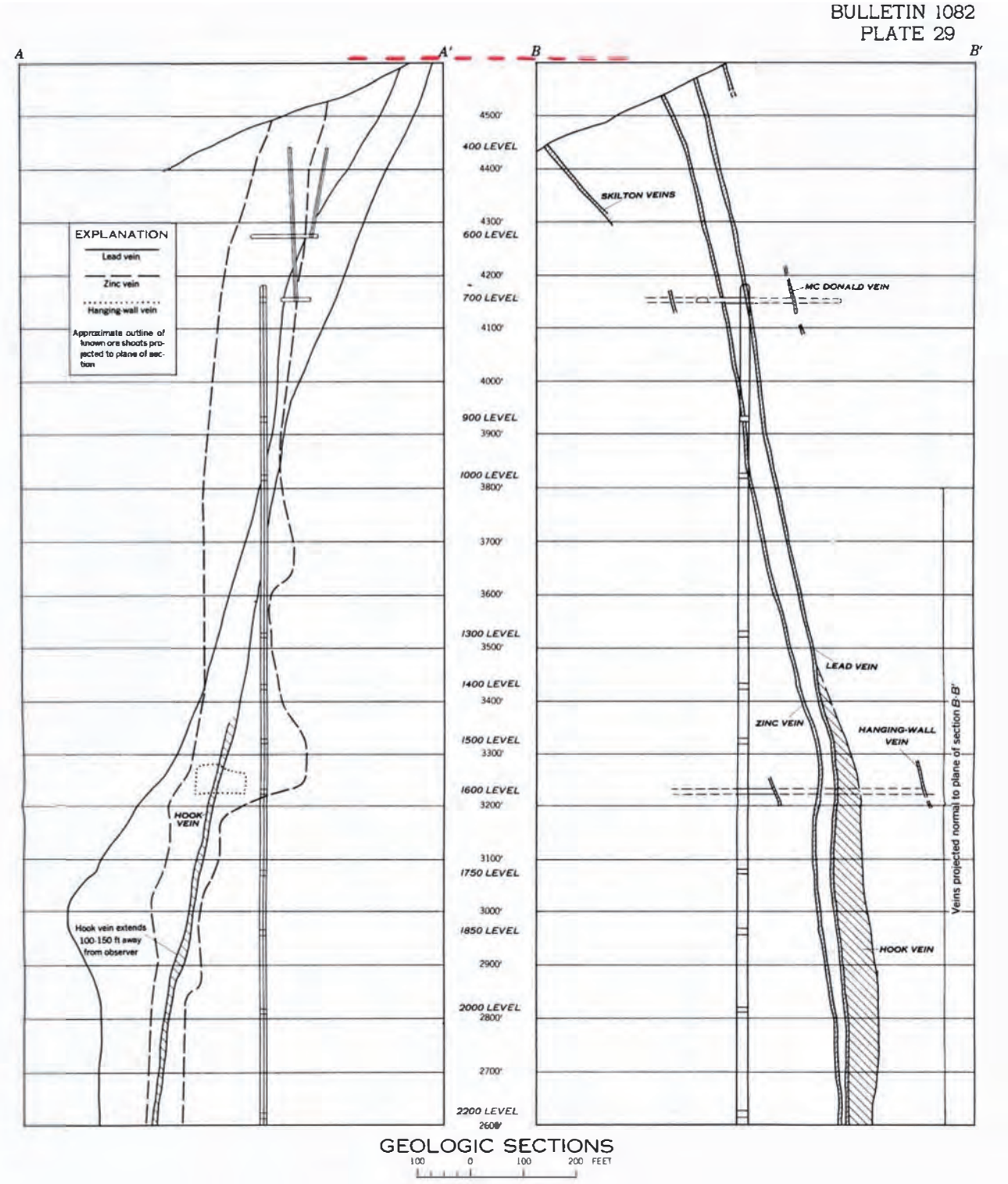

Figure 5. Ore deposit model for the Prosperity Silver Veins. Cross-section of the Iron Mountain mine workings are modified from Campbell, 1960, plate 29. Elevation of the Prosperity mine Blue Cabin Vein apex is shown in red.

chalcopyrite, ± sphalerite, and one report of ruby silver. Vein gangue minerals include: quartz, barite, pyrite, ankerite, siderite (?), and Fe + Mn oxides.

Hypothesized Structural Evolution of East Coeur D'Alene Veins

The following model for evolution of East Cour D'Alene mesothermal veins has been developed from the authors' field observations and data files and from work of previous investigators (refer to the work of: Campbell, 1960; Ruff and others, 2005; Sears and others, 2010; Wallace and Hosterman, 1956; White, 1998; and Zartman and Stacey, 1971).

- Synsedimentary deposition of silver and base metals along growth faults in the Proterozoic Belt Basin, e.g., Sullivan mine, Idaho Cobalt district, Black Butte, Montana. Lead isotopes yield 1.5–1.4 Ma ages for inherited lead in mesothermal vein samples from the Coeur d'Alene district in Idaho to as far east as Missoula County, Montana.
- Tectonic evolution of the Lewis and Clark Lineament (LCL) produces folding and high-angle fault geometries in multiple episodes.
- Principal displacement zones of regional shearing and normal faulting are (north-to-south):
    - Thompson Pass Fault–Mount Bushnell Fault
    - Deadman shear zone–Goat Mountain Fault
    - Osburn Fault[1]
    - Big Creek Fault–Placer Creek Fault–Silver Creek Fault
- LCL shearing produces shear heating, remobilizing disseminated metals that migrate into adjacent dilational domains to form mesothermal veins. Mapped vein structures and mineralogy indicate multiple episodes of shearing, brecciation, recirculation of ore and gangue minerals, and influx of new metal.
- Deep weathering of vein systems produces broad areas of gossan breccia.

Recent Exploration

Silver Trend Mines LLC has leased its East Coeur d'Alene properties to Gold Express Mines Inc., which is exploring the properties under Plans of Operations approved by the U.S. Forest Service. The approved work includes trenching and core drilling along the trend of historic workings to confirm the results of recent exploration and reports of previous operators. The highest rank targets are:

- Extension of two unmined "ore shoots" in shaft workings of the Prosperity mine "Blue Cabin" vein reported to average 12 oz silver/ton; historic surface samples locally yielded grades exceeding 50 oz silver/ton, 8% lead, and 3.5% copper.
- Open extensions of the unmined Tarbox 600–1000 level "ore reserve" block reported to contain 200,000 tons grading 2.2 oz silver/ton, 4.3% lead, and 6.6% zinc with grades increasing to nearly twice these values on the 1,000-ft level.
- Downdip extension of the broad surface gossan and sub-ore grade veins exposed in the historic Meadow Mountain mine adits. Exploration of this target is coupled with the Tarbox Plan of Operations.
- Downdip extension of the Black Traveler–Saltese Consolidated fault zone reported to contain a 2- to 3-ft-wide vein grading greater than 3.5 oz silver/ton and 9% copper.

Induced polarization geophysical surveys, soil geochemistry surveys, and trench sampling during the summer of 2021 confirmed the strength of the noted targets and provides direction for core drilling during the upcoming 2022 field season.

References

Campbell, A.B., 1960, Geology and mineral deposits of the St. Regis-Superior area, Mineral County, Montana: U.S. Geological Survey Bulletin 1082-I, p. 545–612.

Hobbs, S.W., Griggs, A.B., Wallace, R.E., and Campbell, A.B., 1965, Geology of the Coeur d'Alene district, Shoshone County, Idaho: U.S. Geological Survey Professional Paper 478, p. 139.

Mining Review, 1918, author/reporter not listed, Development and equipment of the Tarbox Mine in Montana, p. 21–23.

Ruff, T., Gibson, R.I., and Thomas, R.C., 2005, The Garnet Stock: Magma generation by shear heating and emplacement as a dike: Northwest Geology, v. 34, p. 28–38.

[1] Veins on the STMLLC properties are located directly north of the Osburn fault zone.

Sears, J.W., McDonald, K., Lonn, J., Morgan, L.A., and Quane, S.L., 2010, Lewis and Clark Line, Montana: Tectonic evolution of a crustal-scale flower structure in the Rocky Mountains: Field Guide, Geological Society of America, v. 18, p. 1–20.

Wallace, R.E., and Hosterman, J.W., 1956, Reconnaissance geology of western Mineral County, Montana: U.S. Geological Survey Bulletin, p. 575–612.

White, B.G., 1998, New tricks for an old elephant—Revising concepts of Coeur d'Alene geology: Mining Engineering, v. 50, no. 8, p. 27–35.

Zartman, R.E., and Stacey, J.S., 1971, Lead isotopes and mineralization ages in Belt Supergroup rocks, northwestern Montana and northern Idaho: Economic Geology and the Bulletin of the Society of Economic Geologists, v. 66, no. 6, p. 849–860.

Leslie Lake in the Elkhorn 7.5' quadrangle. Photo by Joel Dietrich.

The Stillwater Complex: A Review

Alan Boudreau

Division of Earth & Climate Sciences, Duke University, Durham, North Carolina

The 2.71 Ga (Wall and others, 2018) Stillwater Complex is a layered ultramafic–mafic intrusion located along the northern front of the Beartooth Mountains in south-central Montana (fig. 1). It has a maximum exposed stratigraphic thickness of 6.5 km and an exposed strike length of ~45 km. Beneath the central and western part of the complex, the footwall to the Stillwater Complex contains a variety of ~3,270 Ma meta-sedimentary rock types. Also present are sills, dykes, and small bodies of massive sulfides immediately below the complex. The upper portion of the intrusion was eroded prior to the mid-Cambrian and then subsequently covered by Paleozoic and Mesozoic sediments. The Late Cretaceous Laramide orogeny led to the current tilting (typically ~70° to the NNE but locally overturned in the vicinity of the Stillwater River) and exposure of the complex along the northern edge to the Beartooth plateau. Stratigraphic subdivisions of the Stillwater Complex are shown in figure 2.

In the past few decades, there have been several major advances in the interpretations of layered intrusions, including the importance of crystal aging, compaction, and compaction-driven recrystallization as drivers of rock texture, the recognition of isotopic disequilibrium, the increasingly precise age determination, and the potential of volatiles to affect crystallization sequences or cause changes in the originally precipitated mineral assemblages. This paper represents a synthesis of this newer work, with a particular emphasis on the ore deposits of the complex and the potential importance of volatiles in their formation.

Conventional models for most of the ore deposits of the Stillwater envision them as having formed by direct precipitation from a magma that itself may have been perturbed by a magma mixing event. More recently, the

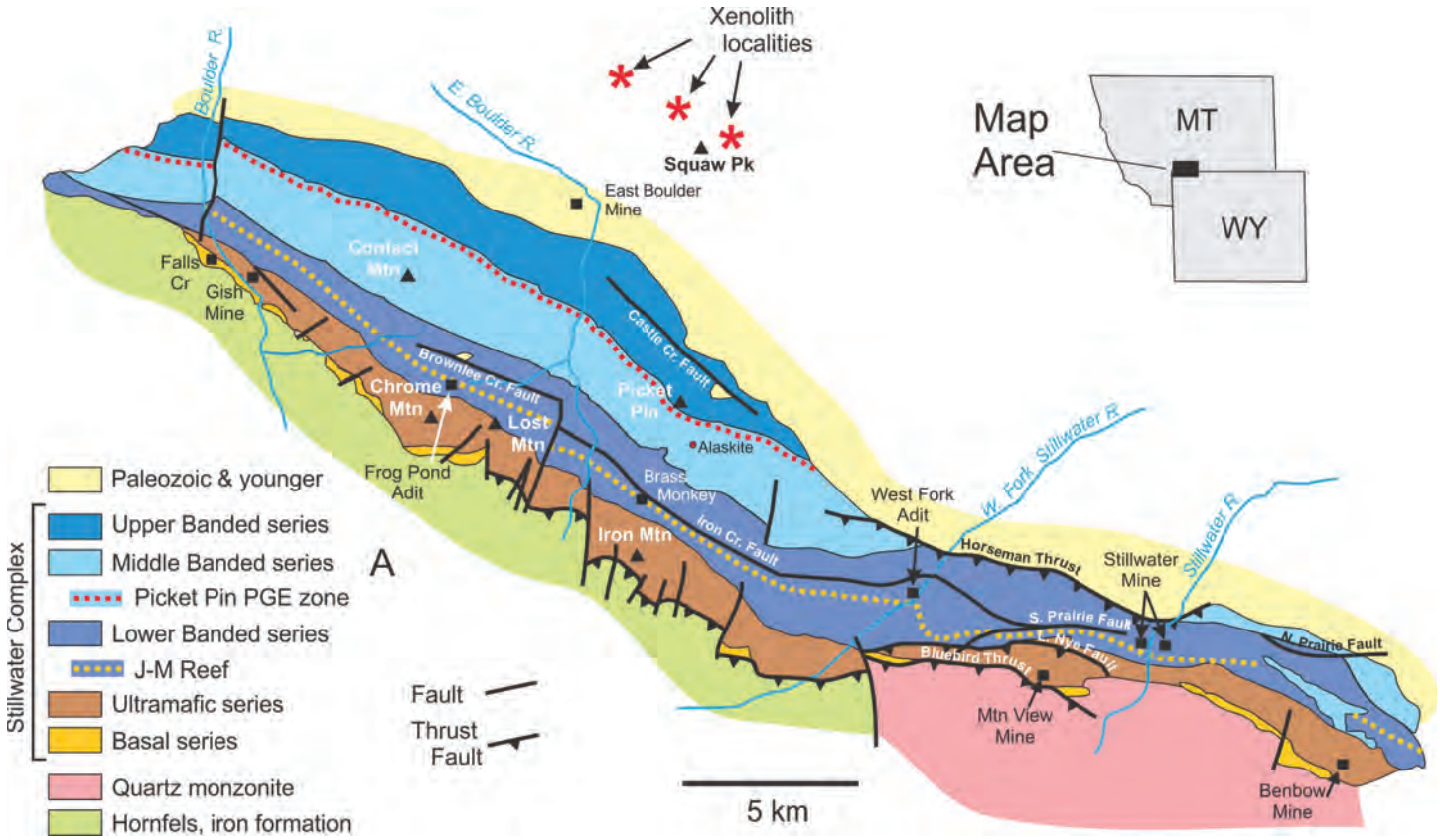

Figure 1. Regional geology of the Stillwater Complex

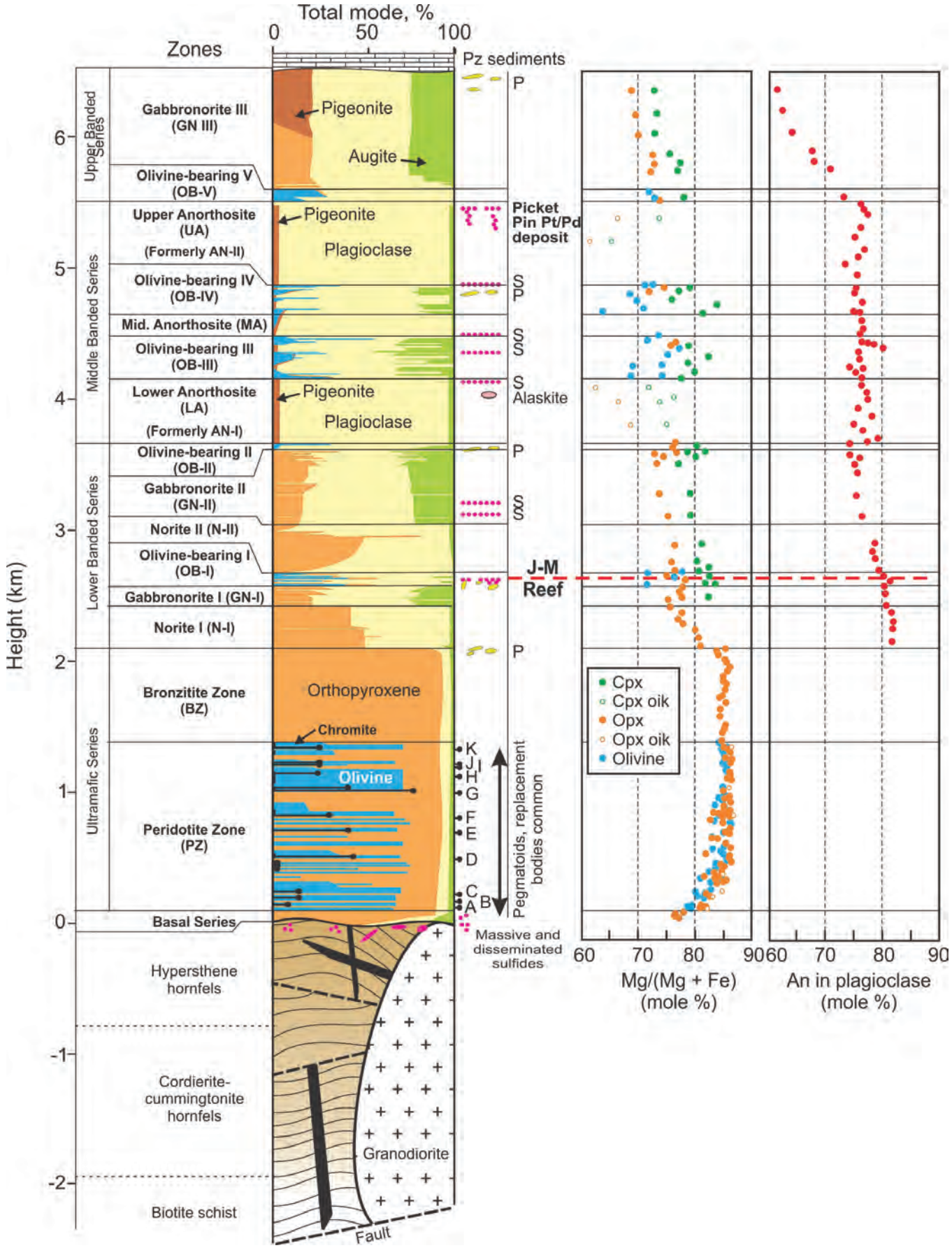

Figure 2. Stratigraphic subdivision of the Stillwater Complex and major mineral compositional trends.

importance of volatiles has been emphasized. This follows from two important effects of volatile components, particularly H_2O, on the behavior of silicate liquid. First, H_2O has a pronounced fluxing effect on a solid-liquid assemblage and can promote incongruent melting of the original assemblage. Second, an increase in H_2O can cause substantial changes in the crystallization order of a magma. This is illustrated in figure 3, in which the increase in $P(H_2O)$ on a magma that nominally would crystallize a gabbronorite assemblage (plagioclase + two pyroxenes) at low $P(H_2O)$ can crystallize an olivine + chromite or chromite alone at high $P(H_2O)$.

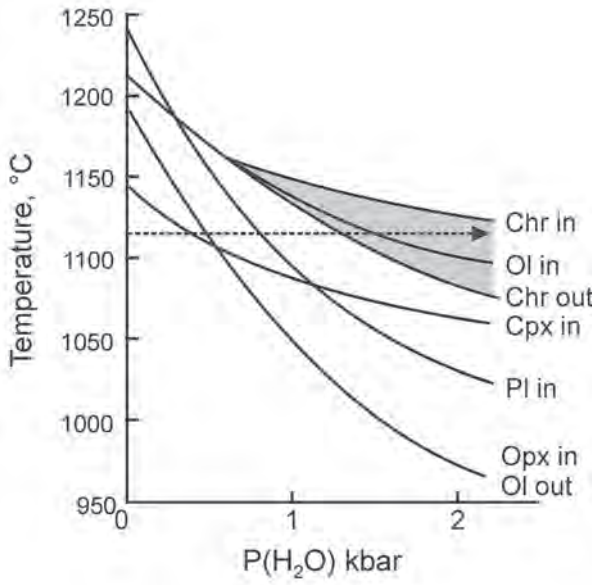

Figure 3. Example of experimental work showing the strong effect of H_2O on the crystallization behavior of a basaltic liquid. After Mathez and Kinzler (2017).

Chromitites and Petrogenetic Models

Massive and disseminated chromite layers occur in the lower portions of many of the cyclic units that make up the Peridotite zone of the Ultramafic series, where individual chromitites range from a single crystal thick to several tens of decimeters in thickness. Orthomagmatic models for the formation of the chromitite deposits found in the Stillwater and other layered intrusions most commonly envision a magma mixing event that pulls a opx + chromite- or olivine + chromite-saturated magma into the chromite field. More recently, the finding of polyphase hydrous mineral inclusions in chromite from both the Stillwater and Bushveld intrusions have been interpreted to have crystallized from a trapped, volatile-rich liquid (e.g., Spandler and others, 2005). One model suggests that mixing of vapor into a multiply saturated magma can lead to the magma becoming saturated in chromite alone, the vapor perhaps generated by dehydration and formation of the extensive metamorphic aureole at the base of the complex. This author has noted that the contacts between the poikilitic harzburgite (that hosts the majority of the chromitites) and the overlying granular harzburgite is irregular, with fingers of the poikilitic harzburgite intruding the granular harzburgite. It was suggested that fluids exsolved lower in the complex rise up into hotter rocks where they induce incongruent melting, leaving chromite as a restite (residual solid) mineral phase (fig. 4).

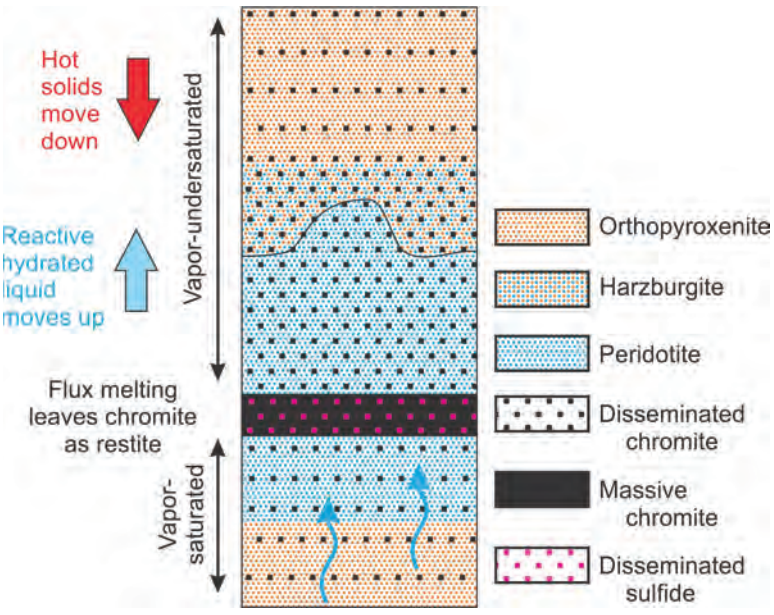

Figure 4. Hydration melting model for the formation of chromitites in the Peridotite zone of the Stillwater Complex.

The J-M Reef

Although the Stillwater Complex contains a number of deposits of potential economic interest, currently it is only the J-M Reef, a platinum-group element (PGE) deposit occurring in Olivine-Bearing zone I (OB-I) of the Lower Banded series, that can be mined without government support. The J-M Reef is generally defined by disseminated PGE-bearing sulfides, and although regionally stratabound, mineralization is heterogeneous on smaller scales and variable in its stratigraphic location. Typically described as a zone of mineralization 2–5 m thick below the contact of the Gabbronorite–Anorthosite subzones of OB-I, mineralization can be discontinuous such that effective mining requires drilling at ~15 m centers to avoid excessive mining of barren rock.

As with the chromitites, there are a number of competing models for the concentration of the

PGE and the associated host rocks. The association of mineralization with olivine ± chromite has again led to a number of orthomagmatic models by which mixing of resident magma with more primitive liquids leads to a change in crystallization from plagioclase + 2 pyroxenes to become olivine- and sulfide-saturated, the sulfide acting as collector for the PGE. Others have noted the extensive evidence for a role by hydrothermal fluids, and envision these fluids as both being carriers of the ore component and fluxing agent that induces the formation of olivine ± chromite by incongruent melting of an original, partly molten plagioclase + 2 pyroxene protolith. A simplified model is shown in figure 4.

Evidence for the role of Cl-rich, aqueous fluids in the introduction of the mineralization and formation of the olivine-bearing rock is extensive and includes the following: (1) The common presence of heterolithic, pegmatoidal olivine-bearing rocks is consistent with increasing H_2O favoring olivine over plagioclase and pyroxene. (2) Lateral changes from gabbronorite and norite to olivine-bearing lithologies. (3) Potholes and their similarities with seafloor pockmarks produced by degassing sediments. (4) The presence of "ballrooms" defined by discordant sulfide mineralization that cuts across layering for up to 30 m or more below the typical level of the reef. (5) Common occurrence of biotite and amphibole largely restricted to the more olivine-rich lithologies. (6) Rounded, embayed, and reversely zoned plagioclase in olivine-bearing assemblages. (7) Unusually high Cl in the hydrous minerals, particularly apatite, which approaches chlorapatite endmember composition. (8) Highest tenor PGE-sulfides are associated with higher Cl-assemblages, consistent with experimental work on the solubility on the PGE in Cl-bearing fluids at high temperatures (e.g., Sullivan and others, 2022a,b). (9) The presence of polyphase hydrous mineral inclusions in chromite and olivine, interpreted to have crystallized from trapped, hydrated silicate liquids similar to those seen in the chromitites of the Peridotite zone. (10) The lack of any mineral compositional offsets that might reflect the influx of a more primitive magma. Instead, the mineral trends show a monotonic fractionation trend throughout the Lower Banded series (fig. 2). (11) PGE-bearing fluid inclusions occur in quartz in discordant pegmatoids found well below the J-M Reef, occurring into the Bronzitite zone of the Ultramafic series. These fluid inclusions range from hypersaline to carbonitic, can contain up to 16 solid phases, and have Pd/Cu ratios similar to that of the J-M Reef (Hanley and others, 2005). (12) Some of these pegmatoids are well-mineralized and overlap the compositional field of the J-M Reef, consistent with fluid transport of the ore component. (13) The rocks below the J-M Reef contain relatively high PGE concentrations and are a better source rock for the PGE than the parent magma, even accounting for a maximum of 42% loss for the J-M reef (Boudreau and McCallum, 1992); similar modeling from the Bushveld complex suggests that the underlying rocks would have lost no more than about ~30% of the original PGE concentration to make the Merensky and UG2 PGE Reefs in that intrusion (Kanitpanyacharoen and Boudreau, 2013).

The Picket Pin Pt-Pd Zone

Sulfides modestly enriched in the platinum-group elements occur in the uppermost part of the Upper Anorthosite zone and have been described by Boudreau and McCallum (1986). The sulfide zone is stratabound in the sense that it is traceable at the same stratigraphic interval over 22 km of exposed strike length. However, in detail, the zone is characterized by erratically developed podiform and lenticular accumulations of 1–5 vol.% disseminated sulfides (mainly chalcopyrite, pyrrhotite, and minor pentlandite). Discordant trails of spotty disseminated sulfides and larger transgressive sulfide-rich "pipes" occur to depths of ~150 m into the Upper Anorthosite zone (figs. 5A,5B). These discordant zones of mineralization typically underlie the better-mineralized sections near the top of the anorthosite. Sulfide mineralization is most commonly associated with the pyroxene-poor, incompatible-element-rich parts of the Upper Anorthosite zone (fig. 6), where it is associated with relatively common accessory minerals that include quartz and apatite.

The transgressive zones of sulfide leading up to the main sulfide concentrations, the association of the sulfides with the late-crystallizing minerals quartz and apatite, and the incompatible-element-rich nature of the sulfide pipes and pods led Boudreau and McCallum (1986) to the interpretation that the ore component was introduced by the percolation of mineralizing solutions during solidification of the Upper Anorthosite. The discordant pipes and sulfide trails were interpreted as fossil channelways or the plutonic equivalent of fumarolic zones, through which both late-evolved liquid and the mineralizing fluids migrated upwards.

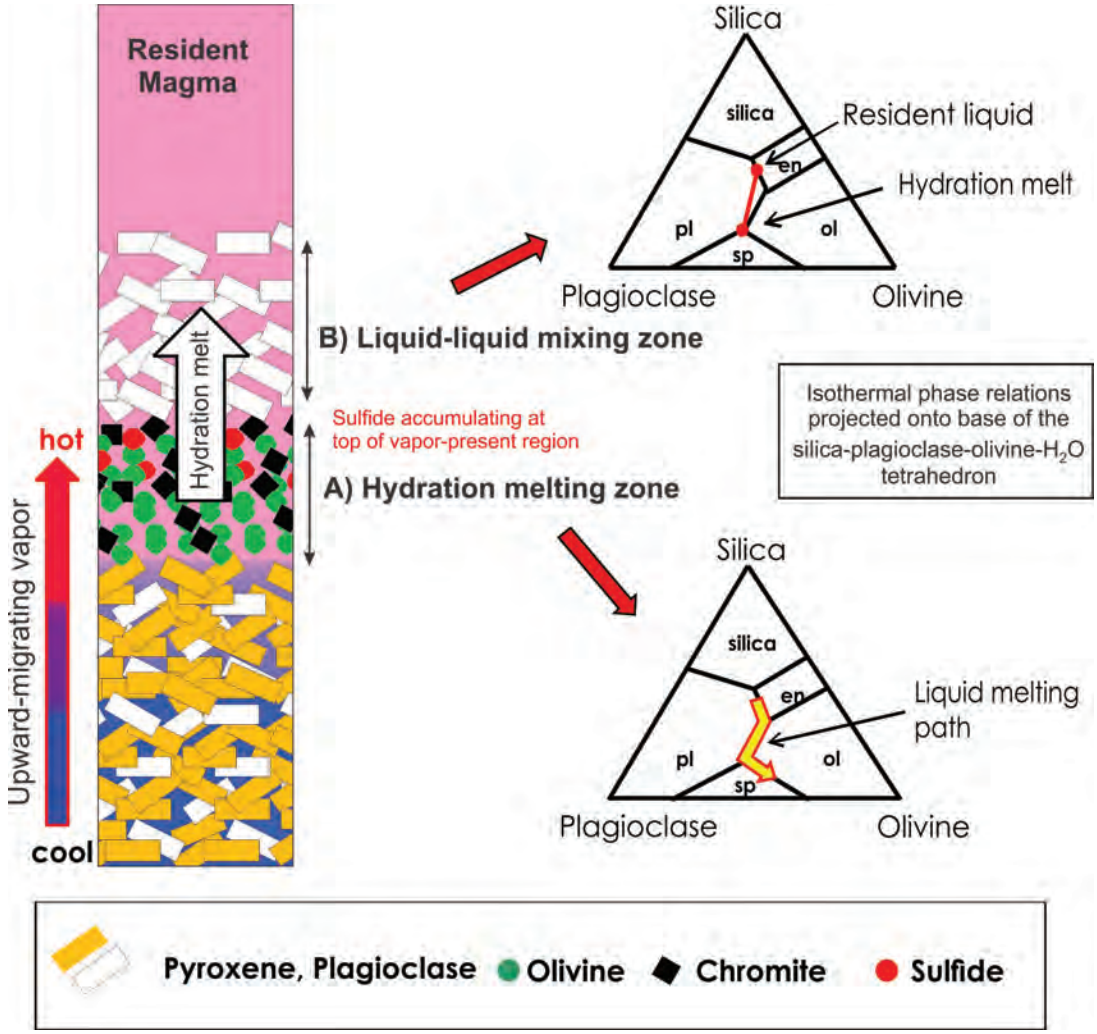

Figure 5. A simplified hydromagmatic model for the formation of the J-M Reef and associated rocks as a combination of (A) hydration melting to produce olivine ± chromite assemblages and (B) the formation of anorthositic hanging wall rocks, as the hydrated melt produced by the hydration event mixes with drier resident magma in the chamber. Sulfide mineralization is concentrated at the top of the vapor-saturation region as vapor redissolves in fluid-undersaturated silicate liquid.

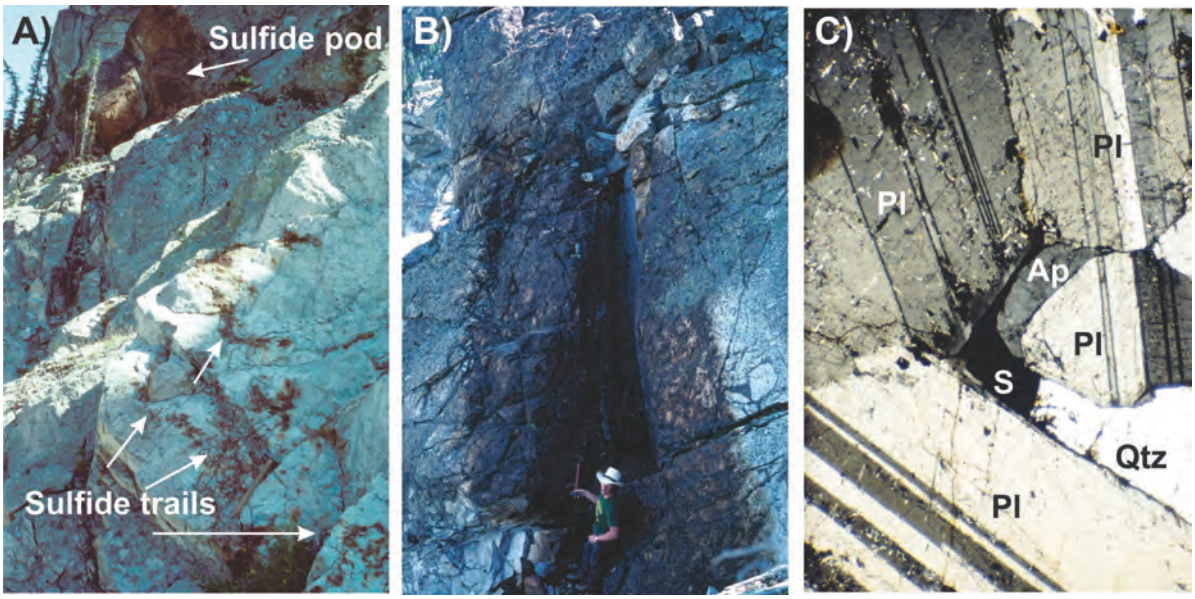

Figure 6. Features of the Picket Pin PGE zone of the Upper Anorthosite zone. (A) Example of trails of disseminated sulfides in the upper part of the Upper Anorthosite zone leading up-section to the sulfide pod at the top of the photo. Note hammer for scale to the right of the 'Sulfide trails' label. (B) Discordant pipe with several percent disseminated sulfide ~100 m below the top of the Upper Anorthosite zone, Lewis Gulch area. (C) Photomicrograph of sulfide (S) associated with quartz (Qtz) and apatite (Ap) interstitial to plagioclase (Pl) from the pipe shown in (B).

Conclusions: A Paradigm Shift in the Interpretation of Layered Intrusions

Conventional cumulus theory envisions that the rocks that formed layered intrusions crystallize directly from a fractionating magma. The hydromagmatic model summarized here and in much more detail by Boudreau (2019) for layered intrusion in general, and by Boudreau (2016) and Boudreau and others (2020) for the Stillwater Complex in particular, point to a new petrogenetic paradigm for how these rocks formed. In this new interpretation, igneous and country fluids are not simply passive actors moving through a partially solidified mush with only minor effect on the original assemblage. Instead, these fluids are active agents both in the ore-forming process and in directing the major minerals of the resultant rocks by the combined processes of modifying the liquidus phase relationships and remelting of the originally precipitated assemblage. These ideas go back at least as far as McBirney (1987), who suggested that a process of "constitutional zone refining" of the interstitial liquid in a growing and solidifying crystal pile can lead to extensive modal variations over time owing to both the buildup of volatile components in the silicate liquid and the eventual separation of an aqueous fluid. More broadly, a growing crystal mush can act as a chromatographic column leading to efficient ore metal enrichment as reactive silicate liquids and O-H-C- Cl-S-rich fluids move upward within the growing crystal pile.

References

Boudreau, A.E., 2016, The Stillwater Complex, Montana—Overview and the significance of volatiles: Mineralogical Magazine, v. 80, p. 585–637.

Boudreau, A.E., 2019, Hydromagmatic processes and platinum-group element deposits in layered intrusions: Cambridge University Press, 275 p.

Boudreau, A.E., Butak, K.C., Geraghty, E.P., Holick, P.A., and Koski, M.S., 2020, Mineral deposits of the Stillwater Complex, *in* Geology of Montana, vol. 2: Special Topics: Montana Bureau of Mines and Geology Special Publication 122, available at https://mbmg.mtech.edu/pdf/geologyvolume/BoudreauChapterFinal.pdf [Accessed January 2022].

Boudreau, A.E., and McCallum, I.S., 1986, Investigations of the Stillwater Complex. Part III. The Picket Pin Pt-Pd deposit: Economic Geology, v. 81, p. 1953–1975.

Boudreau, A.E., and McCallum, I.S., 1992a, Concentration of platinum-group elements by magmatic fluids in layered intrusions: Economic Geology, v. 87, p. 1830–1848.

Hanley, J., Pettke, T., Mungall, J., and Spooner, E.T.C., 2005, Fluid and melt inclusion evidence for platinum-group element transport by high salinity fluids and halide melts below the J-M reef, Stillwater Complex, Montana, U.S.A., 10th Platinum Symposium (Abstract).

Kanitpanyacharoen, W., and Boudreau, A., 2013, Sulfide-associated mineral assemblages in the Bushveld Complex, South Africa: Platinum-group element enrichment by vapor refining by chloride–carbonate fluids: Mineralium Deposita, v. 48, p. 193–210.

Mathez, E.A., and Kinzler, R.J, 2017, Metasomatic chromitite seams in the Bushveld and Rum Layered Intrusions: Elements, v. 13, no. 6, p. 397–402.

McBirney, A.R., 1987, Constitutional zone refining of layered intrusions, *in* Parsons, I., ed., Origins of Igneous Layering: NATO ASI Series C, v. 196, p. 437–452.

Spandler, C., Mavrogenes, J., and Arculus, R., 2005, Origin of chromitites in layered intrusions: Evidence from chromite-hosted melt inclusions from the Stillwater Complex: Geology, v. 33, p. 893–896.

Sullivan, N.A., Zajacz, Z., Brenan, J.C., Hinde, J.D., Tsay, A., and Yin, Y., 2022a, The solubility of gold and palladium in magmatic brines: Implications for PGE enrichment in mafic-ultramafic and porphyry environments: Geochemica et Cosmochemica Acta, doi: https://doi.org/10.1016/j.gca.2021.09.010

Sullivan, N.A., Zajacz, Z., Brenan, J.C., and Tsay, A., 2022b, The solubility of platinum in magmatic brines: Insights into the mobility of PGE in ore-forming environments. Geochemica et Cosmochemica Acta, doi: https://doi.org/10.1016/j.gca.2021.09.014

Wall, C.J., Scoates, J.S., Weis, D., Friedman, R.M., Amini, M,. and Meurer, W.P., 2018, The Stillwater Complex: Integrating zircon geochronological and geochemical constraints on the age, emplacement history and crystallization of a large, open-system layered intrusion: Journal of Petrology, v. 59, no. 1, p. 153–190.

Acid Mine Drainage discharge near Basin, MT. Photo by Chris Gammons.

Radersburg Pass in the Elkhorn 7.5’ quadrangle. Photo by Joel Dietrich.

View to north of Elkhorn Peak and Elkhorn Ghost Town. Photo by Joel Dietrich.

Stable Isotope Applications to the Architecture of Magmatic-Hydrothermal Systems

Peter B. Larson

School of the Environment, Washington State University, Pullman, Washington

The convective circulation of heated water is a natural consequence of the emplacement of magmas into the intermediate and shallow crust. Interaction between these circulating fluids and their wall rocks produces distinctive patterns of hydrothermal alteration, and these environments host several important styles of hydrothermal mineralization. For example, porphyry mineralization can form in the near-magmatic environment, and epithermal deposits are characteristic of the shallowest parts of these systems. Oxygen isotope analyses of the hydrothermally altered rocks can be applied as an important monitor of hydrothermal water–rock interaction, and they can provide a useful map of the scale of hydrothermal activity. Stable isotope analyses, coupled with mineralogic studies of the alteration, have been carried out at several large hydrothermal systems (both active and fossil) that are exposed at different erosional levels. These studies can be compiled to construct three-dimensional pictures of magmatic-hydrothermal systems from deeper levels to the surface, with special emphasis on caldera-related hydrothermal systems.

The Rico, Colorado, hydrothermal system hosts a deep stockwork Mo deposit and shallower epithermal vein mineralization that produced rich Ag deposits. With deep drilling and steep mountainous topography, the hydrothermal system can be sampled over a vertical interval of nearly 4 km. Stable isotope analyses of the altered rocks show that the hydrothermal effects can be mapped in both host intrusive and sedimentary rocks (fig. 1) for more than 5 km from the system's center (Larson and others, 1994; Meuzelaar, 1996). Shallower examples of large hydrothermal systems that have been examined using stable isotopes include alteration around Eocene plutons in the Idaho batholith (Criss and Taylor, 1983), and a 23 Ma hydrothermal system associated with the

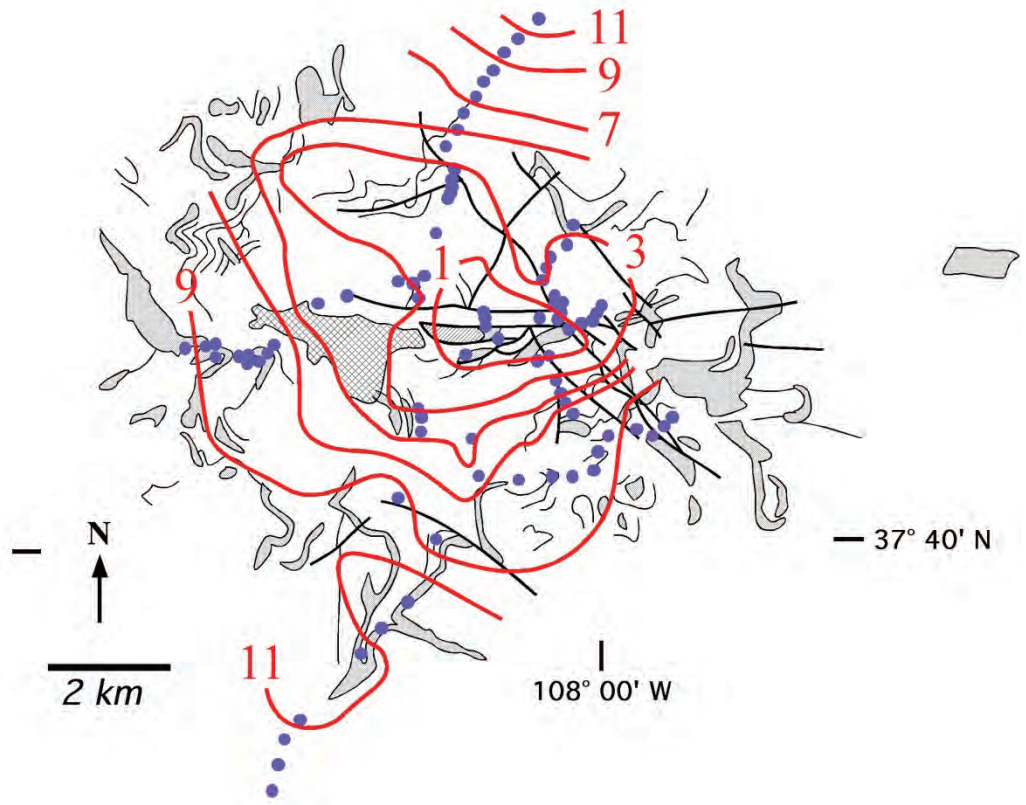

Figure 1. Whole-rock clastic sedimentary rock oxygen isotope ratios for the Rico dome, Colorado. The $\delta^{18}O$ contours (red lines) vary systematically from values near 12‰ (VSMOW) for fresh rock 10 km from the system's center, to values near 0‰ directly above the deeper stockwork Mo deposit (Meuzelaar, 1996).

formation of the Lake City Caldera, Colorado (fig. 2; Larson and Taylor, 1986). In both cases, hydrothermal circulation was strongly controlled by permeable zones that include fractures associated with calderas. Finally, research on the active hydrothermal system at the Yellowstone Caldera provides important information about the shallowest part of a large hydrothermal system (Larson and others, 2009; McMillan and others, 2018), where fluids rise along the hydrostatic boiling curve through permeable plumbing.

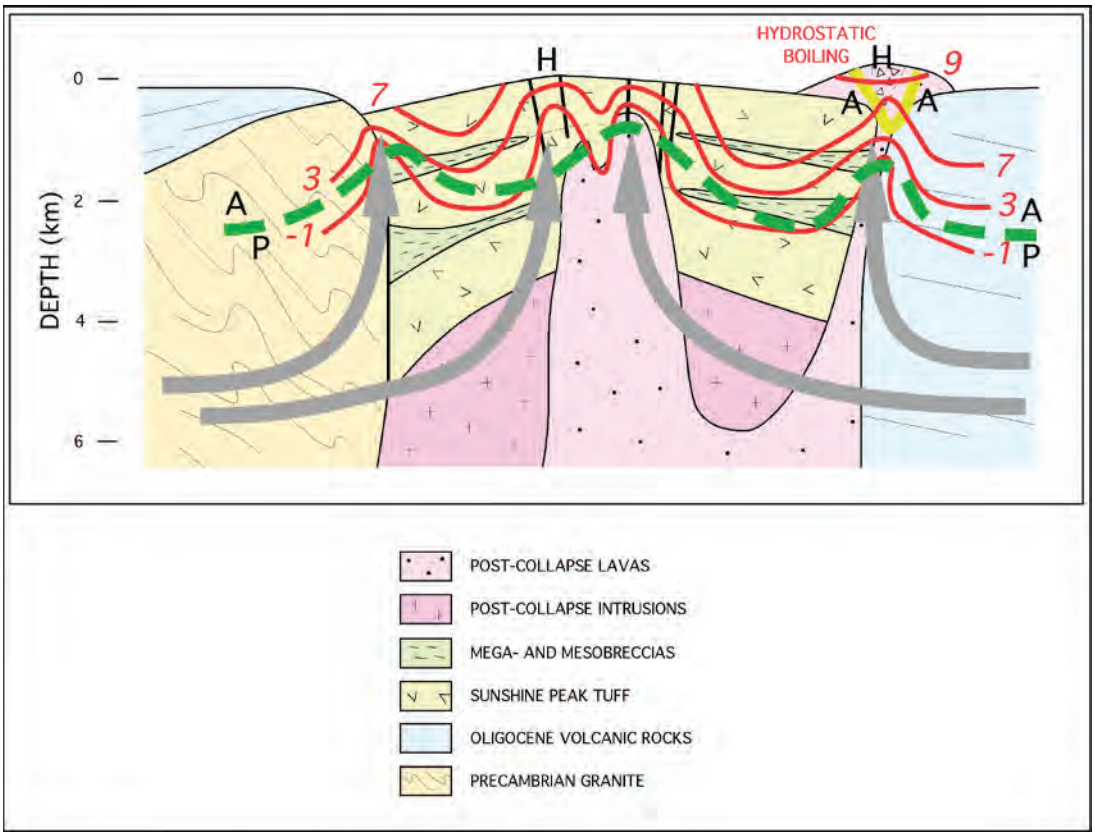

Figure 2. A schematic hydrothermal flow model for the 23 Ma Lake City caldera, southwest Colorado. Whole-rock oxygen isotope ratios (‰, VSMOW) are contoured in red. Large arrows are generalized hydrothermal flow paths. The green line marks the boundary between deeper propylitic (P) and shallower argillic (A) alteration. Alteration produced by a rising and boiling hydrothermal fluid can produce advanced argillic alteration (H). Modified from Larson and Taylor (1986).

Compiling these examples yields some interesting features of the magmatic-hydrothermal environment. Even at the deeper levels near where magmas are emplaced (~4-6 km), hydrothermal effects can extend kilometers away from the driving heat source for the circulation. Porphyry style mineralization with potassic alteration and a strong magmatic fluid component can form in and around the intrusions. Distal alteration is dominated by ambient groundwater (meteoric in most cases) with a minimal magmatic component. Hydrothermal alteration in these areas is characteristically propylitic with chlorite, albite, calcite, and pyrite as important alteration products, among others. Fluids rise along permeable zones (e.g., fractures, permeable sedimentary units, flow contacts) and ultimately reach the surface, where they boil upon rising. The boiling imparts a steep thermal gradient and the drop in temperature can produce drastic changes in fluid chemistry. The shallowest alteration is dominated by clays and can contain sulfate minerals.

References

Criss, R.C., and Taylor, H.P., Jr., 1983, An $^{18}O/^{16}O$ and D/H study of Tertiary hydrothermal systems in the southern half of the Idaho batholith: Geological Society of America Bulletin, v. 94, p. 640–663.

Larson, P.B., and Taylor, H.P., Jr., 1986, An oxygen isotope study of hydrothermal alteration in the Lake City caldera, San Juan Mountains, Colorado: Journal of Volcanology and Geothermal Research, v. 30, p. 47–82.

Larson, P.B., Cunningham, C.G., and Naeser, C.W., 1994, Large-scale alteration effects in the Rico paleothermal anomaly: Economic Geology, v. 89, p. 1769–1779.

Larson, P.B., Phillips, A., John, D., Cosca, M., Pritchard, C., Andersen, A., and Manion, J., 2009, A preliminary study of older hot spring alteration in Sevenmile Hole, Grand Canyon of the Yellowstone River, Yellowstone Caldera, Wyoming: Journal of Volcanology and Geothermal Research, v. 188, p. 225–236.

McMillan, N., Larson, P., Fairley, J., Mulvaney-Norris, J., and Lindsey, C., 2018, Direct measurement of advective heat flux from several Yellowstone hot springs, Wyoming, USA: Geosphere, v. 14, p. 1860–1874.

Meuzelaar, T., 1996, Metasomatism and oxygen isotope exchange within hydrothermally-altered sedimentary rocks, Rico, Colorado: Pullman, Washington State University, M.S. thesis, 194 p.

Hidden Lake in the Elkhorn 7.5’ quadrangle. Photo by Joel Dietrich.

Old mill at Coolidge Ghost Town, Polaris, MT. Photo by Chris Gammons.

A Review (with New Data) of S-Isotopes from Hydrothermal Mineral Deposits of Montana

Christopher H. Gammons[1] and Simon R. Poulson[2]

[1]Montana Technological University, Butte, Montana
[2]University of Nevada-Reno, Reno, Nevada

Introduction

Montana contains a great variety of metallic mineral deposits that span a huge time range, from the Archean to the recent (Gammons and others, 2020a). A large body of data on the S-isotope composition of sulfide minerals exists in the literature for most of the major deposits. As well, the current authors have collected new S-isotope data on many hydrothermal deposits in western Montana, some of which are published, and some of which are tabulated for the first time in this paper. Some general trends are presented herein and briefly discussed.

Sediment-Hosted Deposits of the Belt Basin

Important sediment-hosted deposits in the Mesoproterozoic Belt Supergroup include the Revett-style, Cu-Ag deposits of NW Montana (e.g., Spar Lake, Rock Creek, Montanore) as well as the SEDEX-style Cu-Pb-Zn deposits of the lower Belt sequence (e.g., Black Butte, Soap Gulch). Data on the S-isotope composition of sulfide minerals from Spar Lake, reported by Hayes and others (2012), show a large range from +2.1 to +23.9‰. Hayes and others presented a number of lines of evidence to show that sulfide-S was sourced from a reservoir of sour (H_2S-rich) natural gas that mixed with an oxidized, Cu-rich brine at the site of ore-mineral deposition. The H_2S in the sour gas presumably came from a combination of maturation of organic matter and/or thermochemical reduction of seawater or sedimentary sulfate. Lyons and others (2000) presented data on the S-isotope composition of pyrite from the Zn-rich Soap Gulch deposit east of Melrose, Montana, and the Cu-rich Black Butte (formerly named Sheep Creek) deposit near White Sulphur Springs. Both of these deposits are in dolomitic black shale of the lower Belt Supergroup. The ranges in $\delta^{34}S$-pyrite were -0.5 to +17.3‰ for Soap Gulch, and -8.7 to +36.3‰ for Black Butte. Lyons and others concluded that the pyrite most likely formed near the sea floor by bacterial or thermochemical reduction of seawater sulfate. In contrast to the huge range in $\delta^{34}S$ of pyrite, several studies (Zieg and Leitch, 1998; Graham, 2011; Saintilan and others, 2021; Allard and others, 2022) have noted a much narrower range in $\delta^{34}S$ clustering near 0‰ for chalcopyrite, the main ore mineral at Black Butte. This led Zieg and Leitch (1998) and Saintilan and others (2021) to suggest that magmatic fluids may have played a role in the formation of the high-grade and coarser-grained chalcopyrite zones that replace fine-grained, exhalative pyrite.

Porphyry-Cu-Mo Deposits

Porphyry-Cu-Mo deposits, including Butte and Heddleston, have a relatively restricted range in $\delta^{34}S$ clustering between 0 and +5‰ (fig. 1). However, Field and others (2005) argued that the $\delta^{34}S$ of the primary magmatic fluid at Butte was closer to +11‰, and that most of the isotopically heavier S deposited as hydrothermal sulfate minerals (anhydrite, barite), leaving the economically important sulfide minerals relatively depleted in ^{34}S. Field and others further hypothesized that the overall heavy S-isotope signature of Butte may have been caused by assimilation of heavy S from sediment-hosted deposits of the Belt Basin. Two molybdenite samples from the Turnley Ridge stock in the Elkhorn (Boulder) district have $\delta^{34}S$ near the expected mantle values of 0‰. To the authors' knowledge, no S-isotope data exist for other porphyry Mo deposits in Montana.

Skarn Deposits

Relatively few S-isotope data exist on the skarn deposits of Montana. Sulfide minerals (pyrite, pyrrhotite) associated with gold-rich skarns at Silver Star and Elkhorn (Boulder) have a relatively narrow range in $\delta^{34}S$ between about +1 and +5‰ (fig. 1). Both of these skarn deposits are sulfide-rich, and likely inherited most of their S from co-genetic magmatic-hydrothermal fluids. In this respect, it is interesting and perhaps surprising that the

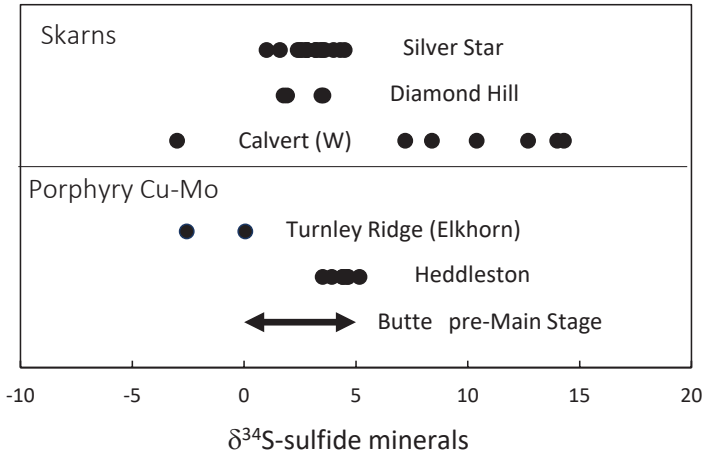

Figure 1. S-isotope composition of sulfide minerals from porphyry and skarn deposits of Montana. Sources of data: Butte (Field and others, 2005); Heddleston (Schubert and Gammons, 2018); Turnley Ridge at Elkhorn (Brown and others, 2019), Silver Star (Sotendahl, 2012); Diamond Hill, Calvert (this study, table 1).

skarn deposits at Elkhorn have a dissimilar S-isotope signature compared to MoS_2 in the nearby Turnley Ridge porphyry stock (see Brown and others, 2019). Sulfide minerals from the scheelite skarn at Calvert have a much wider range in $\delta^{34}S$, from -3 to +14‰ (fig. 1, table 1). Unlike the gold skarns, sulfide minerals are very scarce at Calvert. The wide range in $\delta^{34}S$ values may be due to mixing of a small amount of juvenile (magmatic) S with heavier S inherited from the crust.

Table 1. S-isotope composition of sulfide minerals from miscellaneous mineral deposits.[1]

Mineral	$\delta^{34}S$, ‰	Mineral	$\delta^{34}S$, ‰	Mineral	$\delta^{34}S$, ‰
Calvert W skarn		**York/Bar Gulch "Reefs"**		**Jackrabbit District (E. of Melrose)**	
Pyrite	7.2	Pyrite	-14.7	**Jackrabbit Mine**	
Molybdenite	14.0	Pyrite	-15.2	Galena	5.1
Pyrite	12.7	Pyrite	-14.5	Galena	8.1
Molybdenite	14.3	Pyrite	-15.6	Galena	6.5
Pyrite	10.4	Pyrite	-13.4	Galena	7.6
Pyrite	8.4	Pyrite	-13.8	Galena	5.0
Chalcopyrite	-3.0	Pyrite	-7.7	Galena	4.9
Diamond Hill Au Skarn		**Confederate Gulch**		**Calvin Mine**	
Pyrite	1.8	**Hummingbird Mine**		Galena	4.1
Pyrite	3.5	Pyrite	-8.6	Galena	5.0
Pyrite	3.5	Pyrite	-0.5	Galena	6.3
Pyrite	1.9	**Miller Mine**		Galena	4.5
Radersburg District		Pyrite	-5.7	**Mine between Calvin and Jackrabbit**	
Keating Mine		Pyrite	13.9	Galena	6.0
Pyrite	-0.4	Pyrite	12.9	Galena	5.2
Pyrite	2.3	Pyrite	12.8	Galena	5.7
Pyrite	2.5	Pyrite	12.1	Galena	4.5
Ohio-Keating Mine		**Mayflower (Cardwell)**		**Winston Mine (Custer vein)[2]**	
Pyrite	1.2	Pyrite	-18.4	Pyrite	2.7
Pyrite	1.1	Pyrite	3.8	Sphalerite	2.8
Pyrite	1.2	Pyrite	-28.1	Galena	1.1
Ruby Mine		**Montana Tunnels**		Pyrite	4.4
Galena	2.8	Sphalerite	5.4	Pyrite	4.5
Santa Anita Mine		Sphalerite	5.4	Molybdenite	6.3
Galena	1.6	Pyrite	6.0		
Pyrite	2.7	Pyrite	6.4		

[1]Samples were collected by CHG from abandoned mine dumps and hand-picked under a binocular microscope to obtain sulfide mineral separates.
[2]Samples from the Custer Vein at Winston were collected from new underground mine workings.
Note. All isotopic analyses were performed using isotope ratio mass spectrometry (IRMS) at the University of Nevada-Reno by SRP. All S-isotope data are referenced to the VCDT standard and have an estimated uncertainty of ±0.2‰.

Polymetallic Lode Deposits

Most polymetallic, Ag-Pb-Zn-(Cu-Au) deposits in central and western Montana, including Hecla and Jackrabbit (near Melrose), Philipsburg, Elkhorn (Holter mine), Emery (near Deer Lodge), Mike Horse (near Lincoln), and Barker-Hughesville, have a range in S isotope values that is similar to that of the polymetallic Main Stage veins of Butte (fig. 2). One possible explanation is that, like Butte, most of these vein and carbonate-replacement deposits are related to porphyry systems. As reviewed by Gammons and others (2020a), the majority of the productive polymetallic vein districts of Montana contain associated porphyry-style mineralization. This is contrary to McClernan (1983), who suggested that many of the carbonate-hosted Ag-Pb-Zn deposits of SW Montana, including Hecla, Jackrabbit, and Elkhorn (Boulder), belonged to the Mississippi-Valley Type (MVT) category. McClernan (1983) argued that an MVT origin was most consistent with the huge spread in his S-isotope data for galena from the Jackrabbit mine (+4.7 to +58.8‰). However, we suspect that some of McClernan's data for the Jackrabbit district may have been faulty, since our own analyses for galena from the same area (table 1) show a tight range in $\delta^{34}S$, between +4.1 and +7.6‰, similar to other Ag-Pb-Zn districts of Montana.

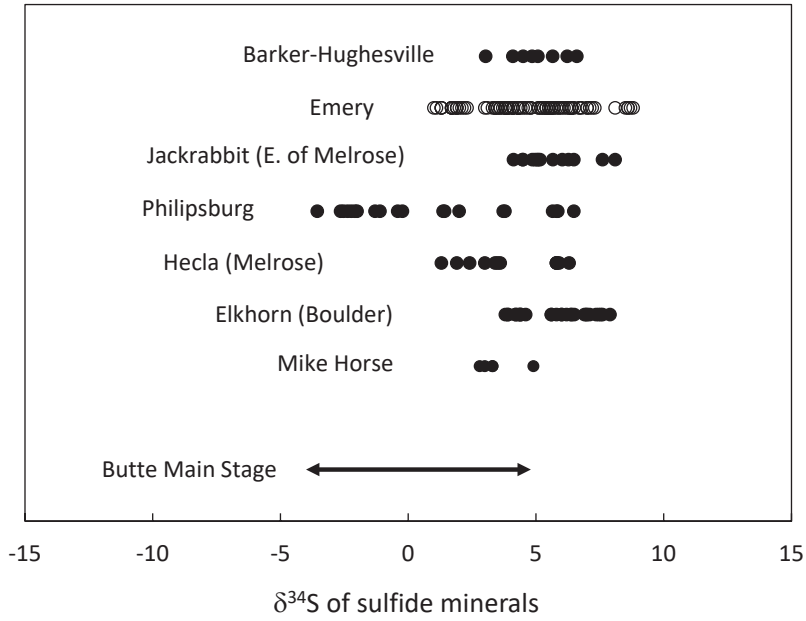

Figure 2. S-isotope composition of sulfide minerals from Ag-Pb-Zn-(Cu-Au) veins and carbonate replacement deposits of Montana. Sources of data: Butte Main Stage (Lange and Cheney, 1971); Mike Horse (Schubert and Gammons, 2018); Elkhorn (Brown and others, 2019); Hecla (Eastman and others, 2017); Emery (Korzeb and others, 2018); Barker-Hughesville (Neaville, 2021); and Jackrabbit district (this study, table 1).

Epithermal Deposits

Isotopic data for sulfide minerals from epithermal deposits of Montana, as well as gold-rich deposits of uncertain origin, are summarized in figure 3. Many of these deposits have $\delta^{34}S$ in the range of 0 to +6‰, overlapping with data for the polymetallic deposits discussed in the previous section. However, the two largest epithermal gold deposits in Montana, Golden Sunlight and Zortman-Landusky, show a wide range in $\delta^{34}S$ values, including some that are very light ($\delta^{34}S < -5‰$). A few other gold-rich deposits, including the Mayflower mine near Cardwell, Golden Messenger, Hummingbird, and Miller mines of the Big Belt Mountains, as well as the lode mines of the Virginia City district, also have anomalously light S, between -18 and -5‰. One sample of high-grade Au-Ag telluride ore from Mayflower (AMC #5262) contained pyrite with $\delta^{34}S = -28.1‰$ (analyzed twice by SRP with similar results). The gold-rich, feldspathic "reefs" in the Greyson Formation near York (Thorson and others, 1999) also contain isotopically light pyrite (-15.6 to -7.7‰, table 1). The origin of the isotopically light S in all of these deposits is uncertain. Gammons and others (2020b) speculated that isotopically light pyrite at Golden Sunlight formed by low-temperature equilibration of H_2S with oxidized forms of S (SO_4^{2-}, SO_2). It is also possible that the gold-rich hydrothermal fluids inherited their light S from an unrecognized crustal source. Regardless of origin, it is interesting to consider that the presence of isotopically light sulfide minerals with $\delta^{34}S < -5‰$ could be a favorable indicator for gold-rich hydrothermal systems in Montana.

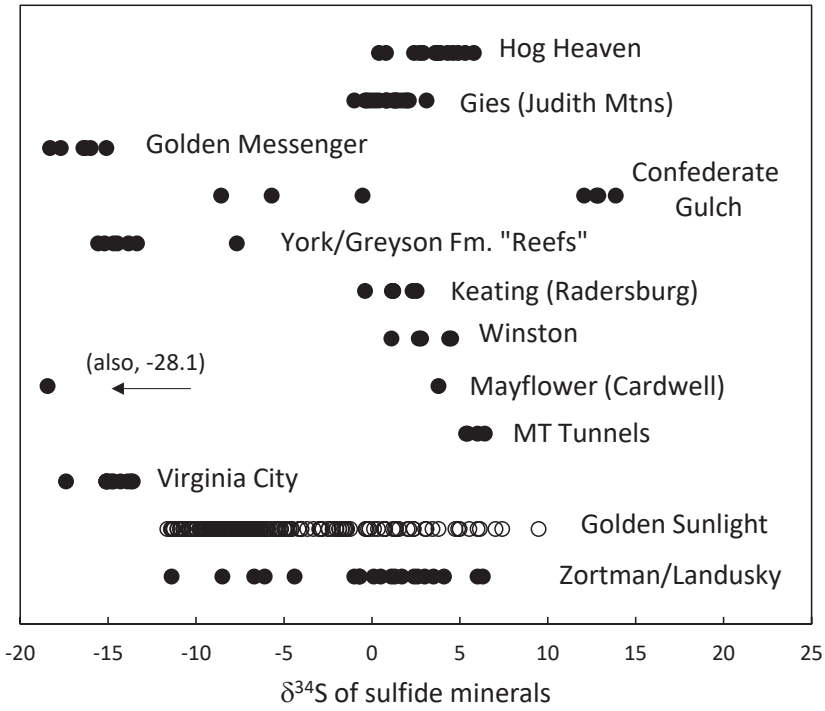

Figure. 3. S-isotope composition of sulfide minerals from epithermal deposits and miscellaneous gold-rich vein and lode deposits of Montana. Sources of data: Zortman-Landusky (Wilson and Kyser, 1988); Golden Sunlight (Porter and Ripley, 1985; Gammons and others, 2020b); Virginia City (Gammons and others, 2019); Golden Messenger (Lange and others, 1995); Gies (Zhang and Spry, 1994); and Hog Heaven (Kallio, 2020). All other data are from this study (table 1).

References Cited

Allard, J., Gammons C.H., and Hatcherian, J., 2022, Stable isotopes and geothermometry of the Lowry deposit, Black Butte Copper Project, Meagher County, Montana: Proceedings of the 2021 Montana Mining and Minerals Symposium (this volume, p. 145–154).

Beaucamp, C. and Gammons, C.H., 2022, New investigations of the Philipsburg polymetallic lode deposits, Granite County, Montana: Proceedings of the 2021 Montana Mining and Minerals Symposium (this volume, p. 131–136).

Brown, A.H., Gammons, C.H. and Poulson, S.R., 2019, New investigations of the economic geology of the historic Elkhorn mining district, Jefferson County, Montana: Montana Bureau of Mines and Geology Special Publication 120, p. 101–112.

Eastman, K.A., Gammons, C.H., Messenger, J.M., Zimmerman, J., Poulson, S.R., Gnanou, H., and Kaplan, J.M., 2017, Geochemical investigation of the Hecla District; a magmatic-hydrothermal Pb-Zn-Ag carbonate replacement deposit, Pioneer Mountains, Beaverhead County, Montana: Montana Bureau of Mines and Geology Open-File Report 685, p. 10–20.

Field, C.W., Zhang, L., Dilles, J.H., Rye, R.O., and Reed, M.H., 2005, Sulfur and oxygen isotopic record in sulfate and sulfide minerals of early, deep, pre-Main Stage porphyry Cu–Mo and late Main Stage base-metal mineral deposits, Butte district, Montana: Chemical Geology, v. 215, p. 61–93.

Gammons, C.H., Mosolf, J., and Poulson, S.R., 2019, Precious metal mineralogy, S-isotopes, and a new LA-ICP-MS date for the Easton and Pacific lode mines, Virginia City district, Montana: Montana Bureau of Mines and Geology Special Publication 120, p. 91–100.

Gammons, C.H., Korzeb, S., and Hargrave, P., 2020a, Metallic ore deposits of Montana, *in* Metesh, J.J., and Gammons, C.H., eds., Geology of Montana—Special Topics: Montana Bureau of Mines and Geology Special Publication 122, v. 2, 30 p.

Gammons, C.H., Gnanou, H., Odt, D., and Poulson S.R., 2020b, Mineralogy and sulfur-isotope geochemistry of polymetallic, porphyry-epithermal mineralization peripheral to the Golden Sunlight gold mine, Montana:

Ore Geology Reviews, v. 126, 103797, 12 p.

Graham, G.E., 2011, Geologic and stable isotope investigations of the Sheep Creek Cu-(Co-Ag) deposit with comparison to other sediment-hosted base metal deposits in Mesoproterozoic basins: Ph.D. Dissertation, Colorado School of Mines, Golden, CO.

Hayes, T.S., Landis, G.P., Whelan, J.F., Rye, R.O., and Moscati, R.J., 2012, The Spar Lake strata-bound Cu-Ag deposit formed across a mixing zone between trapped natural gas and metals-bearing brine: Economic Geology, v. 107, p. 1223–1249.

Kallio, I., 2020, Mineralogy, fluid inclusion, and stable isotope studies of the Hog Heaven Mining District, Flathead County, Montana: Butte, Montana Tech, M.S. thesis.

Korzeb, S.L., Scarberry, K.C., and Zimmerman, J.L., 2018, Interpretations and genesis of Cretaceous age veins and exploration potential for the Emery mining district, Powell County, Montana: Montana Bureau of Mines and Geology Bulletin 137, 53 p.

Lange, I., and Cheney, E., 1971, Sulfur isotope reconnaissance of Butte, Montana: Economic Geology, v. 66, p. 63–74.

Lange, I.M., Krouse, H.R., and Woodward, L.A., 1995, The Golden Messenger Mine, York District, Montana; geologic and isotopic constraints: Economic Geology, v. 90, p. 1322–1328.

Lyons, T.W., Luepke, J.J., Schreiber, M.E., and Zieg, G.A., 2000, Sulfur geochemical constraints on Mesoproterozoic restricted marine deposition: Lower Belt Supergroup, northwestern United States: Geochimica et Cosmochimica Acta, v. 64, p. 427–437.

McClernan, H.G., 1983, Lead-zinc-silver deposits in carbonate host rocks in Montana: Mississippi valley type?, *in* Kisvarsanyi, G., Grant, S.K., Pratt, W.P., and Koenig, J.W., eds. International Conference on Mississippi Valley type lead-zinc deposits: University of Missouri-Rolla, p. 516–525.

Messenger, J., 2016, Paragenesis and geochemistry of the Calvert tungsten skarn deposit, Pioneer Mountains, Montana: Butte, Montana Tech, M.S. thesis.

Neaville, A.C., 2021, Post-reclamation and pre-mining geochemistry of the Galena Creek watershed in the Barker-Hughesville Mining District, Judith Basin County, Montana: Butte, Montana Tech, M.S. thesis.

Porter, E.W., and Ripley, E.M., 1985, Petrologic and stable isotope study of the gold-bearing breccia pipe at the Golden Sunlight Deposit, Montana: Economic Geology, v. 80, p. 1689–1706.

Saintilan, N.J., Sheldrake, T.E., Creaser, R.A., Selby, D., Zieg, J., Boyce, A., and Chelle-Michou, C., 2021, Synsedimentary to diagenetic Cu±Co mineralization in Mesoproterozoic pyritic shale driven by magmatic-hydrothermal activity on the edge of the Great Falls Tectonic Zone–Black Butte, Helena Embayment, Belt-Purcell Basin, USA: Evidence from sulfide Re-Os isotope geochemistry: Lithosphere, v. 2021, no. 1, 7866186.

Schubert, B., and Gammons, C.H., 2018, New mineralogy, fluid inclusion, and S-isotope data for the Heddleston porphyry Cu-Mo deposit, Montana: Montana Bureau of Mines and Geology Open-File Report 699, p. 19–30.

Sotendahl, J.M., 2012, Economic geology of the Madison Gold gold-copper skarn, Silver Star, Montana: Butte, Montana Tech, M.S. thesis.

Thorson, J.P., White, B.G., and Baitis, H., 1999, Gold resources in the Greyson Formation, Big Belt Mountains, Montana, Part II: Mineralization and genesis: Montana Bureau Mines and Geology Open-File Report 381, p. 56–58.

Wilson, M.R., and Kyser, T.K., 1988, Geochemistry of porphyry-hosted Au-Ag deposits in the Little Rocky Mountains, Montana: Economic Geology, v. 83, p. 1329–1346.

Zhang, X., and Spry, P.G., 1994, Petrological, mineralogical, fluid inclusion, and stable isotope studies of the Gies gold-silver telluride deposit, Judith Mountains, Montana: Economic Geology, v. 89, p. 602–627.

Zieg, G.A., and Leitch, C.H.B., 1998, The geology of the Sheep Creek copper deposit, Meagher County, Mon-

Chris Gammons and thrust-faulted Dinwoody Formation near Sandy Hollow, MT. Photo courtesy of Chris Gammons.

The Elkhorn Iron Mine in the Elkhorn 7.5’ quadrangle. Photo by Stan Korzeb.

New Investigations of the Philipsburg Polymetallic Lode Deposits, Granite County, Montana

Celine M. Beaucamp-Stout and Christopher H. Gammons

Department of Geological Engineering, Montana Technological University, Butte, Montana

The Philipsburg Mining District is on the west flank of the Flint Creek Range, Granite County, Montana. It was the second most productive polymetallic-vein district in Montana after Butte and was a major global producer in the late 19th century. The less than 5-mi^2 Philipsburg District produced over 2.4 x10^7 oz of silver, 8.3 x 10^4 oz of gold, 3.6 x 10^7 kg of zinc, 1 x 10^7 kg of lead, 1.8 x 10^6 kg of copper, 4.5 x 10^5 short tons of battery-grade MnO_2 concentrate (Prinz, 1967), and some tungsten (Walker, 1960). Yet the source, timing, and composition of the overall mineralization have never been studied with modern methods.

The U.S. Geological Survey (USGS), the U.S. Bureau of Mines, and a few students studied the geology and mineralization in the twentieth century, while the district was producing. Emmons and Calkins (1913) studied the district extensively as part of their Philipsburg quadrangle USGS report; so did Prinz (1967) for his Geology and Ore Deposits of the Philipsburg District report. These early works provide valuable details from the mines that are no longer accessible, with particular emphasis on the battery-grade manganese dioxide lodes.

Geology Context

The geology of the Philipsburg district (fig. 1) consists of Precambrian to Mesozoic sedimentary rocks truncated to the south and east by the 75 Ma Philipsburg batholith (Emmons and Calkins, 1913; Goddard, 1940). An aureole of contact metamorphism formed around the batholith (Holser, 1950; Prinz, 1967). A 65 Ma, Mo-bearing porphyry stock outcrops at the north end of the district (age: F. Dudas, oral commun.). The ages of the Philipsburg Batholith and associated porphyry are similar to the nearby Butte Granite and quartz–porphyry dikes of the famous Butte porphyry-lode district, located 60 km to the SE.

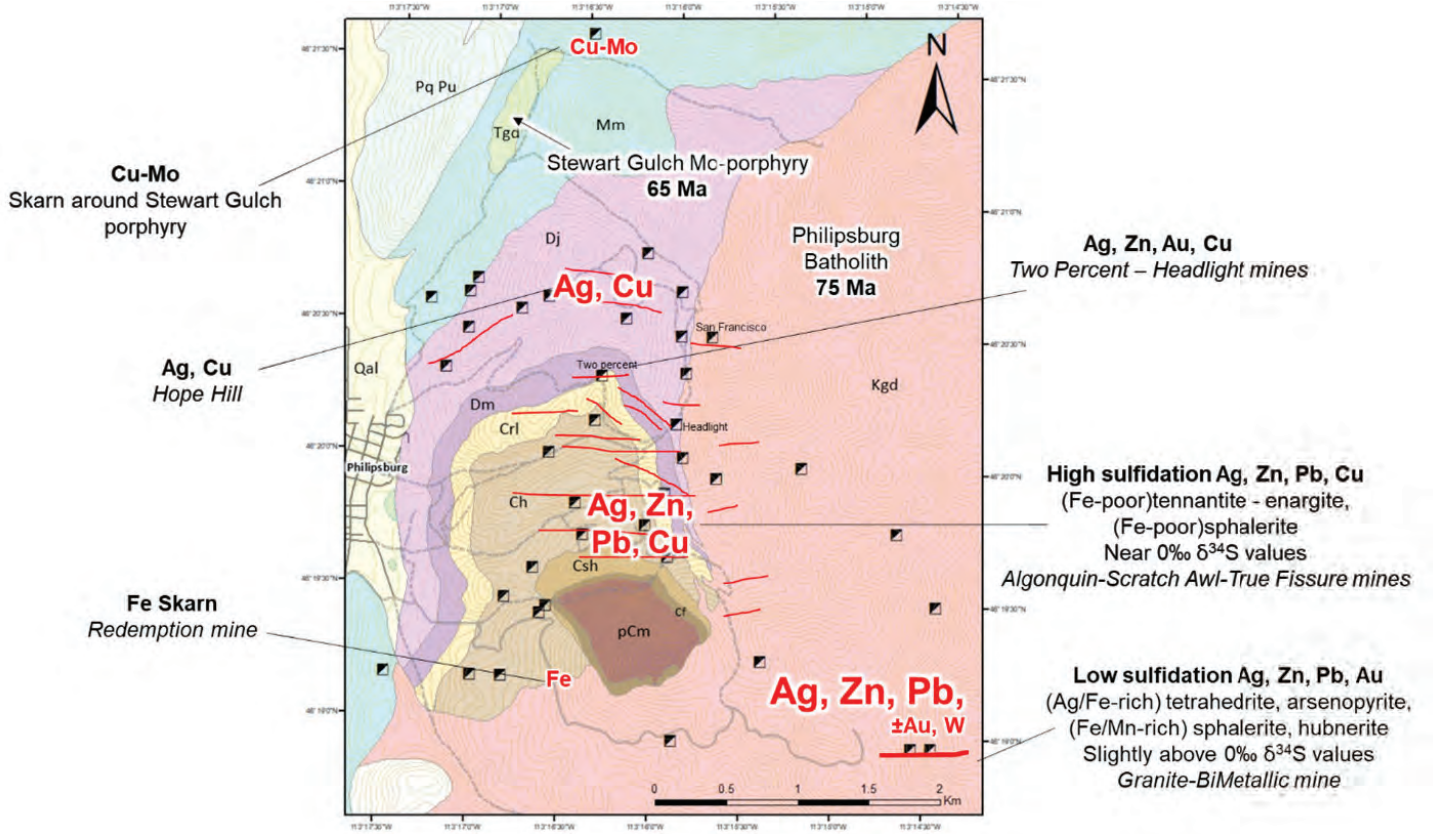

Figure 1. Map of the geology and mineralization throughout the district, showing a zonation of Cu-Mo in the north to Ag-Zn-Pb-Cu in the center and south of the district. Major veins are shown in red.

The dominant structural feature of the Philipsburg district is an asymmetrical north-trending anticline plunging 15°–30° N. The east limb dips 30°–55° E, whereas the west limb dips 45°–70° W (Prinz, 1967). Dozens of nearly vertical quartz-fissure veins strike roughly E–W, while less common, bedding-parallel veins and replacements follow the trace of the anticline. This structural pattern is similar to vein orientations in the Boulder Batholith and associated volcanic rocks and is consistent with E–W shortening in the late Cretaceous. Faults in the district (e.g., Redemption Fault) have steep, reverse displacement.

According to Prinz (1967), four main types of mineralization occur in the district:

1. Steeply dipping quartz veins, mined principally for Ag, Zn, and Pb, occurring in both granodiorite and sedimentary rocks.
2. Quartz veins oriented along bedding, mined principally for Ag, occurring mostly in limestone and marble in the northern part of the district, and yielding the first ores mined in the area.
3. Manganese-rich replacement deposits, consisting mainly of rhodochrosite and manganese oxide deposits, occurring in favorable beds adjacent to or near steeply dipping quartz veins.
4. Contact metasomatic deposits of magnetite occur along the Redemption Fault and along the border of the batholith in the southwestern part of the district.

New Findings

The first author is investigating the mineralization at Philipsburg using modern geochemistry methods, including fluid inclusion, stable isotope, SEM-EDS, LA-ICP-MS, and geochronological methods. The hypothesis to be tested is that Philipsburg, like Butte, is a classic example of Cordilleran style polymetallic lode deposits centered on deeper, porphyry-style mineralization. Some preliminary findings from this ongoing study are summarized herein.

The Philipsburg district is zoned in both metal ratios (from Ag-Cu to Ag-Zn-Pb; see fig.1) and mineral assemblages:

- Copper–molybdenum mineralization is common in the north of the district, where it is directly linked to a skarn around the 65 Ma porphyry stock in the Stewart Gulch area.
- On Hope Hill, the ore bodies are siliceous, argentiferous replacement deposits mostly following bedding planes. The mineralization consists of Cu-rich sulfides, silver, and MnO_2, in a gangue of comb-textured quartz and abundant barite. No zinc is present on Hope Hill.
- South of Hope Hill, the mineralization switches to sphalerite, galena, pyrite, realgar, silver sulfides, copper, and MnO_2, in a quartz–rhodochrosite gangue.
- Going farther south, the mines near the settlement of Tower seem to represent a mineralization bullseye. A lot of silver was produced from the mines in this area: Algonquin, True Fissure, Scratch Awl, Speckled Trout, and Headlight. The coexistence of enargite, tennantite, and Fe-poor sphalerite in the veins indicates a higher sulfidation state (Barton and Skinner, 1979). Other minerals include galena, pyrite, minor chalcopyrite, and a host of silver minerals such as pearceite-polybasite, proustite, jalpaite, acanthite, and trace gold. The gangue is mostly quartz, barite, and a small amount of rhodochrosite. Barite and sphalerite minerals show clear zonation under SEM cathodoluminescence, as well as UV light. LA-ICP-MS analysis on four sphalerite samples is being conducted and will hopefully help explain this.
- In the granodiorite host, at the southern end of the district, the Ruby–Granite–Bimetallic mines were the main producer of the district. Mineralogy consists of a lower sulfidation assemblage of Ag-rich tetrahedrite, Fe-rich sphalerite, and arsenopyrite (Barton and Skinner, 1979), as well as chalcopyrite, pyrite, galena, MnO_2, and silver minerals including pyrargyrite, miargyrite, and trace amounts of gold.

The district's ore zonation indicates a trend of decreasing sulfur fugacity from north to south and matches the trend of zoned base metal veins surrounding porphyry copper mineralization, as described by Einaudi and others (2003; fig. 2). This trend is shown in other Cordilleran deposits, such as Butte (Meyer and others, 1968)

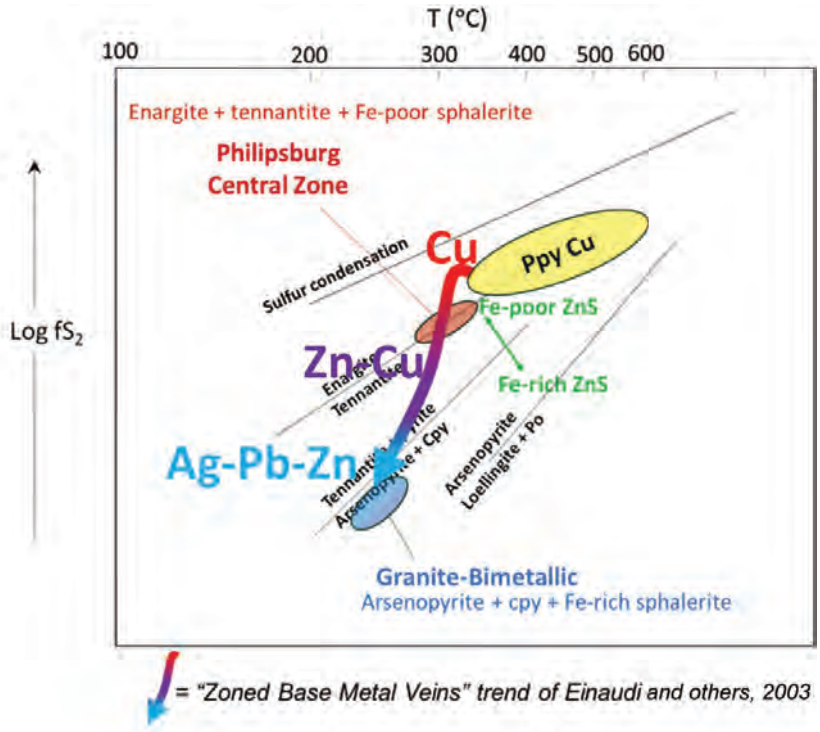

Figure 2. The zonation in sulfidation state shown by the Philipsburg district's ore and mineralogy matches the base metal vein trend of Einaudi and others (2003).

and Morococha, Peru (Catchpole and others, 2015). This type of mineral zonation from Cu-rich to Ag-Pb-Zn-rich could be used to target the source of the mineralized fluids, which is postulated to be one or more porphyry Cu-Mo intrusions.

Preliminary results for stable sulfur isotopes and fluid inclusions also show zonation at a district scale. Stable S-isotopes (n = 20) show somewhat lighter $\delta^{34}S$ values in the Tower area (-3.6 to 5.7‰, avg. = -0.7‰) and heavier values in the Ruby–Granite–Bimetallic area (3.7 to 6.5‰, avg. = 5.1‰). S-isotope geothermometry on sphalerite–galena pairs gives higher temperatures (304–460°C) than on sphalerite–barite pairs (221–246°C). Ongoing work will determine if this disparity reflects disequilibrium or separate mineralizing events. The absolute values and zonation trends in $\delta^{34}S$ of sulfide minerals at Philipsburg are very similar to those displayed in the Butte Main Stage veins (Lange and Cheney, 1971; fig. 3).

Fluid inclusions in Cu-Zn-Ag-rich veins from the Tower area homogenize around 244°C for barite (152.5–324°C, n = 35) and around 197°C for sphalerite (176–215°C, n = 33). Those in quartz from the Hope Hill area homogenize around 215°C (161.4–241°C, n = 30). Inclusions in barite have a wide range in salinity (1.05–34.5 wt% $NaCl_{eq}$, average 9.7 wt% $NaCl_{eq}$), while those in quartz and sphalerite have narrower ranges (respectively 0.53–8.27 wt% $NaCl_{eq}$, average 5.8 wt% $NaCl_{eq}$, and 4.32–7.44 wt% $NaCl_{eq}$, average 6.24 wt% $NaCl_{eq}$; fig.4). At least one CO_2-rich population was observed in barite (three-phase, with CO_2 homogenization to liquid at 23.4°C), suggesting a high pressure of trapping (>1 kbar). The wide range of T_h data for barite could be due to stretching or leaking (Ulrich and Bodnar, 1988). However, stretching cannot explain the existence of three-phase inclusions that are liquid CO_2-rich. More data are necessary to draw any further conclusions from the ongoing fluid inclusion study.

Preliminary Conclusions

The Philipsburg mining district seems to fit well in the Cordilleran polymetallic lode deposit category, as described by Fontboté and Bendezú (2009) and Catchpole and others (2015). The district has a spatial relationship to regional calc-alkaline igneous activity as well as a localized porphyry system(s). The mineralization formed at "deep epithermal" or "mesothermal" conditions and is zoned at a district scale. Overall, the veins of the district are polymetallic (Cu-Zn-Pb-Mn-W-Sn-As-Sb-Ag-Au) and have a very high Ag/Au ratio. Mineralization occurs as both discordant veins and breccias, as well as concordant replacement bodies. The ore-forming fluids

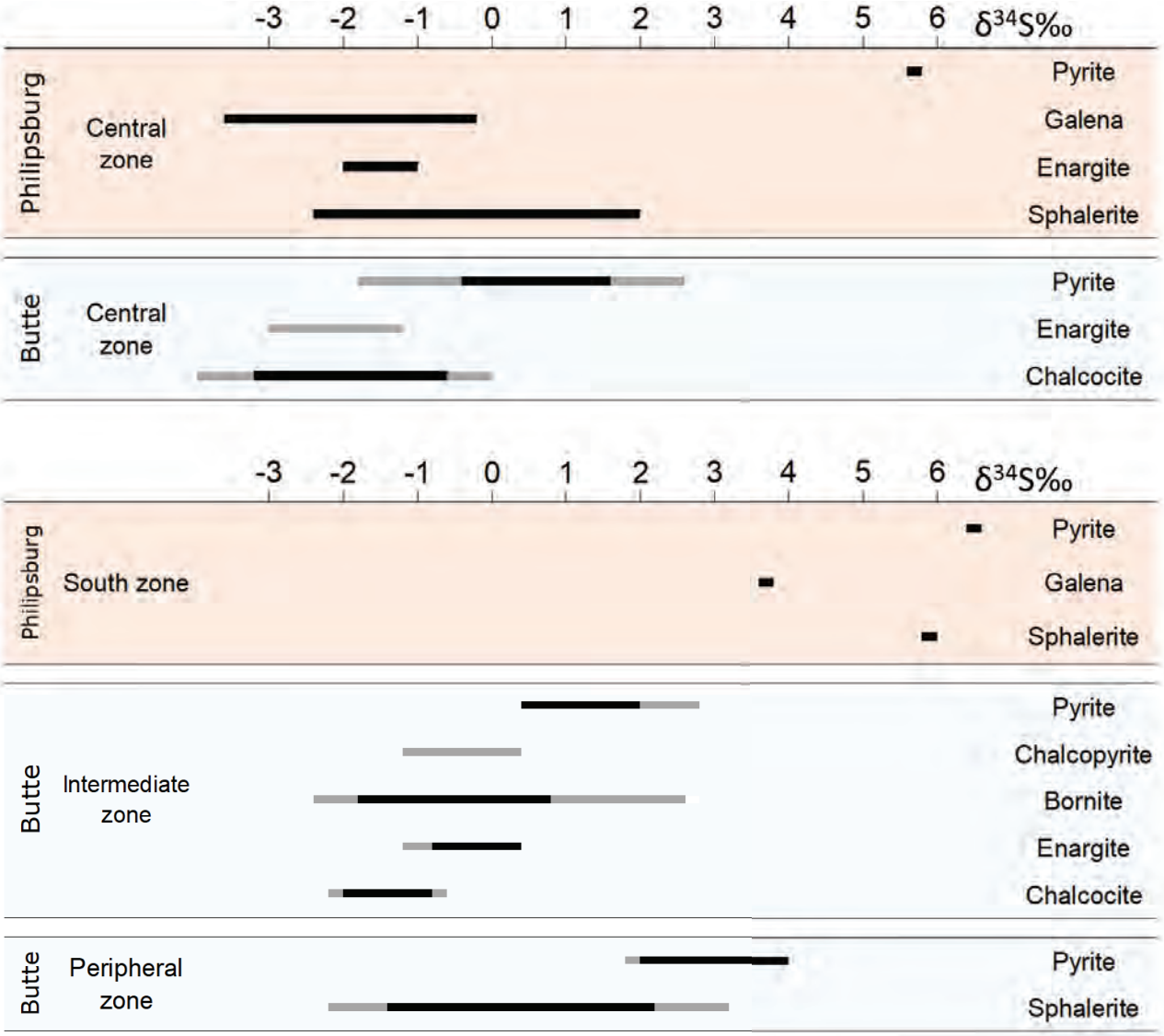

Figure 3. Comparison of the stable sulfur isotopes of Butte (Main Stage data from Lange and Cheney, 1971) and Philipsburg.

Figure 4. Homogenization and ice-melting temperature ranges for fluid inclusions in barite and sphalerite (True Fissure mine), and in quartz (Hope mine). Note that the homogenization temperatures are not pressure-corrected and do not represent trapping temperatures.

had a low to moderate salinity and were likely trapped at temperatures in the range of 200 to 375°C. Lastly, the Philipsburg district has many similarities (and a few differences) to Butte, as summarized in table 1.

Table 1. Comparison of the main characteristics of the Butte mining district and the Philipsburg mining district.

Butte Mining District	Philipsburg Mining District
75 Ma Butte Granite	75 Ma Philipsburg Granodiorite
65 Ma Quartz porphyry dikes with porphyry Cu-Mo	65 Ma Stewart Gulch porphyry with porphyry Mo-Cu
Zoned, east-west (mostly) trending Cu-Ag-Pb-Zn lodes	Zoned, east-west (mostly) trending Ag-Zn- (Pb, Cu) lodes
Mined for Mn (as rhodochrosite)	Mined for Mn (as Mn-oxides)
Granite host rock	Granite and metasedimentary host rock
Cu-rich Main Stage Veins	(Cu)Zn-rich Main Stage Veins

References

Barton, P.B. Jr., and Skinner, B.J., 1979, Sulfide mineral stabilities, *in* Barnes H.L., 1979, Geochemistry of hydrothermal ore deposits, 2nd ed., p. 278–403.

Catchpole, H., Kouzmanov, K., Putlitz, B., Seo, J.H., and Fontboté, L., 2015, Zoned based metal mineralization in a porphyry system: Origin and evolution of mineralizing fluid in the Morococha district, Peru: Economic Geology, v. 110, p. 39–71.

Einaudi, M.T., Hedenquist, J.W., and Inan, E.E., 2003, Sulfidation state of fluids in active and extinct hydrothermal systems: Transition from porphyry to epithermal environments: Society of Economic Geologists, Special Publication 10, p. 285–313.

Emmons, W.H., and Calkins, F.C., 1913, Geology and ore deposits of the Philipsburg quadrangle, Montana: U.S. Geological Survey Bulletin 1237.

Fontboté, L., and Bendezú, R., 2009, Cordilleran or Butte-type veins and replacement bodies as a deposit class in porphyry systems, *in* Williams, P.J., ed., Proceedings of the 10th Biennial Society of Geology Applied to Ore Deposits Meeting, Townsville, Australia, p. 521–523.

Goddard, E.N., 1940, Manganese deposits at Philipsburg Granite County, Montana: A preliminary report: U.S. Geological Survey Bulletin 922-G, p. 157–204.

Holser, W.T., 1950, Metamorphism and associated mineralization in the Philipsburg region, Montana: Geological Society of America Bulletin, v. 61, p. 1053–1090.

Lange, I.M., and Cheney, E.S., 1971, Sulfur isotopic reconnaissance of Butte, Montana: Economic Geology, v. 66, p. 63–74.

Meyer, C., Shea, E., Goddard, C., and Staff, 1968, Ore deposits at Butte, Montana, *in* Ridge, J.D. ed., Ore Deposits of the United States 1933–1967 (Graton-Sales vol.): New York, American Institute of Minerals, Metals, and Petroleum Engineers, v. 2, p. 1363–1416.

Prinz, W., 1967, Geology and ore deposits of the Philipsburg district, Granite County, Montana: U.S. Geological Survey Bulletin 1237.

Ulrich, M.R., and Bodnar, R.J., 1988, Systematics of stretching of fluid inclusions II: Barite at 1atm confining pressure: Economic Geology, v. 83, p. 1037–1046.

Walker, D.D., 1960, Tungsten resources of Montana: Deposits of the Philipsburg batholith, Granite and Deer Lodge counties: U.S. Bureau of Mines Report of Investigations 5612.

Tiffany Ostenburg at the Marget Ann Mine, Butte, MT. Photo by Chris Gammons.

Mineralogy and Fluid Inclusion Study of the Marget Ann Mine, a Gold-Rich Deposit on the North Edge of the Butte District, Montana

Tiffany Ostenburg and Christopher H. Gammons

Department of Geological Engineering, Montana Technological University, Butte, Montana

Introduction

The Marget Ann Mine, located about 1 km northwest of the Alice Pit at the top of Butte Hill (fig. 1), is one of the few mines in Butte that was rich in gold, as well as silver. It is also one of the few mines in the district never to have been operated by the Anaconda Company. The site is relatively well preserved, with several buildings and all of the mine dumps intact. The flooded mine shaft is monitored and sampled by the Montana Bureau of Mines and Geology as part of the Butte Mine Flooding activities. Metesh (1990) conducted a pumping test and evaluation of the flooded Marget Ann shaft. Water in the mine has a near-neutral pH with low concentrations of dissolved metals and elevated concentrations of dissolved H_2S.

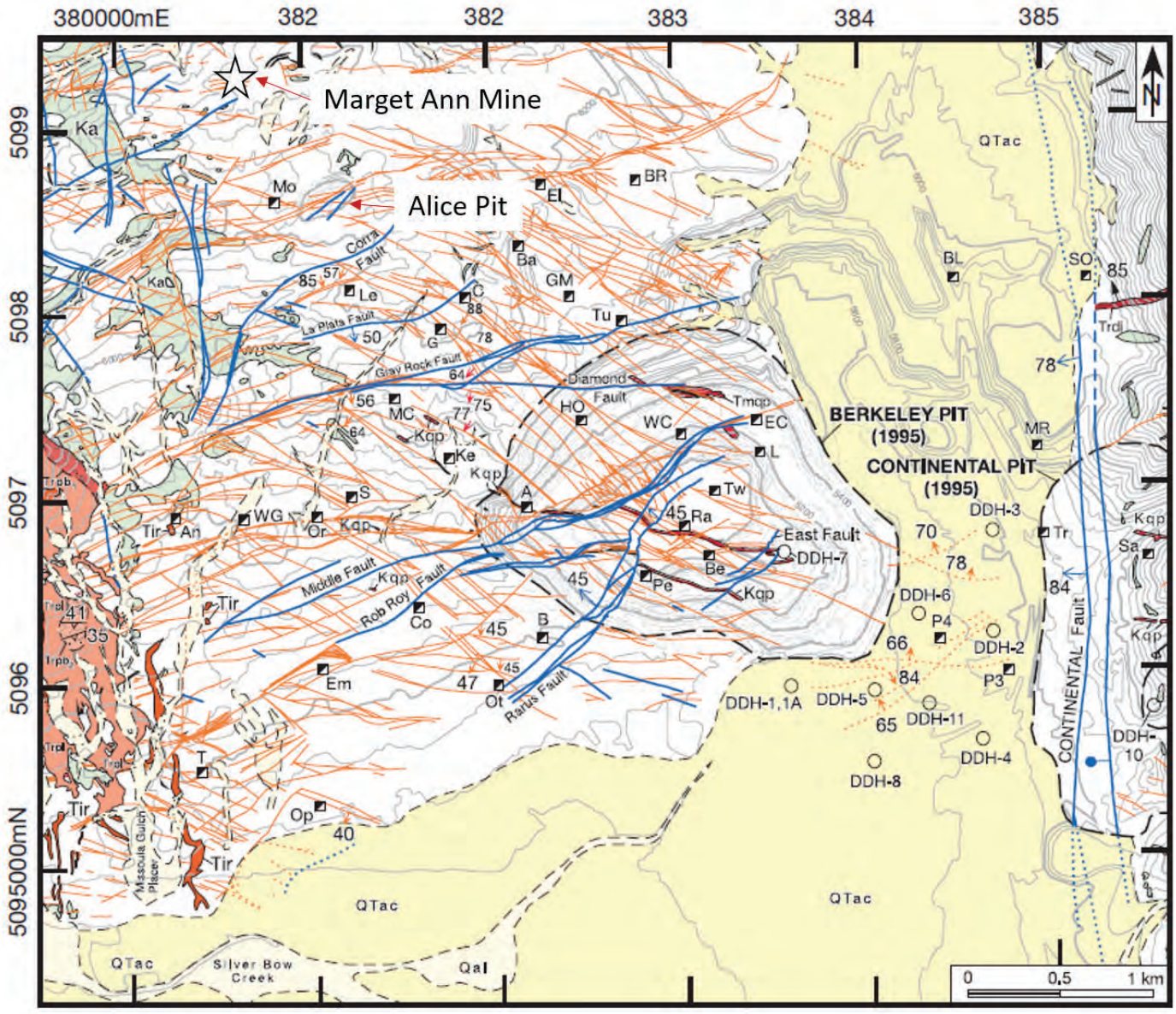

Figure 1. Location of the Marget Ann mine within the Butte District. The base map is from Houston and Dilles (2013).

Previous work on the economic geology of the Marget Ann Mine includes the B.S. thesis of Sahinen (1953) and the M.S. thesis of Win (1955), both of which were completed at Montana Tech during a time when the mine was active. More recently, Gammons and others (2016) examined the mineralogy of some samples from Marget Ann in their district-wide study of silver in the Butte District. The mine is located in the outer, or "peripheral" zone of Main Stage mineralization at Butte (Meyer and others, 1968), and is consequently enriched in Ag-Pb-Zn-Mn (-Au) and depleted in Cu relative to the more famous underground mines in the center of the district. Figure 2 is a composite plan map of the mine (after Win, 1955), showing underground workings at several levels. The Marget Ann shaft, completed to a depth of 650 ft, intersected Butte Granite from top to bottom. Two principal lodes, referred to as the North Vein and South Vein, strike approximately N8°E and dip moderately to steeply northward. Both vein sets are cut off by a NE-striking fault of unknown age and sense of offset (Win, 1955). The north dip of the Marget Ann veins is unusual, as most of the east–west-trending lodes of the Butte district dip to the south (Meyer and others, 1968; Houston and Dilles, 2013).

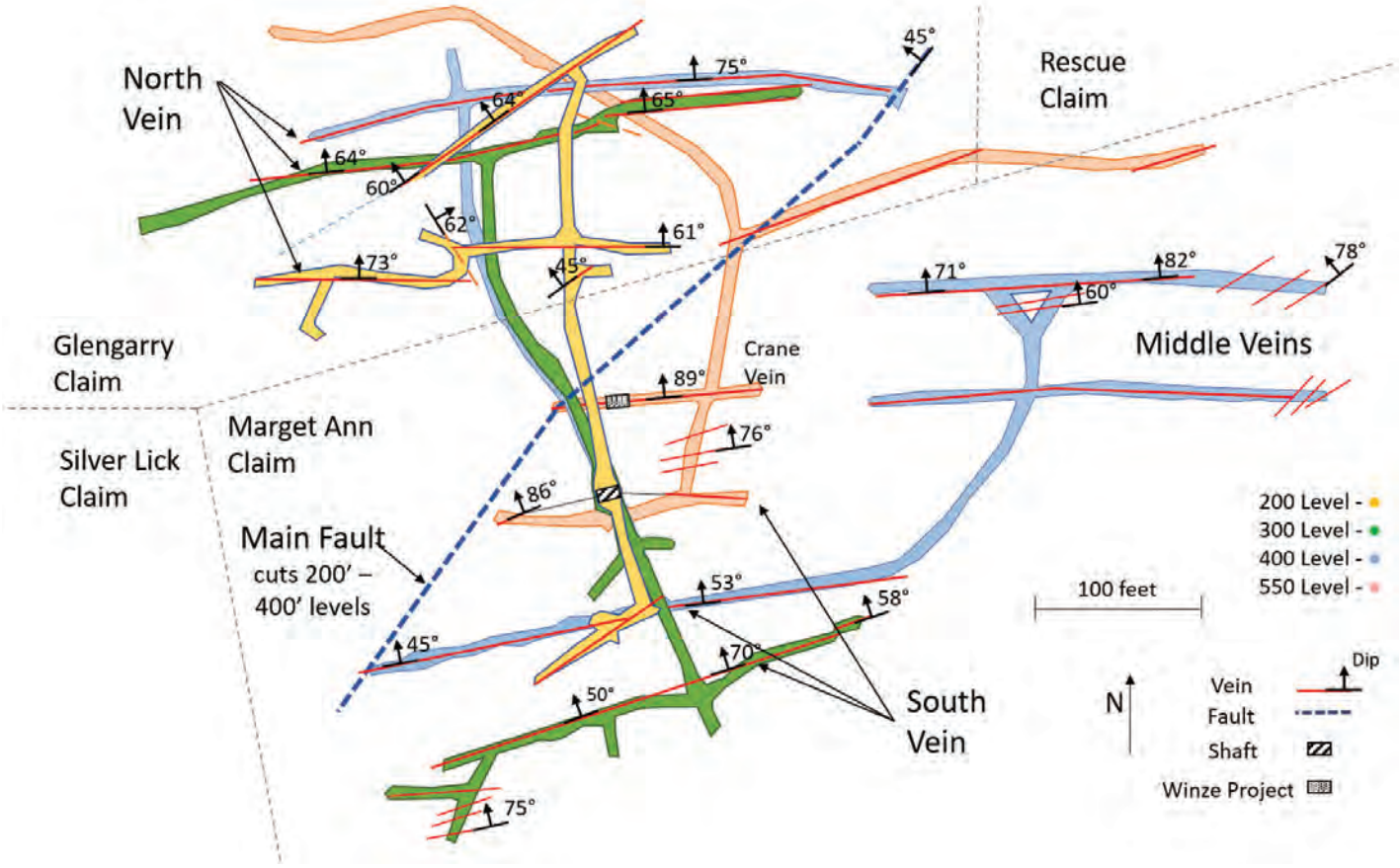

Figure 2. Composite plan map of the Marget Ann Mine. The trace of the Main Fault is shown at the 400 level.

Methods

The current authors have undertaken a study of the Marget Ann deposit using modern methods of ore microscopy and fluid inclusions. (Some stable isotope work is also in progress, but will not be presented here.) Samples of mineralized rock were collected from the mine spoils, from outcrops near the mine, from core drilled in the 1980s by New Butte Mining (now owned by Blackjack Silver), and from samples archived in the Anaconda Research Collection that is housed on the Montana Tech campus. Hand samples were sawn and photographed, with priority samples mounted in epoxy and polished for mineralogy and fluid inclusion work. All samples were examined using reflected light microscopy, and a subset were examined by scanning-electron microscopy–electron dispersive spectroscopy (SEM-EDS) at the CAMP lab at Montana Tech. Doubly polished sections of vein quartz were cut into small chips and examined via fluid inclusion microthermometry using equipment in the Department of Geological Engineering at Montana Tech.

Mineralogy

The mineralogy of the Marget Ann Mine is summarized in table 1. Early "Stage 1" minerals constitute most of the volume of vein material, and consist of coarse-grained, banded quartz ± rhodochrosite, rhodonite, and dolomite, with disseminated to semi-massive sulfides including pyrite, low-Fe sphalerite (<1 wt% Fe), galena, chalcopyrite, and Ag-rich tetrahedrite (up to 14.9 wt% Ag). Figure 3 shows a few photographs of Stage 1 mineralized veins. The abundance of carbonate minerals (rhodochrosite, dolomite) explains the near-neutral pH of the water in the flooded shaft, despite the presence of pyrite in the veins and altered granite (see also Metesh, 1990; Gammons and others, 2009). Stage 2 consists of localized pockets of very high-grade Au-Ag ore containing jalpaite (Ag_3CuS_2), argentite, and electrum disseminated in a compact gangue of rhodochrosite, rhodonite, and fine-grained quartz (chalcedony), with minor calcite and hydrothermal K-feldspar (adularia). Representative photomicrographs from Stage 2 are shown in figure 4. The electrum grains in figure 4 have compositions in the range of 53 to 75 wt% Au. Jalpaite and acanthite are often found together in Stage 2, sometimes intergrown in a "symplectic" texture (fig. 4C) that suggests exsolution from a higher temperature Ag-Cu-S phase. This texture is important because it is hard to imagine it happening from supergene processes. Three small grains of Cu-rich uytenbogaardtite (ideally Ag_3AuS_2, but here containing up to 6 wt% Cu) were found (figs. 4A, 4B), and this study is the first reported occurrence of uytenbogaardtite in the Butte District. The uytenbogaardtite has a distinct brownish color under reflected light (fig. 4B), and was found in contact with electrum. The high Cu content suggests that this phase could possibly be makotoite ($Ag_{12}(Cu_3Au)S_8$). If so, this would be only the second known occurrence of this mineral worldwide. Electron microprobe data are needed to verify the mineral formulas.

Table 1. List of minerals from the Marget Ann mine. Mineral abundance increases with darkness of shading.

	Stage 1	Stage 2	Supergene
Pyrite			
Sphalerite			
Galena			
Chalcopyrite			
Ag-rich tetrahedrite			
Pearceite-Polybasite			
Jalpaite			
Argentite			
Uytenbogaardtite			
Electrum			
Silver			
Covellite			
Chalcocite			
Quartz (coarse)			
Dolomite			
Chalcedony			
Rhodonite			
Rhodochrosite			
Calcite			
Sericite			
Adularia			
Mn-oxides			

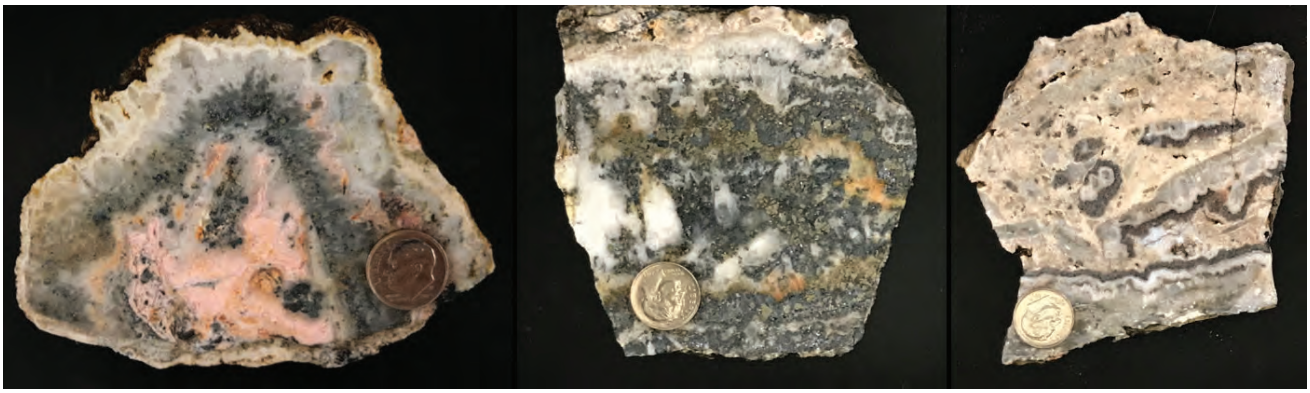

Figure 3. Representative hand samples of mineralized veins from Marget Ann. (A) Central breccia fragment of early rhodonite + rhodochrosite overgrown by Stage 1 quartz with minor base metal sulfides; (B) coarse, milky gray Stage 1 quartz and sulfides (mainly pyrite + sphalerite); (C) Stage 1 quartz (gray) brecciated and rimmed by sphalerite (brown) with late dolomite fill (light tan).

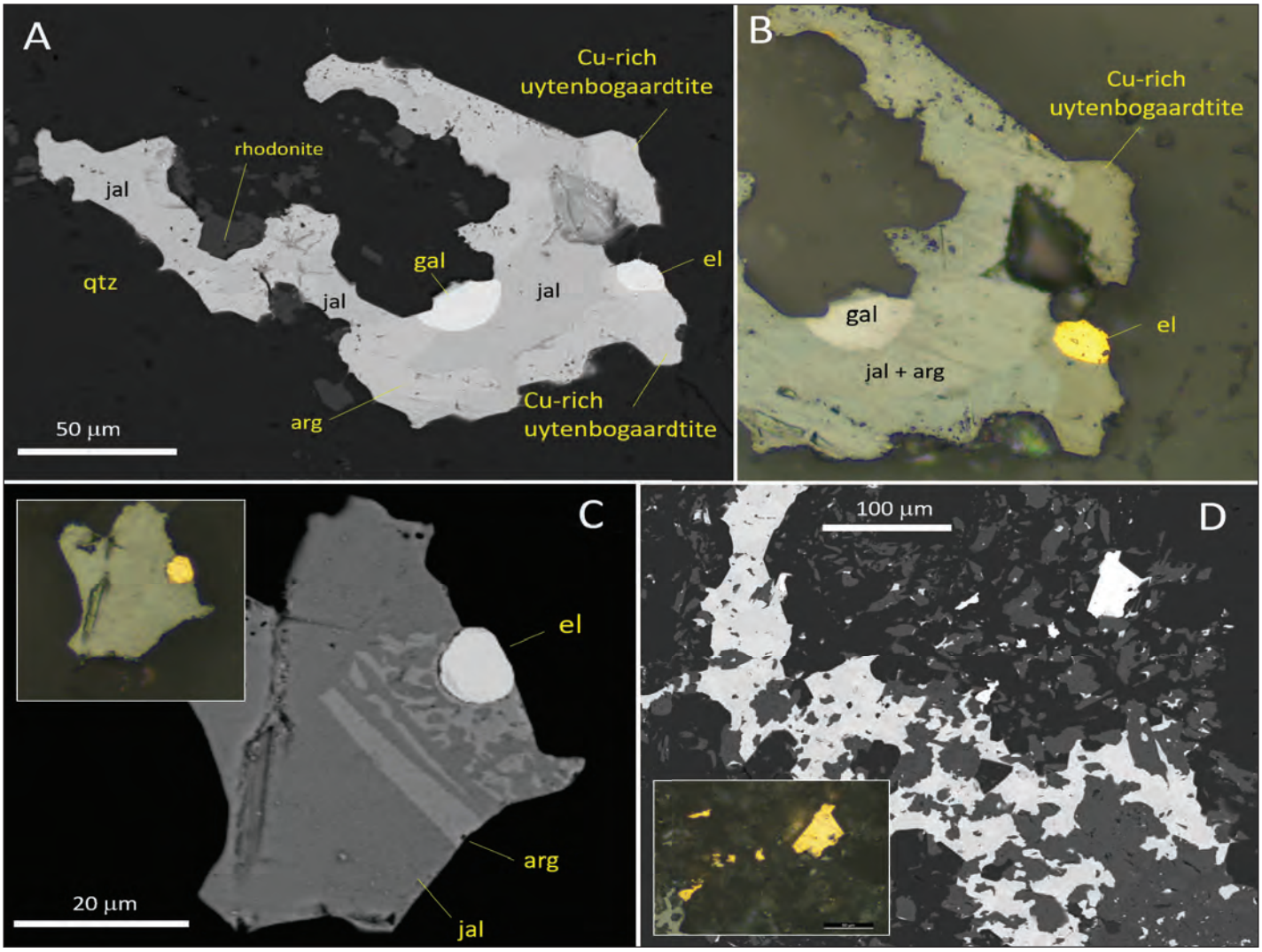

Figure 4. Stage 2 minerals from sample MA-13. (A) Intergrowth of jalpaite (jal), argentite (arg), galena (gal), electrum (el), and Cu-rich uytenbogaardtite in a gangue of quartz (qtz) + rhodonite, viewed in SEM-BSE mode; (B) same as A, reflected light; (C) exsolution intergrowth of argentite + jalpaite with electrum (inset shows same view in reflected light); (D) several electrum grains (easier to see in the reflected light inset) with abundant argentite + jalpaite (light gray) in gangue of rhodochrosite + rhodonite (medium gray) and quartz (darkest gray).

Like many lodes of Butte, supergene weathering of the veins of Marget Ann left behind resistant outcrops of quartz laced by veinlets of black Mn-oxides and brown Fe-oxides. Attempts to determine the mineralogy of the Mn-oxides by X-ray diffraction were unsuccessful, suggesting that they are amorphous or very fine grained. Some polished specimens collected from the mine dumps show evidence of secondary Cu and Ag mobilization with formation of supergene acanthite (Ag_2S), native silver, and Cu-sulfides (covellite and chalcocite). Although supergene Ag-enrichment was probably important for the overall mine production, the mineral assemblages of Stage 1 and 2 mineralization described above are thought to have been hypogene.

Fluid Inclusions

Coarse-grained, “comb” quartz from the Marget Ann mine has abundant fluid inclusions that range in size from <1 µm to >100 µm (fig. 5). Most of the fluid inclusions are simple two-phase inclusions with small vapor bubbles (B20 or roughly 20% bubble by volume, following the labeling convention of Rusk and others, 2008a). Some inclusions contain feathery, anisotropic daughter minerals, believed to be dawsonite ($NaAl(CO_3)(OH)_2$) based on their optical properties and the fact that they do not dissolve on heating (Coveney and Kelley, 1971). Very few vapor-rich inclusions were found, which suggests that boiling was not occurring when the coarse-grained, Stage 1 quartz grew. No three-phase CO_2-rich inclusions were found, and no CO_2-clathrates were seen, indicating a relatively low CO_2 content. Homogenization temperatures (T_h) show a bell-shaped distribution be-

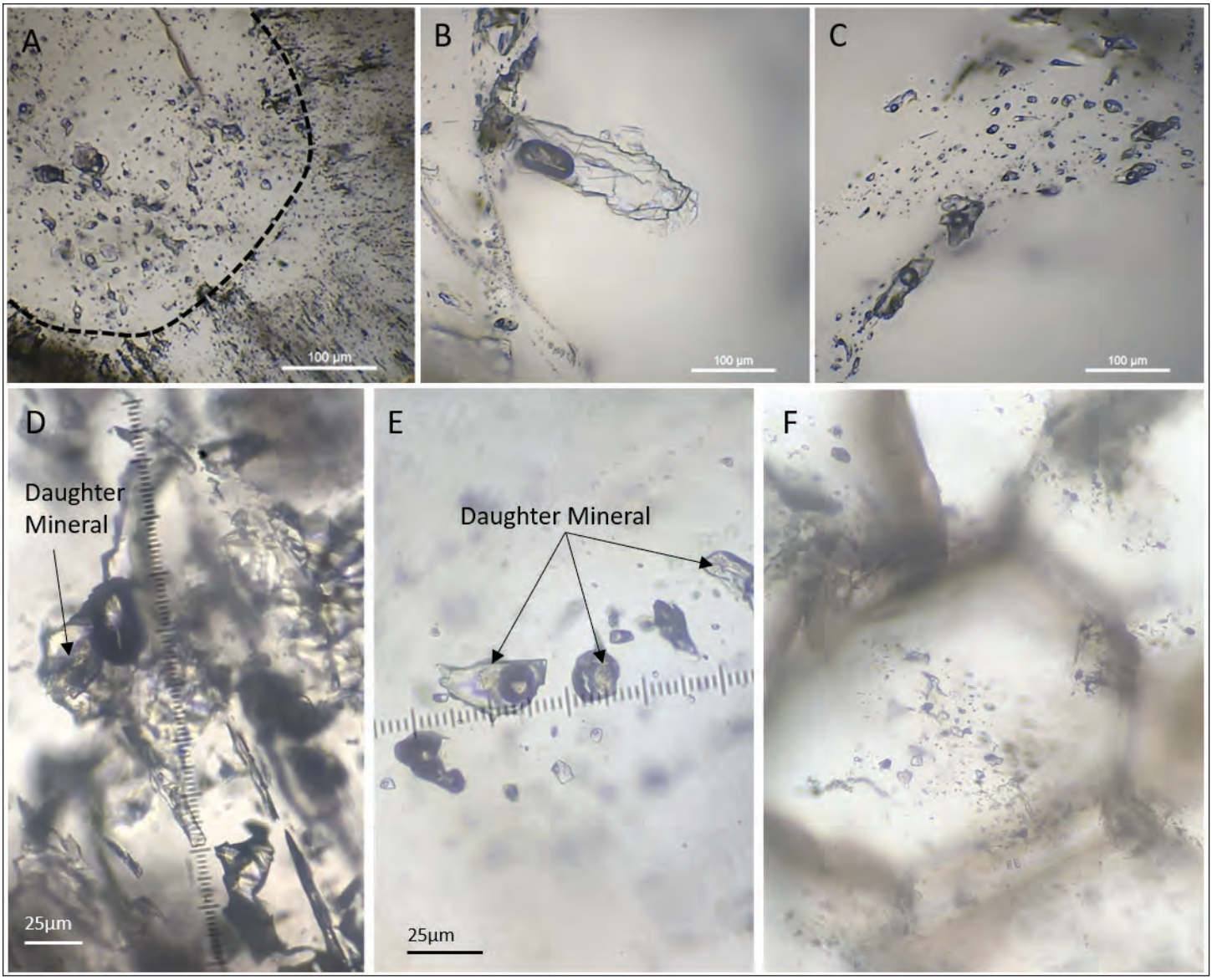

Figure 5. Fluid inclusions in quartz from Marget Ann. (A) Cluster of primary fluid inclusions 5 to 30 µm in diameter in the core of a zoned quartz crystal; (B and C) very large, B20 fluid inclusions in quartz; (D) very large B20 fluid inclusion with daughter mineral (dawsonite?); (E) group of fluid inclusions with daughter minerals (dawsonite?); (F) cluster of primary fluid inclusions in core of a quartz grain.

tween about 220 and 310°C, with a tail to lower temperatures (fig. 6A). The average Th for all measurements (*n* = 131) is 251°C. Salinities based on ice-melting temperatures ranged from 0.5 to 7 wt% $NaCl_{eq}$ (fig. 6B), with an average of 2.2 wt% $NaCl_{eq}$ (*n* = 77). A plot of salinity vs. temperature (fig. 6C) shows a possible mixing trend between three waters: (I) a high-temperature, higher salinity water; (II) a high-temperature, low-salinity water; and (III) a lower temperature, low-salinity water. Our preliminary interpretation is that Fluids I and II were heated groundwater and Fluid I was magmatic-hydrothermal in origin. These observations are more or less in line with what has been reported by Rusk and others (2008b) and Ortelli (2015) for fluid inclusions from other Main Stage veins of Butte.

Discussion

Fluid inclusion data from this study suggest that Stage 1 mineralization at Marget Ann formed when a saline magmatic/hydrothermal fluid mixed with a more abundant, low-salinity groundwater. Most of the metals (Cu-Pb-Zn-Ag-Mn) were probably transported into the veins from the magmatic fluid (e.g., Reed and others, 2013), while the quartz could have precipitated from either the magmatic water or the heated groundwater. A more interesting question is: which of these fluids would have been moving gold? At 250°C, gold is more soluble as a sulfide complex vs. a chloride complex in fluids that contain dissolved sulfide (e.g., Gammons and Williams-

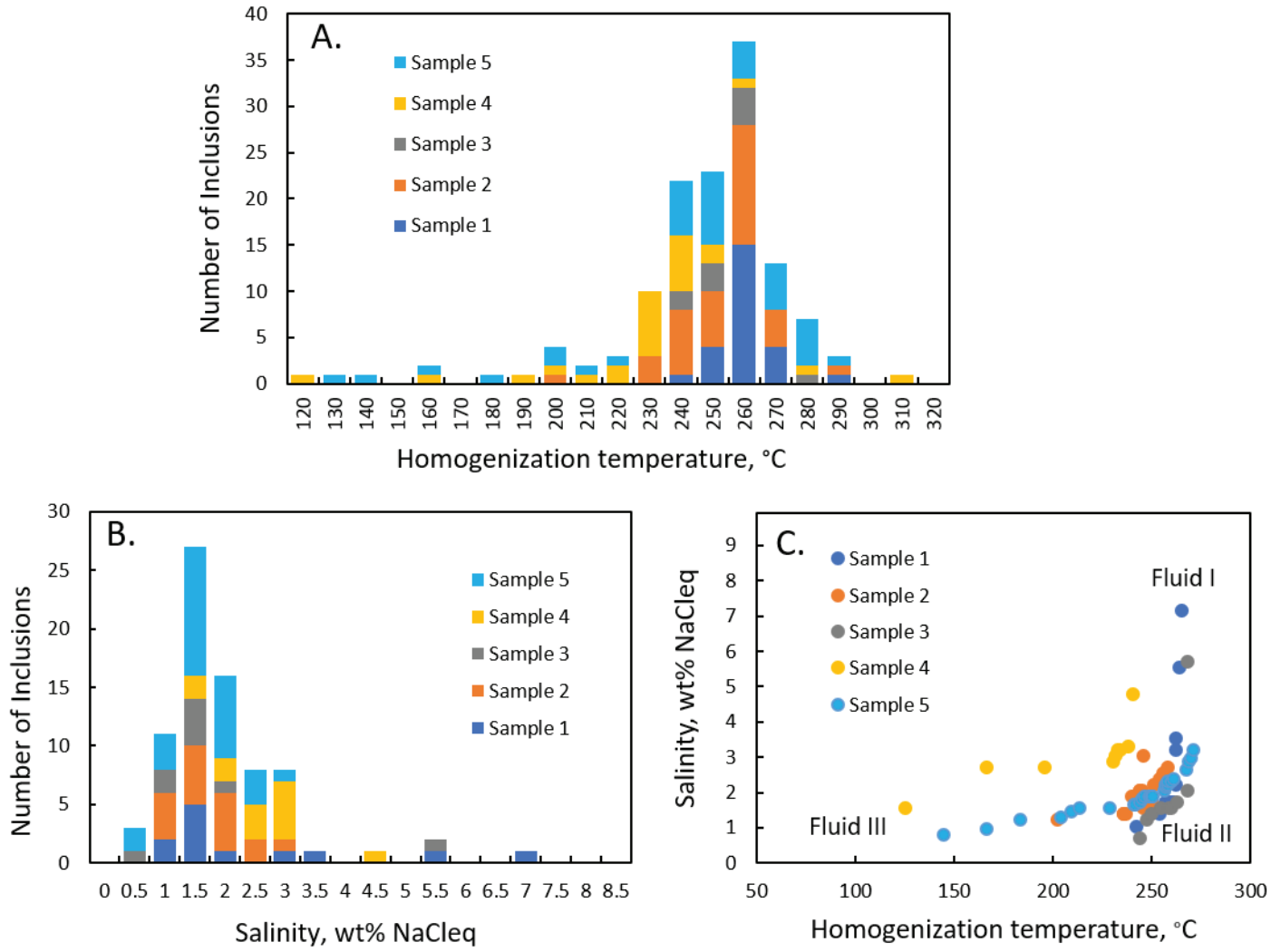

Figure 6. Fluid inclusion data from Marget Ann. (A) Histogram of homogenization temperatures; (B) histogram of salinity values; (C) salinity vs. Th cross plot.

Jones, 1997). If the low-salinity groundwater had an elevated H_2S content, it could have transported gold into the Marget Ann system. The fact that Marget Ann is at the periphery of the Butte district at a high elevation, and has veins that dip north, away from the magmatic-dominated Central Zone, could also help explain the higher gold content at Marget Ann.

An unanswered question is how much time, if any, elapsed between Stage 1 and Stage 2. Although Reed and others (2013) proposed that all of the vein types and metals of Butte formed during a single magmatic-hydrothermal event at roughly 65 Ma, Lund and others (2018) argued that the Ag-rich veins in the Peripheral Zone formed closer to 75 Ma, roughly 10 million years prior to the porphyry Cu-Mo event. If this is correct, then the Stage 1 mineralization at Marget Ann may have formed early, near 75 Ma, while Stage 2 might have formed later, circa 65 Ma. It is also possible that Stage 1 and Stage 2 formed during a single hydrothermal event, but by different processes. For example, the coarse-grained Stage 1 minerals may have formed by simple cooling or fluid mixing, whereas the fine-grained but richer Stage 2 mineral assemblage may have formed by boiling. Although this study did not find many vapor-rich fluid inclusions, we only looked at the Stage 1 quartz. Boiling, if it occurred, would have resulted in a drop in temperature (leading to deposition of chalcedony + rhodonite), an increase in pH (leading to deposition of carbonates + Ag-Cu-sulfide minerals + adularia), and loss of H_2S to vapor (leading to deposition of gold). More work is needed to develop these ideas further.

References Cited

Coveney, R.M., and Kelley, W.C., 1971, Dawsonite as a daughter mineral in hydrothermal fluid inclusions: Contributions to Mineralogy and Petrology, v. 32, p. 334–342.

Gammons, C.H., and Williams-Jones, A.E., 1997, Chemical mobility of gold in the porphyry-epithermal environment: Economic Geology, v. 92, p. 45–59.

Gammons, C.H., Snyder, D.M., Poulson, S.R., and Petritz, K., 2009, Geochemistry and stable isotopes of the flooded underground mine workings of Butte, Montana: Economic Geology, v. 104, p. 1213–1234.

Gammons, C.H., Szarkowski, J., and Stevenson, R., 2016, New investigations of the mineralogy of silver in the world-class porphyry-lode deposits of Butte, Montana: Mining Engineering, Web Exclusive, June 2016.

Houston, R.A., and Dilles, J.H., 2013, Structural geologic evolution of the Butte District, Montana: Economic Geology, v. 108, p. 1397–1424.

Lund, K., McAleer, R.J., Aleinikoff, J.N., Cosca, M.A., and Kunk, M.J., 2018, Two-event lode-ore deposition at Butte, USA: $^{40}Ar/^{39}Ar$ and U-Pb documentation of Ag-Au-polymetallic lodes overprinted by younger stockwork Cu-Mo ores and penecontemporaneous Cu lodes: Ore Geology Reviews, v. 102, p. 666–700.

Metesh, J.J., 1990, Aquifer testing and evaluation at the Travona Mine and Marget Ann Mine, Butte, Montana: Butte, Montana Tech, M.S. thesis,.

Meyer, C., Shea, E., Goddard, C., and Staff, 1968, Ore deposits at Butte, Montana, *in* Ridge, J.D. ed., Ore deposits of the United States 1933–1967 (Graton-Sales vol.): New York, American Institute of Minerals, Metals, and Petroleum Engineers, v. 2, p. 1363–1416.

Ortelli, M., 2015, Chemistry and physical properties of ore-forming fluids trapped in ore and gangue minerals: New insights into mineralization processes in magmatic-hydrothermal systems with special focus on the Butte mining district (USA): University of Geneva, Ph.D. dissertation.

Reed, M., Rusk, B., and Palandri, J., 2013, The Butte magmatic-hydrothermal system: One fluid yields all alteration and veins: Economic Geology, v. 108, p. 1379–1396.

Rusk, B.G., Reed, M.H., and Dilles, J.H., 2008a, Fluid inclusion evidence for magmatic-hydrothermal fluid evolution in the porphyry copper-molybdenum deposit at Butte, Montana: Economic Geology, v. 103, p. 307–334.

Rusk, B.G., Miller, B.J., and Reed, M.H., 2008b, Fluid inclusion evidence for the formation of Main Stage polymetallic base-metal veins, Butte, Montana, USA: Arizona Geological Society Digest 22, p. 573–581.

Sahinen, W.M., 1953, Geology of the Marget Ann mine, Butte district, Montana: Butte, Montana Tech, B.S. thesis.

Win, M.S., 1955, Geology and ore deposits of the Marget Ann Mine, Silver Bow County, Montana: Butte, Montana Tech, M.S. thesis.

John Allard mapping near Cardwell, MT. Photo by Chris Gammons.

Stable Isotopes and Geothermometry of the Lowry Deposit, Black Butte Copper Project, Meagher County, Montana

John Allard,[1] Chris Gammons,[1] and Javin Hatcherian[2]

[1]*Department of Geological Engineering, Montana Tech, Butte, Montana*

[2]*Organic Petrology Lab, United States Geological Survey, Reston, Virginia*

Abstract

The Black Butte copper project is a sedimentary-rock-hosted Cu massive sulfide deposit, hosted in rocks of the ca. 1.5–1.325 Ga Mesoproterozoic Belt Supergroup. The goals of this research were to apply robust geochemical methods to characterize the ore-forming fluids of the Lowry deposit. Sulfur stable isotope analyses of chalcopyrite from the Lowry show a narrow range of $\delta^{34}S$ between ±5 per mil. Carbonate isotopes from hydrothermal gangue have a spread of 22 to 16 per mil $\delta^{18}O$ and 0 to -5 per mil $\delta^{13}C$. When plotted with other S isotopes of pyrite and chalcopyrite from the Black Butte project, a broad range of S isotope values in pyrite reflect bacterial reduction of marine sulfate, whereas the narrow range in chalcopyrite can be explained by higher temperature thermochemical sulfate reduction or an input of magmatic sulfur. When plotted with carbonate values of the Newland Formation from White and others (2014), carbonate values of hydrothermal dolomite from this study show depletion of $\delta^{18}O$, likely through heating from ore-forming fluids. New bitumen reflectance values produced temperature estimates averaging 223 ± 8°C (n = 8), with a range of 213 to 239°C. These geochemical data, combined with observations of mineralized Lowry core, suggest that the Lowry deposit formed under moderate temperature fluids that originated in highly evolved connate brines or magmatic fluids. The number of cross-cutting textures hosted in the Lowry suggest that the host Newland Formation was undergoing compaction during mineralization, but the presence of some laterally extensive sedimentary pyrite replaced by pyrite allows for a late syngenetic to early epigenetic interpretation.

Introduction

The Black Butte copper project, formerly known as Sheep Creek, is located 27 km northwest of White Sulphur Springs, Meagher County, Montana (fig. 1), along the northern margin of the Helena embayment of the Mesoproterozoic Belt–Purcell basin. The deposit is unusual in that it has the geologic setting of a sedimentary-exhalative (SEDEX) deposit but a metal endowment typical of a sediment-hosted stratiform Cu deposit. Black Butte is hosted by the Newland Formation (Fm) of the Lower Belt Group, a black shale/limestone–dolostone with interbeds of debris flow conglomerates. Two centers of Cu mineralization, 2 km apart, have been drilled on the property, termed the Johnny Lee and Lowry deposits: both occur in the Lower Newland Fm (fig. 2).

Multiple workers (Himes and Petersen, 1990; Zieg and Lietch, 1998; Lydon, 2007; Graham and others, 2012; White and others, 2014; Present and others, 2018; Saintilan and others, 2021) have described Black Butte's sedimentary architecture, mineralization, stable isotopes, and similarities to other deposits. The majority of previous work has focused on the Johnny Lee deposit, although the study of Graham and others (2012) included samples from four Lowry drill holes circa 1987. The purpose of this study is to expand upon the geology, stable isotope geochemistry, and thermal conditions at the Lowry deposit to better describe its ore-forming fluids and metal source.

Methods

Over 60 samples were collected of representative intercepts from nine drill holes that intersected the Lowry sulfide zones along N–S and E–W transects. Drill core was accessed at the Sandfire Resources America, Inc. core storage facility in White Sulphur Springs, Montana. A portable x-ray fluorescence instrument was used to select sulfide samples for microscopy. More than 20 1-in-diameter polished plugs were made for reflected light microscopy, 8 of which were used for bitumen reflectance analysis. Bitumen samples were sent as plugs

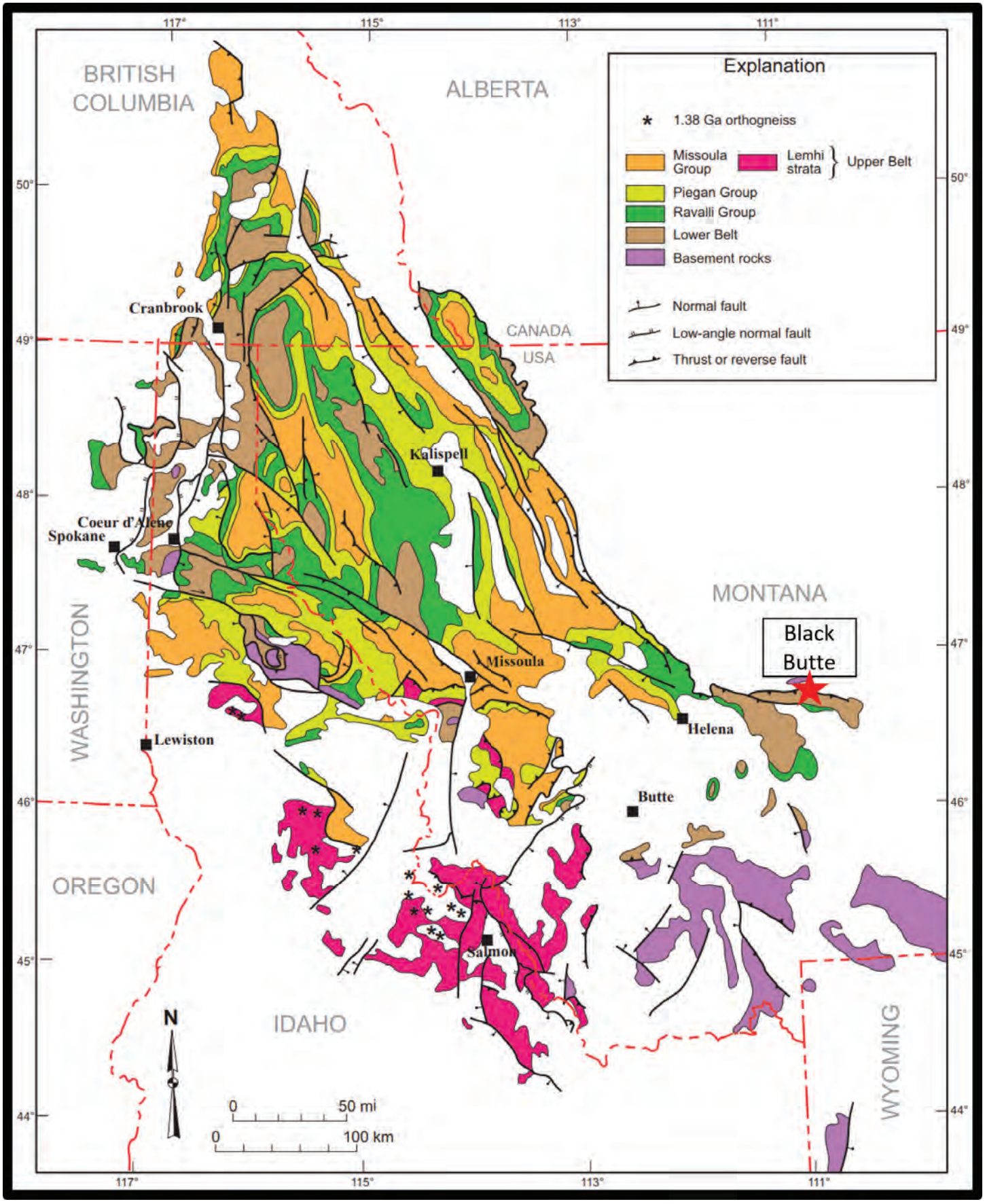

Figure 1. Extent of the Belt–Purcell Supergroup outcrops with the location of Black Butte copper project. From Lonn and others (2020).

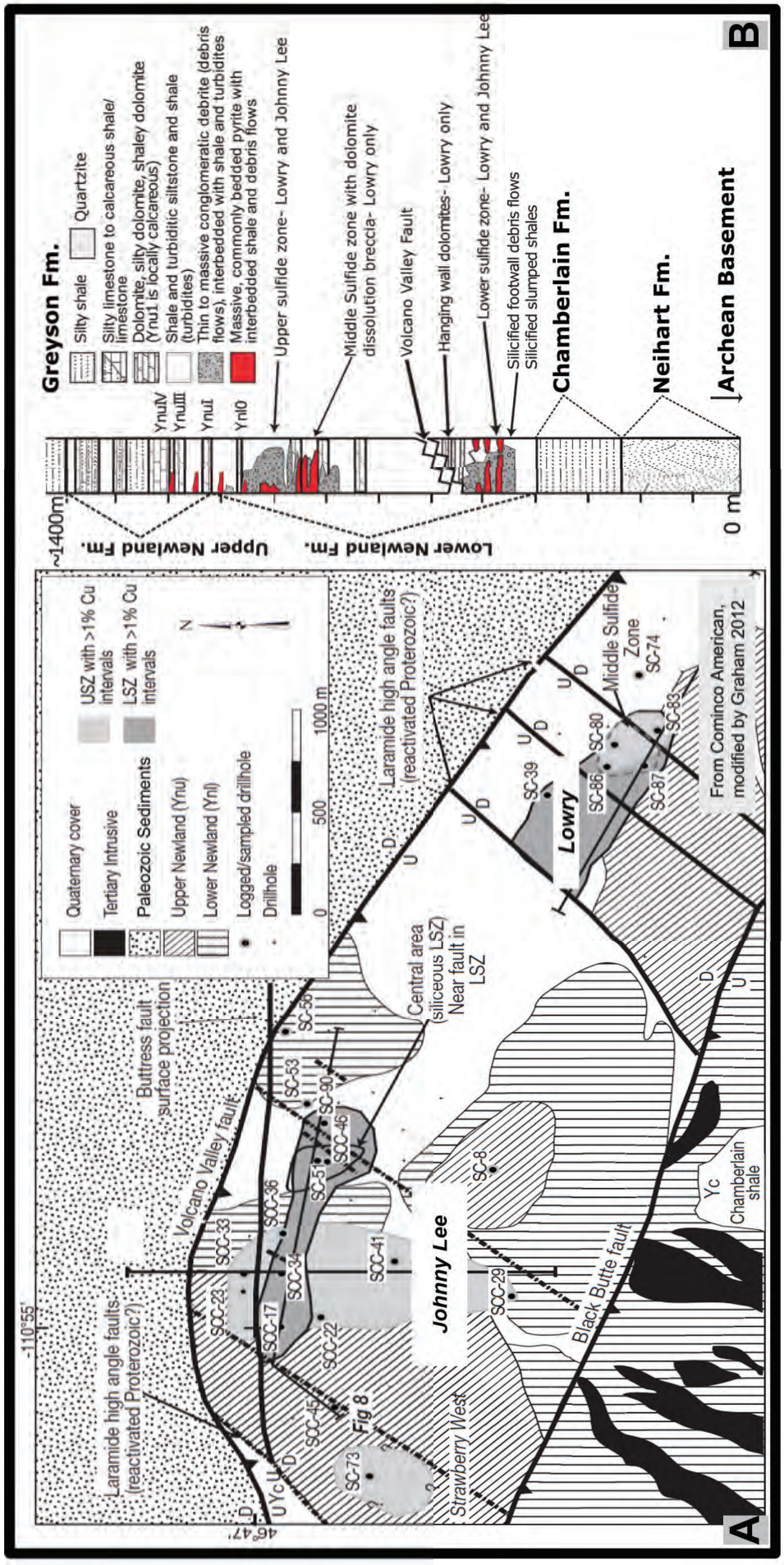

Figure 2. (A) Geologic map of the project area from Cominco American modified by Graham and others (2012). (B) Stratigraphy of the Black Butte project area modified from Graham and others (2012); note that "logged/sampled drillhole" is from Graham and others (2012).

and separates to the U.S. Geological Survey's Organic Petrology Laboratory in Reston, Virginia, for reflection analysis, which used a Leica DM4000 microscope equipped with LED illumination and monochrome camera detection. Fifteen separates of chalcopyrite and one of pyrite were sent to the University of Nevada–Reno for $\delta^{34}S$ analysis, which was performed with a Eurovector elemental analyzer interfaced to a Micromass Isoprime stable isotope ratio mass spectrometer (IRMS). Twenty separates of hydrothermal dolomite were sent to the University of Wyoming's Stable Isotope Facility for $\delta^{13}C$ and $\delta^{18}O$ analyses, which was performed with a Thermo GasBench gas chromatographer coupled to a Thermo Delta V IRMS. Three samples of solid bitumen were analyzed for $\delta^{13}C$ using a Picarro combustion module and cavity ring-down spectrometer in the Montana Bureau of Mines and Geology's geochemistry laboratory. Six separates of hydrothermal quartz were sent to the University of Oregon's Stable Isotope Lab for $\delta^{18}O$ analyses, which was performed with a 35-watt CO_2 laser line coupled with MAT 253 10 kV gas source IRMS using purified BrF_5 reagent.

Results

Ore and Gangue Mineralogy

Sulfide mineralization in the Lowry deposit occurs dominantly as chalcopyrite and pyrite with lesser, typically fine-grained inclusions of tennantite. Multiple styles of mineralization textures most common in the Lowry deposit, specifically the MSZ of the Lowry, are described below.

1. 1–10 cm chalcopyrite and pyrite ± tennantite veins cutting the host lower Newland Fm are common throughout the copper mineralized MSZ (figs. 1A, 1B).
2. Dolostone dissolution breccias with mono-polylithic clasts in a matrix of sparry white dolomite (fig. 3B) replaced or infilled by chalcopyrite and pyrite (fig. 4D). Bitumen and quartz are common accessories to the dolomite dissolution breccias. Dissolution breccias are a laterally extensive subunit within the lower Newland Fm in the Lowry deposit. In hand sample and polished section, copper sulfides appear intergrown (coeval) with sparry dolomite, but it is possible that the copper sulfides grew later than the dolomite gangue as void-fill.
3. Chalcopyrite and late pyrite engulfing and replacing sedimentary pyrite in net-textured pyrite, bedded pyrite, and pyrite clasts in debris flow conglomerates (fig. 4C). Polished plug microscopy revealed that most of the early, sedimentary pyrite (bedded) or net-texured pyrite observed in the Lowry MSZ is engulfed by later copper sulfides and pyrite; little evidence of replacement was observed.
4. Replacement of debris-flow matrices or infill of pore spaces

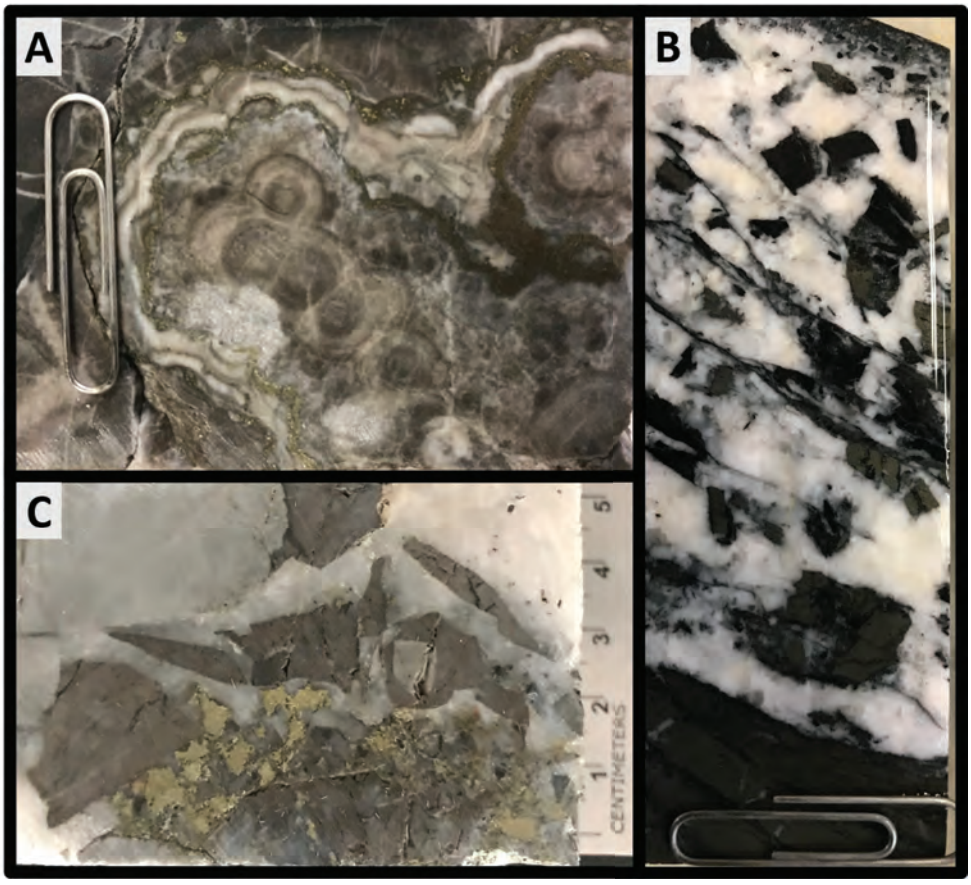

Figure 3. Lowry gangue textures. (A) Crustiform dolomite rimmed by pyrite and chalcopyrite; (B) dolomite dissolution breccia–white sparry dolomite with clasts of black shale and sedimentary pyrite; (C) brecciated dolostone in quartz with pyrite and chalcopyrite.

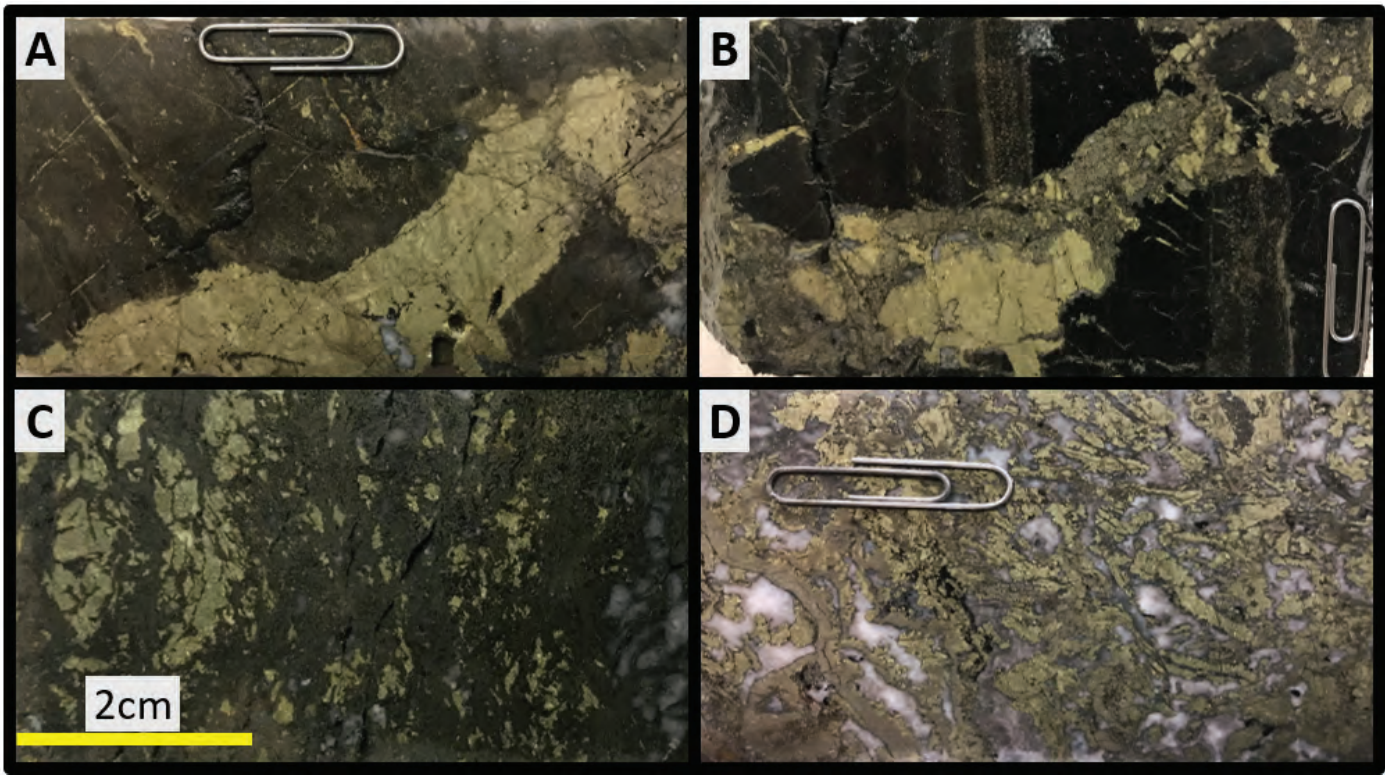

Figure 4. Lowry sulfide textures. (A, B) Chalcopyrite-pyrite ± tennantite veins cutting black shale and sedimentary pyrite in the Lower Newland Formation; (C) chalcopyrite and sedimentary pyrite in pyrite-walled-tube structures (Present and others, 2018); (D) chalcopyrite, pyrite, and bitumen replacing or infilling crustiform dolomite.

Copper mineralization in the Lowry deposit is closely associated with white sparry dolomite and lesser quartz veins and silicification. Sparry dolomite, also described as baroque or saddle dolomite, is a locally derived diagenetic and/or alteration product of the Newland Fm. Dolostone in the Newland was locally recrystallized, as crustiform dolomite and dissolution breccias, then transported as veins. Crustiform textures in dolomite are inferred to be the result of local recrystallization in places where grain size and color are zoned relative to dolostone, fining from coarse white centers to darker gray recrystallized dolostone (fig. 3A). Bitumen often occurs within the coarse cores, likely a result of insoluble carbonaceous material or hydrocarbons from the Newland dolostone beds (fig. 5). Dissolution breccias commonly occur as sparry white dolomite with angular clasts of sedimentary pyrite and/or black shale (fig. 3B). Mosaic breccias consisting of fine-grained, recrystallized dolostone cut by thin white hydrothermal dolomite veins ± sulfides is also common.

Stable Isotopes

Chalcopyrite (n = 12) and pyrite (n = 1) grain separates from the Lowry Middle Sulfide Zone (MSZ) and Lower Sulfide Zones (LSZ) were analyzed for $\delta^{34}S$, reported here relative to the Vienna Canon Diablo Troilite (fig. 6A). The $\delta^{34}S$ values range from -3.6 to + 3.4‰, with a mean of -0.4‰ (n = 13). Dolomite (n = 19) separates from the Lowry MSZ and LSZ were analyzed for $\delta^{13}C$ and $\delta^{18}O$, reported here relative to the Vienna Pee Dee Belemnite (VPDB) and Vienna Standard Mean Ocean Water (VSMOW), respectively (fig. 6B). The $\delta^{13}C$ values ranged from -4.8 to +0.7‰, with a mean of +2.1‰, while the $\delta^{18}O$ values ranged from +18.7 to +22.2‰, with a mean of +20.6‰. Bitumen (n = 3) separates from the Lowry deposit were analyzed for $\delta^{13}C$, reported here relative to the VPDB. The $\delta^{13}C$ values of the three samples were -30.4, -30.7, and -33.5‰.

Finally, six samples of vein quartz from the Lowry USZ and LSZ were analyzed for $\delta^{18}O$, reported here relative to VSMOW (table 1). The $\delta^{18}O$ values ranged from +21.0 to +22.8‰, with a mean of +21.9‰.

Bitumen Temperature Estimates

Bitumen reflectance is a widely applied method to constrain hydrocarbon reservoir maturity (Hackley, 2012). Like vitrinite, the reflectivity of solid bitumen increases with increasing thermal maturity. This relation-

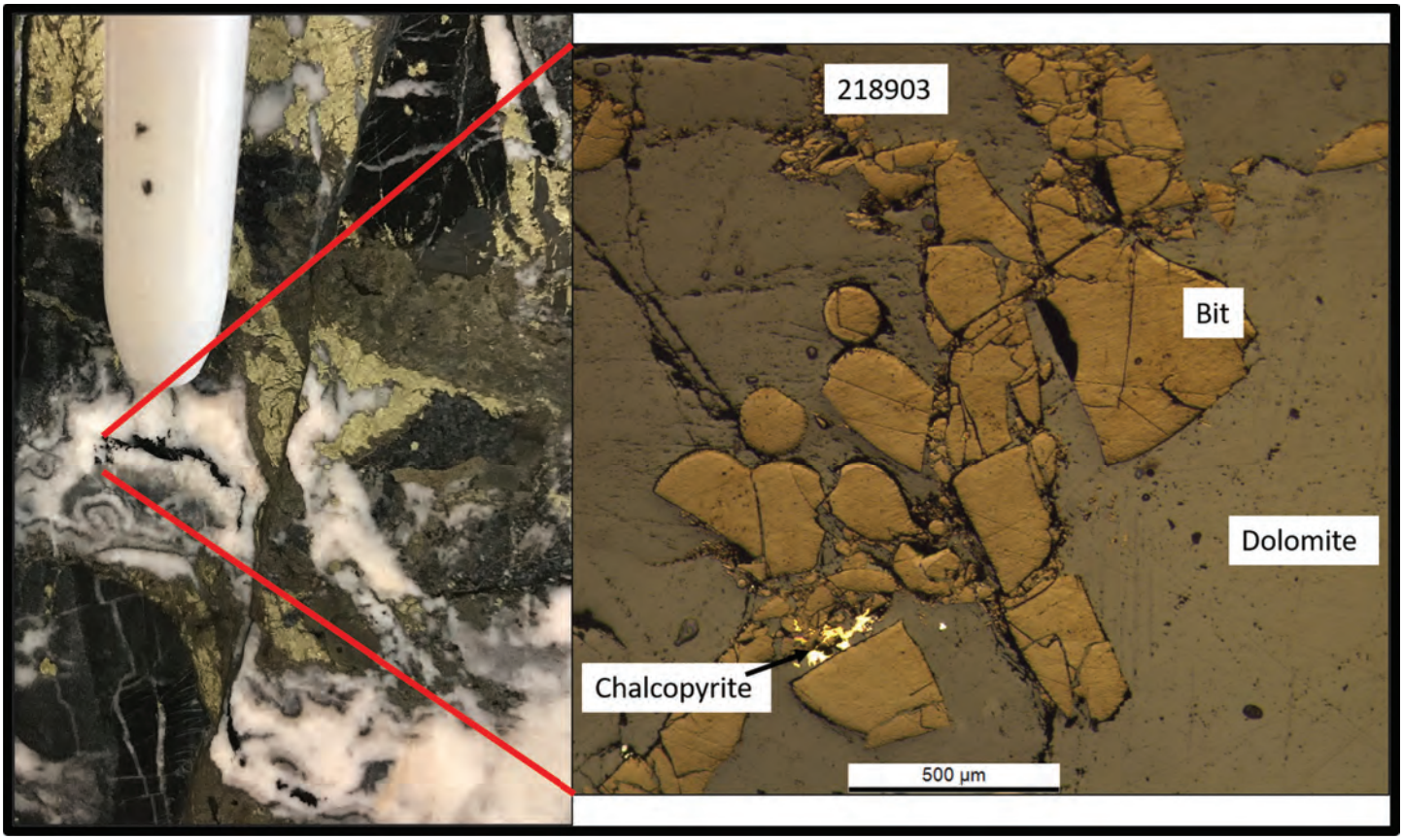

Figure 5. Hand sample and photomicrograph of solid bitumen with dolomite and chalcopyrite. The mean T_{peak} of 218903 was 236.1°C (table 2).

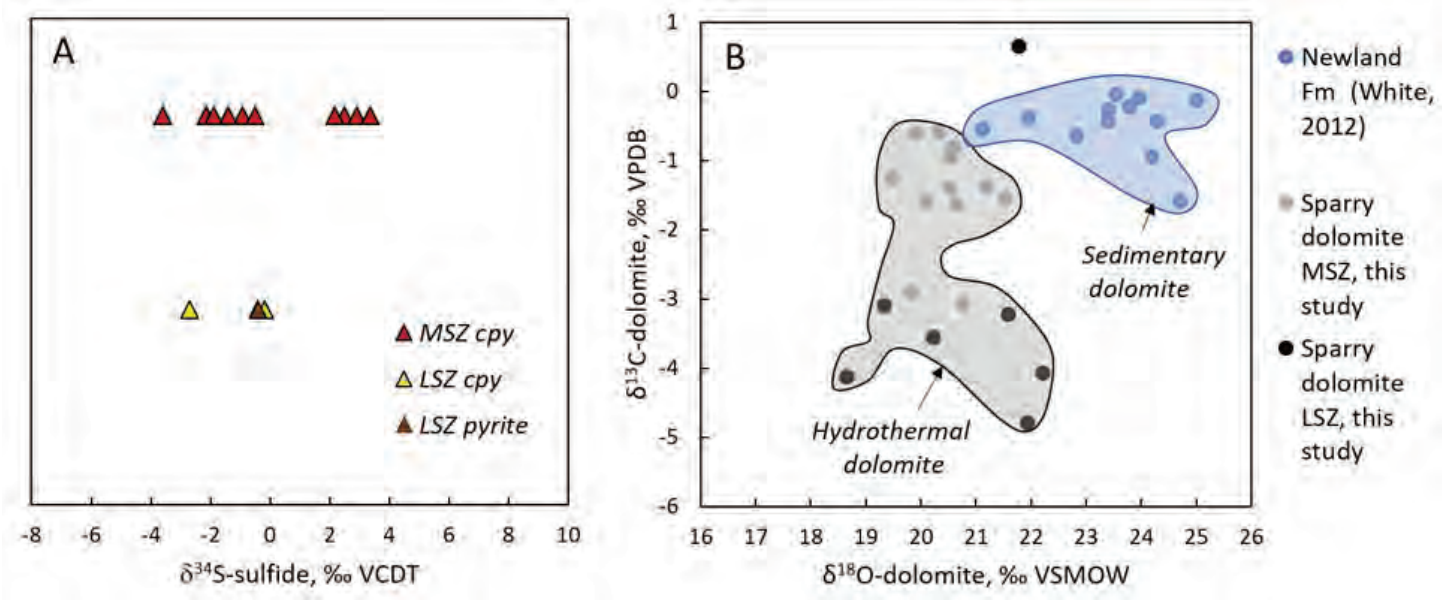

Figure 6. New stable isotope data from the Lowry deposit. (A) S-isotopes of chalcopyrite and pyrite; (B) C- and O-isotopes of hydrothermal dolomite (data for sedimentary dolomite from White, 2012, are shown for comparison).

ship can be used to estimate the peak temperature experienced by solid bitumen (Riediger, 1993; Barker and Bone, 1995; Landis and Castaño, 1995; Hackley, 2012). For this study, reflectance of solid bitumen occurring with gangue and sulfides was measured. The reflectance values of solid bitumen were used to calculate peak temperatures from 212.8 to 239.5°C (avg = 223 ± 8°C, *n* = 8) following the regression of Barker and Bone (1995; table 2). Additional work is in progress at Montana Technological University to estimate the temperature of the same bitumen samples based on Raman spectroscopy.

Table 1. $\delta^{18}O$ of quartz from the Lowry deposit.

Sample	$\delta^{18}O_{SMOW}$	Lowry Sulfide Zone
223505	21.1	MSZ
218909	21.9	MSZ
218911	22.8	MSZ
223516	21.0	USZ
223515	22.7	USZ
218913	21.9	USZ

Table 2. Bitumen reflectance and temperature estimates Barker and Bone (1995) regression-$(BR_o+0.9787)/0.0202$.

Sample	$\%BR_o$	±	T_{peak}	±
223507	3.3	0.1	212.8	7.1
223529	3.3	0.1	213.8	6.6
218919	3.4	0.1	215.3	6.5
223507B	3.4	0.1	218.3	7.3
223525	3.4	0.2	218.7	8.1
218917	3.6	0.2	228.2	11.4
218903	3.8	0.2	236.1	8.4
223525	3.9	0.2	239.5	8.9

Discussion

The estimated maximum temperature experienced by bitumen at the Lowry deposit was roughly 220°C. This agrees with temperatures of 125° to 225°C estimated by White and others (2014) based on the thermodynamic stability of ore minerals at Black Butte. These results suggest that the Black Butte deposit formed at relatively low temperatures, consistent with other SEDEX and sediment-hosted stratiform copper deposits worldwide that are believed to have formed by circulating basinal brines. Saintilan and others (2021) reported un-radiogenic Os values from Black Butte chalcopyrite, which reflects a magmatic Os source; they suggested that a buried Mesoproterozoic intrusive body, akin to the ca. 1,455 Ma tholeiitic dikes cutting the Archean basement in the Tobacco Root Mountains near the Perry Line (Wooden and others, 1978) was responsible for the metalliferous fluids. Whereas it is reasonable to expect that syn-rift magmatism in the Belt–Purcell Basin would have created an elevated thermal gradient to drive connate fluid convection, this study shows no evidence of temperatures that would indicate the involvement of magmatic-hydrothermal fluids, as was recently proposed for Black Butte by Saintilan and others (2021).

The S-isotope results presented above are in close agreement with previous studies (Zieg and Lietch, 1998; Lyons and others, 2000; Graham, 2011; Present and others, 2018; Saintilan and others, 2021) of the Black Butte district. Whereas early, sedimentary pyrite of the Newland Fm shows a huge range in $\delta^{34}S$ from -8.7 to +36.3‰ (Lyons and others, 2000), the $\delta^{34}S$ of epigenetic chalcopyrite in both the Johnny Lee and Lowry deposits is more restricted to values closer to 0‰. This result suggests that copper in the Lowry MSZ/LSZ and Johnny Lee USZ and LSZ deposits had a similar origin, despite differences in the style of mineralization. Multiple authors have proposed two distinct mechanisms for these ore-stage $\delta^{34}S$ values: (1) a magmatic sulfur source (Zieg and Lietch, 1998; Saintilan and others, 2021) and (2) thermochemical-sulfate reduction, by which hydrothermal fluids reduced seawater sulfate to H_2S (Graham, 2012).

As shown in figure 5B, the sparry, hydrothermal dolomite in the Lowry deposit is depleted in both $\delta^{18}O$ and $\delta^{13}C$ relative to sedimentary dolomite in the Newland Fm. The depletion in $\delta^{18}O$ was likely caused by water–rock interaction at temperatures up to 200°C, as has been modeled for dolomite from the MacArthur River deposit of Australia (Large and others, 2001). Some of the depletion in $\delta^{13}C$ could have been caused by incorporation of inorganic carbon sourced by the breakdown of bitumen. As shown above, bitumen from the Lowry deposit is very light ($\delta^{13}C < -30$ per mil). Therefore, incorporation of even a small amount of bitumen-C could have lowered the $\delta^{13}C$ of dissolved inorganic carbon in the hydrothermal fluid.

The $\delta^{18}O$-quartz values reported above are the first published data for hydrothermal quartz from Black Butte. At 200°C, quartz is predicted to be about 1.5‰ enriched in $\delta^{18}O$ relative to dolomite (Zheng, 1999). This agrees with the results of this study. Whereas hydrothermal quartz from Lowry had an average $\delta^{18}O$ of +21.9‰, hydrothermal dolomite from Lowry has an average $\delta^{18}O$ of +20.6‰, which is +1.3‰ lighter than the quartz.

Overall, the results of this study are consistent with an ore-forming fluid, probably a hot connate brine, depositing quartz, dolomite, and chalcopyrite at temperatures near 200°C in the Lowry deposit.

Acknowledgments

We would like to thank Tintina Montana, Inc. for their ongoing support of this research. Jerry Zieg, Eric LeLacheur, and Adam Wiest have provided access to drill core and discussion that were invaluable to this study. Dr. Paul Hackley has provided a wealth of information regarding solid bitumen, for which we are extremely grateful. Funding for this project was provided through the generous support of the Society of Economic Geology, the Tobacco Root Geological Society, and Tintina Montana, Inc.

References

Barker, C. E., and Bone, Y., 1995, The minimal response to contact metamorphism by the Devonian Buchan Caves Limestone, Buchan Rift, Victoria, Australia: Organic Geochemistry, v. 22, p. 151–164.

Graham, G. E., 2011, Geologic and stable isotope investigations of the Sheep Creek Cu-(Co-Ag) deposit with comparison to other sediment-hosted base metal deposits in Mesoproterozoic basins: Ph.D. Dissertation, Colorado School of Mines, Golden, CO.

Graham, G., Hitzman, M. W. H., and Zieg, J., 2012, Geologic setting, sedimentary architecture, and paragenesis of the Mesoproterozoic sediment-hosted Sheep Creek Cu-Co-Ag deposit, Helena Embayment, Montana: Economic Geology, v. 107, p. 1115–1141.

Hackley, P. C., 2012, Geological and geochemical characterization of the Lower Cretaceous Pearsall Formation, Maverick Basin, south Texas: A future shale gas resource? AAPG Bulletin, v. 96, p. 1449–1482.

Himes, M.D., and Petersen, E.U., 1990, Geological and mineralogical characteristics

of the Sheep Creek copper-cobalt sediment-hosted stratabound sulfide deposit, Meagher County, Montana, *in* Hausen, D.M., Halbe, D.N., Petersen, E.U., and Tafuri, W.J., eds., Proceedings of the Gold ’90 Symposium, Salt Lake City, Utah: Littleton, Colorado, Society for Mining, Metallurgy and Exploration, p. 533–546.

Landis, C. R., and Castaño, J. R.,1995, Maturation and bulk chemical properties of a suite of solid hydrocarbons: Organic Geochemistry, v. 22, p. 137–149.

Large, R. R., Bull, S. W. and Winefield, P. R., 2001, Carbon and oxygen isotope halo in carbonates related to the McArthur River (HYC) Zn-Pb-Ag deposit, North Australia: Implications for sedimentation, ore genesis, and mineral exploration: Economic Geology, v. 96, p. 1567-1593.

Lonn, J. D., Burmester, R. F., Lewis, R. S., and Mcfaddan, M. D., 2020, The Mesoproterozoic Belt Supergroup: Montana Bureau of Mines and Geology, Special Publication 122, Geology of Montana, vol. 1: Geologic History.

Lydon, J. W., 2007, Geology and metallogeny of the Belt-Purcell basin: In Mineral Deposits of Canada: A Synthesis of Major Deposit-Types, District Metallogeny, the Evolution of Geological Provinces, and Exploration Methods, 5(5), 581–607.

Lyons, T. W., Luepke, J. J., Schreiber, M. E., and Zieg, G. A., 2000, Sulfur geochemical constraints on Mesoproterozoic restricted marine deposition: Lower Belt Supergroup, northwestern United States: Geochimica et Cosmochimica Acta, v. 64, p. 427-437.

Present, T. M., Bergmann, K. D., Myers, C., Slotznick, S. P., Creveling, J. R., Zieg, J., Fischer, W. W., Knoll, A. H., and Grotzinger, J. P., 2018, Pyrite-walled tube structures in a Mesoproterozoic sediment-hosted metal sulfide deposit: Bulletin of the Geological Society of America, v. 130, p. 598–616.

Riediger, C. L., 1993, Solid bitumen reflectance and Rock-Eval Tmax as maturation indices: an example from the “Nordegg Member”, Western Canada Sedimentary Basin: International Journal of Coal Geology, v. 22, p. 295–315.

Saintilan, N. J., Sheldrake, T. E., Creaser, R. A., Selby, D., Zieg, J., Boyce, A., and Chelle-Michou, C., 2021, Synsedimentary to diagenetic Cu ± Co mineralization in Mesoproterozoic pyritic shale driven by magmatic-hydrothermal activity on the edge of the Great Falls Tectonic Zone–Black Butte, Helena Embayment, Belt-Purcell Basin, USA: Evidence from sulfide Re-Os: Lithosphere, v. 2021(1), p. 01–20.

White, J., 2012, Paragenesis of cobalt and nickel at the Black Butte Copper Project, Meagher County, Montana: M.S. Thesis. Montana Tech, Butte, MT.

White, J., Gammons, C. H., and Zieg, G. A., 2014, Paragenesis of cobalt and nickel in the Black Butte shale-hosted copper deposit, Belt Basin, Montana, USA: Mineralium Deposita, v. 49, p. 335–351.

Wooden, J. L., Vitaliano, C. J., Koehler, S. W., & Ragland, P. C., 1978, The late Precambrian mafic dikes of the southern Tobacco Root Mountains, Montana: geochemistry, Rb-Sr geochronology and relationships to Belt tectonics: Canadian Journal of Earth Sciences, v.15, p. 467–479.Zheng Y.-F., 1999, Oxygen isotope fractionation in carbonate and sulfate minerals: Geochemical Journal, v. 33, p. 109-126

Zieg, G. A. and Lietch, C.H., 1998, The geology of the Sheep Creek copper deposits, Meagher County, Montana: In: Berg R (ed) Belt Symposium III Abstracts, Montana Bureau of Mines and Geology, Open File Report 381.

Kaleb Scarberry on way to Hidden Lake in the Elkhorn 7.5’ quadrangle. Photo by Joel Dietrich.

Tizer Lake in the Elkhorn 7.5’ quadrangle. Photo by Joel Dietrich.

Geochemistry of Naturally Occurring Acid Rock Drainage in the Judith Mountains, Montana: A Synoptic Study of Chicago Gulch

Sara C. Edinberg[1,2] and Christopher H. Gammons[1]

[1]*Department of Geological Engineering, Montana Technological University, Butte, Montana*

[2]*Montana Bureau of Mines and Geology, Butte, Montana*

Acid rock drainage (ARD) poses a continuing environmental challenge to the mining industry. However, few studies have documented pre-mining (baseline) groundwater and surface-water chemistry prior to large-scale mining operations (Nordstrom, 2015). Here, we summarize baseline water chemistry from an unmined watershed with naturally occurring acid rock drainage. Further details of this study are available in Edinberg (2016) and Gammons and others (2021).

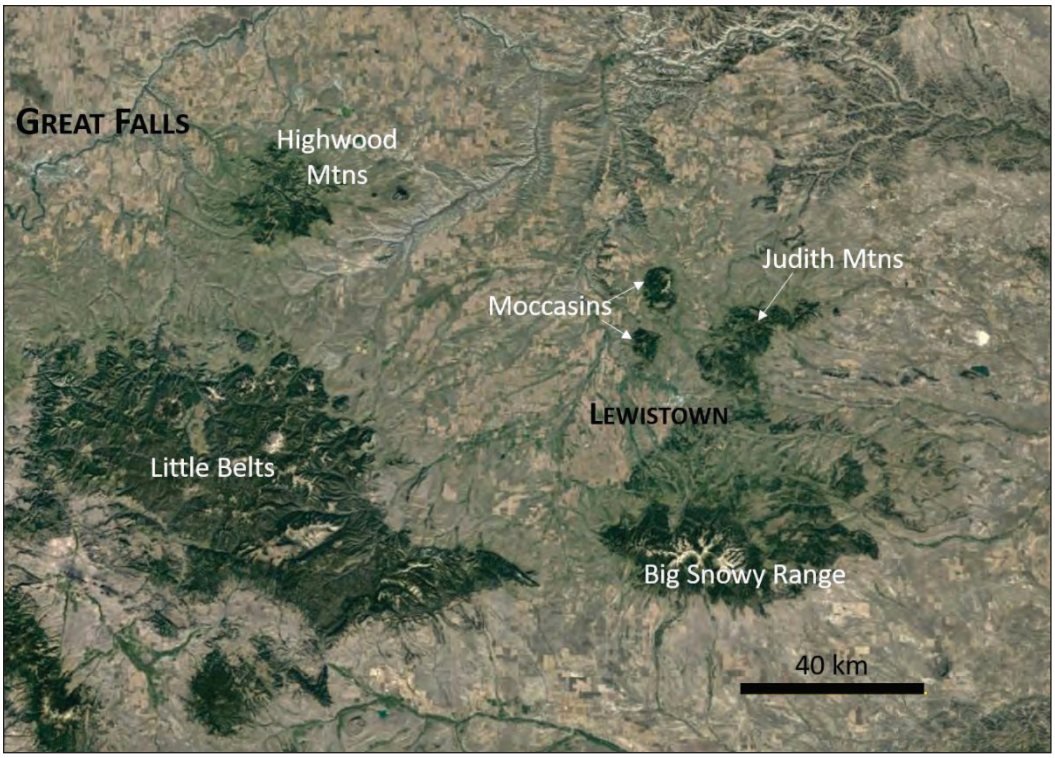

Figure 1. Map showing the location of the Judith Mountains, northeast of Lewistown, Montana.

The Judith Mountains are located in central Montana northeast of Lewistown (fig. 1). The mountain range is composed of a cluster of late Cretaceous to Tertiary laccoliths, stocks, dikes, and sills that intruded Paleozoic and Mesozoic sedimentary formations toward the end of the Laramide orogeny. Red Mountain, a prominent peak in the Judiths, is composed of hydrothermally altered quartz monzonite with disseminated pyrite (Goddard, 1988). Although the Red Mountain area was never mined, the three streams that radially drain Red Mountain are naturally acidic in their headwaters (fig. 2). A previous study (Williams and others, 2015) examined the geochemistry of two streams draining Red Mountain—Armells Creek and Collar Gulch—using synoptic sampling events and flow measurements. This study presents results from the third stream, Chicago Gulch, and compares data between the three drainages. Estimates of solute fluxes (load divided by watershed area) for the three drainages are also presented as a potential analogue for baseline solute flux in a disturbed watershed.

Total and dissolved (filtered to 0.45 μm) metal concentrations were measured at over 20 locations along Chicago Gulch and its tributaries during low-flow (August 2014) and high-flow (May 2015) conditions (fig. 3). In the headwaters, pH is less than 4 and extensive iron oxide (ferricrete) deposits are observed along the floodplain and in iron bogs (fig. 4A). The source of the ferricretes is from the oxidation of pyrite in the hydrothermally altered bedrock that feeds weakly acidic springs. These springs contain >10 mg/L of Fe^{2+}, which quickly oxidizes to Fe^{3+} and precipitates as unstable hydrous ferric oxide (HFO) minerals (fig. 4B). These HFOs mature into the aged ferricrete deposits visible along the drainage. Geochemical modeling suggests the mineralogy of the actively forming HFOs is a mix of schwertmannite, jarosite, and ferrihydrite; once the HFOs have aged, the resulting ferricretes are composed of mostly goethite.

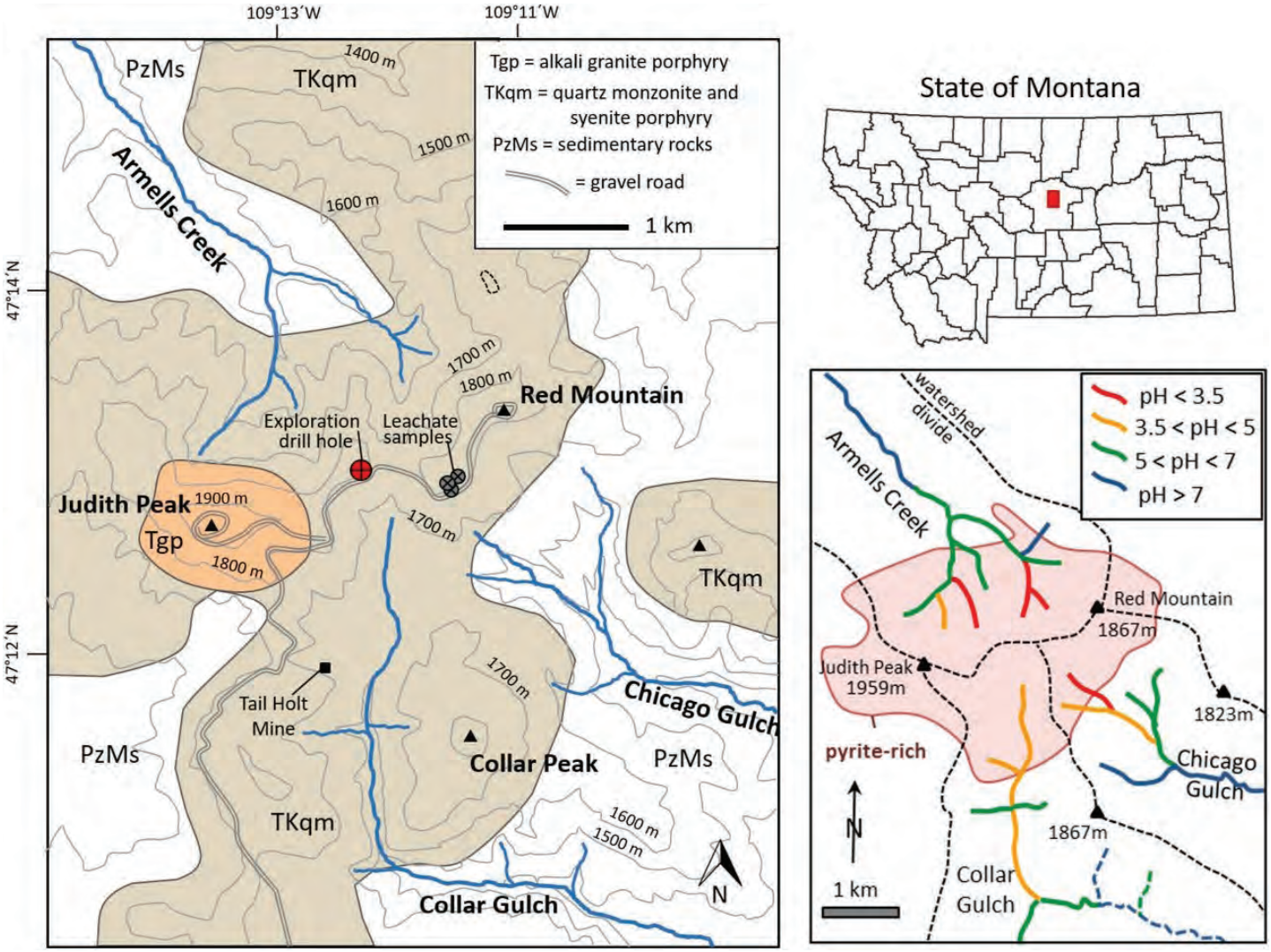

Figure 2. The study area encompasses the three streams that radially drain Red Mountain; this paper focuses on Chicago Gulch. All of the streams are acidic in the headwaters due to mineralization on Red Mountain. (From Gammons and others, 2021.)

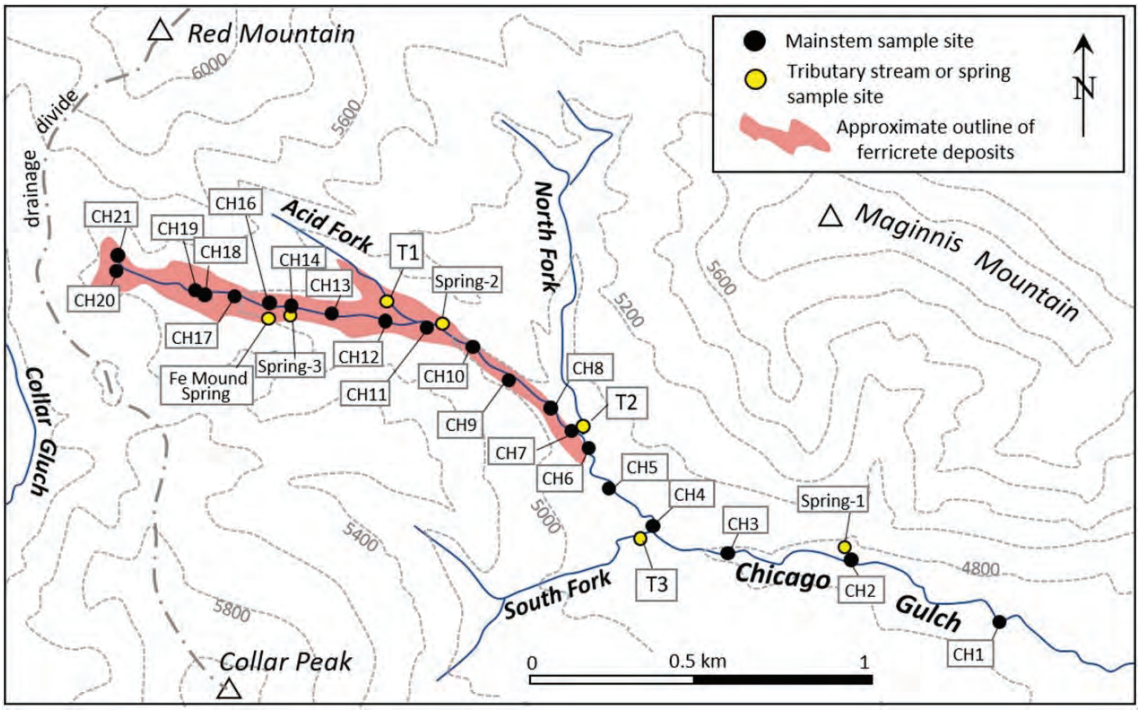

Figure 3. Synoptic sample locations in Chicago Gulch (Gammons and others, 2021).

Figure 4. (A) The “Iron Mound Spring,” named for the terraced ferricrete deposits that formed from Fe-rich groundwater emitting from the spring. From the spring source to the bottom of the ferricretes, pH decreases from 4.44 to 3.56, and Fe concentrations decrease from 18 ppm to 9 ppm as a result of oxidation of the Fe-rich groundwater. (B) Actively forming HFO deposits on a white marble boulder. This rock was placed in Armells Creek in August 2014; this photo was taken in May 2015 showing the formation of HFOs over a period of about 9 months. (C). Aluminum precipitates (white) form as pH increases above 5. This photo was taken at the confluence of the mainstem of Chicago Gulch with a neutral tributary (North Fork) entering from the top left of the photo. Mixing of these waters causes a rapid increase in pH from 3.5 to >5.

Both total and dissolved water samples collected for this study from the upper reaches of Chicago Gulch exceed the U.S. EPA maximum concentration limits for protection of aquatic life for lead, cadmium, zinc, and copper, and human health standards for thallium (data available in Edinberg, 2016). Montana DEQ-7 standards were also exceeded for these same constituents. Lead concentrations are especially high in the headwaters of Chicago Gulch, which may indicate the presence of a concealed lead-sulfide deposit. Synoptic pH values generally increase with distance downstream, due to influx of more basic groundwater and tributary streams. Dissolved Fe and Al loads increase from the headwaters to approximately 700 m downstream due to influx of Fe- and Al-rich groundwater (fig. 5). Fe precipitates out of solution where pH increases above 3.5, resulting in decreasing Fe load in the stream. Where stream pH increases above 5, white hydrous aluminum oxide (HAO) flocs form (fig. 4C). A comparison of dissolved and total metal concentrations shows that copper and lead adsorbed strongly onto the HAO particles at pH >5, whereas zinc, cadmium, manganese, and thallium remained dissolved. Based on our sampling, where Chicago Gulch flows past the boundary of BLM-owned land, it meets aquatic-life standards for all trace metals.

The method of Nimick and others (2009) was used to estimate pre-modern pH conditions of Chicago Gulch. In this method, the concentrations of Cu and Fe are measured in freshly formed HFO and HAO in the stream. The ratios of concentrations of Cu/Fe of these HFOs and HAOs are then regressed as a function of stream pH. Using the measured Cu/Fe ratio of pre-modern ferricrete deposits, the pH of the pre-modern stream can be estimated using the same regression. The results (fig. 6) indicate that the pH of Chicago Gulch was simi-

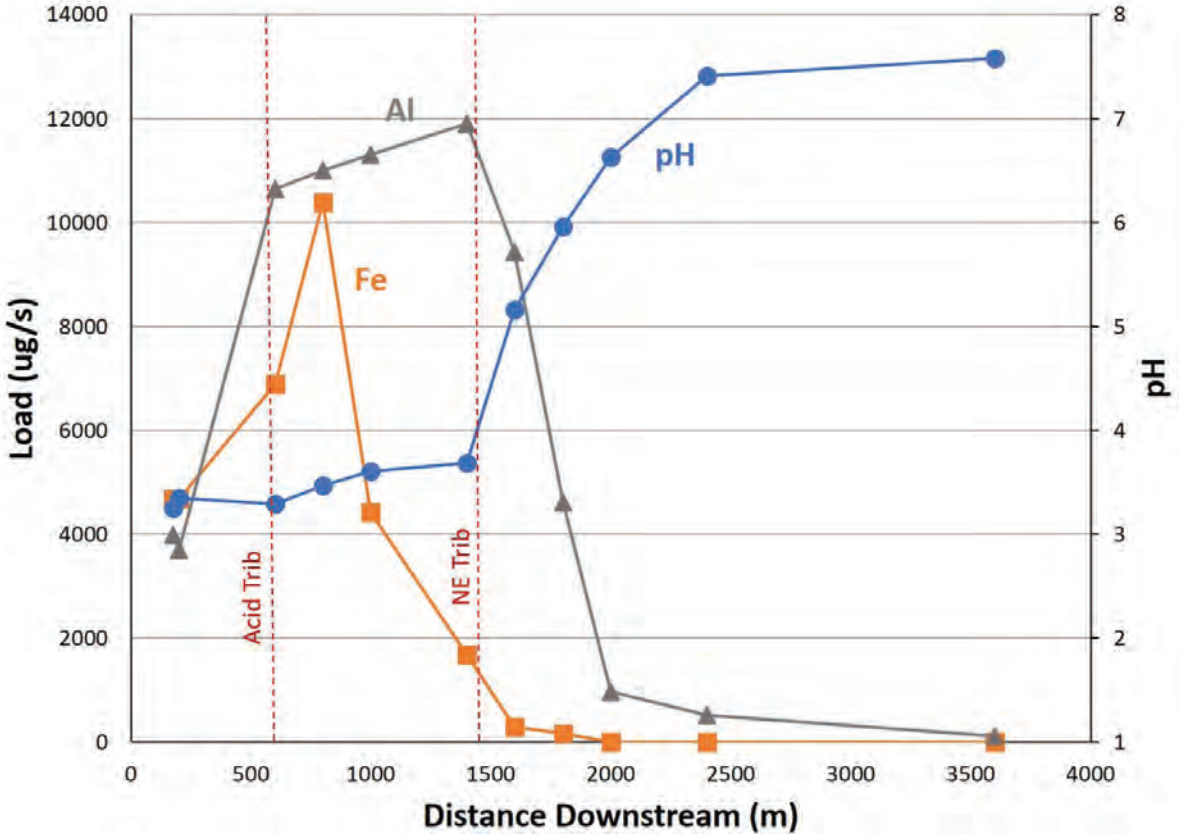

Figure 5. Synoptic pH measurements plotted with corresponding Fe and Al loads.

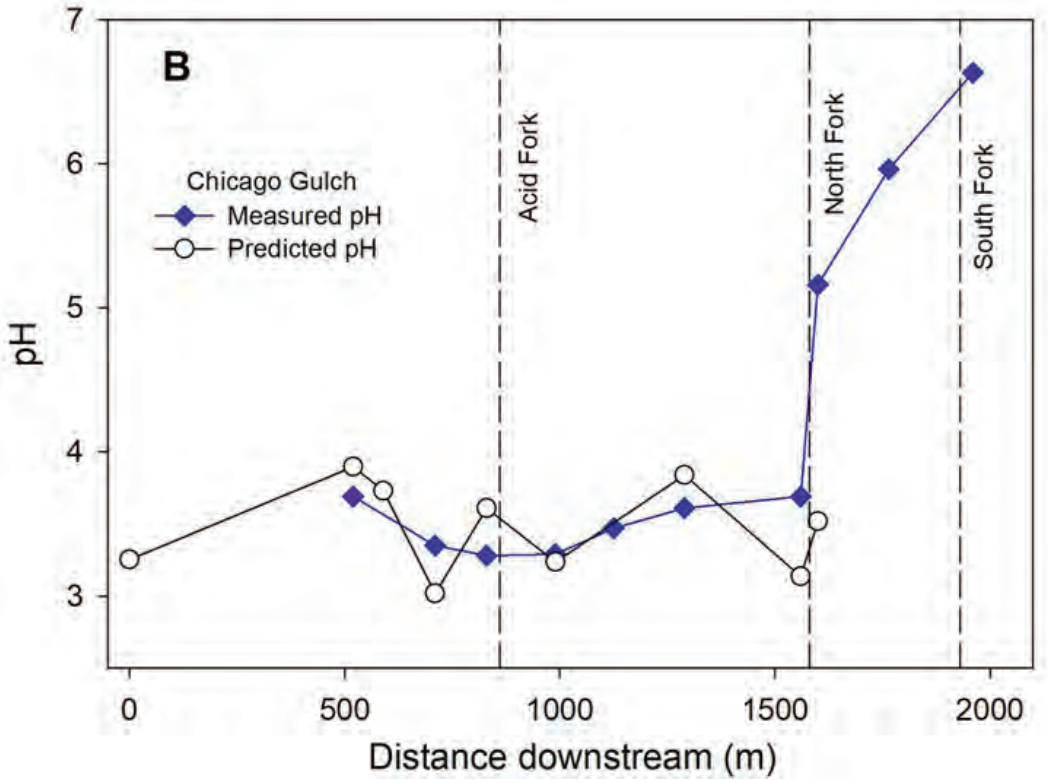

Figure 6. Measured pH versus predicted pre-modern pH in Chicago Gulch. The values match well, suggesting that pre-modern stream conditions were very similar to those observed today.

lar during formation of the ferricrete deposits. Similar conclusions were reached in the study of Williams and others (2015) for two other streams in the Red Mountain area. Our attempts to date the ferricrete deposits were unsuccessful, due to a lack of organic carbon in the samples. However, dating of similar ferricrete deposits in other Montana streams (Furniss and others, 1999; Nimick and others, 2009) suggests that the ferricretes on Red Mountain are probably more than 1000 years old, possibly >10,000 years old.

The streams draining Red Mountain are naturally acidic, and have likely had similar hydrogeochemical conditions for thousands of years. This makes the Judith Mountains an ideal case study for the determination of baseline conditions to apply to a mining-impacted area. We combined the results of this study with those of Williams and others (2015) to estimate the fluxes of sulfate ions exiting at the mouth of all three streams. We normalized these estimates to the area of each stream's watershed (km^2) that is underlain by pyrite-rich, hydrothermally altered bedrock (as mapped by Goddard, 1988). The calculated SO_4-fluxes were similar for each stream draining Red Mountain (see Gammons and others, 2021). This indicates that the rate of pyrite oxidation is similar in all three watersheds, and is likely to be at steady-state with respect to the rate of physical erosion of Red Mountain. Further work is in progress to examine the stable isotope composition of pyrite and dissolved sulfate in the streams of the study area.

References

Edinberg, S.C., 2016, Natural acid rock drainage and ferricrete deposit chemistry of the Judith Mountains, Montana: Butte, Montana Tech, M.S. thesis.

Furniss, G., Hinman, N.W., Doyle, G.A., and Runnells, D.D., 1999, Radiocarbon-dated ferricrete provides record of natural acid rock drainage and paleoclimate changes, New World Mining District, MT, U.S.A: Environmental Geology, v. 37, p. 102–106.

Gammons, C.H., Edinberg, S.C., Parker, S.R., and Ogawa, Y., 2021, Geochemistry of natural acid rock drainage in the Judith Mountains, Montana, Part 2: Seasonal and spatial trends in Chicago Gulch: Applied Geochemistry, v. 129, paper no. 104968.

Goddard, E.N., 1988, Geologic map of the Judith Mountains, Fergus County, Montana: U.S. Geological Survey Miscellaneous Investigation Series, Map I-1729.

Nimick, D.A., Gurrieri, J.T., and Furniss, G., 2009, An empirical method for estimating instream pre-mining pH and dissolved Cu concentration in catchments with acidic drainage and ferricrete: Applied Geochemistry, v. 24, p. 106–119.

Nordstrom, D.K., 2015, Baseline and premining geochemical characterization of mined sites: Applied Geochemistry, v. 57, p. 17–34.

Williams, G.P., Petteys, K., Gammons, C.H., and Parker, S.R., 2015, An investigation of acidic head-water streams in the Judith Mountains, Montana: Applied Geochemistry, v. 62, p. 48–60.

Sara Edinberg (right) at the field trip to Elkhorn Ghost Town. Photo by Peter Larson.

Metal Mining in the Western Washington Cascade Mountains

Gabe Cangelosi

Department of Geologic Engineering, Montana Tech, Butte, Montana

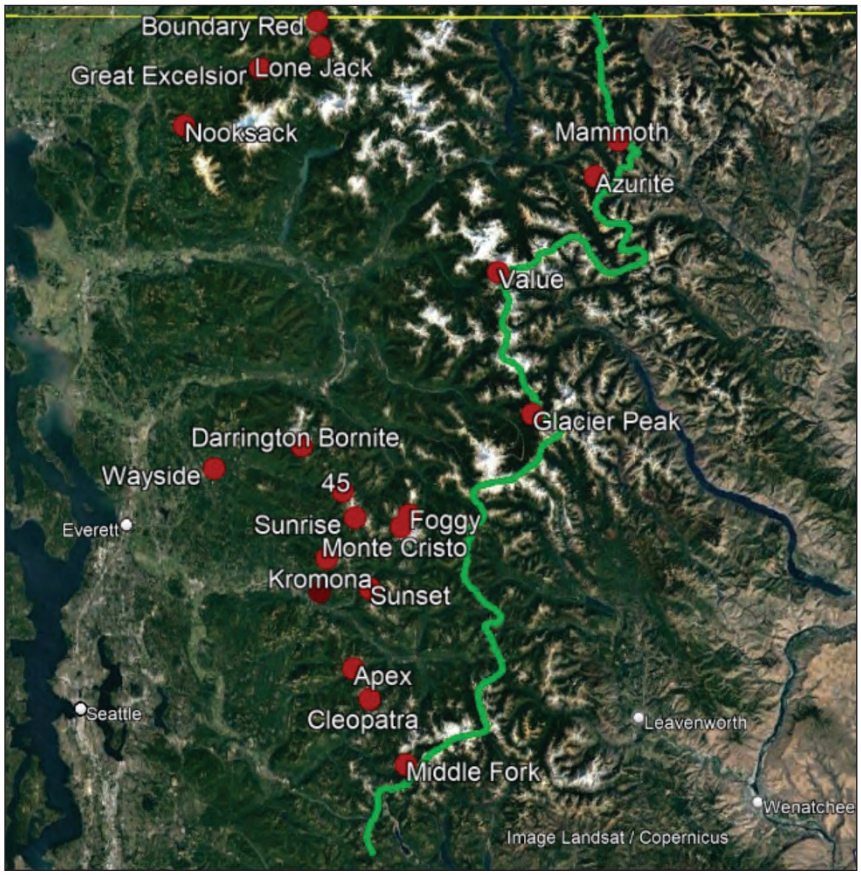

Figure 1. Map of major historical mining operations in the region (green line is the divide between the east and west sides; image is from Google Earth).

The metal mines of the western Washington Cascade Mountains (fig. 1) have a long and unproductive history. While there were some notable successes, most of the mining-related effort in the area was without much reward. In the early years of development, access issues were the most significant impediment. As roads were built and technology improved, the region was gradually locked up in legal designations closed to mining.

In general, this region is poorly understood in the realm of economic geology. The access and regulatory problems that have hindered mining have largely prevented much in the way of in-depth exploration to be completed. Many of the high-grade veins that were mined in the early years were shown to decrease in grade at depth, but the massive deposits were never fully explored.

The eastern slope of these mountains has proven over the years to be host to some highly successful mines. The Holden (Cu) mine produced almost ¼ of a billion pounds of copper, and the Cannon and Lovitt Mines (Au) have brought out millions of ounces of gold. While their success is largely due to good geology, they did not encounter the same issues that hindered mining on the other side of the range. For whatever reason, the southern end of the range in the State never saw much in the way of mineral development.

While the number of “mines” and “prospects” in this region greatly depends on one’s definition of the terms, the total amount of mining ventures here likely number in the thousands. For the purpose of this overview, each mine in the region was individually reviewed, mainly using the publication by Marshall Huntting (1956). Much information was also gained though verbal conversations with Bart Cannon (oral commun., 2015–2019). Which operations to focus on was somewhat subjective, but in general the larger operations were highlighted. It is likely that there some small groups or individuals were able to profit from the hand operation of small deposits, but the records of these are spotty. If one were to limit “prospects” to those with over 100 ft of development work, less than 1% of them saw any sort of production, and only a handful turned a profit.

To best understand the region, it is important to know its largest inherent challenge, access. The Cascades are quite vertical, with many peaks gaining half a mile of elevation in less than half a mile of distance. Many trails had to be blasted into the hillsides, and roads could not come near many mining ventures. Heavy wet snow was a nightmare to maintain buildings in, and those that survived the crushing weight were eventually swept away by avalanches. The high number of rainy days also proved to be problematic since any structure made

of wood was fated to rot at an alarming rate. Finally, brush of a thickness that would put many true jungles to shame clogged up river valleys, preventing people from conducting thorough examinations to this day.

As far as successes go, there were no great bonanzas in the western Cascades. The total production for the region would likely total well under 1 million tons. A few operations turned a profit, and some of them knew when to quit while they were ahead. The most prominent among the successes were the Sunset mine (Cu), Lone Jack/Boundary Red mines (Au), and Azurite mine (Au).

The Sunset mine (fig. 2) was near the town of Index and ran sporadically from 1905 to 1949. It produced just short of 13 million pounds of copper (Huntting, 1956). Little remains as evidence of the size of the operation, since the rock was generally nonreactive and the site has almost completely grown over. The ore averaged 2.5% Cu, and occasionally massive blocks of solid bornite were found. This led to comparisons between it and Butte, Montana in promotional material of the day. The mine was drilled and explored after closure, but no ore body continuous enough was found to incentivize reopening (Woodhouse and others, 2008).

Figure 2. Sunset Mine circa 1929 (Lee Pickett photo).

The Lone Jack and Boundary Red mines were located just a few miles shy of the Canadian border around 5,000 ft elevation. They were geologically and operationally similar, producing 45,000 oz of gold combined from the 1900s to the 1930s (Moen, 1969). The primary issue that plagued both mines was the snow. Nearby the mines is Mt. Baker, home to the U.S. snowfall record of 95 ft falling in a season. Avalanches swept away countless buildings at the mines, and eventually both were abandoned. For most of the year there would be snow on the ground, and the workings were always wet and cold. The Boundary Red Mine found it next to impossible to keep workers in these horrible conditions, with a 1-month turnover rate of 96% at one time (Moen, 1969). The Lone Jack had a revival with some production around 2010, but since then it has remained dormant.

The Azurite mine was notable as being a successful depression-era mine operating in the late 1930s. It was run by ASARCO, and was the only success story of a large mining company in the region. It produced 72,000 oz Au, and closed largely due to depletion (Moen, 1969). The mine was notoriously difficult to reach even though the nearest town was less than 20 mi away. It was located on the west side of the mountain range, but could only be accessed from the east side over a high pass due to impassible canyons to its west. The road was narrow, and custom vehicles had to be built to meet its width requirements. In the winter, plowing the road was sometimes not an option and supplies had to be dropped by plane.

As mentioned before, most of the mine development in the region was for naught. The largest producing mine in the western Cascades ended up being one of the greatest losses for investors (Woodhouse and others, 2008). The Monte Cristo mine (Au) ended up having a town of over 1,000 people associated with it, and direct-

ly led to the formation of the now bustling city of Everett. Originally the mine consisted of various groups of separated workings including the Mystery, Pride of the Woods, and Pride of the Mountains. They were eventually combined into the Monte Cristo mine. The mine managed to remove around 300,000 tons of ore before closing (Huntting, 1956). While the ore was generally rich, the lack of technology to concentrate sulfides proved to be an issue. Even more problematic was the railway to the mine being inundated by the river multiple times, with miles of track destroyed.

Another notable productive but unprofitable mine was the 45 mine located above Spada Lake in the Sultan Basin. It ran from 1896 to 1902, producing 279,000 oz of silver (Carithers and Guard, 1945). The workings of the mine were located on a cliffside over the ridge from the small town of Silverton along the Monte Cristo railway. The verticality of the ridge, however, prohibited easy transport, leading to most of the production coming from pack mules. A 3-mi-long tramway was built to bring ore down from the mine, then back over a high pass to the railway, but the railway suffered one of its worst washouts right when the tram was completed and little ore was moved over it. The company at this point was frantic to try and make the mine produce, and largely bankrupted itself trying to build a 23-mi-long puncheon road (Woodhouse and others, 2008).

There are countless unproductive prospects in any mining region, but the western Cascades hold some impressive ventures that failed to turn a pound of ore (B. Cannon, oral commun., 2015–2019). The chief among these in the early days was the Foggy Prospect, which was located near the Monte Cristo mine. A visitor to the mine had to go several miles along a puncheon road to a lake, which was then barged across, then a glacier had to be climbed to the main portal on a cliff face. All of the buildings and equipment had to be secured to the cliff with cables (fig. 3). The building were constructed flush with the cliffs, with roofs shaped like ramps to try and deflect the avalanches. Even with these difficulties, the miners managed to drive around 10,000 ft of workings including a seven-level internal shaft. The vein was fairly consistent here, but not in a good way, with generally quite low grades (Church and others, 1984).

Figure 3. Foggy Prospect (University of Washington photo).

The few producing mines in the region largely stopped producing by the late 1940s, and most effort after this was exploration. One of the larger modern exploratory ventures was the Sunrise prospect, which was active in the 1960s–1970s. Miles of core were drilled and a 5,000 ft crosscut adit was driven into the deposit. A measured and indicated resource of 50 million tons running almost 0.4% Cu was discovered (Glass, 1971), but the miners faced an issue that their predecessors had not. Even though there was a good road right to the portal, they were unable to come to an agreement with local land management agencies on where they could construct their facilities. The tailings pond was the largest item of contention. This project had multiple revisions, but was ultimately stopped due to these regulatory reasons (B. Cannon, oral commun., 2015–2019).

The Glacier Peak prospect is another example of contemporary exploration in the region. From a considerable amount of drilling in the 1950s–1960s, a porphyry was proven with at least 30 million tons averaging 0.7% Cu (Church and others, 1984). It would have made an excellent mine, but was highly opposed by the community. Eventually, a wilderness area was designated around the property, largely to prevent the operation of the mine (B. Cannon, oral commun., 2015–2019). This trend of regulation stopped the region from ever becoming

an important minerals producer in the later years, and currently the majority of the area is closed to mineral entry (fig. 4).

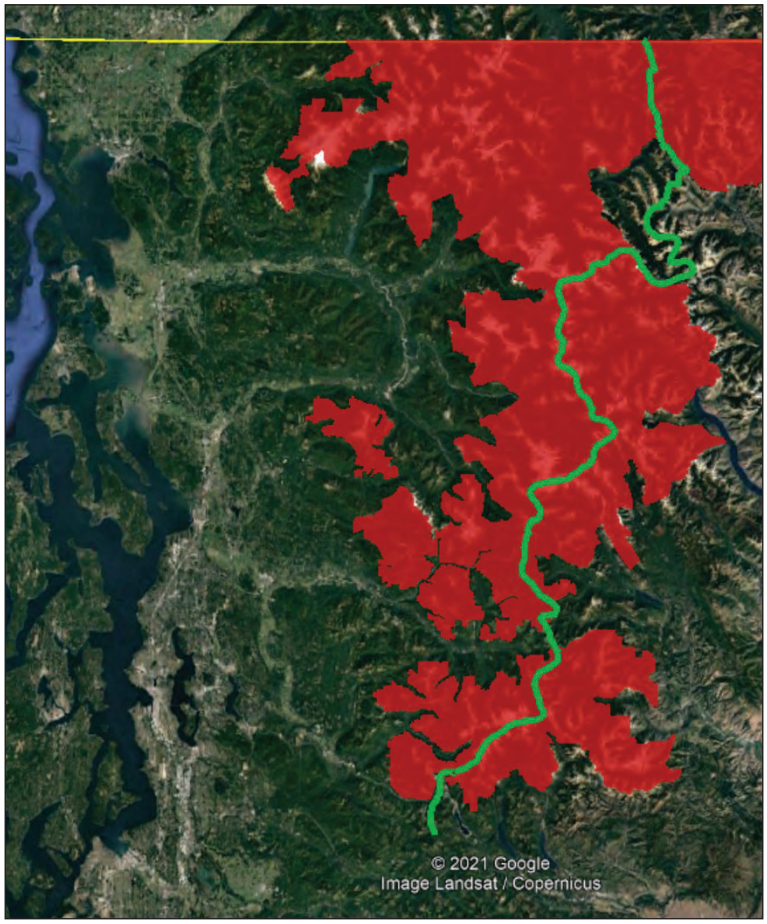

Figure 4. Map of area closed to mineral entry in the region (Google Earth).

References

Church, S.E., Ford, A.B., and Flanigan, V.J., 1984, Mineral resource potential of the Glacier Peak wilderness and adjacent areas, Chelan, Skagit, and Snohomish Counties, Washington: U.S. Geological Survey Pamphlet 1652-A.

Glass, J.R., 1971, Report on Sultan Basin properties for Brenmac Mines Ltd.: Snohomish County, Washington, USA.

Huntting, M.T., 1956, Inventory of Washington minerals—Part II, Metallic minerals: Washington Division of Mines and Geology Bulletin 37, v. 1.

Moen, W., 1969, Mines and mineral deposits of Whatcom County, Washington: Washington Department of Natural Resources Division of Mines and Geology Bulletin 57.

Woodhouse, P.R., Jacobson, D., Pisoni, V., and Cady, G., 2008, Discovering Washington's historic mines, v. 1: The West Central Cascade Mountains: Northwest Mining Publishers.

Skarn Mineralization Geology and Geochemical Exploration, JWD Lodes, Jefferson County, Montana: Boulder Mining District

Jim Gruber

Geologist, Joliet, Montana

Introduction

At the northeast corner of the Bull Mountain fault block, in the JWD Lodes project area (fig. 1), veins in Paleozoic marble containing galena, sphalerite, and pyrite are mineralized and most likely relate to skarn deposits in the adjacent, historically prolific Elkhorn mining district.

Multi-element geochemical tests of rock and soil confirm the presence of a polymetallic mineral system. The area's mineralization, indicative of skarn, represents only a small part of a much larger mineralized unit.

Skarn deposits are coarse-grained metamorphic rocks composed of calc-silicate minerals formed by replacement of carbonate-bearing rocks during contact or regional metamorphism and metasomatism. They are formed by early calc-silicate alteration followed by oxide-sulfide mineralization. These are mineral deposits formed at relatively high temperatures related to magmatic hydrothermal activity associated with granitic plutons in orogenic tectonic settings. Skarn generally forms where a granitic pluton has intruded sedimentary strata that includes limestone, dolomite, or other carbonate-rich rocks.

Geologic literature suggests that metal zoning in skarn systems generally follow a concentration pattern of elements Fe to Cu(Au, W, Mo) to Cu, Zn(Ag) to Zn, Pb(Ag) to Mn to Hg from the inner to the distal parts of the system (fig. 2).

Geologic Setting

Regional tectonics began in Precambrian time followed by the collision between the Archean Wyoming and Medicine Hat provinces and an intervening volcanic island arc event; tectonism continues to the present in the form of activity within the Intermountain Seismic Belt. The JWD Lodes project area lies at the intersection of several important geologic provinces, including the northwestern edge of the Archean Wyoming Province and eastern edge of the bounding Great Falls Tectonic Zone; the southern edge of the Proterozoic Belt Basin; the easternmost edge of Sevier–Laramide thrusting; the eastern edge of the Cretaceous Boulder Batholith; and the northern extent of the Cenozoic Basin and Range Province. There are many hundreds of structures in the map area, with a variety of styles and orientations (fig. 3).

In the JWD Lodes project area, and exposed in outcrop, are Paleozoic carbonate rocks (Pzm) in contact with the Cretaceous-age Elkhorn Mountains Volcanics (Keld; fig. 4). Mesozoic, Paleozoic, and Middle Proterozoic sedimentary rocks are presumed to underlie Elkhorn Mountains Volcanics (Keld) and in close proximity to the Boulder Batholith and/or satellite stocks of Late Cretaceous age (figs. 5A, 5B).

Previous Work

Mineral prospecting in this area dates back to the late 1800s. Numerous pits, glory holes, and shafts indicate that work was performed using hand tools along with some drilling and blasting. Courthouse records reveal that mining claims were staked, and assessment work was performed between 1894 and 1921. Optimism was evident in a November 6, 1915 article in the Boulder Monitor about the area that reads as follows:

> *There is a splendid prospect near Boulder that gives every indication of soon becoming a paying proposition to the owner, Henry Reer, and this property is within a few miles of town. Henry has assurances from the quality of ore so far revealed that he has a bonanza. The vein is nearly eight inches thick and runs largely in gold and silver. It is the old Gibson property, and as it is only about one mile from the Reer ranch, and very easy of access. The working of it will be a comparatively easy*

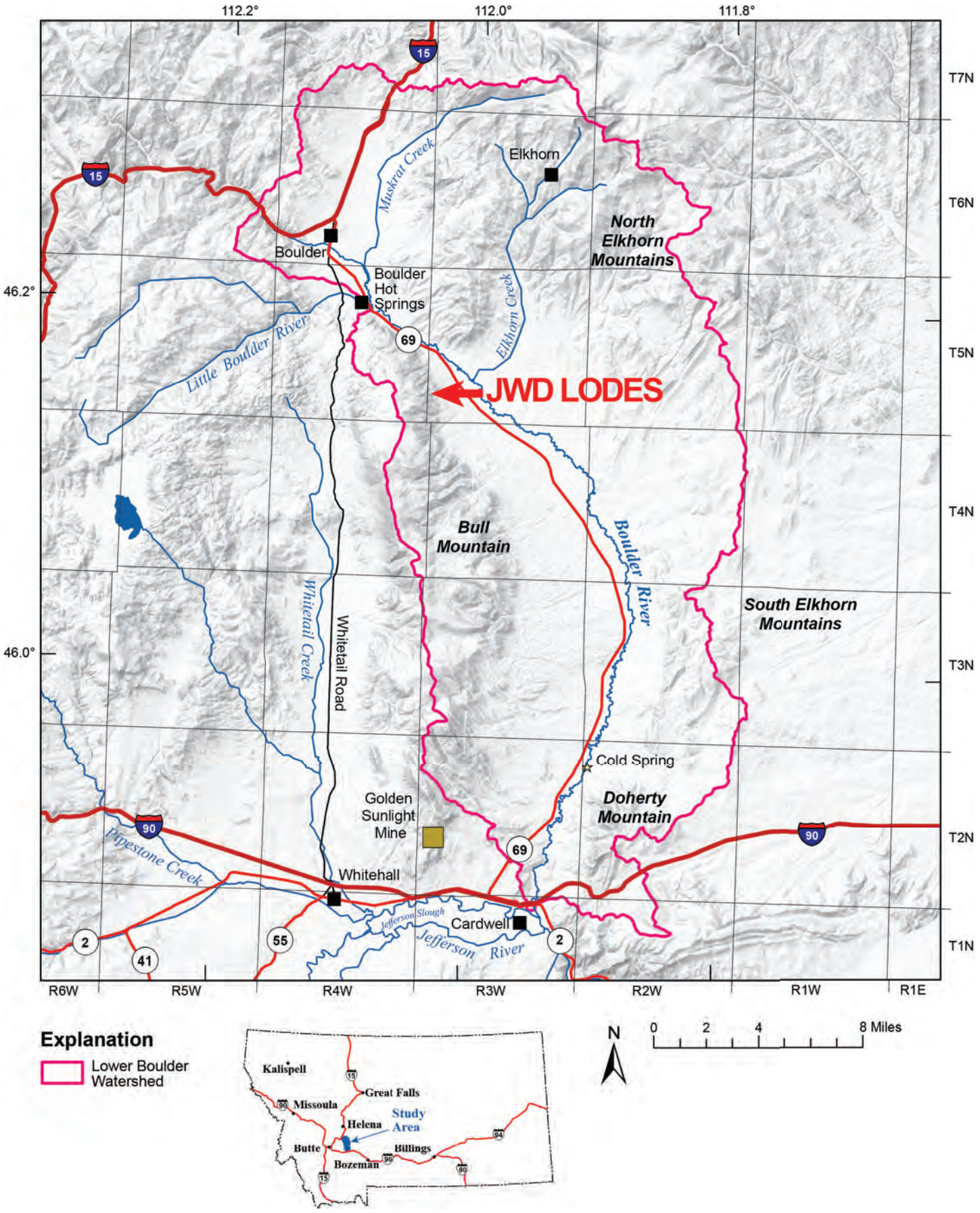

Figure 1. Map showing the location of the JWD Lodes at the north end of Bull Mountain.

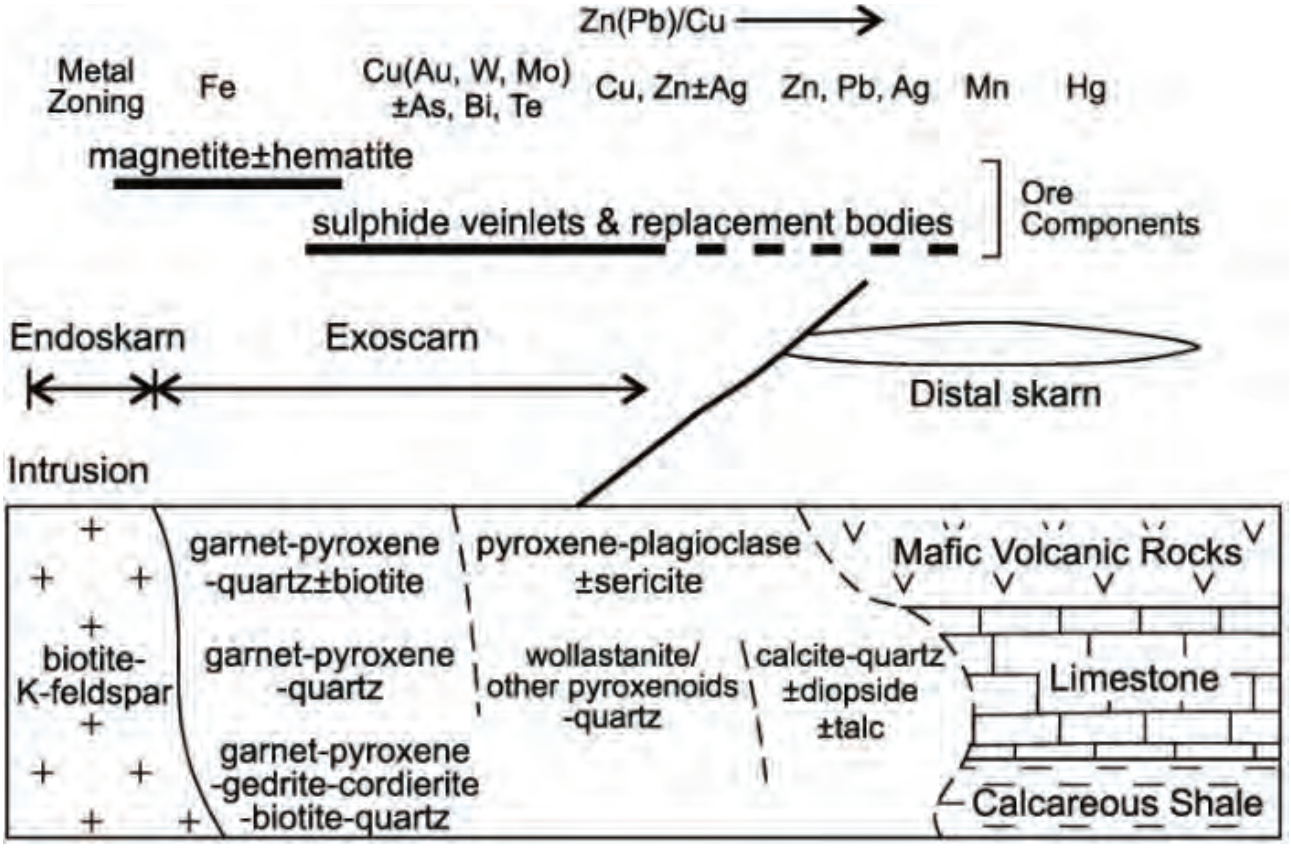

Figure 2. Schematic structure of skarn deposits showing typical alteration mineralogy and metal zoning (Megaw, 1998).

matter. He is now busily engaged in baling several tons of hay for shipment, but when that is completed, he intends putting on all the force he can handily work in order to open up and begin shipment, as he already has several tons on the dump. Several fine tons have already been sent to the East Helena smelter in days gone by, and there is no reason in sight why this mine cannot be made to pay splendidly in the near future. We have often predicted that good mines would eventually be opened up in close proximity to Boulder and judging by the way the Reer proposition looks at present, we have no hesitancy in saying that this might be one of them.

Records indicate that Edward Gibson prospected this area before the turn of the century and died in 1904. Henry Reer continued prospecting until developing health problems around 1920 and passing in 1924. Based on field observations, this area has been relatively untouched since before World War II.

The most ambitious signs of exploration in the area is an accessible 140 ft cross-cut tunnel that was driven to intersect a well-worked mineralized shaft that lies 60 ft vertically above the tunnel. Measurements indicate that the cross-cut tunnel was abandoned about 50 ft before the mineralized objective.

Current Exploration Methods and Results

Geologic Mapping

Geologic investigations were aided greatly by recently published mapping by the Montana Bureau of Mines and Geology (Scarberry and others, 2017). The geologic map of the Boulder East 7.5' quadrangle describes the mineralized area in the JWD Lodes study area as Paleozoic metamorphosed carbonate (Pzm) of crystalline dolomitic marble with vein material containing galena, sphalerite, and pyrite (fig. 4).

Rock Sampling

Since 2017, 21 rock samples have been collected in mineralized carbonates (Pzm) from outcrop (fig. 6), and historic underground workings, shafts, pits, and mine dumps. Highlights include: lead (Pb), returning values of 30,000, 39,000, and 68,000 ppm (equivalent to 3.0%, 3.9%, and 6.8%); zinc (Zn), with 5,130 and 1,090 ppm

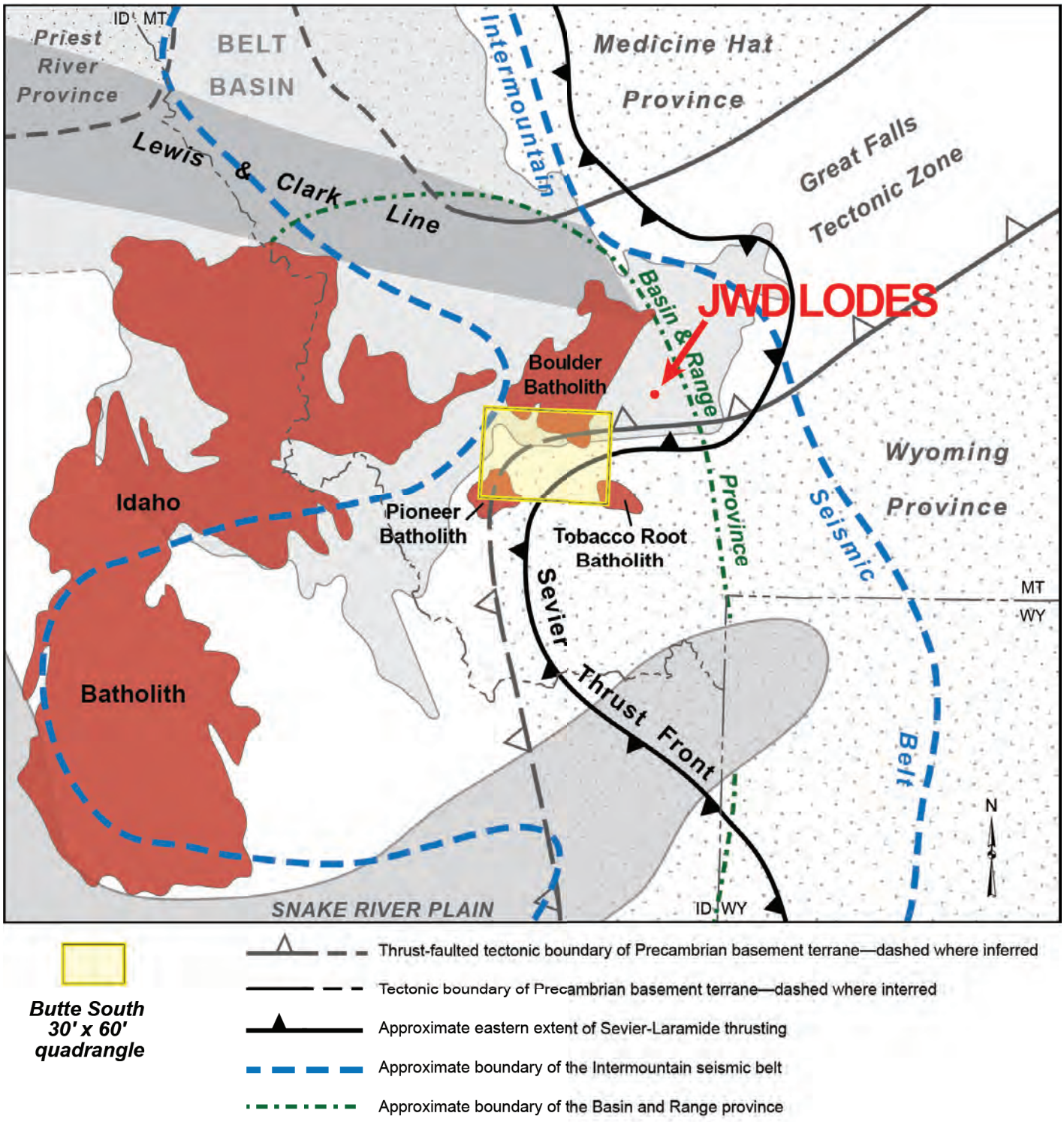

Figure 3. Major Precambrian basement provinces and regional tectonic boundaries and zones in relation to the JWD Lodes project area. The figure also shows the outline of the Proterozoic Belt Basin, the Cretaceous batholitic complexes, and the Tertiary Snake River Plain (modified from McDonald and others, 2012).

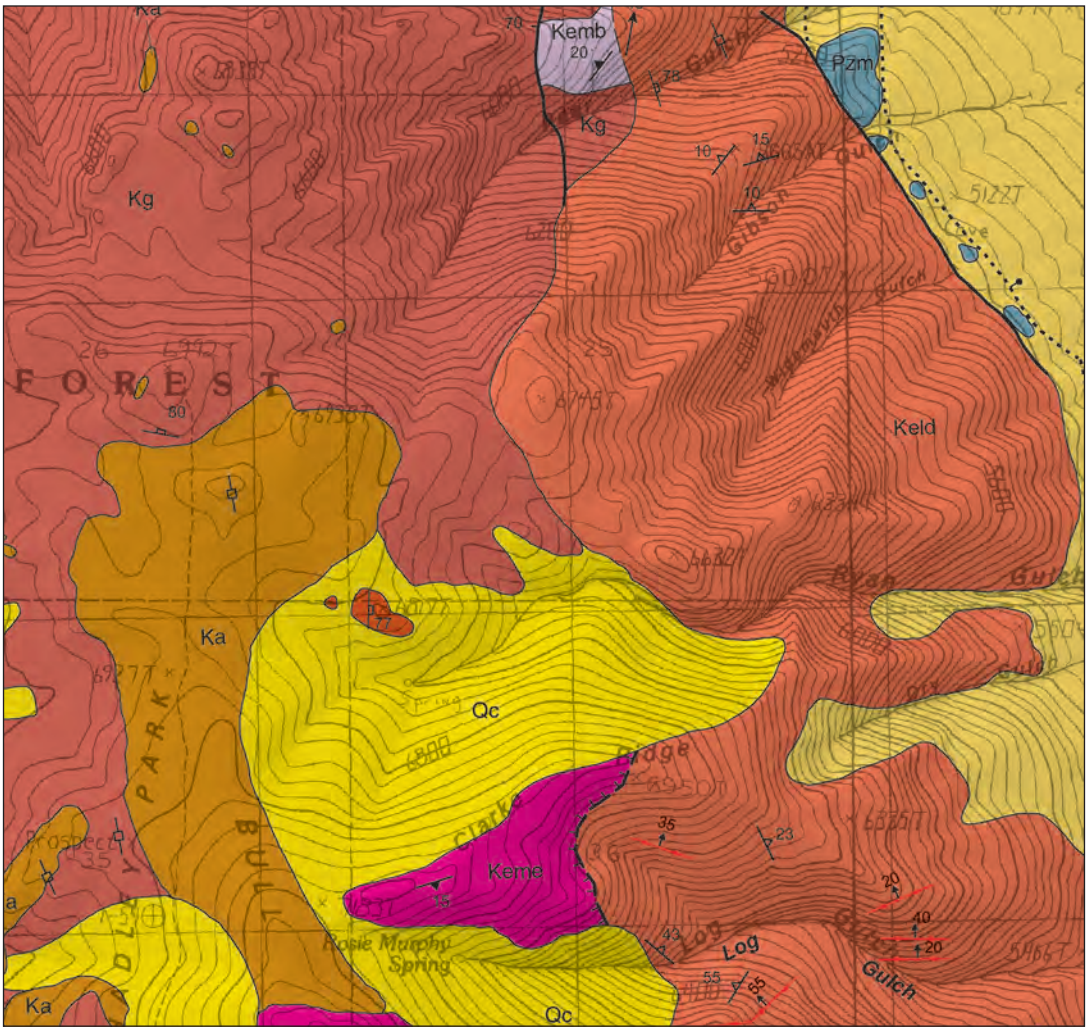

Figure 4. JWD project area: geologic map of part of the Boulder East 7.5' quadrangle from Scarberry and others (2017). Note outcrops of Paleozoic carbonate rocks (Pzm) along the margin of dacite porphyry flow-domes of the Elkhorn Mountains Volcanics (Keld); ignimbrite (Kemb, Kema); Butte granite (Kg) and aplite (Ka) of the Boulder Batholith. Quaternary–Tertiary sediments (QTs) and Quaternary colluvium (Qc). Red dashes near Log Gulch are quartz veins that show sulfide minerals in fractures.

(equivalent to 0.5% and 0.1%); molybdenum (Mo), 2,080, and 1,070 ppm (equivalent to 0.2% and 0.1%); silver (Ag), 120, 97, and 94 ppm (equivalent to 3.5 opt, 2.8 opt, and 2.7 opt); and gold (Au), 2.71, 2.40, and 2.09 ppm (equivalent to 0.08 opt, 0.07 opt, and 0.06 opt). Other metals showing high values include antimony (Sb), 1,650, and 1,420 ppm; manganese (Mn), 1,215 and 944 ppm; tungsten (W), 800 ppm; and copper (Cu), 969 ppm. Samples were analyzed by ALS Global, Reno, NV for 33 elements using the four acid ICP-AES method and FA-AA method for gold.

Soil Sampling

Soil sampling began in 2019 (fig. 7). To date, 111 samples have been collected and analyzed, mostly on a 150 ft x 300 ft grid (figs. 8–14) in and around the exposed Pzm carbonates (fig. 4). Samples were analyzed by ALS Global, Reno, NV for 53 elements using the aqua regia and ICP-MS Super Trace for Gold method.

Within and around the mapped Pzm carbonates, multi-element soil anomalies define overlapping metal zones using element values exceeding the 80th percentile of the data population. Using values for metals of interest (i.e., Au, Ag, Cu, Mo, Pb, Zn, Sb, Mn) along with pathfinder elements that include As, Hg, Te, Mn, Bi, Mg, W, Fe, Ni, Se, four patterns have emerged that suggest polymetallic skarn zonation exists within the Paleozoic-age dolomitic marble (Pzm) that outcrops at various locations within the project area. The emerging skarn mineral suites are: lead–zinc–silver, gold–silver, antimony–copper–molybdenum, and copper–manganese.

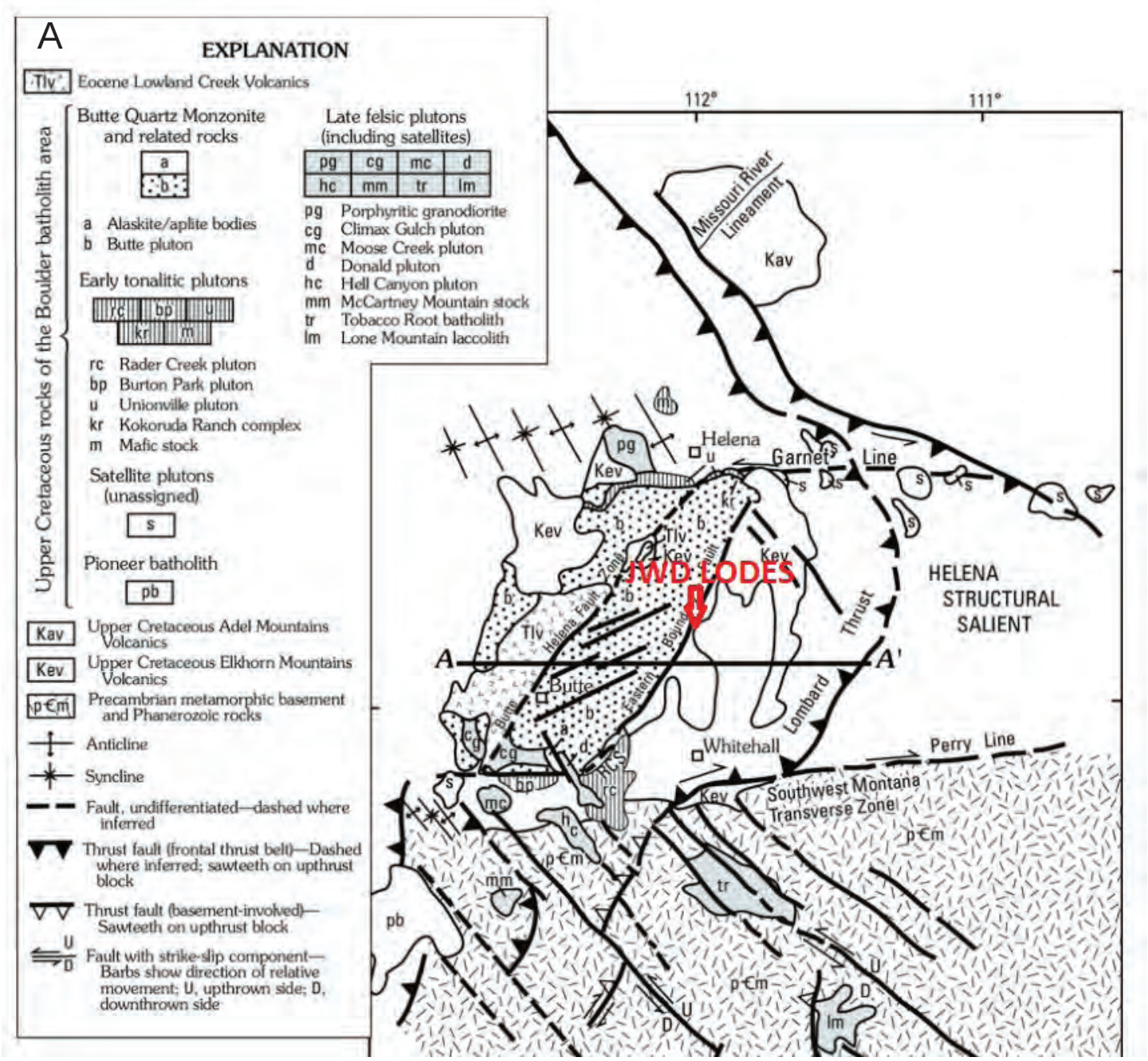

Figure 5. (A) Regional geologic structural map (modified from Schmidt and others, 1990). (B) Cross section of regional geologic structural map (modified from Schmidt and others, 1990).

Figure 6. Rock sample site in JWD Lodes project area.

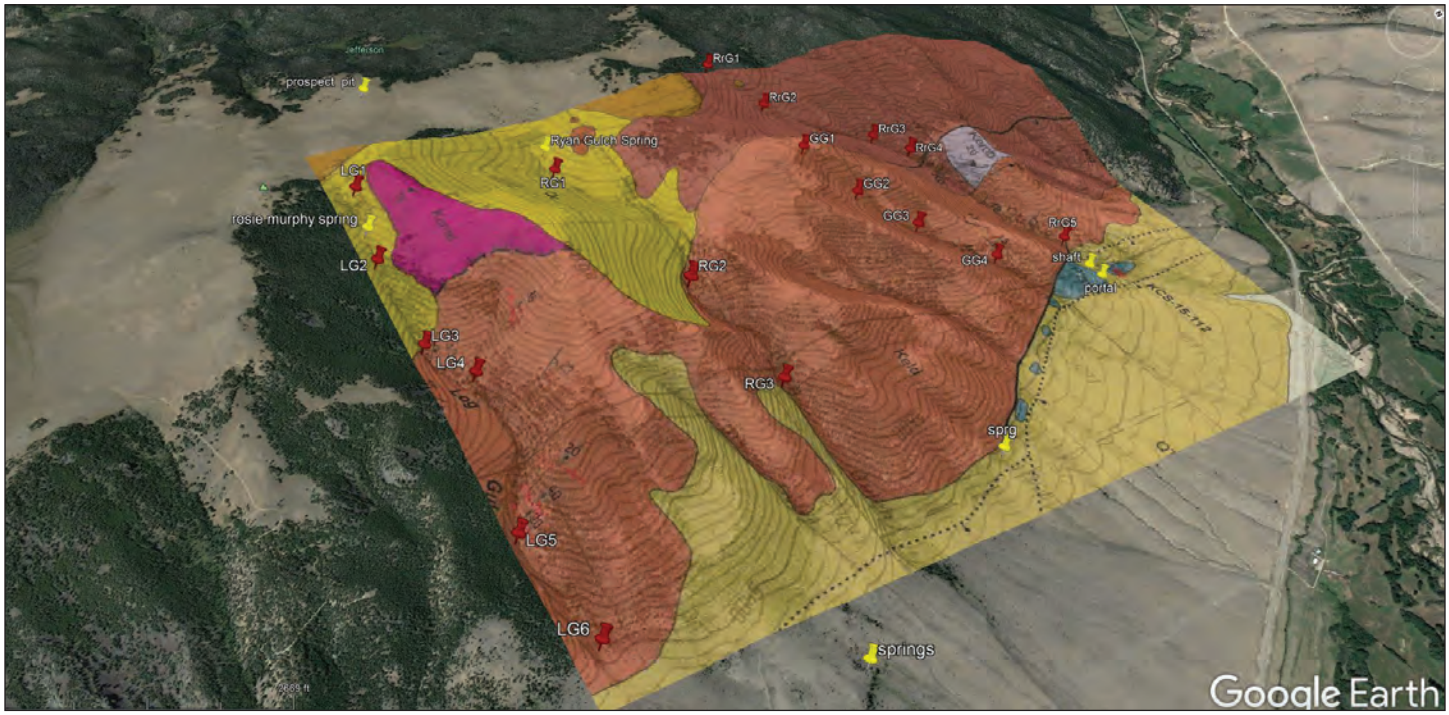

Figure 7. Soil sample site in JWD Lodes project area.

In 2020 and 2021, 18 soil samples were taken along four drainages that are mapped as Cretaceous-age dacite porphyry lava domes and flows (Keld) of the Elkhorn Mountain Volcanics (fig. 15). Elements exhibiting anomalous values in all four drainages are Cd and Mn. Sporadic anomalous metals include Au, Ag, Cu, Pb, Sb, Mo, W, and Zn (table 1). Potential pathfinder elements with high values include As, Bi, Hg, Te, and Fe.

Conclusions

Klepper and others (1957) identify the Elkhorn mining district, to the northeast and adjacent to the JWD Lodes project area, as the only place along the eastern margin of the Boulder Batholith where Paleozoic carbonate rocks, which are favorable hosts for replacement ore deposits, outcrop in contact with or close to the batholith. Elsewhere along its eastern margin, the batholith is in contact with Late Cretaceous volcanic rocks that overlie Paleozoic and Mesozoic sedimentary rocks that may contain replacement deposits that are from several hundred to a few thousand feet beneath the surface. If any districts similar to the Elkhorn district occur at depth elsewhere along the intrusive contact, their presence may be indicated by an unusual amount of fracturing in the overlying volcanic rock and by leakage of abnormal amounts of heavy metals into these fractured rocks (Klepper and others, 1957).

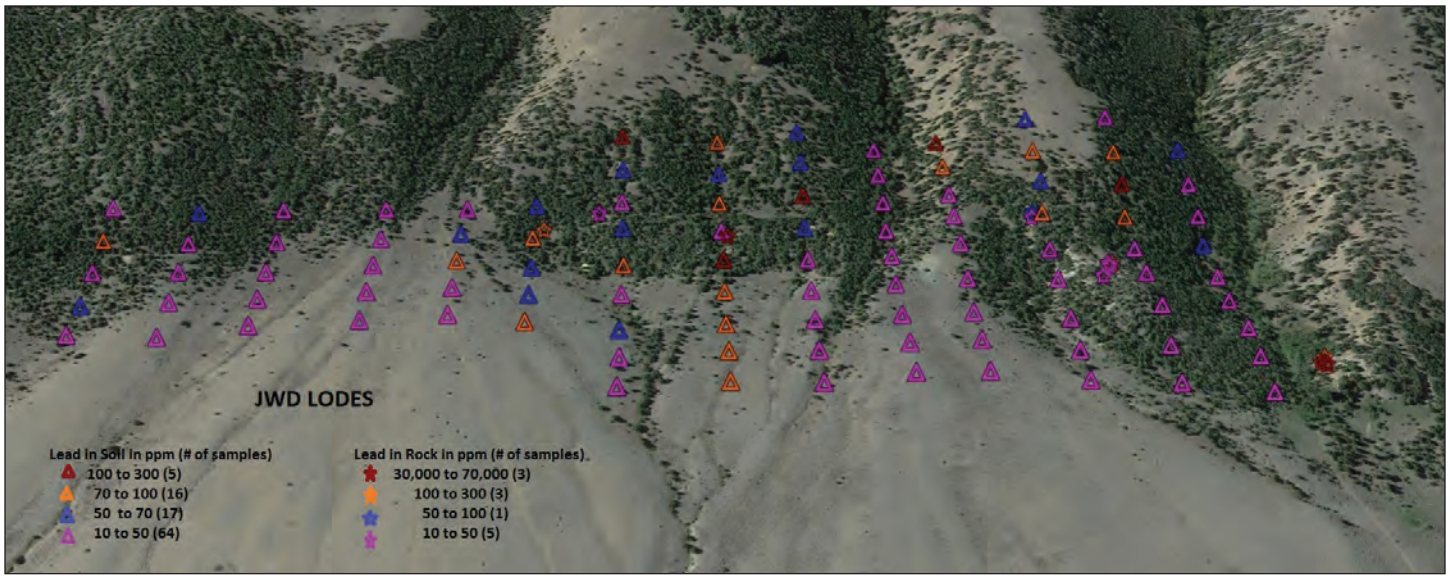

Figure 8. Lead.

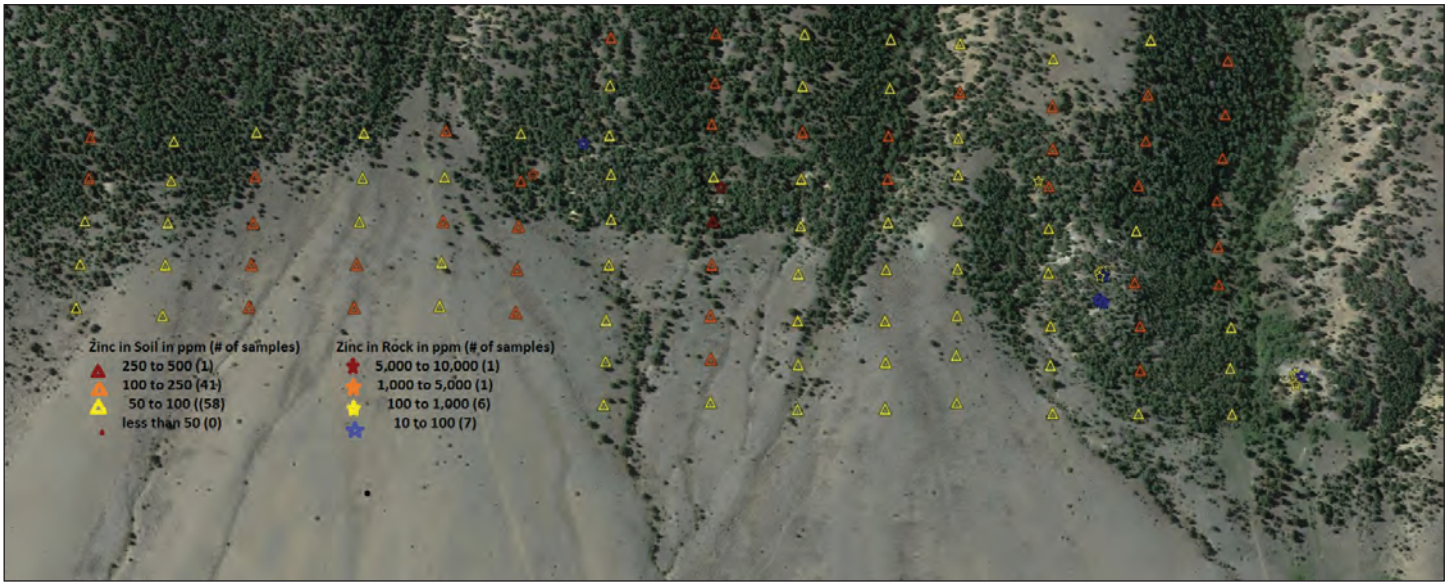

Figure 9. Zinc.

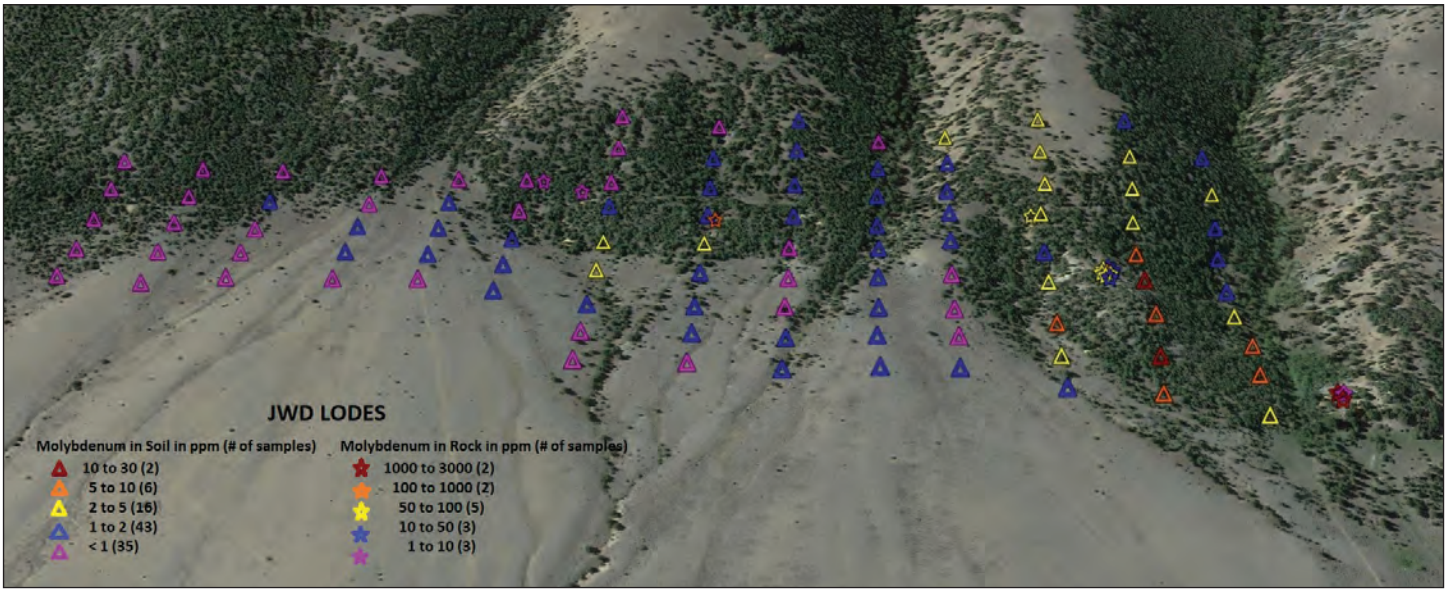

Figure 10. Molybdenum.

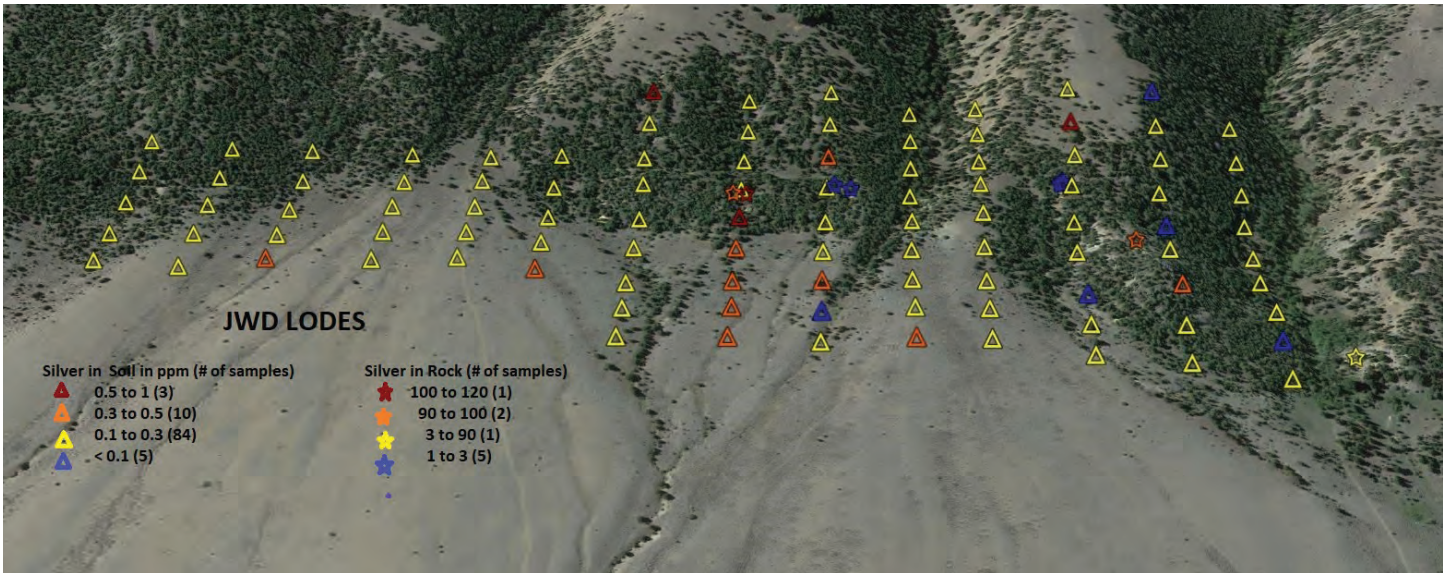

Figure 11. Silver.

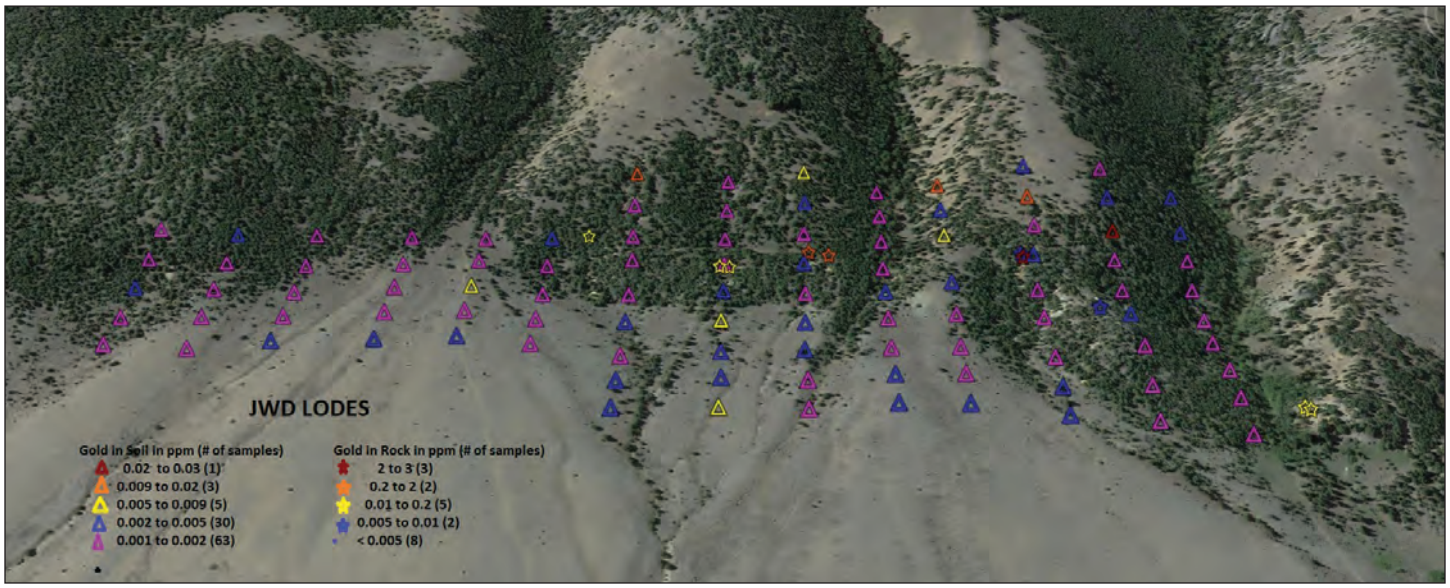

Figure 12. Gold.

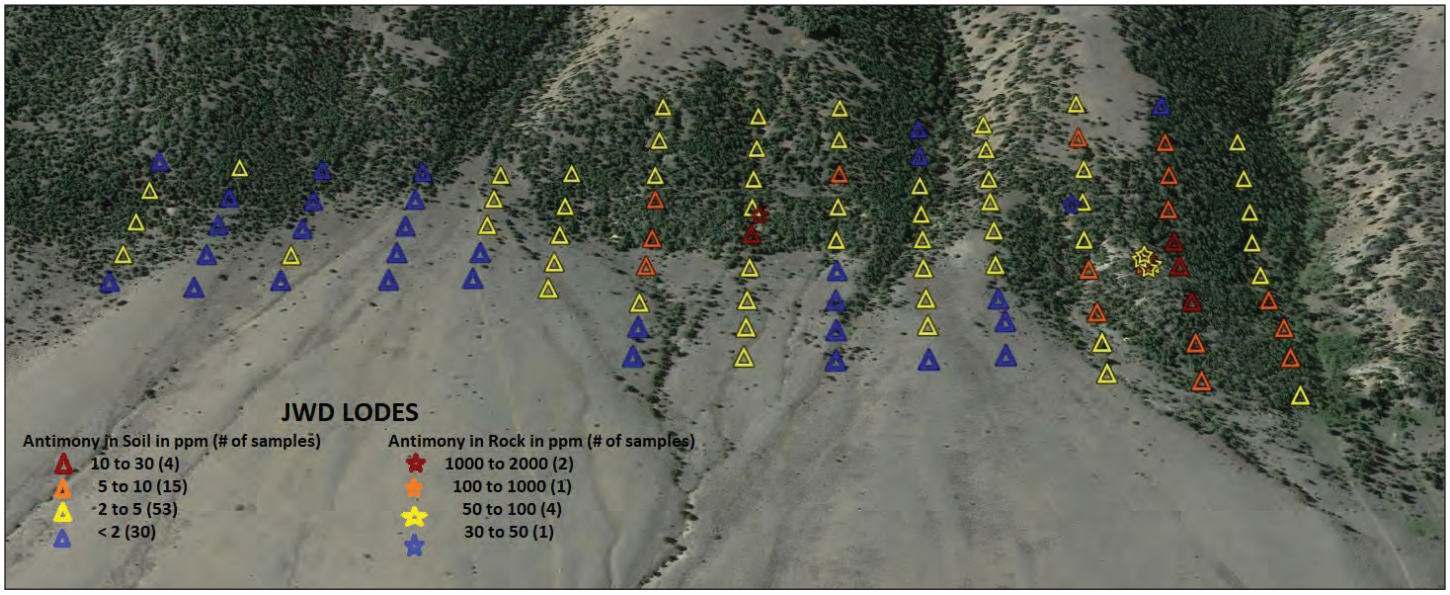

Figure 13. Antimony.

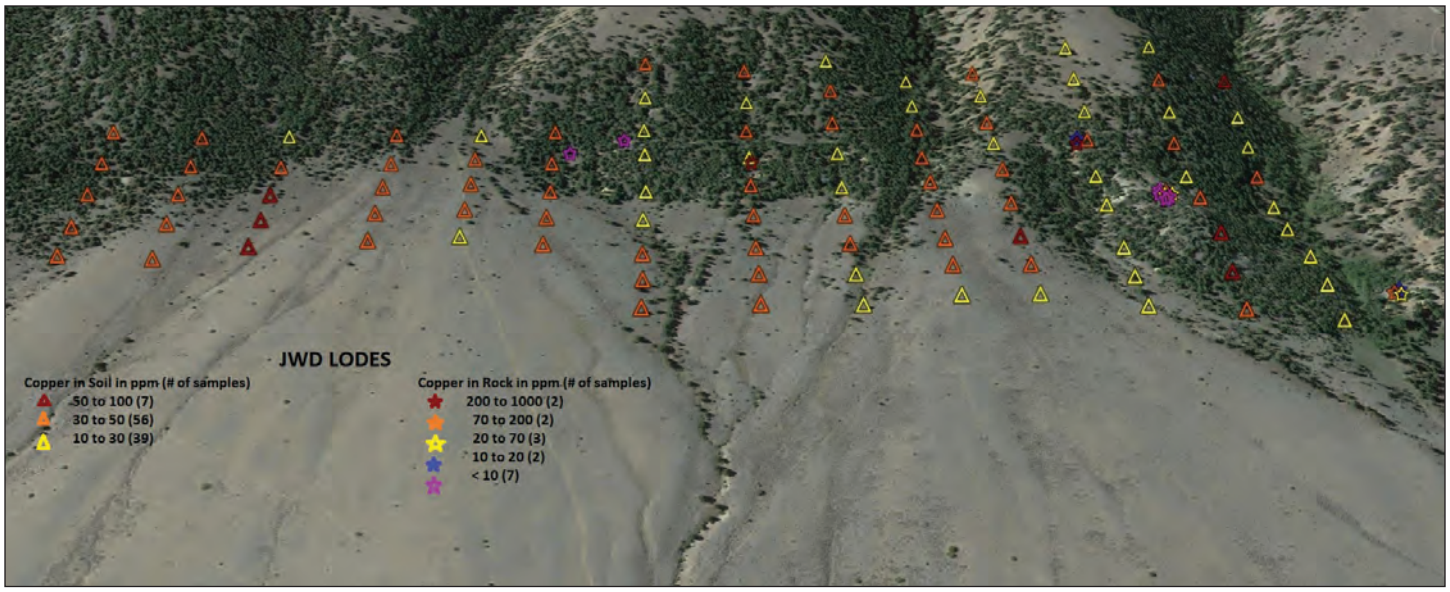

Figure 14. Copper.

Figure 15. Geochemical soil sample sites. Geologic map overlay (Scarberry and others, 2017) of Google Earth image of JWD Lodes study area.

Table 1. Threshold values for various important elements in rocks, soils, and, “silts” (stream sediments). To be used as a general guide only. Source: Amor, 2013.

		Range of Threshold–For Anomalous Values		
Elements	**Crustal Abundance**	**Rocks (ppm)**	**Soils (ppm)**	**Silts (ppm)**
Au	4 ppb	50–100 ppb	40–100 ppb	20–50 ppb
Ag	70 ppb	0.5–1	0.2–0.5	0.2–2.5
Cu	55 ppm	100–200	50–200	100–200
Pb	13 ppm	40–100	40–100	40–100
Zn	70 ppm	100–500	200–300	200–300
Mo	1.5 ppm	5–20	2–5	2–5
W	1.5 ppm	10–50	2–10	2–10
Ni	75 ppm	100–200	100–200	100–200
As	1.8 ppm	5–10	5–20	2–5
Sb	0.2 ppm	5–10	5–20	2–5
Co	25 ppm	10–40	5–20	–
Hg	80 ppb	100–500 ppb	–	5–200 ppb
Te	10 ppb	2–5	–	–
Pt	10 ppb	50–100 ppb	–	–
Ba	425 ppm	500–10,000	500–10,000	500–10,000

At the northeast corner of the Bull Mountain fault block in the JWD Lodes project area, veins in Paleozoic marble are mineralized, and most likely relate to skarn deposits in the adjacent, historically prolific Elkhorn mining district. This Paleozoic marble, which is probably the lower Amsden to upper Mission Canyon Formations of Mississippian age (Weeks, 1974), outcrops in numerous knobs for about 1 mi in a north–south direction and is overlain by cliff debris and alluvial sediments to the east and in contact with Elkhorn Mountain Volcanics to the west (fig. 4).

Geologic mapping and sampling since 2017 confirm that polymetallic replacement mineralization is present and widespread within this Paleozoic marble. Mineralization is concentrated along the north–south-trending fault contact of the Paleozoic marble (Pzm) and Cretaceous dacite porphyry (Keld) of the Elkhorn Volcanics. Quartz veins that show sulfide minerals in fractures near Log Gulch (Scarberry and others, 2017), and similar unmapped veins near Rear Gulch (oral commun., Kaleb Scarberry, MBMG, 2021), most likely indicate leakage of heavy metals from skarn mineralization at depth. Geologic structure (fig. 5B) and anomalous metals in soils in gulches of dacite (Keld) to the west of Paleozoic marble (Pzm; fig. 15) suggest that skarn is widespread throughout the project area. Mineralization appears to exist in both carbonate and volcanic rock.

Suggestions for Further Work

Surface mapping along with rock and soil geochemical data are sufficient within the project area to warrant geophysical surveys and/or drilling as next steps for defining mineral resources and reserves.

In the interim, rock and soil sample data will continue to be analyzed using statistical methods and computer mapping techniques. Additional geochemical exploration methods will continue to be investigated. Geochemistry in soil, for instance, could be instrumental in identifying the areal extent of undetected Au given its unique

characteristics related to leachability of fine gold versus particulate gold. Secondary dispersion haloes from pathfinder elements may result in a more accurate geochemical footprint than just gold alone.

Acknowledgments

I thank Pat Dawson, my indispensable partner, for his encouragement, inquisitiveness, and neverending drive to unlock the secrets of Bull Mountain and Dr. Kaleb Scarberry for his field mapping expertise and helpful suggestions. I'm grateful to the Montana Bureau of Mines and Geology for providing a platform to present our findings.

References

Amor, Steve, 2013, An overview of geochemical methods, geological survey of Newfoundland and Labrador, CIM Short Course.

Beus, A.A., and Grigorian, S.V., 1977, Geochemical exploration methods for mineral deposits: Applied Publishing Ltd.

Klepper, M.R., Weeks, R.A., and Ruppel, E.T., 1957, Geology of the southern Elkhorn Mountains, Jefferson and Broadwater Counties, Montana: U.S. Geological Survey Professional Paper 292, 88 p.

McDonald, C., Elliott, C.G., Vuke, S.M., Lonn, J.D., and Berg, R.B., 2012, Geologic map of the Butte South 30' x 60' quadrangle, southwestern Montana: Montana Bureau of Mines and Geology Open-File Report 622, 1 sheet, scale 1:100,000.

Megaw, P.K.M., 1998, Carbonate-hosted Pb-Zn-Ag, Cu-Au replacement deposits: An exploration perspective, *in* Lentz, D.R., ed., Mineralized intrusion-related skarn systems: Mineralogical Association of Canada, Short course series 26, chap. 10, p. 337–358.

Rose, A.W., Hawkes, H.E., and Webb, J.S., 1979, Geochemistry in mineral exploration: London, Academic Press, 2nd ed.

Scarberry, K.C., Kallio, I.M., and English, A.R., 2017, Geologic map of the Boulder East 7.5' quadrangle, southwest Montana: Montana Bureau of Mines and Geology Geologic Map 68, 1 sheet, scale1:24,000.

Schmidt, C.L., Smedes, H.W., and O'Neill, J.M., 1990, Syncompressional emplacement of the Boulder and Tobacco Roots Batholiths: Geological Journal, v. 25, p. 305–318.

Weeks, R.A.,1974, Geologic map of the Bull Mountain area, Jefferson County, Montana: U.S. Geological Survey Open File Report 74-354. Scale 1:48,000.

Geochemical Evaluation of Hydrothermal Alteration in the Scatter Creek Formation, Republic Mining District, Washington

Jonathan Stanfield and Peter B. Larson

School of the Environment, Washington State University, Pullman, Washington

The Eocene Scatter Creek Formation of Ferry Co., Washington, is a group of complex dikes and sills that intrude Permo-Triassic limestone and clastic sediments and Eocene volcanics and volcanoclastics across the Republic Graben (Parker and Calkins, 1964). These have been interpreted as the hypabyssal variants of the region's Sanpoil Volcanics (Muessig, 1967) originating from the Devil's Elbow Pluton suite (Moye, 1984; Holder, 1985) and the Herron Creek Pluton suite (Holder, 1986). Namely, these are the Devil's Elbow, Kettle Crest, and Fire Mountain Plutons, respectively. This correlates with later work suggesting multiple magma sources were sampled during an extensional environment, rather than subduction, resulting in subsequent emplacement of the Coleville Batholith within post-Laramide metamorphic core complexes (Morris, 1996).

In the Belcher Mining District, these intrusions, and the sediments into which they were emplaced, exhibit widespread propylitic alteration that is focused on the contact between meta-sediments and intrusions (e.g., Lowe and Larson, 1996; Lowe, 1998). Observations, data, and modeling from active Au- exploration near the Key West deposit suggest that contacts of sills and dikes served to control hydrothermal fluid flow as indicated by the distribution of geochemical signatures and perhaps hydrothermal alteration minerals. However, a geochemical analysis dedicated strictly to alteration (briefly mentioned in the literature) has not yet been performed and may corroborate these models.

Preliminary field and geochemical work have been characterizing the Scatter Creek's petrology and alteration within the Mt. Cooke field area; this has occurred predominantly on the southern slope within BLM access and the Key West pit (figs. 1, 2). Field observations show a variety of Scatter Creek compositions from apparent trachyandesite to dacite and hypabyssal textures ranging from matrix dominated to phenocryst dominated. The result is a diverse color palette of pink, light to dark gray, and green depending on dominant mineral composition. Contact textures sometimes include enclaves between intermediate and more mafic compositions and the rare entrainment of quartz xenoliths from unidentified country rock. These observations may indicate multiple origins or events accounting for the variable compositions found around Mt. Cooke.

Microscopy and electron microprobe analysis (EPMA) show various feldspar compositions altering to albite; reactions of hornblende to epidote, apatite (F-Cl), and calcite; and biotite to hematite, magnetite, pyrite (some galena-bearing), and chalcopyrite (figs. 3, 4). Chlorite mineralization is widespread. While primary quartz is mostly lacking, hydrothermal alteration has resulted in diminutive quartz vugs throughout and calcite veining along fracture planes. Individual mineralization effects have been noted in some areas by the presence of ilmenite (extensive), barite, rutile, primary zircon, and sphene (Fe, Al bearing). A single sample was identified at lower elevation containing miniscule almandine–pyrope garnets. EPMA of these detected solid inclusions of Pb- Ni- sulfides; while not yet interpreted, this suggests some degree of metasomatism has occurred. Scatter Creek garnets may then indicate endo-skarn formation and possibly an alteration temperature progression from low to high elevation. While not within the study's scope, EPMA has also shown the presence of tetragonal cerium-bearing grains in epidote surrounding altered hornblende. Element totals suggest these grains may be a vesuvianite member (Ca-Mg, Fe-Ti, Al-silicate), a mineral consistent with skarns but normally within carbonate units. These and garnets may serve as topics of future work to understand alteration from different geochemical perspectives.

Stable isotope analyses using laser fluorination mass spectrometry offers another approach to understand alteration (fig. 5) while fractionation values yield temperature data. $\delta^{18}O$ values of ubiquitous feldspars (Vienna Standard Mean Ocean Water, VSMOW) average between 4 and 6‰, while carbonates (Vienna Pee Dee Belem-

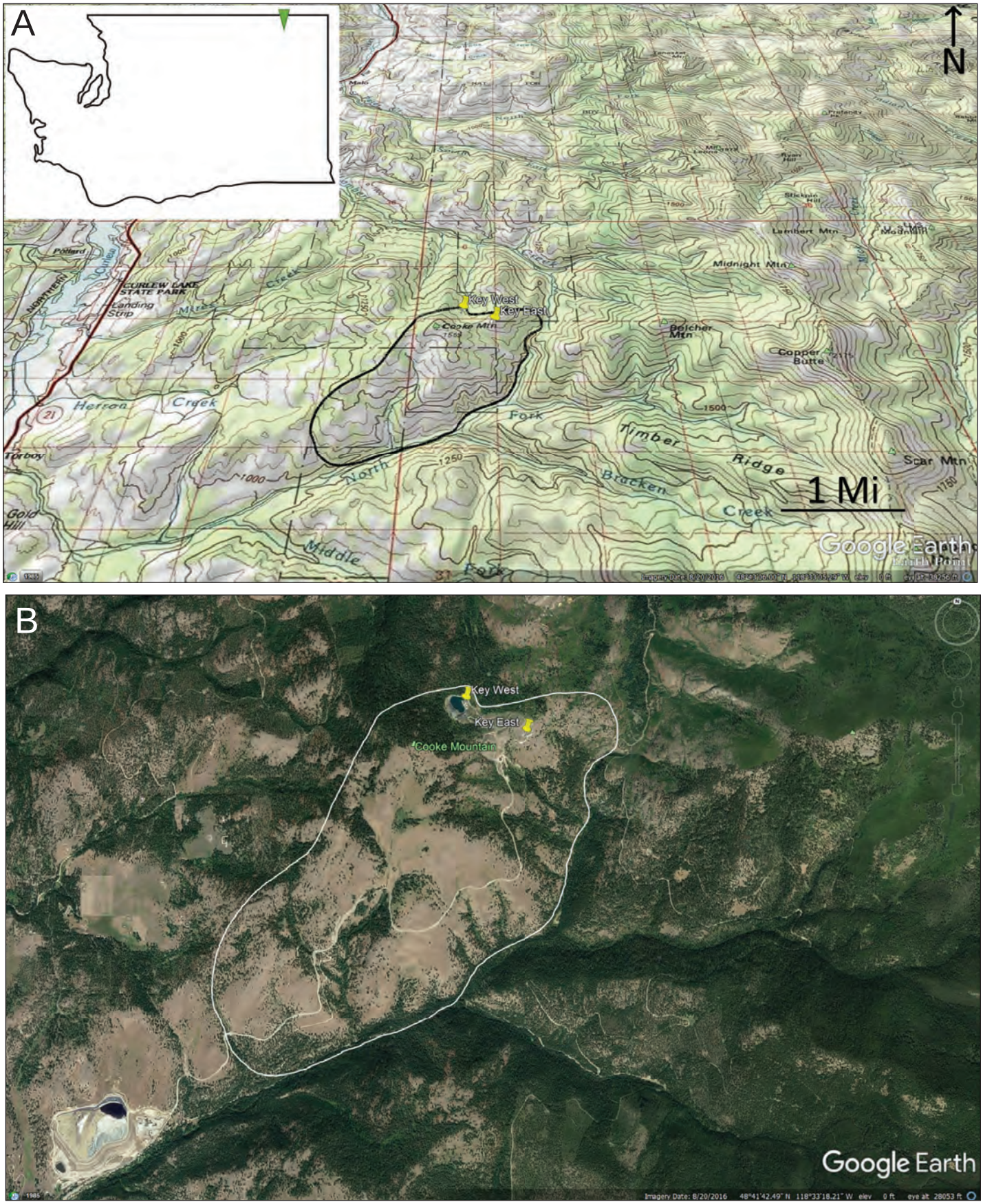

Figure 1. Regional and topographic map (A) and satellite imagery (B) of the Cooke Mountain field area located northeast of Republic, WA. Key East pit (Lowe, 1998) and the Key West pit (this study) are marked.

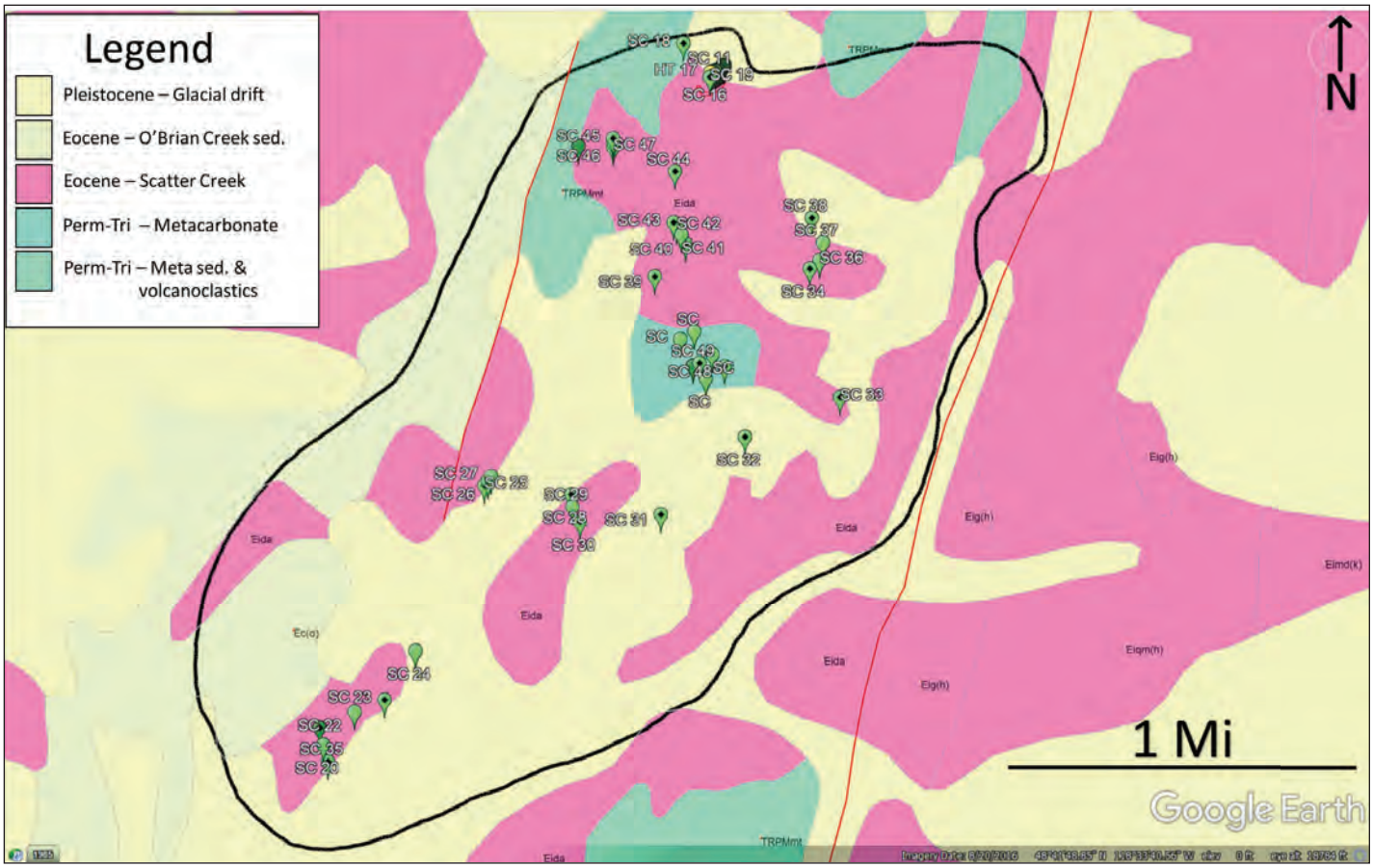

Figure 2. Geologic map of the field area showing sampling locations. Eocene Scatter Creek lies stratigraphically between the Perm-Tri metacarbonate and clastic hornfel units.

nite, VPDB) consistently yield -29‰ (-5 to -8‰ $\delta^{13}C$). Hydrothermal pyrite/chalcopyrite quartz veins within contacting hornfels exhibit $\delta^{18}O$ values between 14‰ (chilled margin) and 11‰ (proximal distance). Fractionation calculations between quartz<=>H_2O yield 210–170°C, respectively (using Sharp and others, 2016). Fluid inclusions within the main body of other nearby deposits have exhibited similar mesothermal temperatures (e.g., 240°C; Fifarek and others, 1996). Higher concentrations of sulfides in veins would be expected as temperature drops and suggest a parent rock previously enriched in sulfur (Barnes, 1979). Feldspar compositions (fig. 6) and other phases calculated from EPMA are still being correlated to $\delta^{18}O$ values and may offer additional fractionation temperatures.

X-ray fluorescence (XRF) and inductively coupled plasma mass spectrometery (ICPMS) major and trace element whole-rock analyses have been recently acquired and interpretations are in progress. However, preliminary insights about the hydrothermal system suggest a more ande-dacitic rather than trachytic composition (fig. 7); whether these values are primary or the result of alteration is yet to be determined. Furthermore, enrichment in Ba (upwards of 2,000 ppm) suggests significant continental contribution to the original magma(s); these values are consistent with analyses of surrounding meta-sediments also supporting hydrothermal fluid circulation. Notably, both Scatter Creek and contact-metamorphosed hornfels show unexpectedly high concentrations of As and Sb (>100 ppm), which may indicate Au- mineralization given its characteristic association with gold arsenide and stibnite (Volkov, 1989).

Routine powder X-ray diffraction (XRD) analyses have been recently acquired and may offer further mineralogical insights into the hydrothermal system (fig. 8). While diffractograms are still being processed and refined, preliminary phase matches have identified ferrous clinochlore to be the prominent chlorite member, consistent with propylitic alteration and similar to greenschist facies mineral assemblages. Likewise, dickite, a low-pressure high-temperature kaolin member, is the dominant clay. Ferro-magnesian hornblende has been identified as the prominent amphibole; actinolite was a close match but the detection of fluorine during EPMA

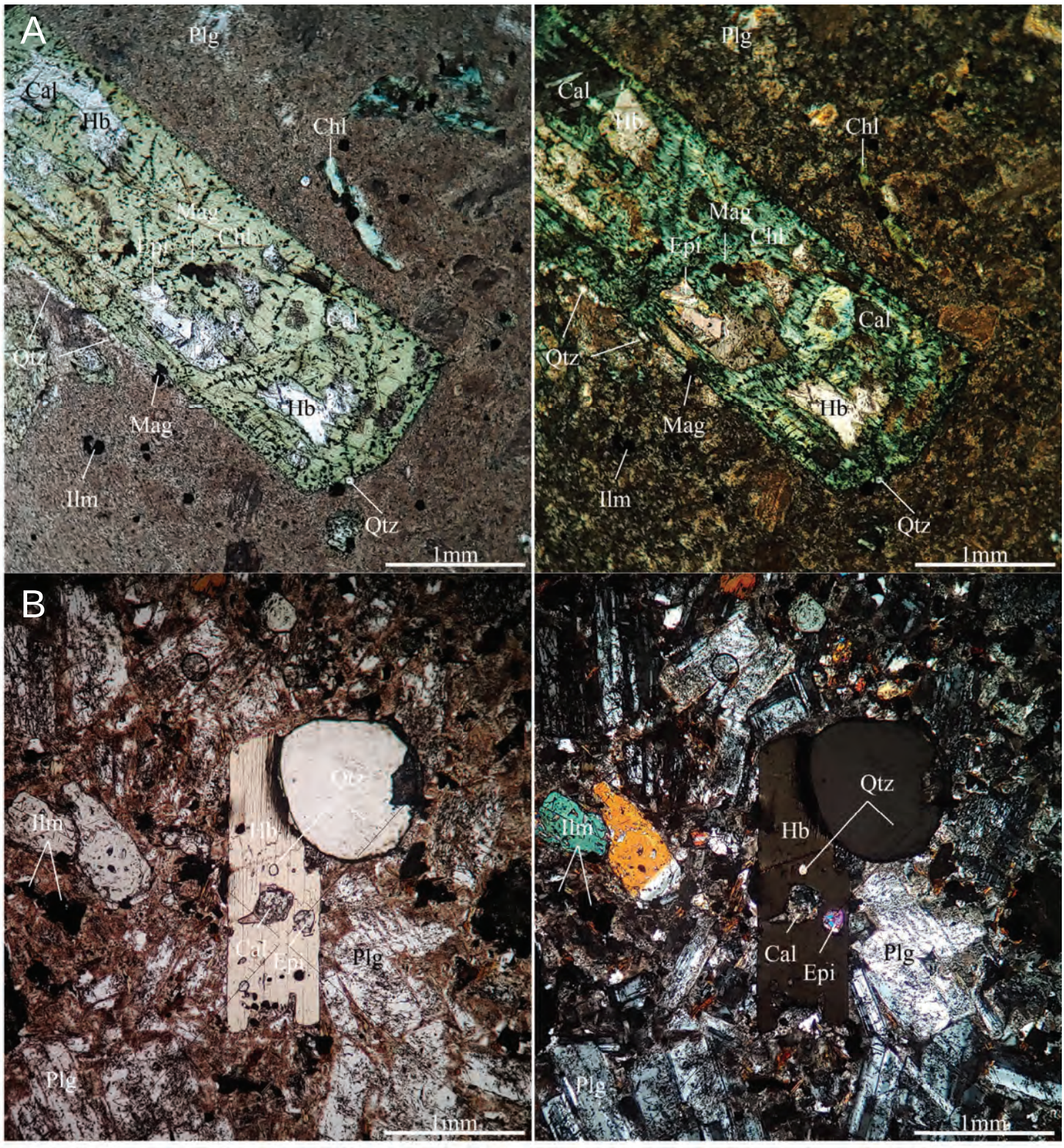

Figure 3. Plain polarized and cross polarized thin section images. Top sample (A) was collected at the Key West pit and exhibits further reaction progress than the bottom sample (B) collected from the southwest slope of Mt. Cooke.

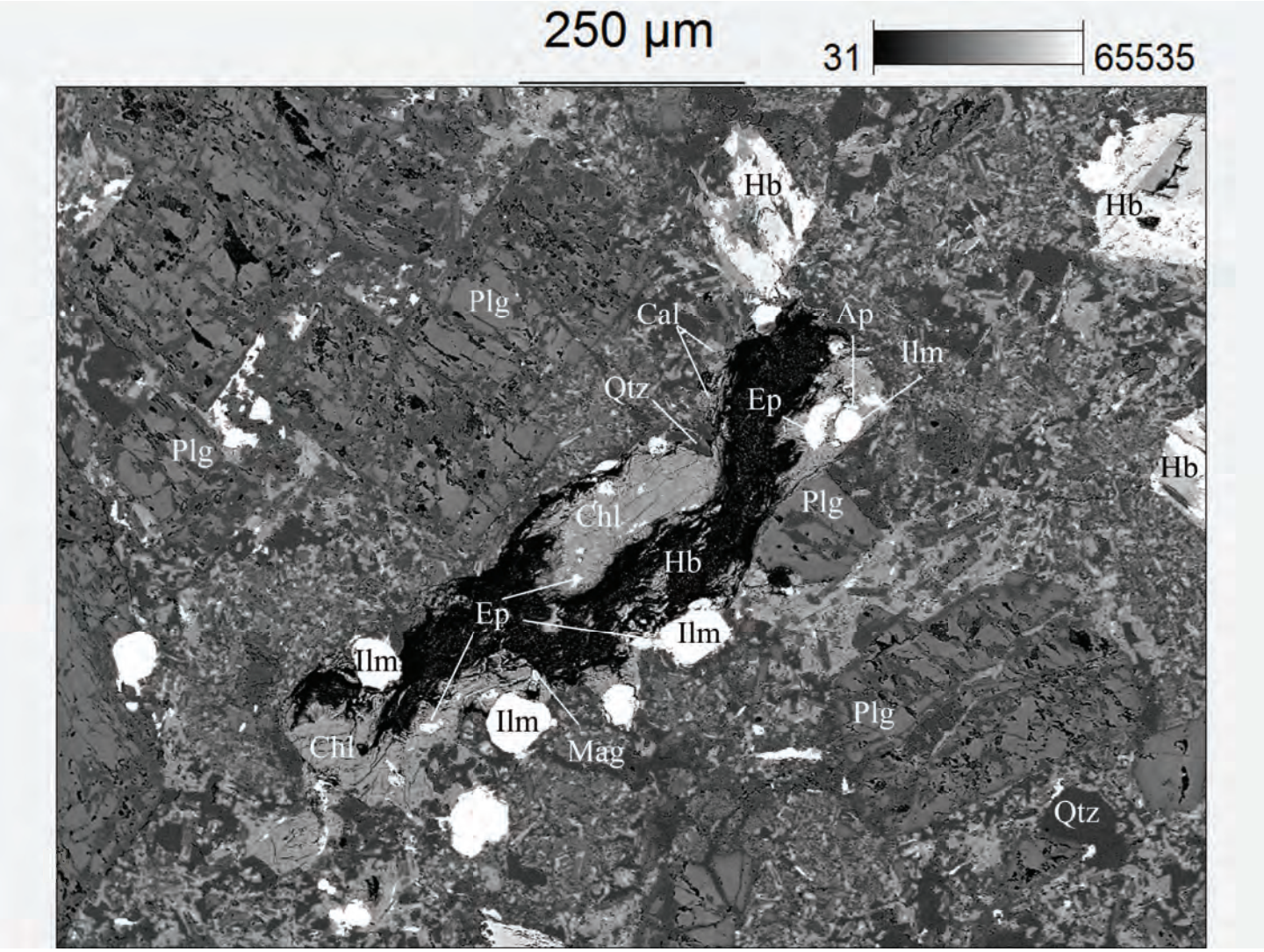

Figure 4. Back scatter electron image showing a characteristic mineral assemblage and reaction progress. Note the central hornblende was preferentially eroded during preparation due to alteration.

corroborates the former. TiO_2 identified during EPMA, thought to be rutile given its stability, was matched as anatase. Matchings of feldspars, quartz, calcite, muscovite, biotite (Fe, Mg), apatite (F, Cl), and sulfides (with the addition of Fe-sphalerite) have been consistent with EPMA identification. Interestingly, there appears to be variation in dominant mica composition (8–2 2θ) across the study area that may correlate to alteration progression spatially.

Another sequence of EPMA routines is underway focusing specifically on feldspars and may offer further insights to alteration within crystal zonations. Nevertheless, the current mineralogical assessment of this thesis agrees with previous nearby studies (Lowe and Larson, 1996; Lowe, 1998) identifying the deposits on Mt. Cooke as a propylitically altered “calcic skarns.” Au- mineralization outside of, and the addition of garnets within, the Scatter Creek suggest both exo- and endo-skarn activity occurred. Future work should involve further characterizations focusing on other minerals (e.g., hornblende, garnet), assessing the age of alteration relative to the emplacement of Scatter Creek, correlations to the structural deformation in the field area, and projections at depth where Au- mineralization is more apparent.

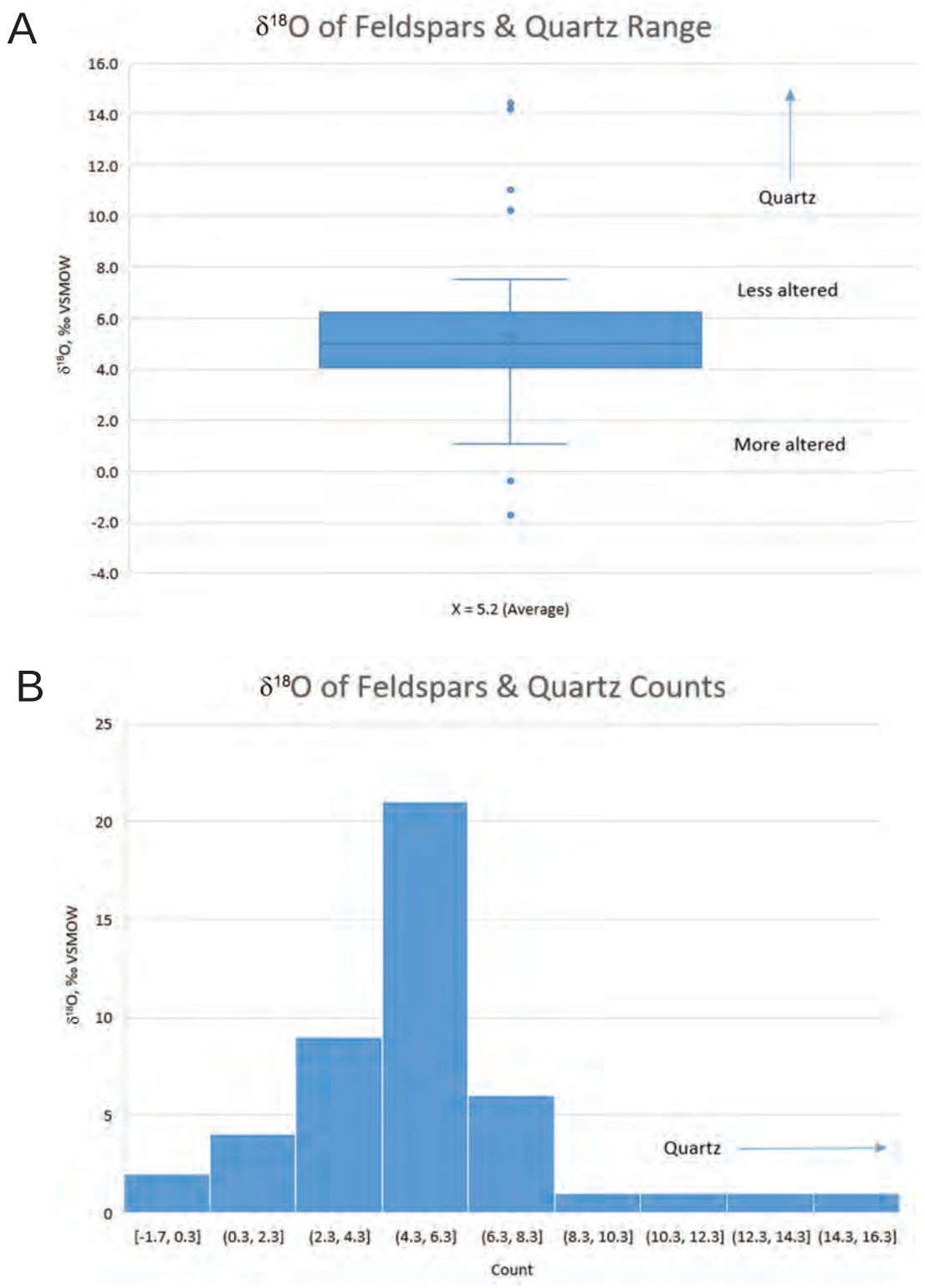

Figure 5. Plots of stable isotope $\delta^{18}O$ value range (A) and counts (B) for feldspar and quartz grains. Average 4–6‰ (VSMOW).

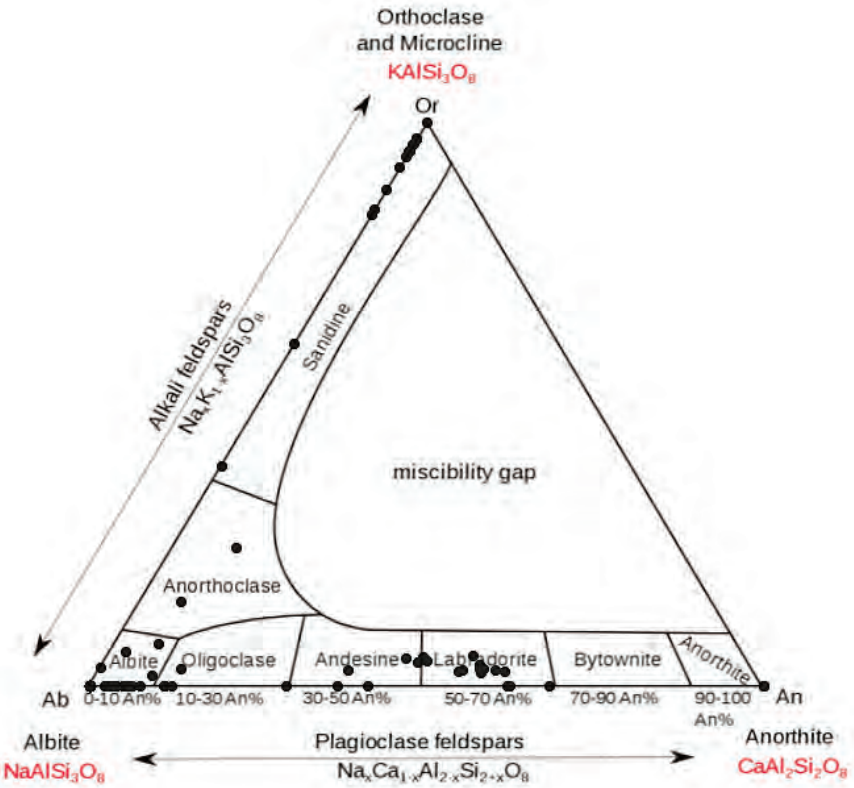

Figure 6. Plot of 65 feldspar compositions calculated from EPMA (after Deer and others, 1992).

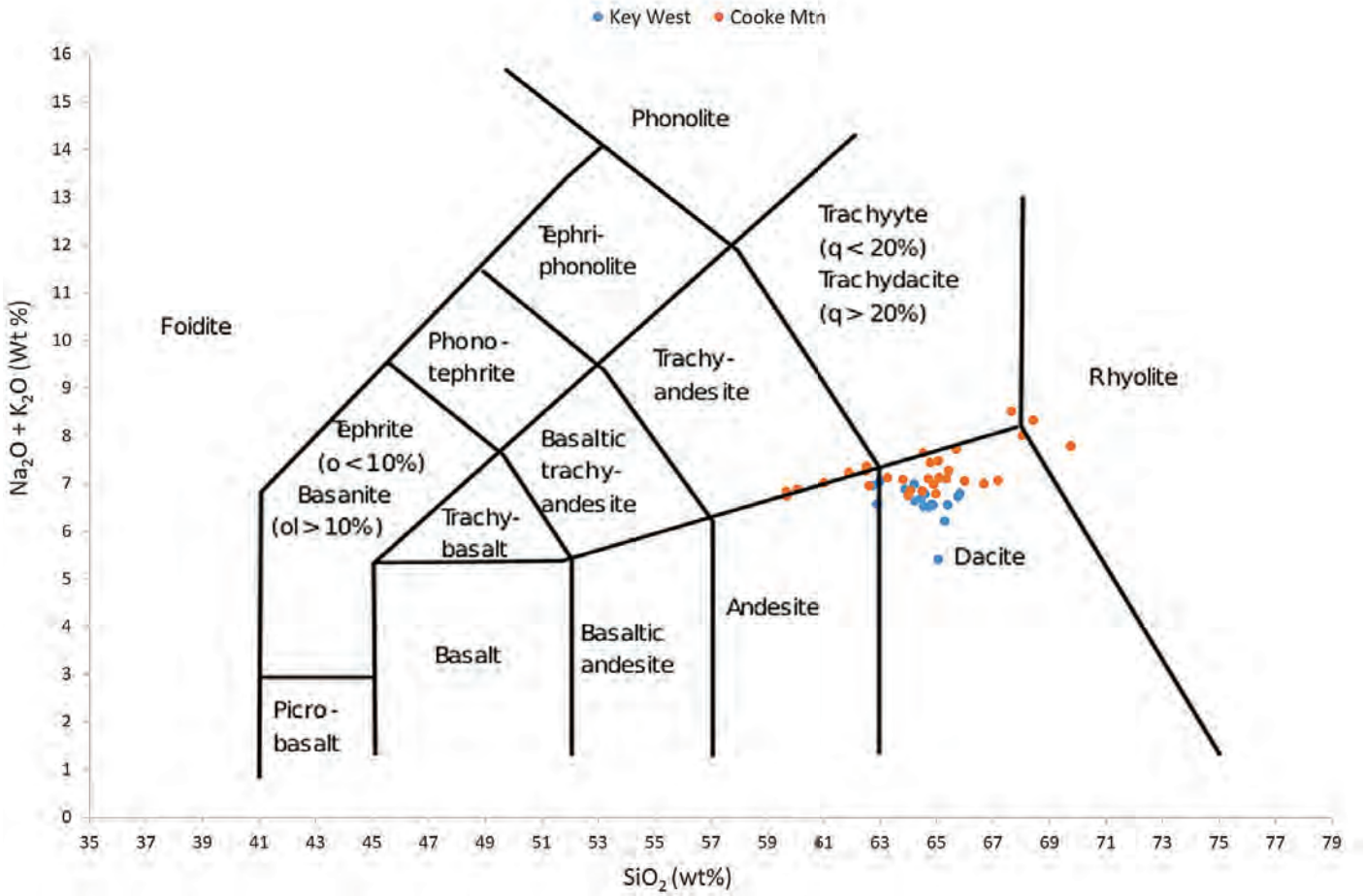

Figure 7. Total alkaline vs. silica XRF plot showing 50 sample compositions from across the field area. Identities fall within the ande-dacite spectrum bordering trachytic varieties. Curiously, samples from the Key West pit (north end of the field area) show lesser alkaline values.

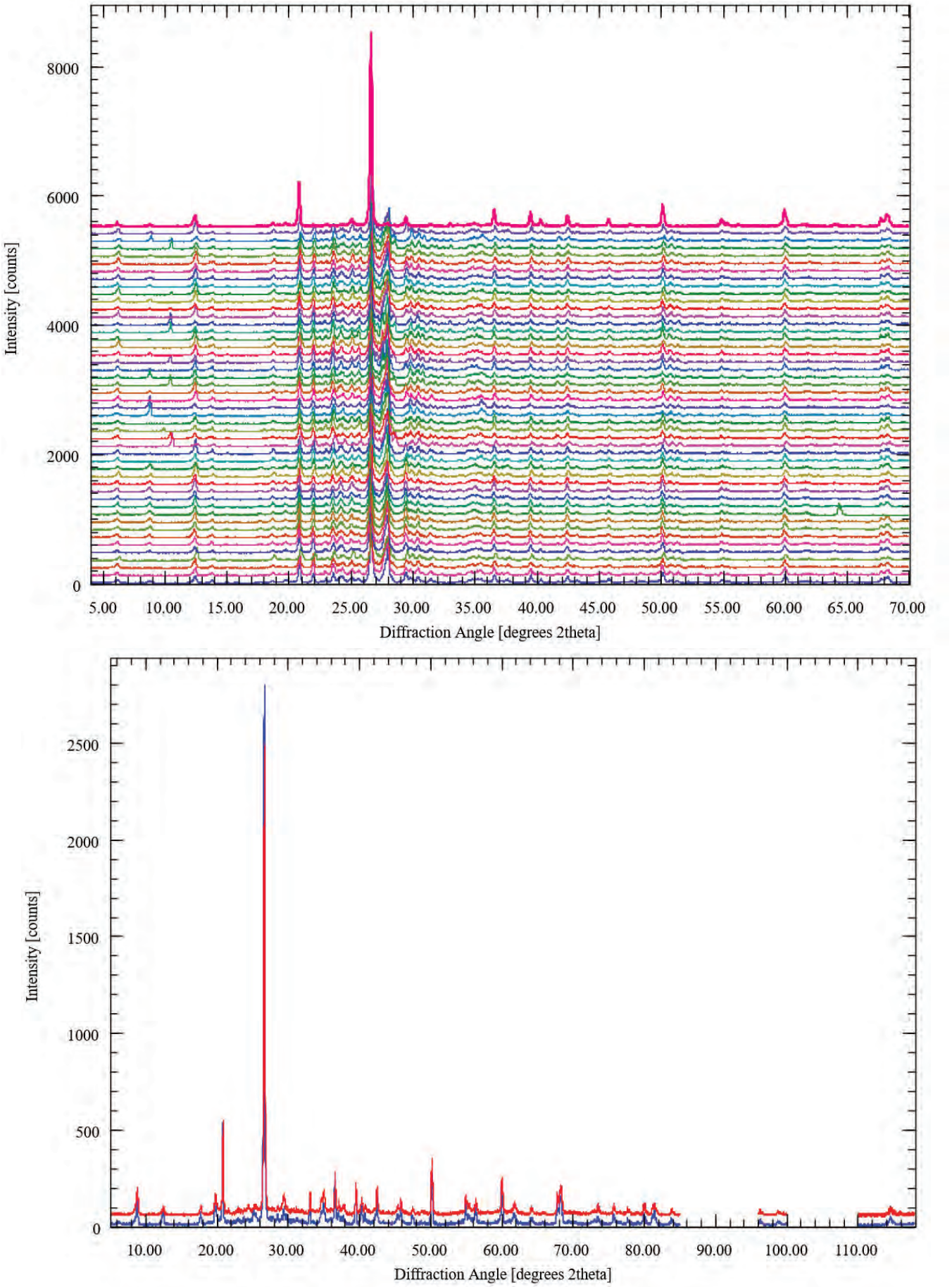

Figure 8. Raw XRD diffractograms of the Scatter Creek (A) and two adjacent hornfels (B).

References

Barnes, H.B., 1979, Geochemistry of hydrothermal ore deposits: New York, Wiley Interscience, p. 1–21.

Deer, W.A., Howie, R.A., and Zussman, J., 1992, An introduction to the rock forming minerals: London, Longman Scientific and Technical, 696 p.

Fifarek, R.H., Devlin, B.D., and Tschauder Jr., R.J., 1996, Au-Ag mineralization at the Golden Promise deposit, Republic district, Washington: Relation to graben development and hot spring processes, *in* Coyner, A.R., and Fahey, P.L., eds., Geology and ore deposits of the American cordillera: Geological Society of Nevada Symposium Proceedings, p. 1063–1088.

Holder, G.A.M., 1985, Geology and petrology of the intrusive rocks east of the Republic Graben in the Republic quadrangle, Ferry County, Washington; Pullman, Washington State University, M.S. thesis.

Holder, R.W., 1986, Emplacement and geochemical evolution of Eocene plutonic rocks in the Colville Batholith: Pullman, Washington State University, Ph.D. dissertation.

Lowe, C.H., 1998, Geology of the Key East gold deposit, Ferry County: Pullman, Washington State University, M.S. thesis.

Lowe, C.H., and Larson, P.B., 1996, Geology of the Key East gold deposit, Ferry County, Washington, *in* Coyner, A.R., and Fahey, P.L., eds., Geology and ore deposits of the American cordillera: Geological Society of Nevada Symposium Proceedings, Reno/Sparks, Nevada, April 1995, p. 1111–1132.

Morris, G.A., 1996, Petrogenesis of calk-alkaline rocks in an extensional environment: The Eocene Coleville Batholith of northeast Washington, USA: Pullman, Washington State University, Ph.D. dissertation.

Moye, F.J., 1984, Geology and petrochemistry of Tertiary igneous rocks in the western half of the Seventeen Mile Mountain 15' quadrangle, Ferry County, Washington: Moscow, University of Idaho, Ph.D. dissertation.

Muessig, S., 1967, Geology of the Republic quadrangle and a part of the Aeneas quadrangle, Ferry County, Washington: U.S. Geological Survey Bulletin 1216, p. 135.

Parker, R.L. and Calkins, J.A., 1964, Geology of the Curlew Quadrangle, Ferry County, Washington: U.S. Geological Survey Bulletin 1169, 95 p.

Sharp, Z.D., Gibbons, J.A., Maltsev, O., Atudorei, V., Pack, A., Sengupta, S., Shock, E.L., and Knauth L.P., 2016, A calibration of the triple oxygen isotope fractionation in the SiO_2<=>H_2Osystem and applications to natural samples: Geochimica et Cosmochimica Acta, v. 186, p. 105–119.

Volkov, AV., 1989, Genesis of Au-Sb mineralization: Tikhookeanskaya Geologiya, no 6., p. 84–87.

Elkhorn Mountains from the Iron Mine in the Elkhorn Mountains 7.5’ quadrangle. Photo by Stan Korzeb.

Barium Mobility in a Geothermal Environment

Jarred Zimmerman and Peter B. Larson

School of the Environment, Washington State University, Pullman, Washington

Barium is a large divalent cation that is not easily accommodated in rock-forming minerals (Johnson and others, 2017). In igneous rocks, Ba^{2+} substitutes for K^{+} in potassium feldspar and mica, as well as in apatite and plagioclase to a lesser extent (Johnson and others, 2017). Under oxidizing conditions, Ba is precipitated most commonly as barite ($BaSO_4$) or witherite ($BaCO_3$). Most barium compounds have low solubility, but solubility increases in reducing or acidic conditions (Johnson and others, 2017). Because of these properties, Ba is a good indicator of major upwelling zones in a hydrothermal environment and an indicator of fluid properties. Despite the large area influenced by the Yellowstone hydrothermal system, approximately 65 km^2 (Lowenstern and others, 2015), water chemistry reported by the USGS (i.e., Ball and others, 2002, 2010) indicates relatively low levels of dissolved Ba, potentially indicating Ba sequestration is occurring before the fluids reach the surface. Barium mobility and sequestration in argillic and advanced argillic alteration environments may act as vectors to major fluid flow pathways, especially where alteration is intense and pervasive or where the paleosurface has been eroded. This study used electron microprobe analysis (EMPA) and optical petrographic methods to identify barium-bearing minerals and altering minerals and compare the findings to previous studies on the Tuff of Sulphur Creek in Yellowstone National Park.

While most of the volcanic flows produced by the Yellowstone hotspot are not enriched in Ba, there are several that have elevated concentrations: the Huckleberry Ridge Tuff–Member C, Tuff of Sulphur Creek, and Canyon Flow (Pritchard and Larson, 2012). Of these units, the Tuff of Sulphur Creek (Tsc) was studied because of the good exposure on canyon hillsides and a fossil hydrothermal system that allows for examination of how Ba moved in the hydrothermal environment. The Tsc covers an elongate area of approximately 119 km^2 to the north and northeast of Sour Creek Dome, contained primarily within the 0.64 Ma (Yellowstone) caldera, and constitutes the walls of the Grand Canyon of the Yellowstone River, the east of Lower Falls (fig. 1A; Larson and others, 2009; Pritchard and Larson, 2012). This unit was deposited by a pyroclastic flow and consists of three sections: a poorly to moderately welded basal ash, a thick devitrified stony interior, and a seldom-exposed upper portion (Pritchard and Larson, 2012). The thick (approximately 300 m in Seven Mile Hole) stony interior has roughly 20–35% phenocryst abundance in hand sample, primarily alkali feldspar with lesser amounts of plagioclase and quartz and trace oxides (Pritchard and Larson, 2012). Ba in the Tsc is primarily contained in sanidine phenocrysts, generally about 1 wt% (Pritchard and Larson, 2012).

Hydrothermal fluids at Yellowstone have three end members: acid-sulfate, circumneutral, and bicarbonate. Bicarbonate fluids are only seen at Mammoth Hot Springs, where travertine mounds and terraces are formed as carbonate minerals precipitate from the cooling water (Hurwitz and Lowenstern, 2014). Inside the caldera, fluid type is controlled by topography and location. Circumneutral springs are most common in topographic lows and along the margins of impermeable volcanic units (Fournier, 1989). These fluids generally have a neutral to slightly basic pH, elevated Cl^{-} concentrations, and tend to precipitate siliceous sinter mounds due to saturation with SiO_2 at high temperatures (Fournier, 1989; Hutwitz and Lowenstern, 2014). Acid-sulfate fluids are most common at topographic highs and areas with little water flow (Fournier, 1989). The preferred model for acid-sulfate fluid generation at Yellowstone is the volatilization of H_2S and CO_2, among other volatile molecules, from a boiling circumneutral water table. Rising volatiles condense into perched meteoric water tables where pH is driven down by a two-stage process: CO_2 dissolves into the water, generating carbonic acid, and H_2S oxidizes to sulfuric acid (Fournier, 1989; Hurwitz and Lowenstern, 2014). These fluids are sulfate-rich, have a pH generally less than 5, and create depressions due to the low pH with little to no water discharge (Fournier, 1989; Hurwitz and Lowenstern, 2014). In addition to topographic discrepancies, circumneutral and acid-sulfate fluids are broadly separated by which portion of the Yellowstone caldera they erupt. Acid-sulfate fluids are dominant

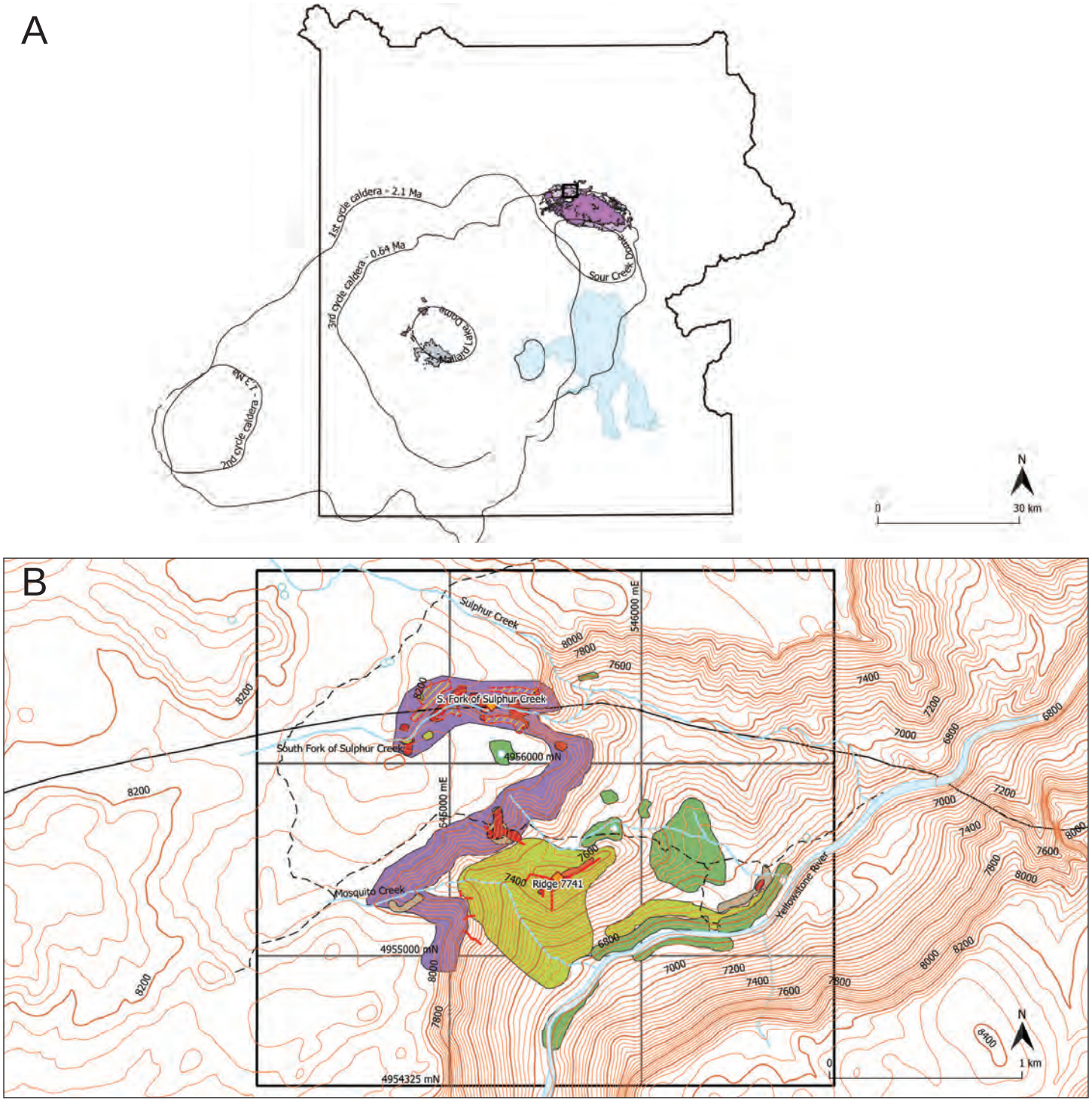

Figure 1. (A) Outline of Yellowstone National Park with the three most recent caldera ring-fault zones and resurgent dome fracture zones noted in thin lines. Purple patches mark the flows of the Upper Basin Members of the Plateau Rhyolites. The small black rectangle denotes the study area along the caldera margin. (B) Alteration map of the study area. Colors represent the major alteration mineral: purple, kaolinite; light green, illite; gray, dickite; maroon, alunite; orange, adularia; yellow hatched area, residual silica; and dark green, sinter fields. Orange diamonds mark the type areas for alteration styles (see text). Images modified from Christiansen, 2001 and Larson and others, 2009.

in the eastern portion of the Yellowstone caldera, likely due to the partial melt and rising mantle plume being closer to the surface (Fournier, 1989; Hurwitz and Lowenstern, 2014), thus steepening the geothermal gradient and producing more steam than liquid water. To the west, the partial melt and plume are deeper, which allows more liquid water than steam to reach the surface, expressed as circumneutral fluids. At times, acid-sulfate and circumneutral fluids may mix to generate fluids of intermediate chemistry (Fournier and others, 2002; Hurwitz and Lowenstern, 2014).

In Seven Mile Hole, approximately 9 km east of Lower Falls between the Yellowstone River and Mt. Washburn, the Tsc is hydrothermally altered by acid-sulfate and circumneutral fluids (fig. 1B; Larson and others, 2009). Despite the elevated Ba concentrations in the Tsc, previous studies found only three Ba-bearing alteration minerals: barite ($BaSO_4$), walthierite ($Ba_{0.5}Al_3(SO_4)_2(OH)_6$), and hyalophane $(K,Ba)(Al,Si)_4O_8$ (Larson and others, 2009). In the study area, alteration appears to be structurally controlled and altering fluid chemistry is controlled by relative permeability. Circumneutral fluid alteration is best exemplified at Ridge 7741 in the Grand Canyon (fig. 1B), approximately 100 m below the modern canyon rim. Ridge 7741 is a silicified, upwelling zone with hydrothermal feldspars and a quartz-illite halo (Larson and others, 2009). Primary feldspar alteration ranges from partial to complete pseudomorphic replacement by adularia, hyalophane, buddingtonite, illite, and quartz. Incomplete alteration reactions show replacement was most efficient along fractures and cleavage planes of sanidine, where Ca was preferentially liberated, followed by Na and Ba (figs. 2B, 2C). Previous workers noted hyalophane in XRD (X-ray diffraction) diffractograms, but it was not noted in this study using EMPA. However, incomplete reactions indicate hyalophane may be a relatively minor intermediate step likely controlled by the original feldspar chemical zonation (fig. 2A).

Acid-sulfate fluid alteration is best exemplified in the South Fork of Sulphur Creek, just north of a dry, broken siliceous sinter field (fig. 1B), and proximal to the permeable caldera ring-fault zone. The area is largely replaced by kaolinite and opaline silica with various sulfate minerals and sits about 50 m below the current canyon rim. Acid-sulfate alteration is noted by residual or “vuggy” silica bodies in the canyon walls and the relative abundance of sulfate minerals. Primary feldspars in this environment were typically more completely altered to kaolinite, alunite ($KAl_3(SO_4)_2(OH)_6$), and silica. When feldspar was replaced by alunite and kaolinite, kaolinite precipitation was preceded by alunite (fig. 2D). Chemical examination of alunite found zonation similar to sanidine altered at Ridge 7741, with elevated K and lesser Ba and Na. This may imply the area was first altered by circumneutral fluids before acid-sulfate fluid incursion. Alunite group minerals were examined for walthierite, noted by previous studies using XRD, but it was not noted via EMPA. However, zonation noted during analysis indicates walthierite and other alunite group minerals likely occur as discrete phases in chemically zoned alunite (fig. 2C). Chemical zonation in alunite was likely inherited from the original feldspar (fig. 2A), also indicating the fluid may have supplied only the sulfate. Additionally, minor amounts of barite were found in silica-sulfide veinlets, signifying that some Ba was liberated to the fluid before being precipitated as barite from the abundant sulfate.

The hydrothermal history in the study area is complicated by the incision of the Grand Canyon and lowering of the local water table (Larson and others, 2009), extending the influence of the acid-sulfate fluids to the south, as well as deepening the steam-heated portion of the system. In areas altered first by circumneutral fluids and later by acid-sulfate fluids in the steam-heated portion of the system, above the water table, paragenesis is muddled. Feldspars were likely altered to patchy combinations of adularia in sanidine with some amount of silica precipitation in upwelling zones. The acidic fluids altered the sanidine phases to pseudocubic alunite group minerals with clay, likely kaolinite given its location above the water table. The process leaves islands of adularia with Ba and Na, patches of alunite with similar concentrations of Ba and minor Na, patchy silica, either opaline or quartz depending on which stage the silica precipitated during, all in a mass of kaolinite (fig. 2D). The original crystal margins may be preserved if the grain was armored by silica or the groundmass was not pervasively replaced by kaolinite. Hydrothermal processes do not seem to have significantly concentrated or dispersed Ba concentrations in the Tsc; they merely changed the mineral to a more stable form for the altering environment.

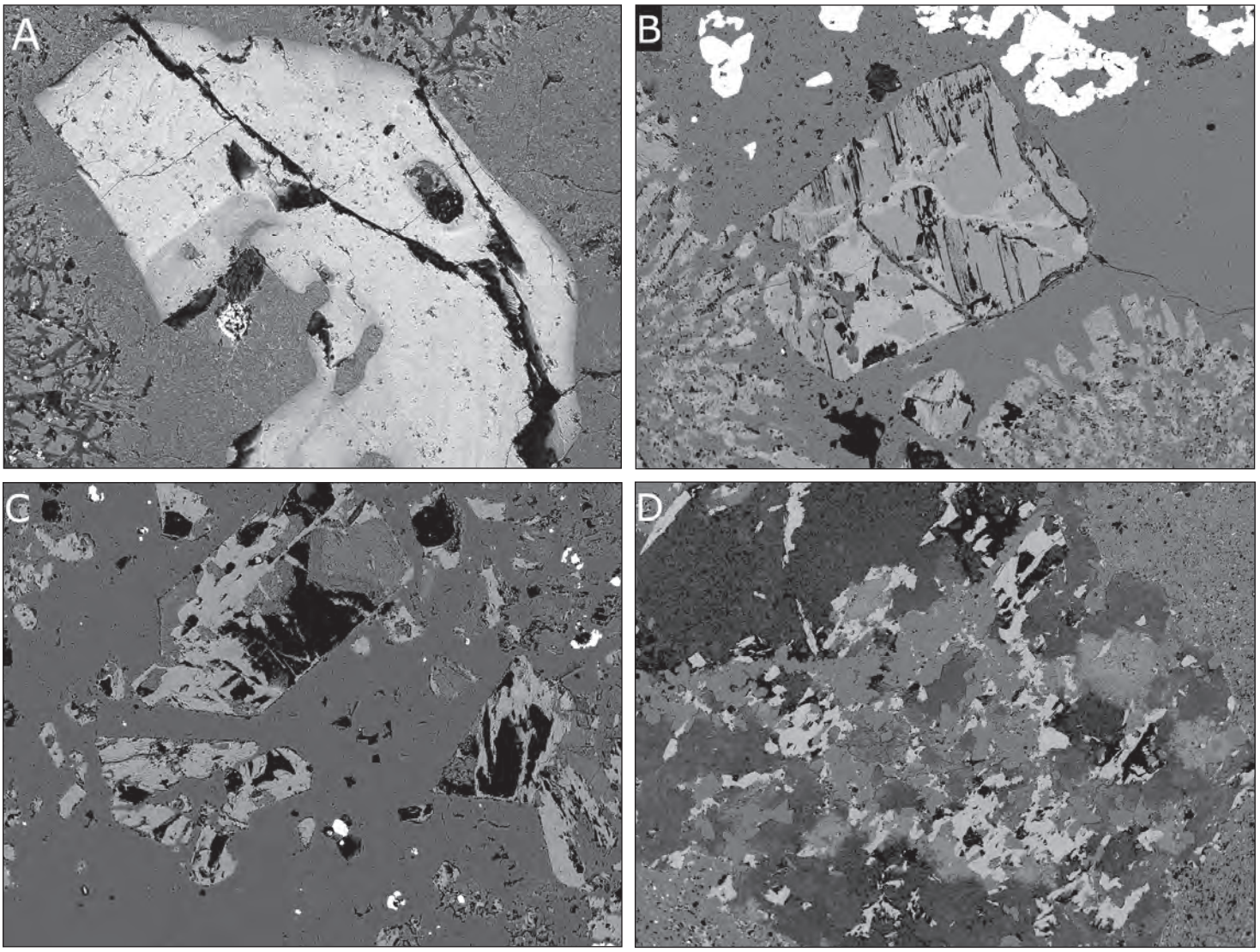

Figure 2. EDS (energy dispersive back-scattered electron) images of feldspars in varying stages of alteration. (A) Relatively unaltered sanidine showing chemical zonation from differences in Ba, Na, and Ca concentrations. (B) Sanidine (darker) phenocryst with veinlets of adularia replacement (lighter) hosted by a quartz (darkest) veinlet. (C) Adularia (medium gray) in a quartz veinlet with zoned alunite (two tone in top middle of image). Lighter gray alunite has a high concentration of Ba with less Ca and Na. (D) Completely altered feldspar with islands of adularia (lightest), patchy silica (smooth medium gray) and alunite (textured medium gray) with clay (dark gray).

References

Ball, J.W., McCleskey, R.B., Nordstrom, D.K., Holloway, J.M., Verplanck, P.L., and Sturtevant, S.A., 2002, Water-chemistry data for selected springs, geysers, and streams in Yellowstone National Park, Wyoming, 1999–2000: U.S. Geological Survey Open-File Report 02-382, 111 p.

Ball, J.W., McCleskey, R.B., and Nordstrom, D.K., 2010, Water-chemistry data for selected springs, geysers, and streams in Yellowstone National Park, Wyoming, 2006–2008: U.S. Geological Survey Open-File Report 2010–1192, 109 p.

Christiansen, R.L., 2001, The quaternary and pliocene Yellowstone Plateau volcanic field of Wyoming, Idaho, and Montana: U.S. Geological Survey Professional Paper 729-G.

Fournier, R.O., 1989, Geochemistry and dynamics of the Yellowstone National Park hydrothermal system: Annual Review of Earth and Planetary Sciences, v. 17, no. 1, p. 13–53.

Fournier, R.O., Weltman, U., Counce, D., White, L.D., and Janik, C.J., 2002, Results of weekly chemical and isotopic monitoring of selected springs in Norris Geyser Basin, Yellowstone National Park during June–September 1995: U.S. Geological Survey Open-File Report 02-344, 49 p.

Hurwitz, S., and Lowenstern, J.B., 2014, Dynamics of the Yellowstone hydrothermal system: Review of Geophysics, v. 51, p. 375–411, doi:10.1002/2014RG000452.

Johnson, C.A., Piatak, N.M., and Miller, M.M., 2017, Barite (Barium), *in* Schulz, K.J., DeYoung, J.H. Jr., Seal, R.R. II, and Bradley, D.C., eds., Critical mineral resources of the United States—Economic and environmental geology and prospects for future supply: U.S. Geological Survey Professional Paper 1802, chap. D, p. D1–D18, doi: https://doi.org/10.3133/pp1802D.

Larson, P.B., Phillips, A., John, D., Cosca, M., Pritchard, C., Andersen, A., and Manion, J., 2009, A preliminary study of older hot spring alteration in Sevenmile Hole, Grand Canyon of the Yellowstone River, Yellowstone Caldera, Wyoming: Journal of Volcanology and Geothermal Research, v. 188, no. 1–3, p. 225–236.

Lowenstern, J.B., Bergfeld, D., Evans, W.C., and Hunt, A.G., 2015, Origins of geothermal gases at Yellowstone: Journal of Volcanology and Geothermal Research, v. 302, p. 87–101.

Pritchard, C.J., and Larson, P.B., 2012, Genesis of the post-caldera eastern Upper Basin Member rhyolites, Yellowstone, WY: From volcanic stratigraphy, geochemistry, and radiogenic isotope modeling: Contributions to Mineralogy and Petrology, v. 164, no. 2, p. 205–228.

Barite (white) with enargite-tennantite-sphalerite from the Philipsburg District. Photo by Chris Gammons.